UNIVERSITY OF CALIFORNIA MERCED

THE COMPLEXITY OF MERCURY CYCLING: STUDYING THE METHYLATION WINDOW AND ASSESSING TWO REMEDIATION TECHNIQUES IN TWO AQUATIC ENVIRONMENTS

A dissertation submitted in partial satisfaction of the requirements
for the degree of

DOCTOR OF PHILOSOPHY

in Environmental Systems

by

Naivy Dennise Rodal Morales

Dissertation Committee:
Thomas Harmon (Chair)
Marc Beutel (Faculty Advisor)
Peggy O'Day
Anne Hansen
Jacob Fleck

Summer 2024

The Dissertation of Naivy Dennise Rodal Morales is approved, and it is acceptable in quality and form for publication on microfilm and electronically:

Thomas Harmon (Chair)

Peggy O'Day

Anne Hansen

Jacob Fleck

Marc Beutel (Advisor)

Table of Content

Introduction **1**
1 Hydrology and Oxygen Addition Drive Nutrients, Metals, and Methylmercury Cycling in a Hypereutrophic Water Supply Reservoir **8**
1.1 Abstract 8
1.2 Introduction 8
1.3 Methods 10
1.3.1 Study Site 10
1.3.2 Field Monitoring 12
1.3.3 Analytical Methods 13
1.3.4 Data Analysis 14
1.4 Results 15
1.4.1 Hydrology 15
1.4.2 Field Parameters 16
1.4.3 Water Chemistry 17
1.4.3.1 Nutrients, Chlorophyll, and Dissolved Organic Carbon 17
1.4.3.2 Metals 18
1.4.3.3 Mercury 18
1.4.4 Internal Loading Dynamics 19
1.5 Discussion 20
1.5.1 Nitrogen Cycle 20
1.5.2 Manganese and Iron Cycling 22
1.5.3 Methylation Window 25
1.6 Management Considerations 27
1.7 References 29
2 Mercury Cycling in Coagulant-Treated Wetland Soils Upon Rewetting: A Controlled Laboratory Incubation **47**
2.1 Abstract 47
2.2 Introduction 47
2.3 Methods 50
2.3.1 Site Description and Sample Collection 50
2.3.2 Soil Characterization 51
2.3.3 Incubation Experiments 51
2.3.4 Water and Sediment Analyses 52
2.3.5 Statistical Analysis 54
2.4 Results 55
2.4.1 Soil Characterization 55
2.4.2 Incubation Experiments 55
2.4.2.1 Inorganic Mercury and Methylmercury 55
2.4.2.2 Aqueous Parameters: Redox Potential, pH, Manganese, and Sulfate 57
2.4.2.3 Aqueous Parameters: Metals, Nutrients, and Dissolved Organic Carbon 58
2.5 Discussion 59

2.5.1 Rewetting Effect 59
2.5.2 Key Drivers of Mercury Cycling 61
2.5.3 Ephemeral Methylation Window 63
2.5.4 Initial Changes in Soil Methylmercury 65
2.6 Conclusions 66
2.7 References 67
3 Algal Organic Matter Addition Opens Ephemeral Methylation Window in Mildly Mercury-Contaminated Soils 93
3.1 Abstract 93
3.2 Introduction 93
3.3 Methods 96
3.3.1 Study Site 96
3.3.2 Spirulina Powder 97
3.3.3 Incubation Design and Sampling 97
3.3.4 Analyses 98
3.4 Results 99
2.4.1 Aqueous Parameters: Redox Potential, pH, Manganese, and Sulfate 99
3.4.2 Mercury and Methylmercury in water and soil 101
3.4.3 Optical Characterization of Dissolved Organic Matter 102
3.5 Discussion 102
3.5.1 Algal Organic Matter Stimulates Microbial Activity 102
3.5.2 Ephemeral Methylation Window 104
3.5.2.1 Stage I: Opening the Methylation Window 105
3.5.2.2 Stage II: Closing the Methylation Window 106
3.5.2.3 Stage III: Anoxic quasi-steady state 107
3.6 Environmental Considerations 108
3.7 References 110
Appendix 128

Figures

Figure A. The mercury cycle in aquatic environments showing main mercury species (mercury gas, Hg(0), divalent mercury, Hg2+ and methyl mercury, MeHg), and processes (deposition and runoff, oxidation-reduction, sedimentation, methylation, bioaccumulation-biomagnification, sediment resuspension, demethylation, volatilization, and deposition). Based on figure developed by Gray (2003) 7

Figure 1-1. Anoxic biogeochemical processes at the sediment-water interface in reservoirs..... 40

Figure 1-2. (A) Picture of the oxygenation cone on construction barge before being submerged (left), and on-shore facilities including liquid oxygen storage tank and evaporators (right). (B) Map of Hodges Reservoir, showing the two sampling stations A and B, location of the pumped storage system, and location of the hypolimnetic oxygenation system 41

Figure 1-3. Monthly rainfall (blue bars) and surface elevation (red line) in Hodges Reservoir from 2016-2021..... 42

Figure 1-4. Summer (July or August) profiles at stations A and B from left to right: temperature, pH, dissolved oxygen (DO), and redox potential (ORP) 42

Figure 1-5. Water quality isopleths for temperature (T), dissolved oxygen (DO) and redox potential (ORP) at station B during 2017-2019 and 2021 43

Figure 1-6. Water quality parameters of ammonia (A), manganese (B), nitrate + nitrite (C), and iron (D) at station B for 2017-2021. 43

Figure 1-7. Water quality isopleths from top to bottom: ammonia, nitrate, total phosphorus, phosphate, iron, manganese, methylmercury, and total mercury for 2017- 2019, and 2021..... 44

Figure 1-8. Monthly Hypolimnetic Accumulation Rate (MHAR), top to bottom: ammonia, phosphate, manganese, total mercury, and methylmercury at station A (bright color) and B (light color) during 2017, 2018, 2019 and 2021..... 46

Figure 1-9. Example estimates of hypolimnetic accumulation (dark grey) and mass transfer across the thermocline (i.e., internal nutrient loading) (light grey) for the month of June for 2017 (top) and 2018 (bottom) 46

Figure 2-1. Map of the location of Cache Creek Settling Basin showing Cache Creek watershed, the major mercury points sources, and the connection of the Yolo Bypass with the Sacramento-San Joaquin Delta. Modified from De Parsia and others, (2019). 86

Figure 2-2. Map showing Cache Creek Settling Basing study site and mesocosm locations A, B and C. Numbers represent the different coagulants with 2: the control, 3: Chitovan coagulant, 4: Ferralyte, and 5: Ultrion (compliments of J. Fleck, USGS). 87

Figure 2-3. Mercury and methylmercury in water. Left side, standard test with control and three coagulant treatments (ChitoVan, Ferralyte and Ultrion) replicated at three stations (A, B and C). Error bars are plus/minus one standard error of triplicate incubations. Right side, stress test with spirulina organic matter

(SP) addition in control soil for station C and a water+SP control. From top to bottom: methylmercury concentration, inorganic mercury concentration, ratio of methylmercury to total mercury, and percentage of methylmercury in water relative to methylmercury in water plus sediment. Note difference in vertical scale for all figures. 88

Figure 2-4. Methylmercury (MeHg) in soil. Left side, standard test with mean values from control and three coagulant treatments (ChitoVan, Ferralyte and Ultrion) replicated at three stations (A, B and C). Error bars are plus/minus one standard error of triplicate incubations. Right side, stress test with spirulina organic matter addition in control soil for station C. From top to bottom: methylmercury mass in soil (dw: dry weight) and log methylmercury Kd value (log of methylmercury soil concentration divided by water concentration). 89

Figure 2-5. Primary aqueous parameters. Left side, standard test with mean values from control and three coagulant treatments (ChitoVan, Ferralyte and Ultrion) replicated at three stations (A, B and C). Error bars are plus/minus one standard error of triplicate incubations. Right side, stress test with spirulina organic matter (SP) addition in control soil for station C and a water+SP control. From upper to bottom: redox potential (Eh), pH, manganese, and sulfate. 90

Figure 2-6. Supporting aqueous parameters. Left side, standard test with mean values from control and three coagulant treatments (ChitoVan, Ferralyte and Ultrion) replicated at three stations (A, B and C). Error bars are plus/minus one standard error of triplicate incubations. Right side, stress test with spirulina organic matter addition in control soil for station C. From upper to bottom: iron, aluminum, ammonia, nitrate, and phosphate. Note difference in vertical scale for iron, ammonia, and phosphate. 91

Figure 2-7. Dissolved organic carbon (DOC) concentration (top) and $SUVA_{254}$ (bottom). Left side, standard test with control and three coagulant treatments (ChitoVan, Ferralyte and Ultrion) replicated at three stations (A, B and C) mean values. Error bars are plus/minus one standard error of triplicate incubations. To facilitate statistical analysis, ChitoVan data includes two B incubations since A samples were not available. Right side, stress test with spirulina organic matter addition in control soil for station C. Note difference in vertical scale for DOC 92

Figure 3-1. Variation in Eh, pH, and aqueous parameters with incubation time with the gradient in spirulina organic matter additions, 0.025 g, 0.05 g, 0.1 g, 0.2 g, 0.4 g, and the control. A) oxidation-reduction potential (Eh), B) pH, C) manganese, D) iron, E) sulfate, and F) phosphate concentrations in water. 122

Figure 3-2. Mercury and methylmercury in water and soil with incubation time with the gradient in spirulina organic matter additions, 0.025 g, 0.05 g, 0.1 g, 0.2 g, 0.4 g, and the control. A) Methylmercury (MeHg), B) Inorganic mercury, IHg (total Hg minus MeHg in water), C) %MeHg water (MeHg water / MeHg water plus MeHg soil), D) MeHg:IHg ratio in water, E) Soil MeHg and F) Partitioning coefficient, Log Kd, for MeHg in soil relative to water with Kd units of L/Kg 123

Figure 3-3. Dissolved organic matter (DOM) optical properties with incubation time with the gradient in spirulina organic matter additions, 0.025 g, 0.05 g, 0.1 g, 0.2 g, and 0.4 g, and the control. A) Fluorescence in region F (Flr_F, RU), quinoid-like DOM, B) Fluorescence in region B (Flr_B, RU), a byproduct of microbial activity, C) Fluorescence Index (FI), indicative of microbial DOM source (>1.8), and D) $Sag_{275\text{-}295}$, indicative of low molecular weight DOM (>0.02). 124

Figure 3-4. Changes in the excitation-emission matrix (EEM) fluorescence intensity spectra at day 0, 2, 4, and 8 for the control incubation (top) and the 0.2 g of spirulina organic matter addition (bottom). Colors blue to red indicate lower to higher fluorescence intensities. Named regions and areas used for calculating indicators are labeled in figures on the left. See Table S1 for description of named regions. 125

Figure 3-5. Conceptual model for the production on methyl mercury (MeHg) with the addition of spirulina organic matter with key aspects studied including water quality, dissolved organic matter (DOM) optical properties, and the mechanisms behind the mercury cycle. Top figure presents relative water concentration trends: % MeHg of the total mercury in soil-water system as an indicator of net MeHg production; and manganese, iron, and sulfate as indicators of oxidation-reduction potential status. Bottom figure represents select DOM optical properties including region B as an indicator of a microbial activity byproduct; fluorescence index (FI) and fluorescence region F as indicators of labile carbon (substrate) type, microbial source DOM and quinoid-like DOM, respectively; and $Sag_{275\text{-}295}$ as an indicator of LMW DOM. The intensity of key mechanisms is shown in the middle and includes microbial activity in blue, and Hg methylation in pink, and MeHg demethylation in purple.

Stage I (day 0 to 4): Opening the Methylation Window. SpOM addition leads to high microbial activity with drop in F and FI and increase in B and increases inorganic mercury bioavailability of Hg-LMW DOM with a spike in $Sag_{275\text{-}295}$, opening the methylation window. Main substrate for microbial activity appeared to be quinoid-like DOM and microbial source DOM, region F and FI, respectively. Multiple microbial communities and syntropy interactions were enhanced, including multiple Hg-methylating organisms including iron-reducing (increase in iron) and sulfate-reducing (drop in sulfate) bacteria.

Stage II (day 4 to 8): Closing the Methylation Window. Transition to high MeHg demethylation rates with a decrease in net MeHg production. This is caused by reduced conditions favoring the activity of MeHg-demethylating microbes. Changes in the DOM properties might suggest the shift in microbial communities with a steeper slope in the substrate F and FI regions and ceased accumulation in fluorescence region B. IHg

bioavailability is possibly affected by sulfide build up and DOM, forming Hg-S and Hg-DOM complexes decreasing Hg methylators activity.

Stage III (day 8 to 16): Anoxic quasi-steady state. This period represents high MeHg demethylation rates at the beginning and the transition of the incubations system to a new quasi-steady state where the microbial activity is limited due to a depletion of substrate and sulfate. Iron and mercury are probably complexing/precipitating with sulfide and DOM and returning to the soil phase..... 127

Tables

Table 1-1. Thermodynamic sequence for reduction of inorganic substances by hydrogen at pH 7.0 and 25°C 36
Table 1-2. Average bottom water quality at station A and B for pre-oxygenation years 2017-2019 and post-oxygenation years 2020-2021 38
Table 1-3. Surface water quality during summer months, May to September, for pre-oxygenation years 964 2017-2019 and post-oxygenation year 2021..... 38
Table 1-4. Internal nutrient loading average values for pre-oxygenation years 2017-2019..... 39
Table 2-1. Cache Creek Settling Basin Soil Characterization 79
Table 2-2. Comparison of mercury in water and soil during initial conditions 80
Table 2-3. Standard test significant determinants for mercury parameters estimated using ANOVA 81
Table 2-4. Stress Test compared to Standard Test significant determinants for mercury parameters estimated using ANOVA 82
Table 2-5. Standard Test significant determinants for aqueous parameters estimated using ANOVA 83
Table 2-6. Stress Test compared to Standard Test significant determinants for aqueous parameters estimated using ANOVA..... 85
Table 3-1 Summary of Cache Creek Settling Basin Soil Characteristics in a dry weight basis 121

Acknowledgements

Beautiful, Toxic, yet Indispensable. Almost ten years ago, I was at UNAM in my geochemistry class with Dr. Laura Mori presenting about mine wastes and mercury contamination in the water… who would have thought I would end up doing a whole Ph.D. studying the organic form of mercury, methyl mercury. Some people would say I am "mad as a hatter".

As my doctoral journey comes to an end, I would like to express my gratitude to all those who have supported and contributed to my success. Firstly, I want to acknowledge my mentors, in particular, my advisor Marc. I am incredibly thankful for his guidance and support. I enjoyed being part of his lab, working on multiple projects together, and discussing ideas over a cup of coffee. I also want to extend my thanks to my committee members, Tom, Peggy, Anne, and Jacob, for helping me find my path, providing valuable feedback, and dedicating their time to my research. I am also grateful for the mentorship I received from Mark Marvin DiPasquale and Charles Alpers at USGS, during the CCSB meetings discussing mercury cycling, and for all the support I found in you. As well as Stephen McCord, thank you for your advice and support towards the end of my Ph.D. journey. Special thanks to Sarah and Jeff from the City of San Diego for their collaboration on Hodges paper, despite the challenges posed by COVID. Secondly, I am thankful to all the people at UC Merced who have supported me in various ways. I am especially grateful to Liying Zhao and the Environmental Analytical Lab, as well as my lab mates and friends Shelby, Byran, Edwin, Mark, and the undergrad students Charlotte, Noelia, and Emily. Those long days working in the lab would not have been the same without your help and support. Thirdly, to my friends who have shared laughter, movies, trips, and late-nights conversations. I am incredibly appreciative of your friendship. Fourthly, my partner, Mirko, for your love and support. Last but not least, my family, to whom I owe so much. A big thanks to my parents, Mimis and Gus, for all the love and support and for making me believe I can do everything I set my mind to. Osqui, thank you for always being there for me, for the nights practicing for my presentations, and for the style and design tips. Nenan, thinking about studying geological engineering and even pursuing a Ph.D. is in part thanks to you and all the moments we spent talking about science. Mi hermana, thank you for all the support in making my dreams come true. My uncle Efra and my cousin Efraincito, I am grateful for having you both in my life with your advice and a laugh. My grandma, Mama Martha, I know that wherever you are you would be proud of me. I only wish we could share this moment. This work is dedicated to you.

Finally, I would like to express my gratitude to University of California Alianza Mx and CONACyTH for the three-years of support towards my Ph.D [2020-000017-02EXTF-00298], to the United States Geological Service in combination with the Department of Water Resources for supporting my second chapter, the Cache Creek Settling Basin study, and to the Environmental System Graduate Group for the summer fellowship and professional development supports.

… I would end up saying, thank you. I could not have done it without all of you!

NAIVY DENNISE RODAL-MORALES

Ph.D. Candidate, University of California Merced
Environmental Engineer, Stillwater Sciences

nrodalmorales@ucmerced.edu 209-769-5887
linkedin.com/naivy-dennise-rodal-morales-ab51834b Merced, CA

EDUCATION

Present: Ph.D. Candidate in Environmental Systems, Environmental Engineering concentration, UC Merced. Advisor: Dr. Marc Beutel. Defense Date: July 2024

- Hodges Reservoir, San Diego: Performed multi-year evaluation of nutrient, metals, and mercury cycling in water column before and after reservoir oxygenation in collaboration with the City of San Diego.
- Cache Creek Settling Basin, CA: Assessed potential for coagulant-treated wetland soils to liberate/produce methylmercury after rewetting in collaboration with the USGS (in preparation).
- Cache Creek Settling Basin, CA: Evaluated effects of organic matter addition on methylmercury cycling in a wetland sediment-water environment (in preparation).

Graduate Student Researcher, UC Merced

M.S. Environmental Systems, UC Merced

- Wetland Newman, CA: Modeled nitrate and phosphate removal using the P-k-C* model in constructed treatment wetlands treating agricultural runoff for the City of Newman.

Fall semester 2018 abroad focusing on Environmental Engineering at UC Merced

B.S. equivalent, Geological Engineering. Graduated with Honors at National Autonomous University of Mexico (UNAM), School of Engineering

- **Thesis topic:** Petrographic and Geochemical characterization of igneous rocks in Teziutlan-Cuetzalan, Puebla, Mexico

JOURNAL PAPERS

- Rodal-Morales, Naivy D, Beutel, Marc, Fuhrmann, Byran, Defeo, Shelby, Hansen, Anne, Harmon, Thomas, Brower, Sarah, Pasek, Jeffery. (2024). Hydrology and Oxygen Addition Drive Nutrients, Metals, and Methylmercury Cycling in a Hypereutrophic Water Supply Reservoir. Frontiers in Water, Environmental Water Quality.

TECHNICAL REPORTS

- Beutel, Marc, Rodal-Morales, Naivy D, and O´Day, Peggy. 2021. Cache Creek Settling Basin Sediment-Water Incubation Methylation Study Report. Prepared for the United States Geological Survey.
- Rodal-Morales, Naivy D, Beutel, Marc. 2020a. Newman Constructed Treatment Wetland Pollutant Removal Modeling Report. Prepared for City of Newman, CA.
- Rodal-Morales, Naivy D, Beutel, Marc. 2020b. Newman Constructed Treatment Wetland Water Quality Report. Prepared for City of Newman, CA.
- Rodal-Morales, Naivy D, Beutel, Marc, Zuber, C. and Kandhway, A. 2020. Newman Constructed Treatment Wetland Water Budget Report. Prepared for City of Newman, CA.
- Rodal-Morales, Naivy D. 2019. Petrographic and Geochemical characterization of igneous rocks in Teziutlan-Cuetzalan, Puebla, Mexico.

PRESENTATIONS (2022-2023)

- Rodal-Morales Naivy D. 2023. Mercury Cycle in Two Aquatic Ecosystems in California. Summer Research Talk. Secure Water Future, UC Merced.
- Rodal-Morales Naivy D. 2023. Effects of Organic Matter on the Mercury Cycle. American Ecological Engineering Society, Tampa, FL.
- Rodal-Morales Naivy D. 2023. Effects of Organic Matter on the Mercury Cycle. Sierra Nevada Research Institute, Research Symposium. Awarded top 3 talks.
- Rodal-Morales Naivy D. 2022. Evaluation of Mercury Accumulation in Hodges Reservoir After the Implementation of Hypolimnetic Oxygenation. California Lake Management Society (CALMS), Oakland, CA.
- Rodal-Morales Naivy D., Beutel M., O'Day, P., (UC Merced), Fleck, J., Marvin-DiPasquale M., and Alpers C. 2022. Incubation Experiments on Cache Creek Settling Basin Sediments from Coagulant-Treated Mesocosms. International Conference of Mercury as a Global Pollutant (virtual).
- Rodal-Morales Naivy D., Fuhrmann, B., Defeo S., Beutel M. 2022. Water Quality Benefits of Reestablishing Oxic Conditions in the Bottom of a Hypereutrophic Drinking Water Reservoir. American Ecological Engineering Society, Baltimore,
- Rodal-Morales Naivy D., Beutel M., O'Day, P., (UC Merced), Fleck, J., Marvin-DiPasquale M., and Alpers C. 2022. Incubation Experiments on Cache Creek Settling Basin Sediments from Coagulant-Treated Mesocosms. Delta Tributary Mercury Council (virtual).

UNIVERSITY OF CALIFORNIA MERCED

THE COMPLEXITY OF MERCURY CYCLING: STUDYING THE METHYLATION WINDOW AND ASSESSING TWO REMEDIATION TECHNIQUES IN TWO AQUATIC ENVIRONMENTS

Naivy Dennise Rodal-Morales

PhD in Environmental Systems
Advisor: Dr. Marc Beutel
Committee Chair: Dr. Thomas Harmon

ABSTRACT

The historic gold rush era and atmospheric deposition in California have led to mercury (Hg) contamination in surface waters. The organic form of Hg, methylmercury (MeHg), bioaccumulates in the food chain and poses a negative health effect for wildlife and humans consuming contaminated fish, seafood, and rice. Controlling MeHg production is challenging due to its dependency on multiple site-specific and interrelated environmental conditions. In this dissertation, I examined the factors contributing to MeHg production, the methylation window, in two aquatic environments: Hodges Reservoir (a lake-like environment), and Cache Creek Settling Basin, CCSB (a wetland-like environment). Additionally, I explored two mercury remediation techniques, a hypolimnetic oxygenation system (HOS) and coagulation with metal-based salts. In Hodges Reservoir, a hypereutrophic sulfate-rich water supply reservoir located in San Diego, CA, field monitoring revealed that before oxygenation, winter precipitation and changes in hypolimnion volume mechanistically affected the biogeochemistry processes of the reservoir, especially the Hg cycle (Chapter 1). During wet years, a spring methylation window opened as precipitation provided additional mass of oxygen due to a larger hypolimnion. This maintained mildly reduced conditions that enhanced Hg methylation in bottom waters. But during dry years, the methylation window closed earlier in the season because of the

development of highly reduced conditions favoring demethylation relative to methylation, and due to the buildup of sulfide concentration decreasing inorganic Hg bioavailability. Following HOS implementation, oxygenation appeared to suppress anaerobic bacteria activity responsible for MeHg production, indicating the potential usefulness of techniques designed to keep bottom lake water oxidized for repressing MeHg production. In CCSB, located in the Sacramento Valley, CA, the United States Geological Survey (USGS) studied the use of the coagulants ChitoVan™ (organic/shell amino-based), Ferralyte® (ferric-sulfate-based), and Ultrion® (polyaluminum chloride-based) to immobilize Hg from Cache Creek into the sediment. Bench-scale sediment-water slurry incubations with CCSB soils from USGS field experiments demonstrated that organic matter is the main driver for MeHg production (Chapter 2). The three different coagulant-treated soils were not a source of MeHg under rewetted conditions (standard test). However, under elevated organic matter loading (stress test), inorganic Hg could be potentially released. In a follow-up experiment using CCSB non-treated soils and water under a gradient of algal organic matter (Spirulina powder), the addition of more than 0.1 g of algal organic matter to 250 ml sediment-water slurries appeared to activate a diverse microbial community that led to an ephemeral window of MeHg production (Chapter 3). Analysis of dissolved organic matter (DOM) optical properties using fluorescence spectroscopy indicated that some regions of the DOM (F, B, and FI index) could correlate to the window of MeHg production. This suggests that monitoring DOM optical characteristics in the field could hold promise in better understanding MeHg production and bioaccumulation in aquatic ecosystems. Overall, the outcomes of these studies indicate that oxygenation and controlling organic matter loading are viable management strategies to mitigate Hg contamination in managed aquatic ecosystems. Note, Appendix includes supplementary material and raw data for Chapters 2 and 3.

Summer 2024

INTRODUCTION

Freshwater environments provide important ecosystem services for both wildlife and humans. Unfortunately, these environments are under severe threat with ongoing declines in biodiversity, health, and sustainability (Bogardi et al., 2020). One of the main causes of this decline is the degradation of water quality, driven by demographic growth, economic and agricultural development, urbanization, industrialization, land use changes, and climate change. These factors contribute to the release of harmful chemical substances to the environment from untreated domestic, industrial, and agricultural wastewaters and atmospheric emission (Holt, 2000; Tipping et al., 2014; Velthof et al., 2014). Consequently, water pollution triggers eutrophication, harmful algal blooms, sedimentation, and heavy metals contamination, all of which have adverse impacts on human and ecosystem health. Therefore, it is essential to study and restore water quality to ensure ecological integrity, biodiversity, and human prosperity.

In the United States, 21% of lakes are affected by eutrophication due to extensive phosphorus and nitrogen loading, while 32% of wetlands suffer from degradation due to soil compaction and vegetation removal (Giri, 2021). In California, surface water quality is impacted by eutrophication due to agricultural fertilizers and urban development (Handler et al., 2006). Runoff after large-scale wildfires is also a growing concern (Paul et al., 2022). Climate change projections indicate that rising summer temperatures and increased winter precipitation will lead to higher external and internal nutrient loading in lakes, exacerbating issues of eutrophication and harmful algal blooms (Mosley, 2015). Additionally, the historical legacy of arsenic and mercury (Hg) pollution from the gold rush era continues to impact surface waters in California. For example, in the Cache Creek Watershed, which originates in Clear Lake and flows through the Sacramento Valley, 40 abandoned mines are found in the drainage (Sacramento River Watershed Program, 2024). As a result, half of the Hg entering the Sacramento River system flows from this watershed.

Mercury as a global pollutant gained the world's attention after the methyl-Hg (MeHg) poisoning incidents in Minamata, Japan, and in Iraq in the 1960s and 1970s (Kessler, 2013). As a result, the 2013 UNEP Minamata Convention on Hg was established. The aims of the Convention are to reduce Hg release into the environment and to monitor the success of global efforts (Selin et al., 2018). Hg is a metal which can exist in the environment in three different states: as a gas (Hg(0)), as aqueous forms (inorganic-Hg (IHg), organic MeHg), and as a solid in minerals like cinnabar (HgS). The global extent and impact of Hg pollution is due to the long-lived gaseous Hg(0) form dispersing in the atmosphere, and the microbial methylation of IHg to toxic MeHg (Fig. A) (Sonke et al., 2023). MeHg, the organic form of mercury, diffuses into the cells of organisms and binds into

proteins, bioaccumulating and biomagnifying in the food chain (Fig. A) (USEPA, 1997). Negative health effects of MeHg from fish, seafood, and rice exposure include neurodevelopment dysfunction and cardiovascular disease (Roman et al. 2011). In the United States, 90% of Hg intake in the population comes from the consumption of shellfish and fish (Selin et al., 2008).

In the environment, Hg is mostly produced by anthropogenic emissions, exceeding natural emissions by sevenfold (Sonke et al., 2023). Anthropogenic sources include iron and steel industries, cement industries, gold industries, non-ferrous metal smelting, chloro-alkali industries, and direct Hg production industries (Eckley et al., 2021). Once Hg(0) is emitted to the atmosphere, the mercury cycle starts (Fig. A). Hg gas can be oxidized to ionic forms of Hg in the atmosphere that, through wet and dry deposition, are transported to freshwater ecosystems in rainfall and runoff. In the anoxic water column and sediments of wetlands, rivers, lakes, and reservoirs, the conversion of IHg to MeHg is the primary process of concern (Hsu-Kim et al., 2013; Ullrich et al., 2001). MeHg production is associated with a great variety of microorganisms across the full environmental oxidation-reduction (redox) potential spectrum (Regnell and Watras, 2019; Sonke et al., 2023). MeHg then bioaccumulates into lower trophic levels and biomagnifies up the food chain. The net MeHg production that we see in the environment is the result of Hg methylation and MeHg demethylation processes. MeHg demethylation also occurs in anoxic environments by anaerobic bacteria as the result of co-metabolic process which produce IHg and carbon dioxide and/or methane (Du et al., 2019; Marvin-DiPasquale et al., 2000). Additionally, under oxic conditions, aerobic microorganisms can transform MeHg into Hg(0) in a response to an environment detoxification process (Barkay and Gu, 2022).

In the end, MeHg production and accumulation in aquatic environments depends on several site-specific and interrelated conditions. This complexity of Hg cycling presents a great variety of possible treatments (Eckley et al., 2020; Pavithra et al., 2023; Wang et al., 2020). Some Hg remediation strategies are based on *in situ* removal and immobilization processes into the sediment, involving mechanisms such as adsorption/desorption, coagulation, and oxidation-reduction. The major aim of these technologies is to separate Hg from the contaminated area and/or avoid the transformation of IHg to the toxic MeHg (Wang et al., 2020). This dissertation analyzes two different freshwater aquatic environments, a reservoir (Hodges Reservoir) and a wetland-type settling basin (Cache Creek Settling Basin, CCSB). In addition to studying the main factors that contributed to MeHg production in each aquatic ecosystem, two mercury remediation techniques, hypolimnetic oxygenation system (HOS) (Beutel and Horne, 1999) and coagulation with metal-based salts (Henneberry et al., 2015), are presented.

Chapter 1 is a five-year field study to evaluate the changes in the Hg cycle and water quality before and after the implementation of a HOS in Hodges Reservoir, San Diego, CA. The study has been published in a special edition of Frontiers in Water titled Water Quality in Reservoirs and its Current Challenges (Rodal-Morales et al., 2024). Using a monthly collected dataset, I estimated hypolimnetic accumulation rates of aqueous pollutants (ammonia, phosphate, iron, manganese, and methylmercury) to quantify changes in the water parameters, including Hg, produced in the profundal zone during summer thermal stratification. In addition, I developed an internal nutrient loading assessment to quantify the effects of sediment-water interface processes on eutrophication and as an estimation of possible available MeHg for bioaccumulation. Results highlighted large-scale factors such as inflow from winter precipitation and oxygen content in lake water are key controllers of biogeochemical processes of the lake, especially the Hg cycle. Years with high precipitation and a larger volume of reservoir opened a methylation window allowing for MeHg production under mildly reduced conditions. On the other hand, dry years with low reservoir volume closed the methylation window earlier in the season because of the development of highly reduced conditions. These conditions favored demethylation relative to methylation and promoted the buildup of sulfide concentration which decreased inorganic Hg bioavailability. After HOS implementation, oxygenation appeared to inhibit anaerobic bacteria activity and the production of MeHg. These results highlight that remediation techniques designed to keep bottom water of reservoirs oxidized can suppress the activity of anaerobic bacteria responsible for MeHg production and its consequently bioaccumulation into species, thereby protecting human and wildlife health.

Chapter 2 involves a series of deoxygenated soil-water slurry laboratory incubations to evaluate the potential for three different coagulant-treated soils, ChitoVan™ (organic/shell amino-based), Ferralyte® (ferric-sulfate-based), and Ultrion® (polyaluminum chloride), used for Hg control in the CCSB, Sacramento Valley, CA, to release Hg under rewetted conditions. The experiments, conducted over 16 days, indicate that rewetted coagulant-treated soils are not a source of MeHg (standard test), but under elevated OM loading (stress test), IHg could be potentially released. The stress test, with the addition of algal organic matter (AOM), resulted in a short-lived methylation window in coagulate-treated and control (no coagulant addition) soils. This suggests that OM is the main driver for MeHg production in CCSB. Therefore, the increase in frequency and intensity of algal blooms, and their consequent loading and degradation in this wetland-like environment, could have significant impacts on the ecosystem by promoting MeHg production and bioaccumulation.

Chapter 3 is built on the findings of Chapter 2, using soil-water slurry incubations from CCSB loaded with a gradient in AOM. Results highlight that levels above 0.1 g of AOM per ~250 ml of soil-water slurry incubations appeared to activate a diverse microbial community that led to an ephemeral production of

MeHg, with higher AOM loading leading to higher peak levels of MeHg in soil and water. Back-of-the-envelope estimates suggest that this level of AOM loading is associated with that experienced in eutrophic to hypereutrophic lakes and wetlands. This study also included, in collaboration with the USGS, an assessment of the optical properties of dissolved organic matter (DOM) via adsorption spectra and fluorescence spectroscopy. AOM addition led to an enrichment in quinoid-like moieties, associated with the fluorescence region "F", microbial source DOM, associated with the fluorescence index (FI), and in low molecular weight DOM, as indicated by elevated $Sag_{275\text{-}295}$ values. This suggests that AOM addition provided labile carbon that promoted the activity of syntrophic microbes, including Hg methylators, and enhanced IHg bioavailability. Results showed that the methylation window tended to correlate with some fractions of the DOM corresponding with optical signals in region F, region B and FI. These findings suggest that assessing the optical characteristics of DOM could hold promise in monitoring and ultimately predicting when the window for MeHg production and bioaccumulation opens in aquatic environments.

References

Barkay, T., and Gu, B. (2022). Demethylation─The Other Side of the Mercury Methylation Coin: A Critical Review. ACS Environmental Au, 2(2), 77–97. https://doi.org/10.1021/acsenvironau.1c00022

Bogardi, J.J., Leentvaar, J. and Sebesvári, Z. (2020). Biologia Futura: integrating freshwater ecosystem health in water resources management. Biologia Futura 71, 337–358 https://doi.org/10.1007/s42977-020-00031-7

Du, H., Ma, M., Igarashi, Y., and Wang, D. (2019). Biotic and Abiotic Degradation of Methylmercury in Aquatic Ecosystems: A Review. Bulletin of Environmental Contamination and Toxicology, 102(5), 605–611. https://doi.org/10.1007/s00128-018-2530-2

Eckley, C.S., Gilmour, C.C., Janssen, S., Luxton, T.P., Randall, P.M., Whalin, L., Austin, C. (2020). The assessment and remediation of mercury contaminated sites: A review of current approaches. Science of the Total Environment 707, 136031. https://doi.org/10.1016/j.scitotenv.2019.136031

Eckley, C. S., Luxton, T. P., Stanfield, B., Baldwin, A., Holloway, J., McKernan, J., and Johnson, M. G. (2021). Effect of organic matter concentration and characteristics on mercury mobilization and methylmercury production at an abandoned mine site. Environmental Pollution, 271, 116369. https://doi.org/10.1016/j.envpol.2020.116369

Gray, J.E. (2003). Geologic studies of mercury by the US Geological Survey (No. 1248). US Geological Survey.

Giri, S. (2021). Water quality prospective in Twenty First Century: Status of water quality in major river basins, contemporary strategies and impediments: A review. Environmental Pollution, 271, 116332.

Handler, N. B., Paytan, A., Higgins, C. P., Luthy, R. G., & Boehm, A. B. (2006). Human development is linked to multiple water body impairments along the California coast. Estuaries and Coasts, 29, 860-870.

Henneberry, Y., Kraus, T. E. C., Krabbenhoft, D. P., and Horwath, W. R. (2016). Investigating the Temporal Effects of Metal-Based Coagulants to Remove Mercury from Solution in the Presence of Dissolved Organic Matter. Environmental Management, 57(1), 220–228. https://doi.org/10.1007/s00267-015-0601-2

Holt, M. S. (2000). Sources of chemical contaminants and routes into the freshwater environment. Food and chemical toxicology, 38, S21-S27.

Hsu-Kim, H., Kucharzyk, K. H., Zhang, T., and Deshusses, M. A. (2013). Mechanisms Regulating Mercury Bioavailability for Methylating Microorganisms in the Aquatic Environment: A Critical Review. Environmental Science & Technology, 47(6), 2441–2456. https://doi.org/10.1021/es304370g

Kessler, R. (2013). The Minamata Convention on Mercury: a first step toward protecting future generations.

Marvin-DiPasquale, M., Agee, J., McGowan, C., Oremland, R. S., Thomas, M., Krabbenhoft, D., and Gilmour, C. C. (2000). Methyl-Mercury Degradation Pathways: A Comparison among Three Mercury-Impacted Ecosystems. Environmental Science & Technology, 34(23), 4908–4916. https://doi.org/10.1021/es0013125

McAlpine, D. O. U. G. L. A. S., and Araki, S. (1959). Minamata disease: late effects of an unusual neurological disorder caused by contaminated fish. AMA Archives of Neurology, 1(5), 522-530.

Mosley, L.M. (2015). Drought impacts on the water quality of freshwater systems; review and integration. Earth-Science Reviews 140, 203–214. https://doi.org/10.1016/j.earscirev.2014.11.010

Nichols, J. W. (1997). Mercury study report to Congress. Volume 6. An ecological assessment for anthropogenic mercury emissions in the United States (No. PB-98-124787/XAB; EPA-452/R-97/008). Environmental Protection Agency, Research Triangle Park, NC (United States). Office of Air Quality Planning and Standards

Paul, M. J., LeDuc, S. D., Lassiter, M. G., Moorhead, L. C., Noyes, P. D., and Leibowitz, S. G. (2022). Wildfire induces changes in receiving waters: A review with considerations for water quality management. Water Resources Research, 58(9), e2021WR030699.

Pavithra, K. G., SundarRajan, P., Kumar, P. S., & Rangasamy, G. (2023). Mercury sources, contaminations, mercury cycle, detection and treatment techniques: A review. Chemosphere, 312, 137314.

Regnell, O., and Watras, Carl. J. (2019). Microbial Mercury Methylation in Aquatic Environments: A Critical Review of Published Field and Laboratory Studies. Environmental Science & Technology, 53(1), 4–19. https://doi.org/10.1021/acs.est.8b02709

Rodal-Morales, N. D., Beutel, M., Fuhrmann, B., Defeo, S., Hansen, A. M., Harmon, T., ... & Pasek, J. (2024). Hydrology and oxygen addition drive nutrients, metals, and methylmercury cycling in a hypereutrophic water supply reservoir. Frontiers in Water, 6, 1356994.

Roman, H. A., Walsh, T. L., Coull, B. A., Dewailly, É., Guallar, E., Hattis, D., ... & Rice, G. (2011). Evaluation of the cardiovascular effects of methylmercury exposures: current evidence supports development of a dose–response function for regulatory benefits analysis. Environmental Health Perspectives, 119(5), 607-614.

Sacramento River Watershed Program. (2024). Cache Creek Watershed . June 2024. https://sacriver.org/explore-watersheds/westside-subregion/cache-creek-watershed/

Selin, N. E., Sunderland, E. M., Knightes, C. D., & Mason, R. P. (2010). Sources of mercury exposure for US seafood consumers: implications for policy. Environmental Health Perspectives, 118(1), 137-143.

Sonke, J. E., Angot, H., Zhang, Y., Poulain, A., Björn, E., and Schartup, A. (2023). Global change effects on biogeochemical mercury cycling. Ambio, 52(5), 853–876. https://doi.org/10.1007/s13280-023-01855-y

Tipping, E., Benham, S., Boyle, J. F., Crow, P., Davies, J., Fischer, U., ... & Toberman, H. (2014). Atmospheric deposition of phosphorus to land and freshwater. Environmental Science: Processes & Impacts, 16(7), 1608-1617.

Ullrich, S. M., Tanton, T. W., and Abdrashitova, S. A. (2001). Mercury in the Aquatic Environment: A Review of Factors Affecting Methylation. Critical Reviews in Environmental Science and Technology, 31(3), 241–293. https://doi.org/10.1080/20016491089226

Velthof, G. L., Lesschen, J. P., Webb, J., Pietrzak, S., Miatkowski, Z., Pinto, M., ... & Oenema, O. (2014). The impact of the Nitrates Directive on nitrogen emissions from agriculture in the EU-27 during 2000–2008. Science of the Total Environment, 468, 1225-1233.

Wang, L., Hou, D., Cao, Y., Ok, Y. S., Tack, F. M., Rinklebe, J., & O'Connor, D. (2020). Remediation of mercury contaminated soil, water, and air: A review of emerging materials and innovative technologies. Environment International, 134, 105281.

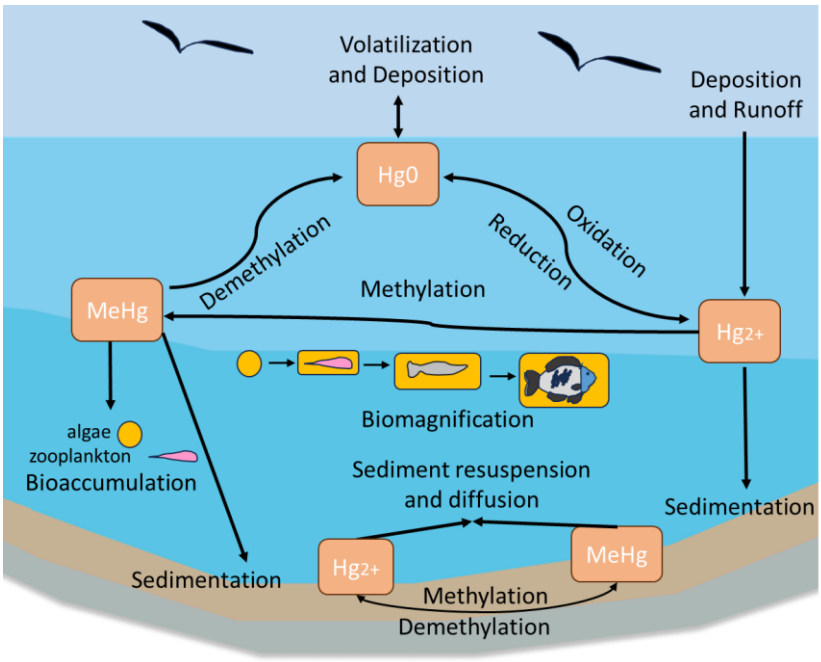

Fig A. The mercury cycle in aquatic environments showing main mercury species (mercury gas, Hg(0), divalent mercury, Hg^{2+} and methyl mercury, MeHg), and processes (deposition and runoff, oxidation-reduction, sedimentation, methylation, bioaccumulation-biomagnification, sediment resuspension, demethylation, volatilization, and deposition). Based on figure developed by Gray (2003).

1. Hydrology and Oxygen Addition Drive Nutrients, Metals, and Methylmercury Cycling in a Hypereutrophic Water Supply Reservoir

1.1 Abstract

Impaired water quality in mediterranean climate reservoirs is mainly associated with eutrophication and internal nutrient loading. To improve water quality in hypereutrophic Hodges Reservoir, California, USA, a hypolimnetic oxygenation system (HOS), using pure oxygen gas, was implemented in 2020. This study encompasses three years of pre-oxygenation data (2017-2019) and two years of post-oxygenation data (2020-2021) to understand the cycling of nutrients, metals, and mercury in the reservoir. During the wet year of 2017, mildly reduced conditions lasted until mid-summer in the enlarged reservoir. Nutrients and metals were seen in the hypolimnion including ammonia (~2 mg-N/L), manganese (~0.5 mg/L), phosphate (~0.5 mg-P/L), and sulfide (~10 mg/L). Production of methylmercury (MeHg), an important bioaccumulative toxin, was favored from April to June with a hypolimnetic accumulation rate of around 200 ng/m^2·d. In contrast, the dry year of 2018 exhibited higher hypolimnetic concentrations of ammonia (~4 mg-N/L), manganese (~1 mg/L), phosphate (>0.5 mg-P/L), and sulfide (>15 mg/L). The rapid onset of highly reduced conditions in 2018 corresponded with low MeHg hypolimnetic accumulation (~50 ng/m^2·d). It seems that mildly reduced conditions were associated with higher MeHg accumulation, while sulfidic, reduced conditions impaired inorganic mercury bioavailability for MeHg production and/or promoted microbial demethylation. Sulfide also appeared to act as a sink for iron via FeS precipitation, and potentially for manganese via MnS precipitation or manganese coprecipitation with FeS. Mass flux estimates for 2017-2019 indicate that much of the nutrients that accumulated in the hypolimnion moved via turbulent diffusion into the epilimnion at loading rates far exceeding thresholds predicting eutrophic conditions. After oxygenation in 2020-2021, the reservoir water column was highly oxidized but showed a lack of thermal stratification, suggesting reservoir operations in combination with HOS implementation inadvertently mixed the water column in this relatively shallow reservoir. Post-oxygenation, concentrations of ammonia, phosphate, manganese, and mercury in bottom waters all decreased, likely in response to oxidized conditions. Oxygenated bottom waters exhibited elevated nitrate, a byproduct of ammonia nitrification, and iron, a byproduct of FeS oxidation, indicating a lake-wide response to oxygenation.

1.2 Introduction

Water quality management in water supply reservoirs is a significant topic for water security as climate factors and growing populations continue to exacerbate pressure on water availability (USEPA, 2023). Eutrophication, and the subsequent algae decay that results in deoxygenation of deeper zones, is the main concern for productive lakes, especially during periods of stratification. Under

these anaerobic conditions, associated with low oxidation-reduction (redox) potential, sediments tend to liberate ammonia, manganese, phosphate, iron, and in extreme cases, sulfides, degrading raw water quality (Beutel, 2006). In addition, internal nutrient loading, in which nutrients accumulate in bottom waters and diffuse or mix into the photic zone, can reinforce eutrophication. Simultaneously, the accumulation of iron may trigger harmful algal blooms (Leung et al., 2021; Molot et al., 2021), while manganese and iron can complicate drinking water treatment (Krueger et al., 2020). Anaerobic conditions also promote the activity of anaerobic bacteria such as sulfate- and iron-reducing bacteria (SRB, FeRB) that produce toxic methylmercury (MeHg) (Watras, 2009). This organic form of mercury (Hg) readily bioaccumulates in fish resulting in a health threat to wildlife and humans (Mergler et al., 2007).

Another important factor to consider when studying nutrients and metals cycling in reservoirs is the contribution of precipitation and correlated inflow modifying the water surface elevation of reservoirs, particularly now that extreme hydrological events are increasing in frequency due to climate change. The consequences of these changes are variable and dependent on lake depth, surface area, mixing regime, and trophic status. In California, climate change predictions indicate a higher likelihood of droughts (Goss et al., 2020), but also an increase in the strength of atmospheric rivers and associated precipitation events (Mosley, 2015; Payne et al., 2020). Consequently, extreme droughts can increase the relative importance of internal nutrient loading as external loading diminishes, and lower water levels increase the mixing of nutrient-rich bottom waters into the photic zone (Mosley, 2015). Conversely, high precipitation and runoff from atmospheric rivers translate into elevated external nutrient and sediment loading. Changes in water surface elevation are also closely related to Hg cycling in reservoirs because more frequent wetting and drying of littoral sediment correlates with MeHg levels in biota (Seelos et al., 2021; Bigham et al., 2017). Thus, to improve surface water treatability, while having the recreational and environmental benefits of a clean water reservoir, reservoir managers need to understand nutrients, metals, and Hg cycling, and the factors that play a role in their potential management.

The biogeochemical processes that occur during hypolimnetic deoxygenation mostly take place at the sediment-water interface (Fig. 1-1, Table 1-1). When algae die, sink, and are deposited onto profundal sediment, they are decomposed by bacteria consuming dissolved oxygen (DO). Ammonia is produced by the mineralization of organic matter (Forsberg, 1989) and accumulates when nitrification is inhibited under anoxic conditions (Rysgaard et al., 1994). Manganese is also released due to microbial dissolution of manganese-oxides (Davison, 1993; Munger, 2016). Phosphate and iron are released from the sediment to overlaying water by reductive dissolution of iron-oxides and release of associated phosphate (Golterman, 2001; Søndergaard et al., 2003). Finally, sulfide is produced by anaerobic microorganisms such as SRB. These anaerobic bacteria also produce toxic MeHg (Gilmour et al., 2013), which tends to build up in anoxic

bottom waters of lakes and reservoirs (Beutel et al., 2020; Poulin et al., 2023; Regnell and Watras, 2019). In addition, inorganic Hg(II) and MeHg can accumulate in bottom waters when metal oxides are dissolved and release sorbed Hg (Chadwick et al., 2006; Beutel et al., 2020).

One strategy to limit the accumulation of reduced compounds in bottom waters and suppress internal nutrient loading in reservoirs is the addition of pure oxygen gas to bottom waters using hypolimnetic oxygenation systems (HOS) (Beutel and Horne, 1999; Bierlein et al., 2017; Austin et al., 2019). These engineered systems are capable of adding large amounts of DO to the bottom of reservoirs (1-100 metric tons/d), while maintaining thermal stratification, with a relatively small infrastructure size, energy, and cost (Beutel and Horne, 1999). In 2020, the City of San Diego (CSD) installed a HOS in Hodges Reservoir, California, USA, to enhance the quality and treatability of reservoir water. With few management options to lower MeHg levels in fish, water managers are also interested in the potential for HOS to suppress the buildup of MeHg in bottom waters and lower subsequent bioaccumulation into the aquatic food web (Beutel et al., 2020; Eckley et al., 2020).

The study aimed to assess patterns of nutrients, metals, and Hg cycling, over the study period of the years 2017-2021, combining water quality monitoring by the University of California Merced (UCM) and CSD. Key objectives and working hypothesis of this multi-year study included: 1) to assess impacts of interannual variations in precipitation (e.g., wet versus dry years) and hypolimnion volume on nutrients, metals, and Hg cycling. During dry years, we hypothesized to see shallower and warmer reservoir that favor rapid deoxygenation of bottom waters and enhanced accumulation rates of nutrients and metals in the hypolimnion; 2) to evaluate, the impacts of HOS operation on conventional water quality parameters including nitrogen, phosphorus, iron, and manganese, and on the cycling of Hg in the water column. As these compounds are redox-sensitive, their accumulation in the hypolimnion was expected to decrease with the oxidized conditions after HOS implementation; and 3) to determine accumulation rates of nutrients and metals in bottom waters and their subsequent transfer via turbulent diffusion from the hypolimnion to the epilimnion (i.e., internal nutrient loading). The objective was to quantify the changes in internal nutrient loading after oxygenation. We hypothesized that the internal loading would decrease post-oxygenation, which would translate into water quality improvement.

1.3 Methods

1.3.1 Study Site

Hodges Reservoir, located in Northern San Diego County, California, USA is a water supply reservoir for the Santa Fe Irrigation District (SFID) and the San Dieguito Water District, which serve around 15,000 people in the region of Rancho Santa Fe and Solana Beach. The reservoir also serves as a backup water

source for CSD and San Diego County Authority. In addition, Hodges Reservoir is part of a pumped storage system in which water is pumped up to nearby Olivenhain Reservoir and released back to Hodges Reservoir to supply power during peak electrical demands. Hydropower production is predicated on maintaining a reservoir surface elevation of around 89 m above mean sea level (amsl). At this elevation, the reservoir has a maximum depth of 19.2 m, a mean depth of 6.4 m, and a surface area of 2.3 km^2.

Summertime water temperatures are typically around 25°C in surface waters and 16°C in bottom waters. The region has a precipitation season from October to March and hot, dry summers typical of a mediterranean climate. Precipitation in the watershed feeds inflows that increase the surface water elevation by 2-6 m annually in wet years. The trophic state of Hodges Reservoir is categorized as hypereutrophic with sulfate-rich waters. The reservoir's main inflow is the San Dieguito River which yields relatively high external nutrient loading from a large watershed (641 km^2). But during dry summer and fall periods, eutrophication is likely driven by internal nutrient loading. Based on past water quality monitoring, Hodges Reservoir exhibits poor water quality, including low water transparency (Secchi depth < 1 m) and elevated total chlorophyll (chl) levels in surface waters (> 60 µg/L) (Beutel et al., 2020). Warmer temperatures in the reservoir, predicted by climate change models, will result in longer and stronger thermal stratification, which will exacerbate internal nutrient loading and eutrophication (Lee and Biggs 2015). For Hg, the predominant source is atmospheric deposition resulting in low total Hg (THg) levels in sediments typical of California background levels (< 0.05 µg/g dry weight). Nonetheless, Hodges Reservoir is listed on the Clean Water Act Section 303(d) List for elevated levels of Hg in fish (Beutel et al., 2020).

As is typical for hypereutrophic reservoirs, Hodges Reservoir has an anoxic hypolimnion during the warmer months (May-October) and is well mixed during winter (November-April) after the fall turnover. Under typical operating conditions (water surface elevation of 89 m amsl), the reservoir has a relatively low Osgood index (ratio of mean depth in m to square root of surface area in km^2) of around 4, suggesting it is not strongly thermally stratified during summer and fall (Cooke et al., 2013). In fact, the reservoir is known to exhibit polymictic characteristics during periods with maximum depths less than 15 m (Lee and Biggs, 2015). We also estimated the lake number (L_N), a dimensionless parameter indicative of mixing potential in lakes and reservoirs based on Robertson and Imberger (1994) using rLakeAnalyser function in RStudio. Under typical stratified summer conditions, the L_N was around 14 with average wind speed (~2.2 m/s) and around 3 with high wind speed (~4.5 m/s). During fall, L_N was around 0.9 with average wind speed (~6.2 m/s). L_N values indicate moderate stratification strength in summer and low stratification strength in the fall when the lake overturns each year. Hence nutrients presumably diffuse and/or mix into surface waters during summer stratification and fall turnover, supporting algal productivity.

To lower internal nutrient loading and improve raw water quality and treatability, in March of 2020 the CSD installed a “Speece Cone” HOS with a delivery capacity of 6 metric tons/d (Fig. 1-2A) (Horne and Beutel, 2019). This delivery rate was determined based on a detailed assessment of sediment oxygen demand and water column oxygen demand in the reservoir prior to HOS installation (Beutel, 2015). The HOS includes a 49.3 m^3 (13,000 gal) on-shore liquid oxygen storage tank and an evaporator unit to convert the liquid to gas, and a 6 m-tall, submerged cone with a 100-horsepower intake pump secured to the bottom of the reservoir at a depth of around 14.5 m. Oxygen gas is released at the top of the cone which acts as a counter-current contact chamber, resulting in around 95% oxygen transfer efficiency. A 30-m-long pipe diffuser connected to the bottom of the cone discharges oxygenated water with elevated DO (~70 mg/L) horizontally above the sediments into the hypolimnion all year long. The HOS was not installed in the deepest part of the reservoir due to infrastructure constraints including limited access to power.

1.3.2 Field Monitoring

Field monitoring was carried out from 2017-2021 as a collaborative effort between UCM and CSD. The study analyzes four years (2017-2019, 2021) of monthly water column data collected by UCM and five years (2017-2021) of approximately weekly to monthly water quality data collected by CSD (Table 1-2). Water samples were collected at two monitoring stations (Fig. 1-2B). Station A was located at the deepest zone of the reservoir (~19 m depth) near the dam, and station B (~12 m depth) was located about 2 km upstream close to the pump storage connection.

UCM samples were obtained with a 1.2-l Polytetrafluoropolymer Kemmerer sampler every 3 m in depth from the surface to the bottom of the reservoir, including an additional near-bottom water sample (~0.5 m from the bottom), from March/April to October/November. UCM monitored for ammonia, nitrate, phosphate measured as soluble reactive phosphorus (SRP), total phosphorus (TP), iron, manganese, sulfate, chloride, sulfide, dissolved organic carbon (DOC), MeHg, and THg. Hg sampling used the dirty-clean-hands method 1669 with Hg clean Teflon water sampler and 250 ml certified clean bottles (USEPA, 1996). Sulfide samples were preserved in the field with zinc acetate and sodium hydroxide. In the laboratory, nutrients (ammonia, nitrate, and phosphate), anions (sulfate and chloride), and DOC samples were preserved by filtering through prewashed 0.45 µm filters and kept inside a freezer. Water samples for unfiltered iron and manganese were preserved with nitric acid (1.0%) and refrigerated. THg and MeHg samples were preserved with hydrochloric acid (0.4%) and refrigerated. Field data also included Secchi depth and chl measurements in samples collected at 0, 3, 6, and 9 m depth. Chl samples were filtered onto GFC filters and placed inside the freezer for later extraction and analysis.

The CSD monitoring included weekly sampling for DO, pH, redox potential, and temperature at station B from 2017- 2021, and occasional monitoring at station A during the summer months, using a YSI-EX02 multiparameter water quality sonde (YSI Corporation, Yellow Springs, OH, USA). Geosmin, a taste and odor compound produced by phytoplankton that complicates water treatment, was measured weekly at station B, and sporadically at station A, from 2017- 2021. Hydrological data (e.g., rainfall, surface elevation, runoff, discharge) used to manage water elevation in Hodges Reservoir were collected monthly by CSD. Rainfall data were calculated based on an evaporation pan measurement that was scaled to the surface area of the reservoir. CSD also monitored monthly water quality in the surface, mid-depth coinciding with a key water outlet at an elevation of 83.8 m amsl (compared to typical water surface elevation of ~89 m amsl), and bottom waters for ammonia, nitrate, phosphate, iron, and manganese at station B, and sporadically at station A, from 2017-2021.

1.3.3 Analytical Methods

Water quality analyses on UCM samples were performed at the UCM Environmental Analytical Laboratory using standard methods (APHA, 2023). Dissolved nutrients (ammonia, nitrate, phosphate, TP) were analyzed on a LACHAT QuikChem 8500 autoanalyzer using standard colorimetric methods by air-segmented continuous-flow absorption spectrophotometry. TP samples were digested via acid persulfate digestion before colorimetric analysis for SRP. Reporting limits were 0.02 mg-N/L for ammonia, 0.05 mg-N/L for nitrate, and 0.02 mg-P/L for SRP and TP. Iron and manganese were determined by inductively coupled plasma optical emission spectrometry on an Optima 5300 DV ICP-OES with a reporting limit of 0.01 mg/L. Sulfate was measured using ion chromatography on an Agilent 7500cs mass spectrometer with a reporting limit of 0.5 mg/L. Sulfide was analyzed by iodometric titration with a reporting limit of 0.4 mg/L. Chl as total chlorophyll was analyzed using the standard 90% acetone extraction method. DOC was measured using the combustion catalytic oxidation method on a Shimadzu TOC-V analyzer. THg analysis was performed on a MERX-T (Brooks Rand Labs, Seattle, WA, USA) using cold vapor atomic fluorescence spectroscopy (CVAFS) based on method 1631 (USEPA, 2002). Samples for MeHg analysis were distilled (2 h at 125°C with nitrogen gas flow < 50 ml/min) before being measured on a MERX-M (Brooks Rand Labs, Seattle, WA, USA) using ethylation, gas chromatography, and CVAFS based on the method 1630 (USEPA, 2001). Hg analyses followed strict quality control standards including method blanks (<0.1 ng/L), matrix spikes (75-125% range), analytical duplicates, and ongoing procedure recovery (75-125% range). Reporting limits were 0.2 ng/L for THg and 0.02 ng/L for MeHg.

Water quality analyses on CSD samples were performed at the San Diego Water Quality Laboratory following standard methods (APHA, 2023). Phosphate was measured via ion chromatography with a reporting limit of 0.02 mg-P/L. Total ammonia was measured using the phenate colorimetric with a reporting limit of 0.03 mg-N/L. Nitrate was measured with the NED dihydrochloride colorimetric method with a reporting limit of 0.05 mg-N/l. Unfiltered iron and manganese were measured on an Agilent 7900 ICP-MS with a reporting limit of 0.01 mg/l for iron and 0.2 mg/l for manganese. Geosmin was measured via SM6040D using solid phase microextraction and gas chromatography/mass spectrometry with a reporting limit of 5 ng/L.

1.3.4 Data Analysis

To assess patterns of nutrients and metals accumulation in the hypolimnion of Hodges Reservoir, at each sampling station we calculated the rate of areal mass accumulation between sampling events, termed the monthly hypolimnetic accumulation rate (MHAR) (mg/m^2·d) following Equation 1:

$$\boldsymbol{MHAR = \frac{\Delta C_H * h_H}{\Delta t}} \qquad \textbf{(1)}$$

where ΔC_H (g/m^3) is the increase or decrease in hypolimnetic mean concentration between monthly sampling events, h_H (m) is the height of the hypolimnion, and Δt (d) is the time between monthly sampling events. The height of the hypolimnion was estimated from the thermocline to the bottom of the reservoir at the sampling station. The height of the hypolimnion was typically 13-14 m at station A and 8-9 m at station B.

The second part of the data analysis encompassed the application of a 1-D model using a mass transport equation based on the heat-accumulation method described by Chapra (1997). The lake is modeled as a mixed surface layer (epilimnion) overlaying a bottom layer (hypolimnion) separated by a thin transitional layer (metalimnion). Compounds released from anoxic sediment (e.g., ammonia, phosphate, MeHg) accumulate in the hypolimnion and then move across the metalimnion via turbulent diffusion. The flux J (g/m^2·d), termed here in the context of lake management as "internal nutrient loading," is estimated as:

$$\boldsymbol{J = -E_t \frac{dC}{dx}} \qquad \textbf{(2)}$$

where dC/dx (mg/L/L) is the concentration gradient across the metalimnion estimated as the concentration in the upper hypolimnion minus the concentration in the epilimnion, dx (m) is the metalimnion thickness (typically around 2 m), and E_t (cm^2/d) is the vertical diffusion coefficient. We estimated site-specific diffusion coefficients for Hodges Reservoir by first estimating the heat exchange coefficient (v_t, cm/d) based on the observed rate of warming of the hypolimnion as:

$$\boldsymbol{v_t = \frac{V_h}{A_t * t_s} ln\left(\frac{T_e - T_{hi}}{T_e - T_{hs}}\right)} \qquad \textbf{(3)}$$

where V_h (m^3) is the volume of the hypolimnion, A_t (m^2) is the area of the thermocline, T_e (^oC) is the average epilimnion temperature, T_{hi} (^oC) is the hypolimnion temperature at the beginning of summer (typically May-June), T_{hs} (^oC) is the hypolimnion temperature during strong summer stratification (typically May to September), and t_s (d) is the number of days during the strong stratification. The internal nutrient loading for a given month can then be estimated using Equation 2 because the vertical diffusion coefficient (E_t) is equivalent to the heat exchange coefficient (v_t) (Equation 3) multiplied by the thickness of the metalimnion (dx).

1.4 Results

1.4.1 Hydrology

The water balance in Hodges Reservoir is composed of inflows including runoff, direct precipitation, and imported water, and outflows including evaporation and withdrawal for potable water delivery and elevation management. Consequently, runoff driven by regional precipitation strongly affects the water budget. An assessment of annual precipitation near Hodges Reservoir shows an overall mean of around 350 mm (1940-1962 and 2010-2020, World Weather Online 2023; Western Regional Climate Center, 2023). Years experiencing abundant rainfall register precipitation levels above 500 mm, while drier years are associated with values below 100 mm per year. Precipitation was 584 mm in 2017, 130 mm in 2018, 430 mm in 2019, and 160 mm in 2021. Accordingly, in the context of this study, we categorized each of these years as wet, dry, average, and dry, respectively. Based on hydrologic data from CSD, the water balance in water year 2019 (October-September), an average precipitation year, includes runoff of 11.9 million m^3/y, evaporative losses of 3.3 million m^3/y, and withdrawal for potable water delivery and elevation management of 8.6 million m^3/y. Mean reservoir volume in 2019 water year was 18,102,026 m^3 and water residence time was around 1.5 y. In wet 2017 water year, runoff increased to 25.1 million m^3/y, and water residence time decreased to around 0.9 y. In dry 2018 water year, runoff was around 1.1 million m^3/y, and water residence time increased to around 16.4 y. Regional rainfall and associated runoff also affect the volume of the hypolimnion, which was shown in this study to be an important controller of nutrients and metals cycling in Hodges Reservoir. A bigger hypolimnion at the beginning of the wet year set a higher mass of oxygen to be gradually consumed by respiration processes during summer thermal stratification. The hypolimnion volume at the end of spring was around 10,087,000 m^3 in wet 2017, but only 4,293,000 m^3 in dry 2018.

During this multi-year study, precipitation and water surface elevation showed a wide range of variation. In 2016, rainfall was minimal at around 200 mm, and water surface elevation was steady at around 89 m amsl (Fig. 1-3). Winter of 2016 and spring of 2017 showed elevated precipitation of more than 450 mm. High precipitation corresponded with significant runoff into the reservoir and

an increase in elevation to 94 m amsl reflected by April. Then, the elevation decreased throughout the year, as no external runoff occurred, and water was transferred from the reservoir via withdrawals and raw water deliveries. The low precipitation and runoff in 2018 combined with continued water releases resulted in a steady drop in elevation from around 90 m amsl at the start of the year to around 89 m amsl by the end of the year. 2019 had high precipitation during February-March (250 mm) and runoff increased the elevation to 93 m amsl. Water elevation decreased to 89 m amsl by the end of the year via withdrawals and raw water deliveries. 2020 and 2021 had low precipitation and the elevation showed a quasi-steady state of around 89 m amsl.

1.4.2 Field Parameters

From 2017-2019, surface water temperature at stations A and B was around 14°C at the beginning of the year and warmed up to 25-30°C during the summer months (Figs. 1-4 and 1-5). The thermocline formed between 5-7 m depth (14-16 m above the bottom) at station A and between 3-5 m (7-9 m above the bottom) at station B (Fig. 1-4). After stratification, formed during summer, bottom water temperature warmed up from 14°C to 18°C (Figs. 1-4 and 1-5). In 2020-2021 after HOS implementation, at both stations A and B, there was only a very slight thermocline formation, and the entire water column was around 24-25 °C during summertime (Figs. 1-4 and 1-5). From 2017-2019, pH at stations A and B decreased with depth during the summer months with surface water values between 8-9.5 and bottom water values between 7-8 (Fig. 1-4). pH values were lower in magnitude and exhibited a less dramatic vertical gradient down the water column in 2020-2021. 2018 had the highest summertime pH in surface water (9.3) while 2021 had the lowest (8.1).

From 2017-2019, DO in surface water was 5-9 mg/L during summer months at station A. The DO decreased dramatically below the thermocline, going anoxic at 4-6 m deep in 2017 and 2018, and at 8 m deep in 2019 (Fig. 1-4). After HOS implementation in 2020, DO showed a steady decrease down the water column from around 7 mg/L in surface waters to 0 mg/L near the bottom at a depth of 18 m. In 2021, DO showed no dramatic vertical variation with values of 6 mg/L on the surface and 4-5 mg/L in the bottom water. At station B, DO profiles for 2017-2019 looked similar with surface water values of around 9 mg/L and anoxia below 5 m deep (Figs. 1-4 and 1-5). After HOS operation in 2020-2021, DO increased to around 2 mg/L between a depth of 5-8 m. Then, DO decreased to 0 mg/L below 8 m deep (Figs. 1-4 and 1-5). Redox potential at both stations A and B during 2017-2019 was indicative of oxidized conditions (>200 mV) in surface waters and reduced conditions (-300 to -350 mV) in bottom waters (Figs. 1-4 and 1-5). After the HOS operation in 2020-2021, conditions throughout the water column at stations A and B were oxidized (>300 mV) (Figs. 1-4 and 1-5). Redox potential showed a decrease in deep water samples near the sediment-water interface, especially in 2021 at station B (-10 mV at 12 m) (Fig. 1-4). The yearly patterns at

station B showed low redox conditions coincident with anoxia in bottom waters from 2017-2019, and elevated redox potential throughout the water column in 2021 (Fig. 1-5). Finally, Secchi disk transparency typically ranged from 60-100 cm in all study years (Table 1-3).

1.4.3 Water Chemistry

1.4.3.1 Nutrients, Chlorophyll, and Dissolved Organic Carbon

From 2017-2019 at stations A and B, ammonia concentration progressively increased in bottom waters during the summer months peaking at 7-7.5 mg-N/L, followed by a decrease in concentration starting in October (0.05 mg-N/L) (Figs. 1-6 and 1-7). At station B, surface and metalimnion ammonia concentrations were low throughout the year (Fig. 1-6A). Nitrate concentrations showed the opposite behavior, with levels peaking at the beginning of spring (0.4 mg-N/L at station A; 3.5-4.5 mg-N/L at station B) and decreasing with the onset of stratification, being depleted during the summer months throughout the water column (Figs. 1-6B and 1-7). In 2020, when oxygenation started, ammonia and nitrate patterns shifted. There was no ammonia in bottom waters during summer months, while nitrate concentration was low but not depleted (~0.5 mg-N/L) (Fig. 1-7). In 2021, ammonia concentration was almost depleted (~0.3 mg-N/L) throughout the water column, while nitrate progressively increased in the water column during the winter-spring months (Figs. 1-6A-B and 1-7). Peak nitrate concentrations were around 1 mg-N/L at station A and 3 mg-N/L at station B. From July to September 2021, nitrate concentration at stations A and B was low in the surface and metalimnion samples but slightly elevated (~0.5 mg-N/L) in bottom water (Figs. 1-6B and 1-7).

Phosphorus cycling was consistent for 2017-2019 at station A (Fig. 1-7). Phosphate progressively increased in the hypolimnion through the stratified period, with higher concentrations at the end of summertime (September-October). During these three years, phosphate concentrations were around 0.5 mg-P/L starting at 5 m deep to the bottom from May to August. 2018 showed the highest phosphate concentration of around 2 mg-P/L in the hypolimnion, followed by 2019 with 1.3 mg-P/L, and 2017 with 0.8 mg-P/L (Fig. 1-7). TP showed the highest concentration (~0.4 mg-P/L) in surface waters (0-5 m) in 2018, compared to 2017 (0.1 mg-P/L) and 2019 (0.2 mg-P/L), indicating high algae productivity all year (Table 1-2, Fig. 1-7). Still, it seems that whole-lake total chl mass, estimated based on reservoir bathymetry and chl profiles down the water column from June to August, showed higher mass in 2019 (1.03 g/m^2) compared to 2018 (0.58 g/m^2) and 2017 (0.52 g/m^2). However, 2018 chl mass was only calculated considering June and July months due to missing data so it might be underestimated (Table 1-3). In the hypolimnion, TP followed the same pattern as phosphate indicating that most of the phosphorus present in bottom waters is in the soluble reactive form (Fig. 1-7). On the contrary, after oxygenation in 2021, TP and phosphate

concentrations were low (<0.2 mg-P/L) during the entire sampling season throughout the water column (Fig. 1-7, Table 1-3). DOC concentrations in bottom waters did not change dramatically after oxygenation. During 2017 and 2018, DOC values were around 9.8 mg/L, whereas in 2021, DOC was slightly lower with a concentration of 8.6 mg/L (Table 1-2). Chl levels in surface waters were typically 60-150 µg/L in 2017-2019 and 30-40 µg/L in 2021 (Table 1-3). The taste and odor compound geosmin appeared to be elevated in 2017-2019 relative to 2021 after HOS operation (Table 1-3).

1.4.3.2 Metals

From 2017-2019, manganese concentration progressively increased in bottom waters with the onset of hypolimnetic anoxia, peaking between 0.8-1.8 mg/L before fall turnover in November when concentrations decreased to around 0.2 mg/L throughout the water column (Figs. 1-6C and 1-7). Patterns at station B from 2017-2019 also showed a vertical increase in concentration down the water column (Fig. 1-6C). However, the years showed different patterns of peak concentrations in the hypolimnion (Figs. 1-6C and 1-7). In 2017, the peak concentration in the hypolimnion (~0.6 mg/L) was in July and August. 2018 peak manganese concentration in the bottom waters (~1.2 mg/L) was observed in May-July and again in September-October. In 2019, peak manganese concentration (1.3-1.8 mg/L) was observed in August-September. After oxygenation, manganese concentrations were lower in bottom waters (~0.3 mg/L). However, at station A in 2021, there was a peak manganese concentration of 1 mg/L during May-June (Fig. 1-7). This was not seen at station B where the highest concentration in the bottom waters during 2021 was 0.3 mg/L (Fig. 1-6C).

Iron behavior was opposite to manganese during the summertime before and after oxygenation. From 2017-2019, iron concentration was low throughout the water column (0.02 mg/L station A; 0.2 mg/L station B). Iron concentration increased in the hypolimnion during May, July, and August and decreased by the end of the summer months (Figs. 1-6D and 1-7). 2019 also showed an interesting pattern with the highest iron concentration in surface waters at station A in the spring (Fig. 1-7). After oxygenation, 2020-2021, iron concentration was elevated throughout the water column at both stations, an order of magnitude higher than under pre-oxygenation years (0.4 mg/L station A, and 2 mg/L station B) (Figs. 1-6D and 1-7). In 2021 after oxygenation, iron had two peaks of elevated concentration in the water column (Fig. 1-7). The first peak was in the hypolimnion in May-June at station A (0.4 mg/L) and in April at station B (0.8 mg/L). The second peak was at the end of the summer months in the water column at station A (0.25 mg/L) and in August in the hypolimnion at station B (0.7-1.8 mg/L) (Figs. 1-6D and 1-7).

1.4.3.3 Mercury

For 2017-2019, patterns of Hg concentration in the hypolimnion at station A were different according to the year (Fig. 1-7). The wet year of 2017 had the

highest MeHg concentration (>1.5 ng/L) present in bottom waters from May to October. THg peak concentration (~6.5 ng/L) happened from September to November (Fig. 1-7). On the contrary, the dry year of 2018 had the lowest Hg concentration. MeHg (<1 ng/L) was observed in bottom waters only during May and June and THg (~2 ng/L) was observed from June to October. In 2019, MeHg (~ 3 ng/L) was observed from June to October and THg (~5 ng/L) from August to September (Fig. 1-7). After oxygenation in 2021, MeHg was below the reporting limit in the bottom waters, while THg concentration throughout the water column was around 1 ng/L (Fig. 1-7).

1.4.4 Internal Loading Dynamics

We calculated MHAR for ammonia, phosphate, manganese, THg, and MeHg at stations A and B for the study period (Fig. 1-8). The highest accumulation rates for nutrients and metals were generally seen during the dry year 2018, while the highest THg and MeHg accumulation rate was seen during the wet year 2017. Focusing on the pre-oxygenation years of 2017-2019, ammonia MHAR showed similar patterns in all years with rates increasing as summer progressed. Ammonia MHAR typically ranged from 50 to 300 $mg/m^2 \cdot d$, but 2018 showed a massive accumulation in July on the order of 1,000 $mg/m^2 \cdot d$ at station A. For phosphate, there was a continued accumulation throughout the summer months with values ranging from 10-80 $mg/m^2 \cdot d$ and generally peaking in June/July.

Manganese seemed to have a progressive accumulation of 30-250 $mg/m^2 \cdot d$, which generally stopped in June/July, except for 2018 when it stopped in May. THg accumulation started in May, with values ranging from 100-400 $ng/m^2 \cdot d$, and typically exhibited a loss (negative MHAR) during August. 2018 had the lowest THg accumulation with values <100 $ng/m^2 \cdot d$. MeHg MHAR patterns for 2017-2019 showed a progressive accumulation that ended in June with values ranging from 50-350 $mg/m^2 \cdot d$, followed by a loss during July/August, and a small accumulation in September. 2018 also had the lowest MeHg accumulation rate with only around 50 $ng/m^2 \cdot d$ during May. In general, the values calculated from the MHAR were the same order of magnitude as anoxic fluxes measured in chamber experiments with Hodges Reservoir water and sediment conducted previously by Beutel et al. (2020).

Results of the internal loading calculation at station A, which estimated the rate of transport of nutrients and metals across the thermocline for 2017-2019, showed similar heat exchange coefficients (V_t) (1.2-1.6 cm/d) and vertical diffusion coefficient (E_t) values (0.003 cm^2/s) for all years (Table 1-4). Typical vertical diffusion coefficient values for moderately deep systems with mean depths of 5-10 m range from 0.003-0.009 cm^2/s (Chapra, 1997). The wet year of 2017 appeared to have the lowest average fluxes of internal loading of phosphate, ammonia, and manganese, while the dry year of 2018 had the lowest internal loading of MeHg. 2019 had average precipitation during the year but had higher internal nutrient loading values compared to the wet year of 2017, except for

MeHg. 2017 and 2019 exhibited a loss of nitrate while 2018 showed nitrate depletion since June. We present the contrasting patterns of internal loading dynamics for June for the wet year, 2017, and the dry year, 2018 (Fig. 1-9). Values of MHAR and mass transport to the epilimnion were generally on the same order of magnitude, even though the two values were calculated using very different approaches. In general, there was double the magnitude of MHAR and internal nutrient loading for ammonia and phosphate in 2018 compared to 2017, whereas values for MeHg and manganese were higher in 2017 compared to 2018. In addition, MeHg showed a higher transport through thermocline in 2017, which was associated with higher bioaccumulation into seston and zooplankton (Beutel unpublished). Negative values of MHAR and internal nutrient loading for manganese and MeHg in 2018 suggest a manganese and MeHg sink in bottom waters.

After oxygenation in 2021, we barely observed any accumulation of ammonia, phosphate, manganese, THg, and MeHg based on our MHAR assessment (Fig. 1-8). Any accumulation that happened at the beginning of the season was followed by loss and a small release in October. Phosphate showed an interesting pattern of continuous accumulation (30 $mg/m^2 \cdot d$) at station B. But as the water column appeared more mixed in 2021, this calls into question the appropriateness of applying the MHAR metric, since it assumed accumulation into a well-defined hypolimnion. Therefore, we used a whole-lake mass approach (McCord et al., 2016) to assess two parameters of interest, TP and MeHg, which are relatively conservative on a whole-lake basis. We estimated the whole-lake mass of TP and unfiltered MeHg in Hodges Reservoir based on bathymetry and concentration down the water column. We compared July 2019, the average precipitation year, with July 2021, after oxygenation with relatively mixed conditions. 2019 hypolimnetic TP mass of around 4,867 kg (19,026,000 m^3 lake volume; 1.8 mg/L) volume-weighted mean concentration was higher than the 2021 whole-lake TP mass of around 2,084 kg (14,262,000 m^3; 0.55 mg/L). For MeHg, in 2019, hypolimnetic mass of around 2 g (19,026,000 m^3; 1.18 $\mu g/m^3$) volume-weighted mean concentration was higher than the 2021 whole-lake MeHg mass of around 0.6 g (14,262,000 m^3; 0.22 $\mu g/m^3$).

1.5 Discussion

1.5.1 Nitrogen Cycle

At the sediment-water interface of hypereutrophic reservoirs, the nitrogen cycle is dominated by mineralization, the formation of ammonium from the degradation of organic matter, and denitrification, the microbial transformation of nitrate into nitrogen gas (Table 1-1). We can observe these two processes being dominant in Hodges Reservoir in 2017-2019. Ammonia progressively accumulated in the hypolimnion while nitrate was depleted early in the season as anoxic

conditions and redox potential favored these reactions. However, there are some differences in the nitrogen cycle during the years before oxygenation. 2017 and 2019 showed high nitrate concentrations in bottom waters (1-4.5 mg-N/L) at the beginning of the season and a progressive ammonia accumulation in the hypolimnion (MHAR ~200 mg/m^2·d). While 2018 showed low nitrate concentration (0.2-2 mg-N/L) in bottom waters at the beginning of the season, and higher ammonia MHAR (>250 mg/m^2·d) peaking in July (Figs. 1-6, 1-7, and 1-8).

Differences in nitrogen cycling year to year can be explained by the wet versus dry conditions (Fig. 1-3). During the dry year 2018, there was negligible runoff resulting in low external nutrient loading and a relatively small lake volume. Upon the formation of the thermocline and the relatively small hypolimnion, DO was rapidly depleted and redox potential quickly dropped (Figs. 1-4 and 1-5, Table 1-1). Thus, organic matter degradation promoted high ammonia MHAR (>200 mg/m^2·d) and high internal nutrient loading all year long (Figs. 1-8 and 1-9, Table 1-4). Nitrate was only seen at the end of the season due to the fall turnover event mixing ammonia from bottom water into an oxic water column where the nitrification process could occur (Figs. 1-6B and 1-7). Interestingly, high nitrate concentration was seen at the beginning of the season of 2019 (Figs. 1-6B and 1-7). On the contrary, the rain seen at the beginning of the years 2017 and 2019 brought runoff from the watershed that increased the volume of the reservoir and resulted in substantial external nutrient loading (Fig. 1-3). The resulting hypolimnion was around two times the volume of the hypolimnion in dry year 2018, which meant that the hypolimnion started with a much higher mass of oxygen. In addition, lake waters had elevated levels of nitrate, a potent oxidant, due to the nitrification of large ammonia releases during the previous years, as well as elevated levels of nitrate in stormwater inflows (1-2 mg-N/L) (City of San Diego, 2021). As a result, bottom water stayed aerobic with elevated redox levels for a longer time after stratification, resulting in less internal nutrient loading (Figs. 1-5 and 1-9, Table 1-4). By poising redox potential above that at which phosphate-containing iron-oxides in sediment undergo reductive dissolution, nitrate has been shown to be a potent inhibitor of sediment phosphorus release in a range of aquatic ecosystems (Beutel et al., 2016).

As expected, the nitrogen cycle pattern shifted after oxygenation starting in 2020. DO concentrations in bottom waters were around 2 mg/L and redox potential was > 300 mV (Figs. 1-4 and 1-5). As a result, nitrification, the oxidation of ammonium to nitrate, was the dominant reaction (Rysgaard et al., 1994):

$$2NH_4^+ + 3O_2 \rightarrow 2NO_2^- + 2H_2O + 4H^+$$

and

$$2NO_2^- + O_2 \rightarrow 2NO_3^-$$

Ammonia concentrations stayed low (0.3-0.5 mg-N/L) all year long throughout the water column (Figs. 1-6A and 1-7). Nitrate concentrations, between 1-2 mg-N/L, were seen early in the season in bottom waters and stayed at low concentration (0.7 mg-N/L) throughout the water column the rest of the season. As there was weaker stratification, nitrate appeared to be mixed throughout the water column. However, there was lower nitrate concentration in the water column during July to September, which could be associated with higher water temperatures enhancing the activity of denitrifying organisms in anoxic sediments, and more algae growth in the surface waters (Figs. 1-6B and 1-7). These results highlight the paradox of nitrogen cycling in eutrophic lakes: the addition of oxygen can indirectly stimulate the anaerobic process of denitrification (nitrate reduction to nitrogen gas) by promoting nitrification (ammonia oxidation to nitrate), resulting in the net loss of ammonia from the system. This phenomenon of net nitrogen loss has also been observed in Camanche Reservoir, California, USA, which has been oxygenated with a Speece Cone HOS since the early 1990s (Beutel, 2006; Horne and Beutel, 2019).

The difference in relative concentrations of ammonia and nitrate after oxygenation might have repercussions in the phytoplankton taxa seen in Hodges Reservoir. Ammonia is normally the preferred compound for algae and bacteria because of the smaller energy cost for assimilation, but eukaryotic phytoplankton are also able to use nitrate, giving them an advantage under nitrate-rich conditions (Harris et al., 2016). In contrast, high ammonia relative to nitrate favors cyanobacteria growth, especially non-nitrogen-fixing taxa, as well as the production of secondary metabolites such as the common taste and odor compound geosmin (Harris et al., 2016). These dynamics appear to be occurring in Hodges Reservoir. In 2021, when nitrate concentrations increased and ammonia concentration decreased, because of oxygen addition, geosmin measured at station B decreased compared to pre-oxygenation years (Fig. 1-6B, Table 1-3). Another interesting observation is the apparent drop in nitrate concentrations in the water column at stations A and B in the summer of 2021, which appeared to correspond with an increase in chl under elevated iron concentration (Figs. 1-6B and 1-6D, and 1-7, Table 1-3). The loss of summertime nitrate may be linked to the presence of iron since iron is known to facilitate nitrate uptake and stimulate algal productivity in some phytoplankton communities (Havens et al., 2012; Ma et al., 2021; Robertson et al., 2016).

1.5.2 Manganese and Iron Cycling

Similar to nitrate and ammonia, manganese and iron had different behaviors between dry and wet years, as well as before and after oxygenation. Both manganese-oxides and iron-oxides in surficial sediment undergo reductive dissolution under reduced conditions, releasing reduced manganese (Mn(II)) and iron (Fe(II)) into overlaying water, with manganese-oxides being more susceptible to reductive dissolution as redox potential drops (Table 1-1) (Davison, 1993). For

pre-oxygenation years, 2017-2019, manganese hypolimnetic accumulation was observed in all years, but patterns were different for each year and corresponded to the redox status of the system and the hydrology (Figs. 1-4 and 1-8). In the wet year 2017, in which hypolimnetic redox potential dropped slowly, modest manganese accumulation was observed from May to July resulting in low concentration in bottom water. This year also showed a late-season manganese flux in September, which could be associated with the abiotic reduction of refractory Mn-oxides by sulfide (Böttcher and Thamdrup, 2001; Beutel et al., 2020), as sulfide (>15 mg/L) was elevated during this period (Fig. 1-8). In contrast, in dry year 2018, when redox potential dropped to low levels earlier in the year, manganese accumulation was observed only in May (Fig. 1-8). This contrast is highlighted in Fig. 1-9 where in June 2017 there was manganese accumulation in bottom waters (MHAR of 33 mg/m^2·d), whereas in June 2018 there was manganese loss (MHAR of -36 mg/m^2·d). A negative MHAR (manganese loss from the hypolimnion) was also observed later in the stratified season in 2019 (Fig. 1-8). Two mechanisms could account for this observation. As discussed below, iron monosulfide minerals (mackinawite, FeS) likely precipitated under Fe(II)- and sulfide-rich conditions and may have scavenged Mn(II) from bottom waters (Morse and Luther, 1999). Another possible sink for manganese could be precipitation with sulfide forming alabandite (MnS).

$$Mn^{2+} + HS^{-} \leftrightarrow H^{+} + MnS_{(s)}$$

This mineral is typically not observed in freshwaters due to its relatively high solubility product (pK_{sp} ~0.4) (Delfino and Lee, 1968; Davidson, 1993). Solubility calculations (pK_{sp} ~2.9) suggest that MnS precipitation may have been favored at the end of summer in bottom waters of Hodges Reservoir under highly sulfidic (~30 mg/L) and manganese-rich (~1 mg/L) conditions.

Patterns of iron concentration in the hypolimnion before oxygenation (2017-2019) were less obvious than for manganese (Fig. 1-6C-D and 1-7). A similar pattern of modest and sustained increase in concentration during wet 2017, compared to a more intense high concentration during dry 2018, was observed. But in all years, iron concentration diminished in the summer. It seems that the high sulfide concentrations, a byproduct of SRB activity in the relatively high sulfate waters (~200 mg/L) of Hodges Reservoir, favored FeS precipitation in the hypolimnion (Balistrieri et al., 1992; Luther et al., 2003; Wolthers et al., 2005) as:

$$Fe^{2+} + HS^{-} \leftrightarrow H^{+} + FeS_{(s)}$$

Typical concentrations of total sulfide (~15 mg/L) and total iron (~0.07 mg/L) in hypolimnetic water at station A under highly reduced conditions (-200

mV) were indicative of FeS precipitation based on the reported solubility product for FeS (pK_{sp} ~3) (Beutel, 2000). FeS precipitation was also observed during the anoxic phase of laboratory chamber experiments assessing sediment release of nutrients and metals in Hodges Reservoir under oxic versus anoxic conditions (Beutel et al., 2020).

Unlike manganese, iron cycling is linked to the internal loading of phosphorus since the dissolution of iron-oxides in sediment is commonly accompanied by the release of phosphate to overlaying water (Lovley et al., 2004; Golterman, 2001; Søndergaard et al., 2003). This linkage is difficult to see in the water quality dataset, since summertime hypolimnetic iron concentration is low (via FeS precipitation sink) when phosphate concentration is elevated, especially in 2018 and 2019 (Fig. 1-7). But this linkage between iron and phosphate release is more obvious in bottom waters during 2017, when the hypolimnion went anoxic more slowly and phosphate and iron concentrations in bottom waters increased from around July through August (Fig. 1-7). In all years, elevated phosphate concentration was observed late in the season, presumably after more labile iron-oxides were reduced. This may be the result of abiotic reduction of refractory iron-oxides by sulfide under the highly sulfidic conditions of bottom waters in the late summer (Mitchell and Baldwin, 1998; Zak et al., 2006). It also could be the result of the mineralization of decaying algae stimulated by the high rates of internal loading in this hypereutrophic reservoir (Forsberg, 1989). To put the magnitude of internal loading in context, we estimated annual rates of internal phosphate loading for Hodges Reservoir (~18-55 g-P/m^2-y). Values were two orders of magnitude higher than that predicting a eutrophic trophic status (~0.2 g-P/m^2-y) for this relatively shallow reservoir (mean depth ~6 m) using the Vollenweider phosphorus loading curve (Horne and Goldman, 1993).

Manganese and iron cycling appeared to change substantially after oxygenation. At both stations A and B for 2020-2021, manganese values in bottom water no longer showed an increase in concentrations as the season progressed. Instead, it showed low and steady concentrations suggesting some continued release via reductive dissolution of manganese-oxides, especially early in 2021 at station A (Figs. 1-6C and 1-7, Table 1-1). In contrast, iron concentration was elevated throughout the water column, but phosphate and TP were low (Figs. 1-6D and 1-7). Since iron-oxide reductive dissolution typically results in the co-release of iron and phosphate (Golterman, 2001; Søndergaard et al., 2003), there appears to be another source of iron in bottom waters. The source of this iron could be the oxidation of FeS in surficial sediment. FeS is metastable and elevated DO and redox potential at the sediment-water interface can promote FeS dissolution, releasing dissolved Fe(II) which would result in Fe(III)-oxides formation (Chen and Morris, 1972; Wang et al., 2023). Freshly formed iron-oxides produced by Fe(II) oxidation in natural waters tend to exist primarily as colloids (1-100 nm), which are resistant to gravitational settling unless they aggregate and become large enough to sink (Chikanda et al., 2021). Moreover, iron-oxide colloids can bind

with natural organic matter in waters with elevated carbon-to-iron molar ratios (>1.6) via bonding to the humic acids (Liao et al., 2017). DOC measured after oxygenation in Hodges Reservoir was around 8.5 mg/L, yielding a carbon-to-iron ratio of around 20, suggesting inhibition of humic acid/iron-oxide aggregation (Table 1-1). This is a possible explanation for the persistent concentrations of iron observed in the post-oxygenated water column (Figs. 1-6D and 1-7). The mechanism of FeS oxidation forming iron-oxides to the water column, combined with the colloid nature of resulting iron-oxides in high DOC waters, could also explain elevated iron throughout the water column in the early spring during the years before oxygenation, especially in 2018 (Fig. 1-7).

1.5.3 Methylation Window

MeHg accumulation in aquatic environments is the result of the competition of two main cycling processes, Hg methylation and MeHg demethylation (Fig. 1-1) (Barkay and Gu, 2022). Hg methylation is performed mainly by anaerobic microorganisms and thus tends to occur under anaerobic conditions (Ullrich et al., 2001). But inorganic Hg(II) bioavailability for methylation tends to decrease as reducing conditions become more severe (Benoit et al., 1999; Regnell and Watras, 2019). As a result, Hg methylation occurs at the redox boundary in aquatic sediment, which can coincide with SRB activity at the sediment-water interface resulting in MeHg formation as a co-metabolic process (Gilmour et al., 2018). MeHg demethylation is prevalent under oxidized conditions and performed by aerobic prokaryotes using the mer-detoxification pattern under extremely high Hg concentrations (Du et al., 2019). It is also performed by some SRB and methanogenic microorganisms as a cometabolic process under highly reduced and light-deprived conditions in soils and sediments where microbes recognize the methyl group in MeHg as a C1 substrate. For SRB, the proposed reaction suggest an oxidative demethylation as an overall reaction analogous to acetate oxidation by SRB (Marvin-DiPasquale and Oremland, 1998):

$$CH_3Hg^+ + 2H^+ + SO_4^{2-} \leftrightarrow HS^- + CO_2 + 2H_2O + Hg^{2+}$$

For methanogenic archaea the reaction is analogous to monomethylamine or methanol degradation where the methyl group is possibly oxidized via the periplasmic enzyme (Baesman et al., 2015; Lu et al., 2017):

$$4CH_3Hg + 2H_2O + 4H^+ \leftrightarrow 3CH_4 + CO_2 + 4H_2 + 4Hg^{2+}$$

As a result of these complex processes, peak MeHg production in aquatic ecosystems tends to occur under moderately anaerobic and mildly reduced conditions (e.g., manganese reduction), which we call the “methylation window”. In Hodges Reservoir, we saw this methylation window at the end of the spring season of the wet and average years (2017 and 2019), especially in 2017. MeHg

production and accumulation in the hypolimnion happened from May to June (Figs. 1-8 and 1-9). It seems that runoff during winter-spring precipitation provided more initial mass of oxygen due to a larger hypolimnion, which delayed the onset of highly reduced conditions in bottom waters. In addition, the elevated nitrate concentration from the previous high-ammonia year, and the extra nitrate input from storm runoff, likely helped to buffer redox conditions at around 200 mV early in the season (Figs. 1-6A-B and 1-7) (Beutel et al., 2016). These conditions favored denitrification and microbial manganese-oxides reduction during the pre-stratified season. But with the onset of stratified conditions in May, mildly reduced conditions (0-100 mV) prevailed in bottom waters that enhanced Hg methylation by promoting inorganic Hg(II) bioavailability and SRB activity in anoxic profundal sediment. We saw a peak in MeHg accumulation rate (200-300 $ng/m^2 \cdot d$) overlapping with elevated manganese accumulation rate (~230 $mg/m^2 \cdot d$), a decrease in sulfate concentration, and low sulfide buildup in the water by May (Fig. 1-8, Table 1-1), conditions known to stimulate MeHg production in aquatic systems (Gilmour et al., 2018). Other studies of Hg cycling have observed this synchronicity of elevated manganese and MeHg, suggesting that in aquatic ecosystems an increase in dissolved manganese may be the effect of mildly reduced conditions that are also suitable for anaerobic microbes able to methylate inorganic Hg(II) (Peterson et al. 2023; Alpers et al., 2014; Gill et al., 2008, Balogh et al., 2004).

In both years, 2017 and 2019, MeHg showed a negative MeHg accumulation rate (loss from bottom waters) late in the stratified season when the hypolimnion was highly reduced and sulfidic (Fig. 1-8). Apparently, the methylation window closed. Two mechanisms may explain this observation: low Hg(II) bioavailability for methylation (Regnell and Watras, 2019) and elevated rates of demethylation relative to methylation (Marvin-DiPasquale et al., 2000). Experimental sediment-water chamber incubations conducted with samples from Hodges Reservoirs by Beutel et al. (2020) also observed peak MeHg accumulation rates of around 100-300 $ng/m^2 \cdot d$ under mildly reduced conditions. MeHg accumulation rates dropped dramatically under highly reduced conditions. Fuhrmann and Beutel (2021) showed that methanogens were potent demethylators in reduced sediment from Hodges Reservoir, suggesting this mechanism accounts for the observed loss of MeHg in the reservoir late in the stratified season.

In contrast to the wet and average years, during the dry year of 2018, the methylation window occurred during a shorter period (Figs. 1-7, 1-8, and 1-9). With no stormwater runoff, the hypolimnion was much smaller, and reduced conditions in the water column developed earlier in the season (Figs. 1-4 and 1-5). As a result of the mechanisms noted above, MeHg accumulation was relatively low. A similar pattern of low MeHg accumulation throughout the stratified season, due to highly reduced and sulfidic conditions in bottom waters, was observed in Twin Lakes, Washington, USA (Beutel et al., 2014). In that lake system, oxygen addition to enhancing a stocked cold-water trout fishery unexpectedly led to an

increase in Hg uptake into biota. In essence, oxygen addition may have inadvertently opened the methylation window, though MeHg uptake into biota was lower in years with elevated oxygen input compared to years with lower oxygen input.

After oxygenation in 2021, DO concentration (~2 mg/L) and redox (> 300 mV) were elevated in bottom waters during the entire sampling season (Figs. 1-4 and 1-5) and MeHg accumulation was absent (Figs. 1-7 and 1-8). The highly oxidized conditions appeared to close the methylation window, likely via inhibition of SRB activity, which microbes are obligate anaerobes and key methylators (Gilmour et al., 2018). Other potential sinks for MeHg and Hg(II) in surficial sediment include sorption to iron- and manganese-oxides, which have large surface areas and high capacity to sorb and co-precipitate with Hg species (Inoue and Munemori, 1979; Ullrich et al., 2001), and loss via aerobic demethylation (Barkay and Gu, 2022; Du et al., 2019). However, because the reservoir appeared to be more mixed after HOS operations, the low and constant MeHg concentration in the water column could be the result of sediment release followed by mixing and dilution. But whole-lake MeHg mass calculations suggest this is not the case (1.18 µg/m^3 during July 2019 versus 0.22 µg/m^3 during post-oxygenation July 2021). Thus, it appears that oxygenation did indeed suppress the accumulation of MeHg into reservoir waters, which presumably could decrease bioaccumulation in aquatic biota as well.

1.6 Management Considerations

Study results highlight the role that winter precipitation and changes in hypolimnion volume play in mediating nutrients, metals, and Hg cycling in Hodges Reservoir. During the wet and average years (2017 and 2019, respectively), larger water volume in the reservoir resulted in relatively low hypolimnetic concentrations of nutrients and metals but opened a window for high MeHg production under mildly reduced conditions. On the contrary, the dry year (2018) favored rapid deoxygenation of bottom waters, resulting in higher hypolimnetic concentrations of nutrients and metals but a lower accumulation rate of MeHg. This change in hypolimnion volume has implications for the reservoir's productivity and MeHg accumulation in biota. After oxygenation, water quality in Hodges Reservoir showed substantial drops in water column ammonia, phosphate, manganese, and MeHg, but elevated levels of iron and nitrate. Whole-lake TP dropped by over half when comparing pre-and post-oxygenation years (July 2019 vs July 2021). Oxygenation also appears to lower phytoplankton productivity and its potential to produce the potent taste and odor compound geosmin.

Notwithstanding, two observations post-oxygenation merit discussion: first, the apparent loss of thermal stratification in post-oxygenation years, and second, the ongoing accumulation of some reduced compounds (e.g., manganese and iron) in bottom waters despite oxygenation. Based on temperature profiles from 2020 and 2021 (Figs. 1-4 and 1-5), the reservoir water column appeared to be well-mixed

with no thermocline formation. This was unanticipated as cone-based HOS aims to maintain thermal stratification to allow for selective withdrawal of bottom waters free of phytoplankton and their decay by-products and to support cold-water biota in the reservoir and its tailwaters (Beutel and Horne, 1999). Numerous oxygenation cones have been used to successfully oxygenate lakes and reservoirs in the USA while maintaining stratification, including Newman Lake, Washington (max depth ~9.0 m) (Moore et al., 2012), Camanche Reservoir, California (max depth ~34.6 m) (Horne and Beutel, 2019; Horne et al., 2019), and in Indian Creek, California (max depth ~12.8 m) and Marston Reservoir, Colorado (max depth ~17.1 m) (Alex Horne, personal correspondence). Three different factors likely contributed to the mixing of the water column: the relatively shallow depth of the reservoir, the turbulent energy input from a pumped storage hydropower system, and the installation of the HOS cone at an intermediate depth (~14.5 m) rather than at the deepest point in the reservoir (~19 m).

The second observation of note was that, while dramatically affecting chemical cycling in the reservoir, HOS operation did not always maintain a well-oxygenated sediment-water interface throughout the reservoir. Rather, some chemical stratification persisted. Elevated levels of manganese and iron were seen early in the season in bottom waters during 2020-2021 (Figs. 1-6C-D and 1-7). As it does not readily reoxidize to a particulate oxide under aerobic conditions, manganese is an especially good tracer of the occurrence of anoxic conditions at the sediment-water interface (Beutel et al., 2020). Hence, its persistence in bottom waters indicates reduced conditions to some extent at the sediment-water interface. Hodges Reservoir has relatively high sediment oxygen demand (~2 $g/m^2 \cdot d$) and during sediment-water chamber experiments, “oxic” sediment chambers still at times released nutrients and metals into overlaying water (Beutel et al., 2020). Accordingly, it is not surprising to see indications of anoxia at the sediment-water interface, even when oxygen is being added. Long-term operation of HOS at other sites has shown that sediment oxygen demand tends to decrease with time as the historic accumulation of organic matter in sediment is oxidized (Gantzer et al., 2009, Horne and Beutel, 2019). The same effect can be expected at Hodges Reservoir, though because of its extremely productive character it may take a relatively long time. Coupled with this decrease in oxygen demand should be an ability for oxygen addition to suppressing metals release more readily from profundal sediment.

Article published: Rodal-Morales, N. D., Beutel, M., Fuhrmann, B., Defeo, S., Hansen, A. M., Harmon, T., ... and Pasek, J. (2024). Hydrology and oxygen addition drive nutrients, metals, and methylmercury cycling in a hypereutrophic water supply reservoir. Frontiers in Water, 6.
https://doi.org/10.3389/frwa.2024.1356994

1.7 References

Alpers, C.N., Fleck, J.A., Marvin-DiPasquale, M., Stricker, C.A., Stephenson M., and Taylor H.E. (2014). Mercury cycling in agricultural and managed wetlands, Yolo Bypass, California: Spatial and seasonal variations in water quality. Science of the Total Environment 484: 276–287. https://doi.org/10.1016/j.scitotenv.2013.10.096

American Public Health Association (APHA). (2023). Standard Methods for the Examination of Water and Wastewater. 24th ed. Washington, D.C: American Public Health Association.

Austin, D., Scharf, R., Chen, C.F., Bode, J. (2019). Hypolimnetic oxygenation and aeration in two Midwestern USA reservoirs. Lake and Reservoir Management 35, 266–276. https://doi.org/10.1080/10402381.2019.1599087

Baesman, S. M., Miller, L. G., Wei, J. H., Cho, Y., Matys, E. D., Summons, R. E., ... and Oremland, R. S. (2015). Methane oxidation and molecular characterization of methanotrophs from a former mercury mine impoundment. Microorganisms, 3(2), 290-309.

Balistrieri, Laurie S., et al. (1992). The cycling of iron and manganese in the water column of Lake Sammamish, Washington. Limnology and Oceanography 37, 510–528, https://doi.org/10.4319/lo.1992.37.3.0510.

Balogh, S.J., Nollet, Y.H., Swain, E.B. (2004). Redox chemistry in Minnesota streams during episodes of increased methylmercury discharge. Environ Sci Tech. 38, 4921–4927. https://doi.org/10.1021/es049696c

Barkay, T., Gu, B. (2022). Demethylation – The Other Side of the Mercury Methylation Coin: A Critical Review. ACS Environ. Au 2, 77–97. https://doi.org/10.1021/acsenvironau.1c00022

Benoit, J.M., Gilmour, C.C., Mason, R.P., Heyes, A. (1999). Sulfide Controls on Mercury Speciation and Bioavailability to Methylating Bacteria in Sediment Pore Waters. Environ. Sci. Technol. 33, 951–957. https://doi.org/10.1021/es9808200

Beutel, M.W. (2000). Dynamic and control of nutrient, metal and oxygen fluxes at the profundal sediment-water interface of lakes and reservoirs. [dissertation/ Ph.D thesis][California(CA)]: University of California Berkeley

Beutel, M.W. (2006). Inhibition of ammonia release from anoxic profundal sediments in lakes using hypolimnetic oxygenation. Ecological Engineering 28, 271–279. https://doi.org/10.1016/j.ecoleng.2006.05.009

Beutel, M.W., Horne, A.J. (1999). A Review of the Effects of Hypolimnetic Oxygenation on Lake and Reservoir Water Quality. Lake and Reservoir Management 15, 285–297. https://doi.org/10.1080/07438149909354124

Beutel, M.W., Dent, S. R., Reed, B., Marshall, P., Gebremariam, S., Moore, B. C., Cross, B., Gantzer, P., Shallenberger, E. (2014). Effects of hypolimnetic

oxygen addition on mercury bioaccumulation in Twin Lakes, Washington, USA. Science of the Total Environment 496, 688–700. https://doi.org/10.1016/j.scitotenv.2014.06.117

Beutel, M.W. (2015). Lake Hodges Reservoir Oxygen Demand Study. Report to Brown and Caldwell and City of San Diego, June 11, 2015.

Beutel, M.W., Duvil, R., Cubas, F.J., Matthews, D.A., Wilhelm, F.M., Grizzard, T.J., Austin, D., Horne, A.J., Gebremariam, S. (2016). A review of managed nitrate addition to enhance surface water quality. Critical Reviews in Environmental Science and Technology 46(7), 673–700. https://doi.org/10.1080/10643389.2016.1151243

Beutel, M.W., Fuhrmann, B., Herbon, G., Chow, A., Brower, S., Pasek, J. (2020). Cycling of methylmercury and other redox-sensitive compounds in the profundal zone of a hypereutrophic water supply reservoir. Hydrobiologia 847, 4425–4446. https://doi.org/10.1007/s10750-020-04192-3

Bierlein, K.A., Rezvani, M., Socolofsky, S.A., Bryant, L.D., Wüest, A., Little, J.C. (2017). Increased sediment oxygen flux in lakes and reservoirs: The impact of hypolimnetic oxygenation. Water Resources Research 53(6), 4876-4890. https://doi.org/10.1002/2016WR019850

Bigham, G.N., Murray, K.J., Masue-Slowey, Y., Henry, E.A. (2017). Biogeochemical controls on methylmercury in soils and sediments: Implications for site management: Geochemical Controls on Mercury Methylation. Integr Environ Assess Manag 13, 249–263. https://doi.org/10.1002/ieam.1822

Böttcher, M.E., Thamdrup, B. (2001). Anaerobic sulfide oxidation and stable isotope fractionation associated with bacterial sulfur disproportionation in the presence of MnO2. Geochimica et Cosmochimica Acta 65(10), 1573–1581. https://doi.org/10.1016/S0016-7037(00)00622-0

Chadwick, S.P., Babiarz, C.L., Hurley, J.P., Armstrong, D.E. (2006). Influences of iron, manganese, and dissolved organic carbon on the hypolimnetic cycling of amended mercury. Science of The Total Environment 368, 177–188. https://doi.org/10.1016/j.scitotenv.2005.09.039

Chapra, S.C. (1997). Surface Water-Quality Modeling. WCB/McGraw-Hill. 580-585.

Chen, K.Y., and Morris, J.C. (1972). Kinetics of Oxidation of Aqueous Sulfide by Oxygen. Environmental Science and Technology 6, 529–37. https://doi.org/10.1021/es60065a008.

Chikanda, F., Otake, T., Koide, A., Ito, A., Sato, T. (2021). The formation of Fe colloids and layered double hydroxides as sequestration agents in the natural remediation of mine drainage. Science of the Total Environment 774, 145183. https://doi.org/10.1016/j.scitotenv.2021.145183

City of San Diego. Watershed Sanitary Survey (2023). https://www.sandiego.gov/public-utilities/water-quality/watersheds/sanitary-survey

Cooke, G.D., Welch, E.B. and Peterson, S.A. (2013). Lake and Reservoir Restoration. Elsevier. 400 pp.

Davison, W. (1993). Iron and Manganese in Lakes. Earth-Science Reviews 34 (2), 119–63. https://doi.org/10.1016/0012-8252(93)90029-7.

Delfino, J.J., Lee, G.F. (1968). Chemistry of manganese in Lake Mendota, Wisconsin. Environ. Sci. Technol. 2, 1094–1100. https://doi.org/10.1021/es60023a004

Du, H., Ma, M., Igarashi, Y., Wang, D. (2019). Biotic and Abiotic Degradation of Methylmercury in Aquatic Ecosystems: A Review. Bull Environ Contam Toxicol 102, 605–611. https://doi.org/10.1007/s00128-018-2530-2

Eckley, C.S., Gilmour, C.C., Janssen, S., Luxton, T.P., Randall, P.M., Whalin, L., Austin, C. (2020). The assessment and remediation of mercury contaminated sites: A review of current approaches. Science of the Total Environment 707, 136031. https://doi.org/10.1016/j.scitotenv.2019.136031

Forsberg, C. (1989). Importance of sediments in understanding nutrient cyclings in lakes. Hydrobiologia 176/177, 263–277. https://doi.org/10.1007/BF00026561

Fuhrmann, B., Beutel, M., Ganguli, P., Zhao, L., Brower, S., Funk, A., Pasek, J. (2021). Seasonal patterns of methylmercury production, release, and degradation in profundal sediment of a hypereutrophic reservoir. Lake Reserv Manage. 37, 360–377. https://doi.org/10.1080/10402381.2021.1940397

Gantzer, P.A., Bryant, L.D., Little, J.C. (2009). Effect of hypolimnetic oxygenation on oxygen depletion rates in two water-supply reservoirs. Water Research 43(6), 1700-1710. http://doi.org/ 10.1016/j.watres.2008.12.053

Gill, G. (2008). Monomethylmercury photo-degradation studies. Transport, cycling, and fate of mercury and monomethylmercury in the San Francisco Delta and tributaries: an integrated mass balance assessment approach: final report to the California Department of Fish and Game and the California Bay Delta Authority, Task 5.1. [21 pp. http://mercury.mlml.calstate.edu/wp-content/uploads/2008/10/09_task5_1_final.pdf (accessed Nov. 09, 2023)].

Gilmour, C.C., Bullock, A.L., McBurney, A., Podar, M., Elias, D.A. (2018). Robust Mercury Methylation across Diverse Methanogenic Archaea. mBio 9, e02403-17. https://doi.org/10.1128/mBio.02403-17

Gilmour, C.C., Podar, M., Bullock, A.L., Graham, A.M., Brown, S.D., Somenahally, A.C., Johs, A., Hurt, R.A., Bailey, K.L., Elias, D.A. (2013). Mercury Methylation by Novel Microorganisms from New Environments. Environ. Sci. Technol. 47, 11810–11820. https://doi.org/10.1021/es403075t

Golterman, H.L. (2001). Phosphate release from anoxic sediments or `What did Mortimer really write?'. Hydrobiologia, Sediment-Water Interaction 11, 99–106. https://doi.org/10.1023/A:1017559903404

Goss, M., Swain, D.L., Abatzoglou, J.T., Sarhadi, A., Kolden, C.A., Williams, A.P., Diffenbaugh, N.S. (2020). Climate change is increasing the likelihood of extreme autumn wildfire conditions across California. Environ. Res. Lett. 15, 094016. https://doi.org/10.1088/1748-9326/ab83a7

Harris, T., Smith, V., Graham, J., Van De Waal, D., Tedesco, L., Clercin, N. (2016). Combined effects of nitrogen to phosphorus and nitrate to ammonia ratios on cyanobacterial metabolite concentrations in eutrophic Midwestern USA reservoirs. IW 6, 199–210. https://doi.org/10.5268/IW-6.2.938

Havens, S.M., Hassler, C.S., North, R.L., Guildford, S.J., Silsbe, G., Wilhelm S.W., Twiss M.R. (2012). Iron Plays a Role in Nitrate Drawdown by Phytoplankton in Lake Erie Surface Waters as Observed in Lake-Wide Assessments. Edited by Yves Prairie. Canadian Journal of Fisheries and Aquatic Sciences 69, 369–81. https://doi.org/10.1139/f2011-157.

Helmrich, S., Vlassopoulos, D., Alpers, C. N., and O'Day, P. A. (2022). Critical review of mercury methylation and methylmercury demethylation rate constants in aquatic sediments for biogeochemical modeling. Critical Reviews in Environmental Science and Technology, 52(24), 4353-4378.

Horne, A.J., Beutel, M.W. (2019). Hypolimnetic oxygenation 3: an engineered switch from eutrophic to a meso-/oligotrophic state in a California reservoir. Lake and Reservoir Management 35(3), 338–353. https://doi.org/10.1080/10402381.2019.1648613

Horne, A.J., Jung, R., Lai, H., Faisst, B., Beutel, M. (2019). Hypolimnetic oxygenation 2: oxygen dynamics in a large reservoir with submerged down-flow contact oxygenation (Speece cone). Lake and Reservoir Management 35(3), 323–337. https://doi.org/10.1080/10402381.2019.1648612

Horne, A.J., Goldman C.R. (1993). Limnology. McGraw-Hill. Second Edition. 577

Inoue, Y., Munemori, M. (1979). Coprecipitation of mercury(II) with iron(III) hydroxide. Environ. Sci. Technol. 13, 443–445. https://doi.org/10.1021/es60152a001

Krueger, K.M., Vavrus, C.E., Lofton, M.E., McClure, R.P., Gantzer, P., Carey, C.C., Schreiber, M.E. (2020). Iron and manganese fluxes across the sediment-water interface in a drinking water reservoir. Water Research 182, 116003. https://doi.org/10.1016/j.watres.2020.116003

Lee, R.M., Biggs, T.W. (2015). Impacts of land use, climate variability, and management on thermal structure, anoxia, and transparency in hypereutrophic urban water supply reservoirs. Hydrobiologia 745, 263–284. https://doi.org/10.1007/s10750-014-2112-1

Leung, T., Wilkinson, G.M., Swanner, E.D. (2021). Iron availability allows sustained cyanobacterial blooms: a dual-lake case study. Inland Waters 11, 417–429. https://doi.org/10.1080/20442041.2021.1904762

Liao, P., Li, W., Jiang, Y., Wu, J., Yuan, S., Fortner, J.D., Giammar, D.E. (2017). Formation, Aggregation, and Deposition Dynamics of NOM-Iron Colloids at Anoxic–Oxic Interfaces. Environ. Sci. Technol. 51, 12235–12245. https://doi.org/10.1021/acs.est.7b02356

Lovley, D. R., D. E. Holmes, K. P. Nevin. (2004). Dissimilatory Fe(III) and Mn(IV) reduction. Advances in Microbial Physiology 49, 219–286. https://doi.org/10.1016/S0065-2911(04)49005-5

Luther, III, G.W., Glazer, B., Ma, S., Trouwborst, R., Shultz, B.R., Druschel, G., and Kraiya, C. (2003). Iron and Sulfur Chemistry in a Stratified Lake: Evidence for Iron-Rich Sulfide Complexes. Aquatic Geochemistry 9, 87–110. https://doi.org/10.1023/B:AQUA.0000019466.62564.94.

Lu, X., Gu, W., Zhao, L., Farhan Ul Haque, M., DiSpirito, A. A., Semrau, J. D., and Gu, B. (2017). Methylmercury uptake and degradation by methanotrophs. Science Advances, 3(5), e1700041.

Ma, K., Yang, R. Qu, S., Zhang, Y., Liu, Y., Xie, H., Minghan, Z., Mengqi, B. (2021). Evidence for Coupled Iron and Nitrate Reduction in the Surface Waters of Jiaozhou Bay. Journal of Environmental Sciences 108, 70–83. https://doi.org/10.1016/j.jes.2021.02.016.

Marvin-DiPasquale, M., Agee, J., McGowan, C., Oremland, R.S., Thomas, M., Krabbenhoft, D., Gilmour, C.C. (2000). Methyl-Mercury Degradation Pathways: A Comparison among Three Mercury-Impacted Ecosystems. Environ. Sci. Technol. 34, 4908–4916. https://doi.org/10.1021/es0013125

Marvin-DiPasquale, M. C., & Oremland, R. S. (1998). Bacterial methylmercury degradation in Florida Everglades peat sediment. Environmental Science & Technology, 32(17), 2556-2563.

McCord, S.A., Beutel, M.W., Dent, S.R. and Schladow, S.G. (2016). Evaluation of mercury cycling and hypolimnetic oxygenation in mercury-impacted seasonally stratified reservoirs in the Guadalupe River watershed, California. Water Resources Research 52(10), 7726-7743. http://doi.org/10.1002/2016WR019061

Mergler, D., Anderson, H.A., Chan, L.H.M., Mahaffey, K.R., Murray, M., Sakamoto, M., Stern, A.H. (2007). Methylmercury exposure and health effects in humans: a worldwide concern. AMBIO: A Journal of the Human Environment 36(1), 3-11. https://doi.org/10.1579/0044-7447(2007)36[3:MEAHEI]2.0.CO;2

Mitchell, A., Balwin B.S.(1998). Effects of desiccation/oxidation on the potential for bacterially mediated P release from sediments. Limnol. Oceanogr. 43(3), 481-487 https://doi.org/10.4319/lo.1998.43.3.0481

Molot, L.A., Schiff, S.L., Venkiteswaran, J.J., Baulch, H.M., Higgins, S.N., Zastepa, A., Verschoor, M.J., Walters, D. (2021). Low sediment redox promotes cyanobacteria blooms across a trophic range: implications for management. Lake and Reservoir Management 37, 120–142. https://doi.org/10.1080/10402381.2020.1854400

Moore, B.C., Cross, B.K., Beutel, M., Dent, S., Preece, E., Swanson, M. (2012). Newman Lake restoration: a case study Part III. Hypolimnetic oxygenation. Lake and Reservoir Management, 28(4), 311–327. https://doi.org/10.1080/07438141.2012.738463

Morse, J.W., Luther III G.W. (1999). Chemical influences on trace metal-sulfide interactions in anoxic sediments. Geochimica et Cosmochimica Acta 63(19/20), 3373–3378 https://doi.org/10.1016/S0016-7037(99)00258-6

Mosley, L.M. (2015). Drought impacts on the water quality of freshwater systems; review and integration. Earth-Science Reviews 140, 203–214. https://doi.org/10.1016/j.earscirev.2014.11.010

Munger, Z.W. (2016). The Sources and Cycles of Iron and Manganese in Surface Water Supplies. Virginia Polytechnic Institute. [dissertation/Ph.D thesis][Virginia(VA)]: Virginia Tech.

Payne, A.E., Demory, ME., Leung, L.R. et al. (2020). Responses and impacts of atmospheric rivers to climate change. Nat Rev Earth Environ 1, 143–157. https://doi.org/10.1038/s43017-020-0030-5

Peterson, B.D., Poulin, B.A., Krabbenhoft, D.P., Tate, M.T., Baldwin, A.K., Naymik, J., Gastelecutto, N., McMahon, K. (2023). Metabolically diverse microorganisms mediate methylmercury formation under nitrate-reducing conditions in a dynamic hydroelectric reservoir. ISME J 17, 1705–1718. https://doi.org/10.1038/s41396-023-01482-1

Poulin, B.A., Tate, M.T., Ogorek, J., Breitmeyer, S.E., Baldwin, A.K., Yoder, A.M., Harris, R., Naymik, J., Gastelecutto, N., Hoovestol, C. and Larsen, C. (2023). Biogeochemical and hydrologic synergy control mercury fate in an arid land river-reservoir system. Environmental Science: Processes & Impacts 25(5). 912-928. https://doi.org/10.1039/D3EM00032J

Regnell, O., Watras, C.J. (2019). Microbial Mercury Methylation in Aquatic Environments: A Critical Review of Published Field and Laboratory Studies. Environ. Sci. Technol. 53, 4–19. https://doi.org/10.1021/acs.est.8b02709

Robertson, D.M., Imberger, J. (1994). Lake Number, a Quantitative Indicator of Mixing Used to Estimate Changes in Dissolved Oxygen. Int. Revue ges Hydrobiol. 79(2), 159-176. https://www.researchgate.net/publication/263990847

Robertson, E.K., Roberts, K.E., Burdorf, L.D.W., Cook, P., Thamdrup, B. (2016). Dissimilatory Nitrate Reduction Regnell to Ammonium Coupled to Fe(II) Oxidation in Sediments of a Periodically Hypoxic Estuary: DNRA Coupled to Fe(II) Oxidation. Limnology and Oceanography 61 (1), 365–81. https://doi.org/10.1002/lno.10220.

Rysgaard, S., Risgaard-Petersen, N., Niels P., Kim, J., Lars Peter, N. (1994). Oxygen regulation of nitrification and denitrification in sediments. Limnol. Oceanogr. 39, 1643–1652. https://doi.org/10.4319/lo.1994.39.7.1643

Schlesinger, Willliam, H. (1997). Biogeochemistry: an anaysis of global change. Second Edition. Elsevier Science. p 234.

Seelos, M., Meraz, E.R., Beutel, M.W., Traina, S.J., Furhmann, B., Burmistrova, J., Vlassopoulos, D., O'Day, P.A. (2021). Evaluation of Manganese Oxide Amendments for Mercury Remediation in Contaminated Aquatic Sediments. ACS EST Eng. 1, 1688–1697. https://doi.org/10.1021/acsestengg.1c00267

Søndergaard, M., Jensen, J.P., Jeppesen, E. (2003). Role of sediment and internal loading of phosphorus in shallow lakes. Hydrobiologia 506–509, 135–145. https://doi.org/10.1023/B:HYDR.0000008611.12704.dd

Ullrich, S.M., Tanton, T.W., Abdrashitova, S.A. (2001). Mercury in the Aquatic Environment: A Review of Factors Affecting Methylation. Critical Reviews in Environmental Science and Technology 31, 241–293. https://doi.org/10.1080/20016491089226

United States Environmental Protection Agency (USEPA). (1996). Method 1669: Sampling Ambient Water for Trace Metals at EPA Water Quality Criteria Levels.

United States Environmental Protection Agency (USEPA). (2001). Method 1630: methyl mercury in water by distillation, aqueous ethylation, purge and trap, and CVAFS. EPA-821-R-01–020. Washington, D.C.

United States Environmental Protection Agency (USEPA). (2002). Method 1631, revision E: mercury in water by oxidation, purge and trap, and cold vapor atomic fluorescence spectrometry. EPA-821-R-02–019. Washington, D.C

United States Environmental Protection Agency (USEPA). (2023). Climate Impact on Water Utilities. https://www.epa.gov/arc-x/climate-impacts-water-utilities

Watras, C.J. (2009). Mercury pollution in remote freshwater lakes. In Likens, G. (eds), Encyclopedia of Inland Waters. Elsevier, New York: 100–109. https://www.researchgate.net/publication/274699049_Mercury_Pollution_in_Remote_Freshwaters

Wang, T., Zhao, D., Liu, J., Zhang, T., Wang, X., Liu, T., Lui, B. Lui, Y. (2023). Effects of Abiotic Mineral Transformation of FeS on the Dynamic Immobilization of Cr(VI) in Oxic Aquatic Environments. Science of the Total Environment 894, 164-991. https://doi.org/10.1016/j.scitotenv.2023.164991.

Western Regional Climate Center. (2023). Hodges Dam, California, Period of Record Precipitation (1940 to 1962). https://wrcc.dri.edu/cgi-bin/cliMAIN.pl?ca4014

Wolthers, M., Charlet, L., van Der Linde, P., Rickard, S., van Der Weiden, C.H. (2005). Surface chemistry of disordered mackinawite (FeS). Geochimica et Cosmochimica Acta. 69(14), 3469–3481. http://doi.org/10.1016/j.gca.2005.01.027

World Weather Online. (2023). Lake Hodges, San Diego Annual Weather Precipitation (2010-2020). https://www.worldweatheronline.com/fishing/lake-hodges-san-diego-weather-averages/california/us.aspx

Zak, D., Kleeberg, A., Hupfer, M. (2006). Sulphate-mediated phosphorus mobilization in riverine sediments at increasing sulphate concentration, River Spree, NE Germany. Biogeochemistry 80(2), 109–119. https://doi.org/10.10

Table 1-1. Thermodynamic sequence for reduction of inorganic substances by hydrogen at pH 7.0 and 25°C

Reaction	**Eh (mV)**	**ΔG^b**
Reduction of O_2 $O_2 + 4H^+ + 4e^- \leftrightarrow 2H_2O$	812	-29.9
Reduction of NO_3^- (denitrification) $2NO_3^- + 6H^+ + 6e^- \leftrightarrow N_2 + 2H_2O$	747	-28.4
Reduction of Mn^{4+} to Mn^{2+} $MnO_2 + 4H^+ + 2e^- \leftrightarrow Mn^{2+} 2H_2O$	526	-23.3
Reduction of Fe^{3+} to Fe^{2+} $Fe(OH)_3 + 3H^+ + e^- \leftrightarrow Fe^{2+} + 2H_2O$	-47	-10.1
Reduction of SO_4^{2-} to H_2S $SO_4^{2-} + 10H^+ + 8e^- \leftrightarrow H_2S + 4H_2O$	-221	-5.9
Reduction of CO_2 to CH_4 $CO_2 + 8H^+ + 8e^- \leftrightarrow CH_4 + 2H_2O$	-244	-5.6

Modified from Schlesinger, W. Second Edition (1997, p234). Calculated from Stumm and Morgan (1981, p459)

[b] Kcal/mole- e^-, assuming coupling to the oxidation reaction;

$\frac{1}{4}CH_2O + \frac{1}{4}H_2O \rightarrow \frac{1}{4}CO_2 + H^+ + e^-$, and $\Delta G = -RT\ln(K)$

Table 1-2. Average bottom water quality at station A and B for pre-oxygenation years 2017-2019 and post-oxygenation years 2020-2021.

		2017		2018		2019		2020		2021	
Parameter		**A**	**B**	**A**	**B**	**A**	**B**	**A**	**B**	**A**	B
Ammonia, mg-N/L	CSD		2.5 ± 1.2		3.2 ± 2.5		3.0 ± 1.6	0.22	0.25 ± 0.17	0.2	0.13 ± 0.07
	UCM	1.9 ± 1.2	1.9 ± 0.9	4.3 ± 3.1	2.8 ± 1.2	2.4 ± 1.6	2.1 ± 1.2			0.05 ± 0.2	0.01 ± 0.14
Nitrate, mg-N/L	CSD		0.1 ± 0.2		0.1 ± 0.1		0.3 ± 0.3	0.22	0.51 ± 0.76	0.16	0.13 ± 0.1
	UCM	0.1 ± 0.06	0.03	ND	ND	0.05 ± 0.02	0.03 ± 0.01			0.32 ± 0.2	0.23 ± 0.1
Phosphate, mg-P/L	CSD		0.8 ± 0.5		0.5 ± 0.2		0.1 ± 0.04	0.22	0.39 ± 0.07	0.9	0.7 ± 0.12
	UCM	0.5 ± 0.1	0.5 ± 0.05	1.0 ± 0.33	0.7 ± 0.1	0.5 ± 0.14	0.8 ± 0.1			0.10 ± 0.04	0.13 ± 0.07
Iron, mg/L	CSD		0.1 ± 0.02		0.1 ± 0.03		0.1 ± 0.02	0.19	0.21 ± 0.12	0.1	0.4 ± 0.3
	UCM	0.1 ± 0.02	0.1 ± 0.02	0.05 ± 0.03	0.04 ± 0.03	0.03 ± 0.01	0.3 ± 0.01			0.17 ± 0.09	0.17 ± 0.12
Manganese, mg/L	CSD		0.5 ± 0.1		0.8 ± 0.2		1.1 ± 0.3	0.18	0.16 ± 0.05	0.31	0.23 ± 0.09
	UCM	0.5 ± 0.1	0.5 ± 0.08	0.9 ± 0.1	0.6 ± 0.2	0.8 ± 0.3	0.7 ± 0.2			0.27 ± 0.4	0.13 ± 0.1
Total Hg, ng/L	UCM	3.4 ± 0.9	3.8 ± 0.4	1.4 ± 0.2	1.1 ± 0.2	2.1 ± 1.4	1.7 ± 0.3			0.58 ± 0.3	0.53 ± 0.3
Methyl-Hg, ng/L	UCM	1.4 ± 0.4	1.5 ± 0.5	0.2 ± 0.07	0.3 ± 0.09	0.4 ± 0.3	0.5 ± 0.2			0.04 ± 0.01	0.05 ± 0.01
Sulfate, mg/L	UCM	162 ± 13.2	159 ± 7.1	60 ± 10.5	65 ± 8.22	168 ± 17.7	175 ± 16.1			104 ± 24.3	140 ± 86.6
Sulfide, mg/L	UCM	3.7 ± 3.9	2.9 ± 2.4	14.6 ± 8.7	10.3 ± 5.3	11.5 ± 0.3	5.4 ± 4.5			ND	ND
DOC, mg/L	UCM	10.4 ± 0.9		9.3 ± 0.36	9.7 ± 0.8					8.62 ± 0.23	

Notes: The values represent the average plus/minus standard deviation from May to September of the bottom waters. Data from City of San Diego (CSD) and UC Merced (UCM). For UCM

data, bottom waters are considered the deepest three depths sampled (n ~15). For CSD data, bottom waters were collected weekly at station B (n ~20). For CSD data in 2020 and 2021, bottom waters were collected one week in July at station A. ND is not detected. DOC is dissolved organic carbon.

Table 1-3. Surface water quality during summer months, May to September, for pre-oxygenation years 2017-2019 and post-oxygenation year 2021.

	2017		2018		2019		2021	
Parameter	**A**	**B**	**A**	**B**	**A**	**B**	**A**	**B**
Total Chl, µg/L	61 ± 19 (n=5)	74 ± 16 (n=5)	66 ± 40 (n=4)	73 ± 32 (n=4)	92 ± 52 (n=5)	145 ± 101 (n=5)	29 ± 11 (n=5)	37 ± 3 (n=5)
Total Chl mass, g/m^2	0.52		0.58		1.03		0.24	
Total P, mg/L	0.14 ± 0.03 (n=5)	0.15 ± 0.02 (n=5)	0.29 ± 0.08 (n=4)	0.26 ± 0.02 (n=4)	0.21 ± 0.03 (n=5)	0.19 ± 0.04 (n=5)	0.11 ± 0.02 (n=5)	0.11 ± 0.01 (n=5)
Sechi Disk, cm	74 ± 18 (n=5)		67 ± 20 (n=4)	62 ± 16 (n=4)	110 ± 99 (n=5)	100 ± 102 (n=5)	70 ± 22 (n=5)	
Geosmin, ng/L		ND (n=9)		35 (n=18)		18 (n=31)		ND (n=28)

Notes: Values are means, except for geosmin values which are medians, and sample size is noted in parentheses. For chlorophyll and total phosphorus, surface waters represent the average from 0-9 m deep at station A, and from 0-6 m deep at station B. For chlorophyll mass, before oxygenation was considered 0-9 m, after oxygenation (2021) was considered all the water column. ND is not detected.

Table 1-4. Internal nutrient loading average values for pre-oxygenation years 2017-2019.

Parameter	2017	2018	2019
Heat exchange coeff. (V_t), cm/d	1.23	1.39	1.59
Vertical Diffusion Coefficient (Et), cm^2/s	0.0028	0.0030	0.0030
Phosphate, mg-P/m^2·d	11	40	61
Ammonia, mg-N/m^2·d	53	150	168
Manganese, mg/m^2·d	10	38	71
Nitrate mg-N/m^2·d	-56	0	-27
Methylmercury, ng/m^2·d	39	7	16

Notes: Values calculated using a mass transport equation based on the heat-accumulation method described by Chapra (1997); see methods for more details. Values are average of monthly rates estimated for May to August (n=4) for 2017 and 2019, and for May to July (n=3) for 2018 due to missing sampling date.

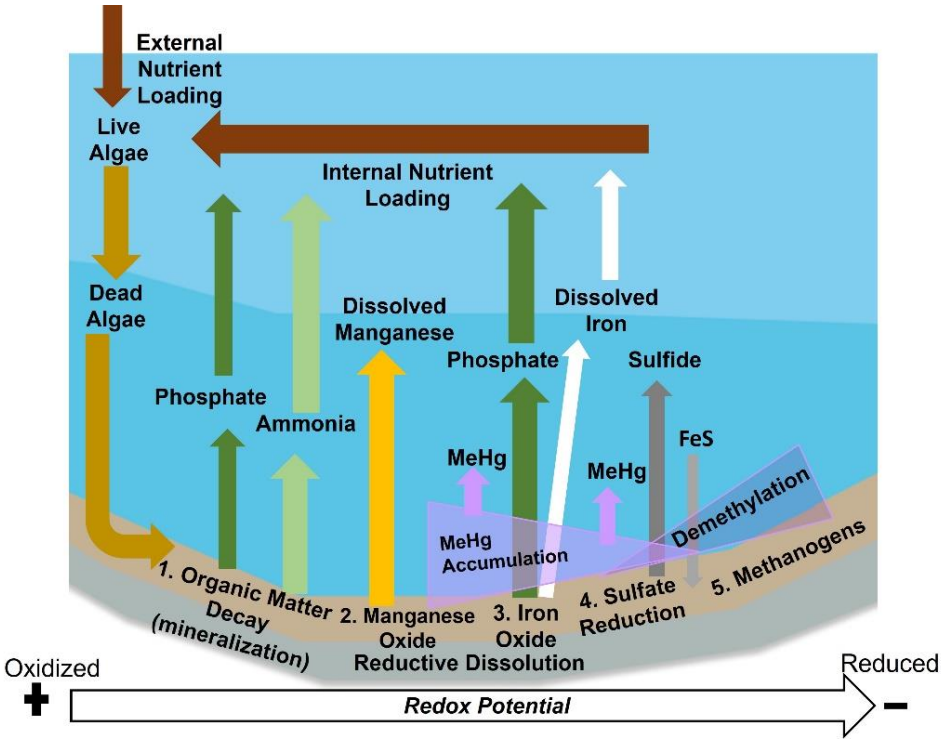

Figure 1-1 Anoxic biogeochemical processes at the sediment-water interface in reservoirs. External nutrient loading leads to sediment accumulation and decay of organic matter, which can release ammonia (light green) and phosphate (dark green) via mineralization. As sediments become mildly reduced metal oxides undergo reductive dissolution, resulting in manganese (yellow), iron (white) and phosphate (dark green) release. These processes lead to internal nutrient loading. Under reduced conditions sulfide is released (dark grey) and can precipitate with iron (light grey). Toxic methylmercury (MeHg) (purple) tends to be released under mildly reduced conditions but lost under highly reduced conditions.

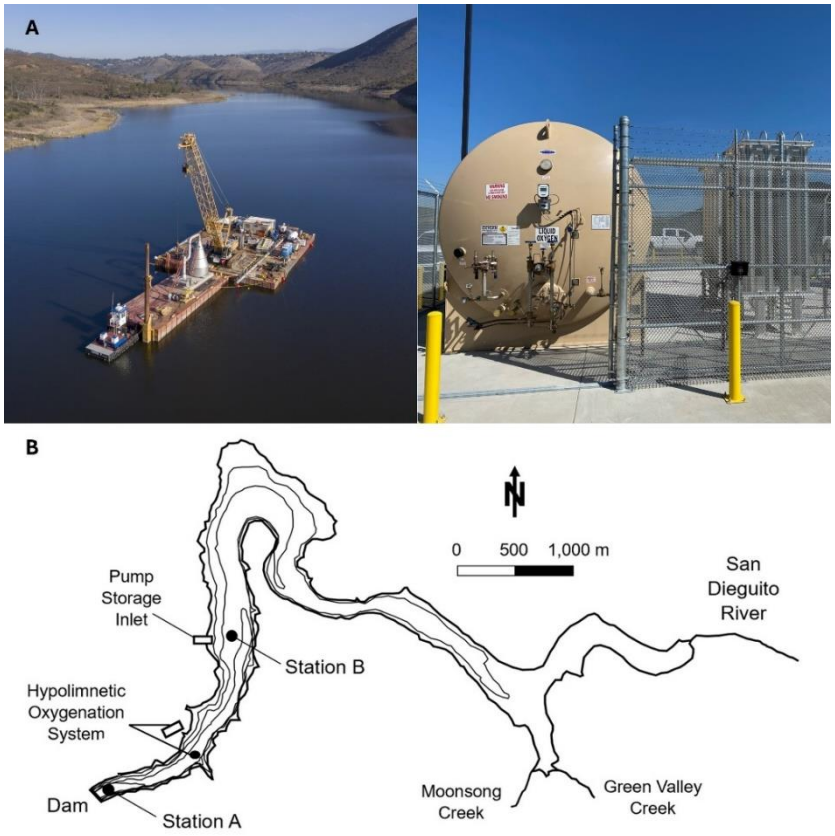

Figure 1-2 (A) Picture of the oxygenation cone on construction barge before being submerged (left), and on-shore facilities including liquid oxygen storage tank and evaporators (right). Photo credit: City of San Diego. (B) Map of Hodges Reservoir, showing the two sampling stations A and B, location of the pumped storage system, and location of the hypolimnetic oxygenation system. Contours are every 5 m and mapped water surface elevation is of ~91 m. Modified from Beutel et al. (2020).

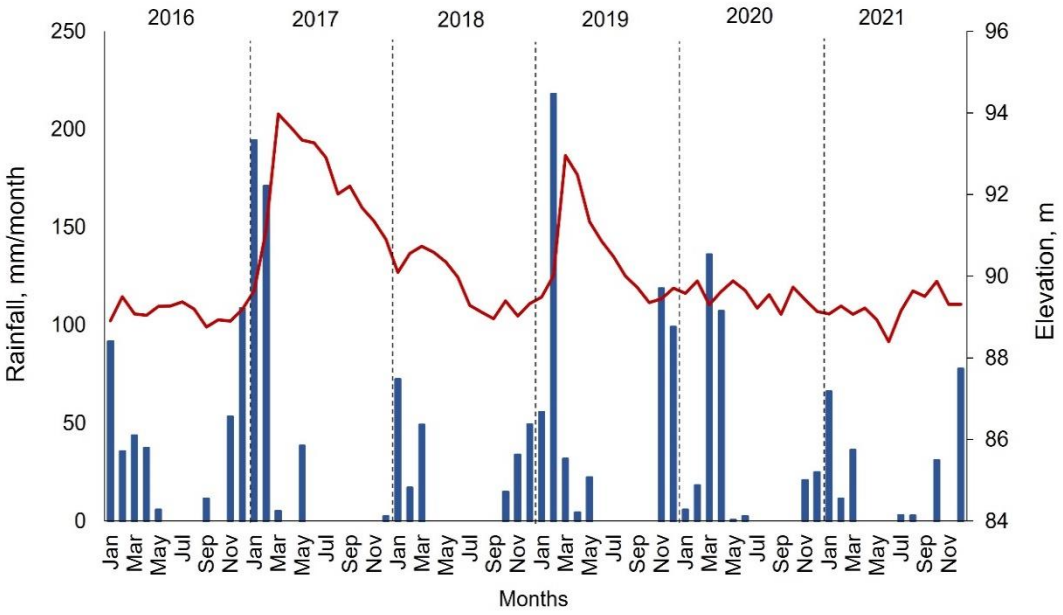

Figure 1-3 Monthly rainfall (blue bars) and surface elevation (red line) in Hodges Reservoir from 2016-2021. Data collected monthly by the City of San Diego. Rainfall represents calculated values based on an evaporation pan measurement that is scaled to the surface area of the reservoir.

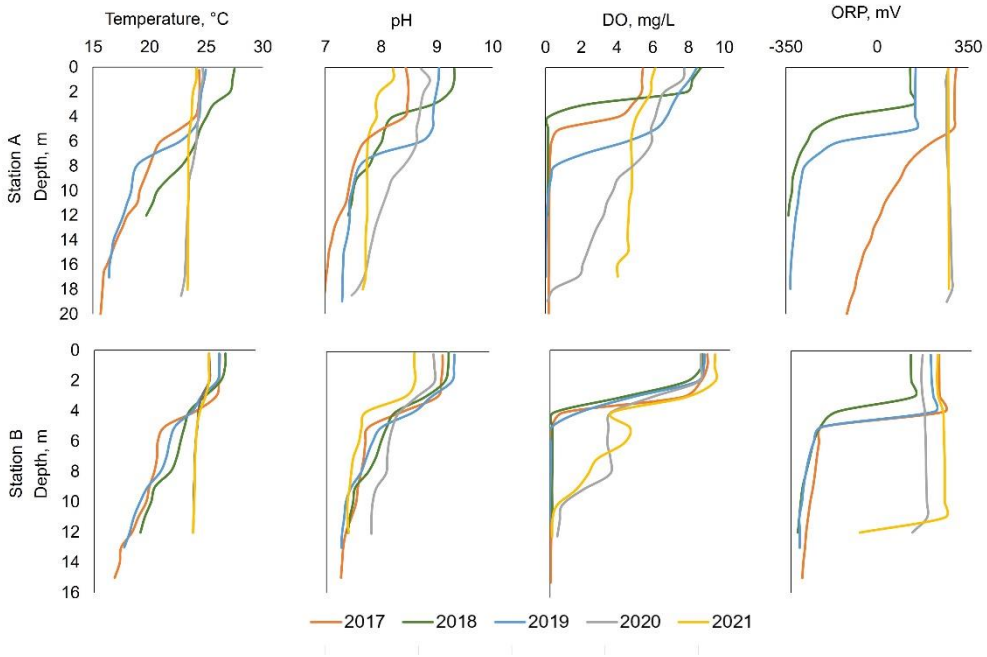

Figure 1-4 Summer (July or August) profiles at stations A and B from left to right: temperature, pH, dissolved oxygen (DO), and redox potential (ORP). Oxygenation occurred during 2020 and 2021. Note that in 2018 at station A data were only collected to a depth of 12 m.

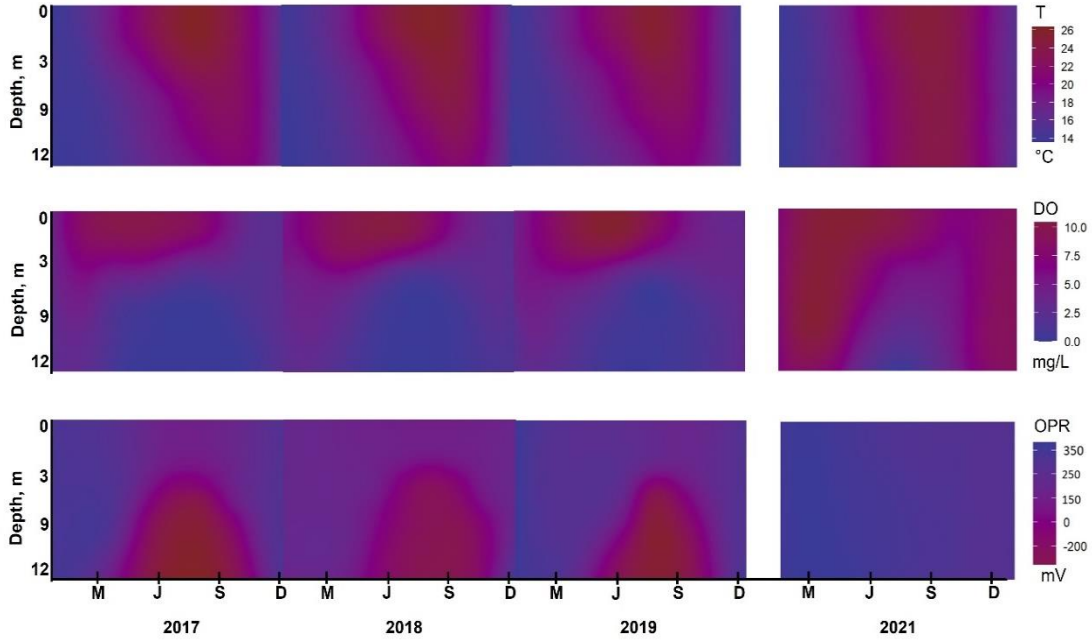

Figure 1-5 Water quality isopleths for temperature (T), dissolved oxygen (DO) and redox potential (ORP) at station B during 2017-2019 and 2021. The isopleths were calculated as an annual interpolation of weekly data collected by the City of San Diego from January through December to a depth of 12 m using RStudio. Note actual elevation of reservoir varied between years; see text for details.

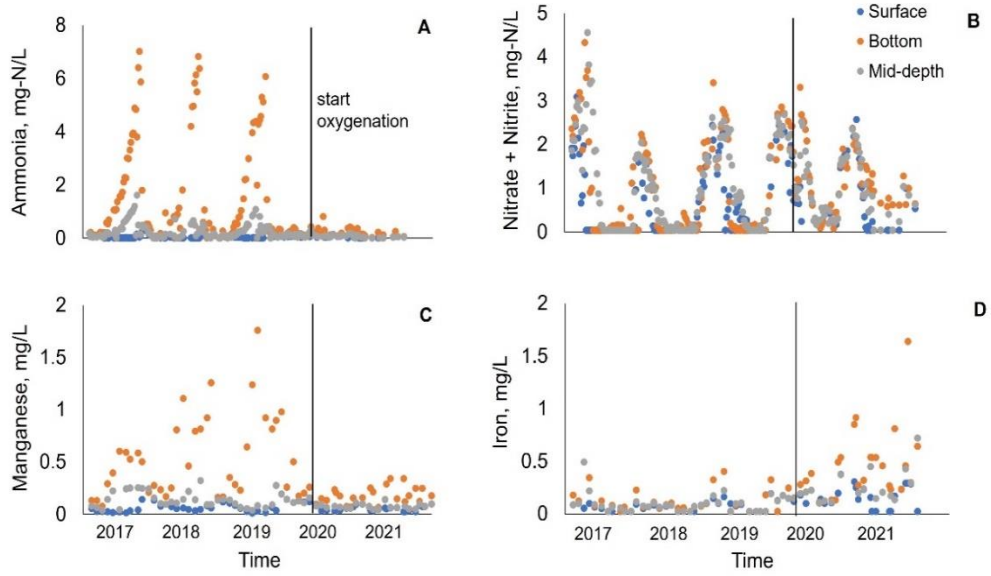

Figure 1-6 Water quality parameters of ammonia (A), manganese (B), nitrate + nitrite (C), and iron (D) at station B for 2017-2021. Data collected by the City of San Diego from January to December at three different depths: surface, bottom, and mid-depth.

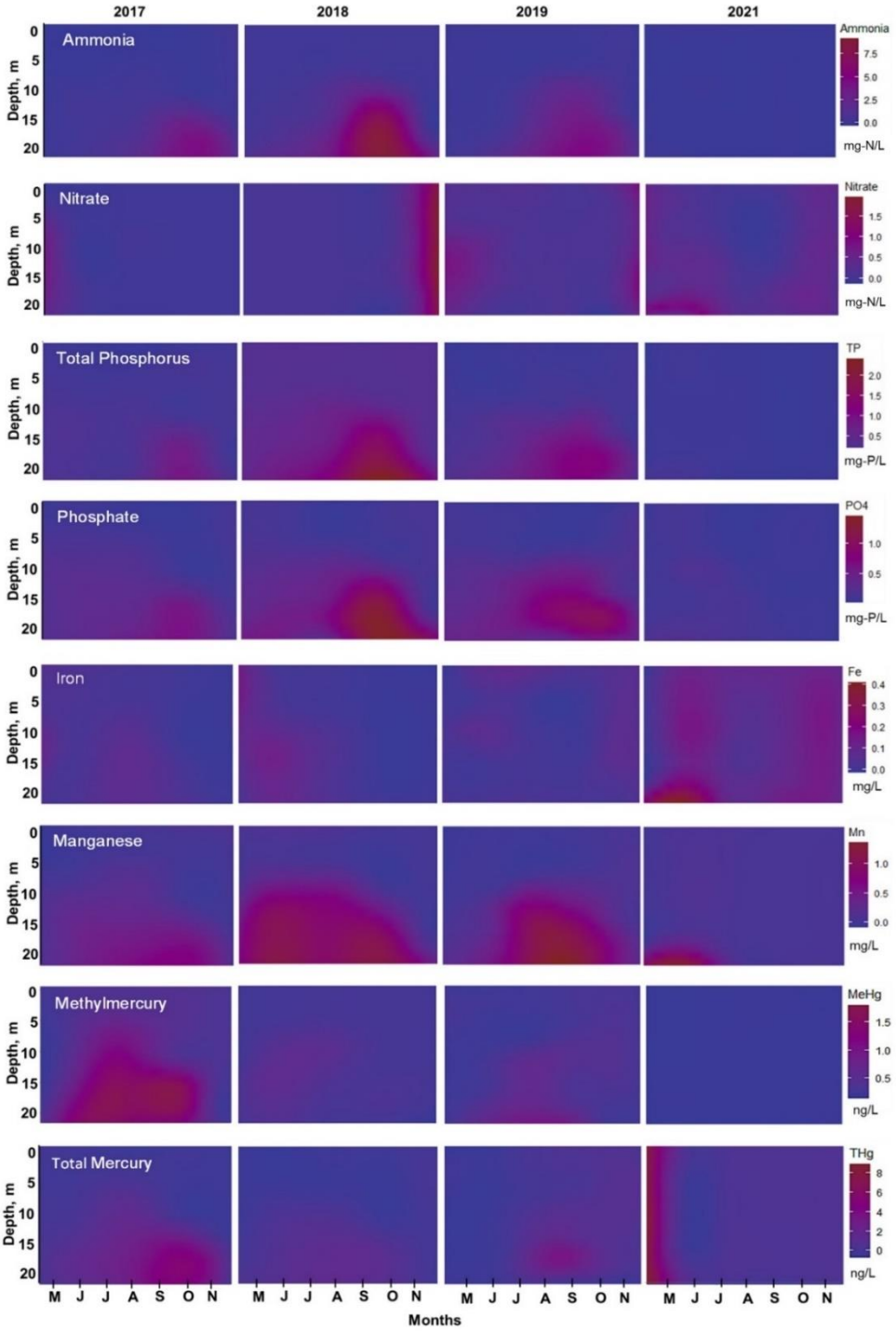

Figure 1-7. Water quality isopleths at station A, from top to bottom: ammonia, nitrate, total phosphorus, phosphate, iron, manganese, methylmercury, and total mercury for 2017-2019, and 2021. Data collected monthly by UC Merced at 3-m-deep intervals April through November and interpolated to a depth of 20 m using RStudio. Note actual elevation of reservoir varied between years; see text for details.

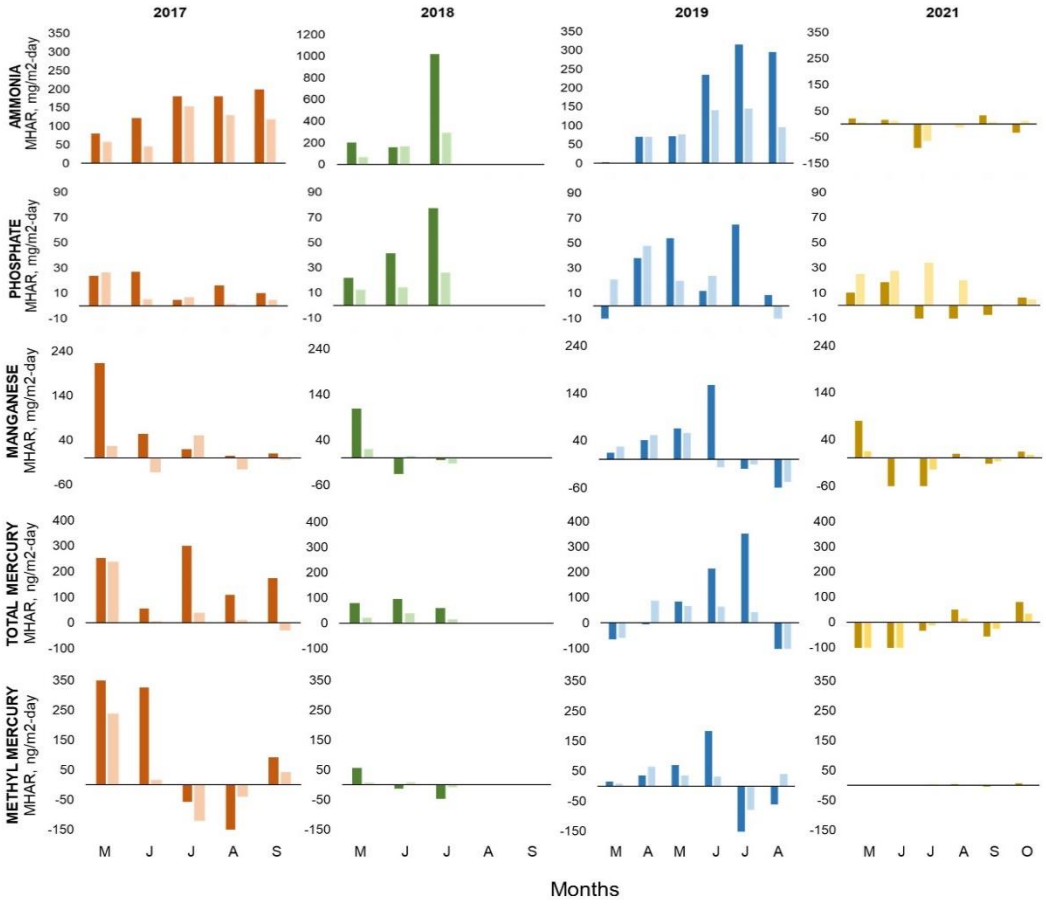

Figure 1-8 Monthly Hypolimnetic Accumulation Rate (MHAR), top to bottom: ammonia, phosphate, manganese, total mercury, and methylmercury at station A (bright color) and B (light color) during 2017, 2018, 2019 and 2021. Data used for the calculation were collected monthly by UC Merced at 3-m-deep intervals from April through November.

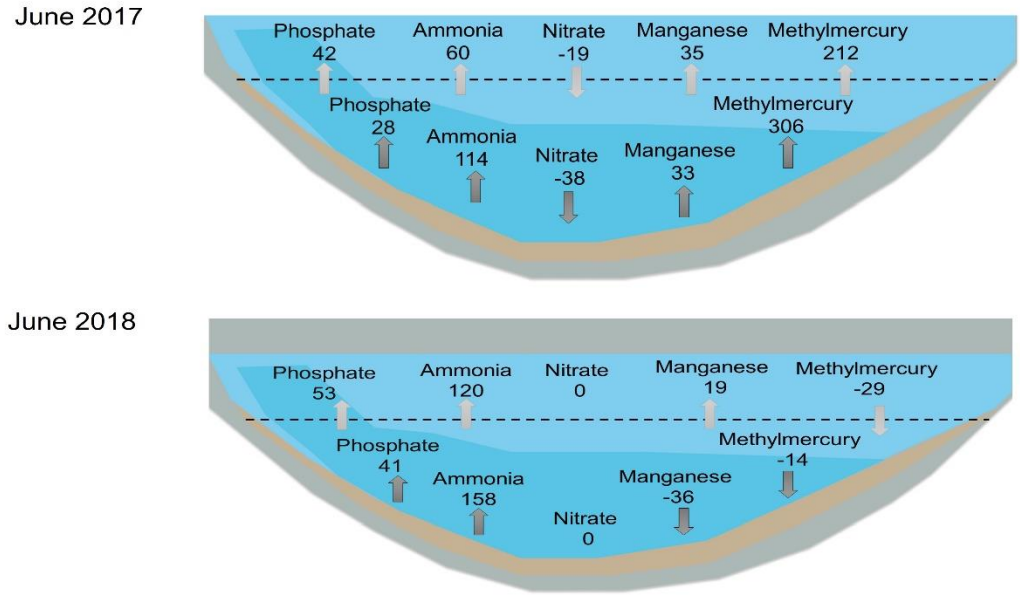

Figure 1-9 Example estimates of hypolimnetic accumulation (dark grey) and mass transfer across the thermocline (i.e., internal nutrient loading) (light grey) for the month of June for 2017 (top) and 2018 (bottom). Units are $mg/m^2 \cdot d$ except for methylmercury which is $ng/m^2 \cdot d$. Note reservoir was substantially smaller in volume in 2018. From left to right: phosphate, ammonia, nitrate, manganese, and methylmercury. Dashed line represents thermocline. Data used for the calculations were collected monthly by UC Merced at 3-m-deep intervals from April through November.

2. MERCURY CYCLING IN COAGULANT-TREATED WETLAND SOILS UPON REWETTING: A CONTROLLED LABORATORY INCUBATION

2.1 Abstract

Negative health effects of methylmercury (MeHg) on wildlife are prime factors of concern in the Sacramento-San Joaquin Delta. The Cache Creek Settling Basin (CCSB), California, USA, was designed to trap sediment from discharging to the Yolo Bypass which ultimately drains into the Delta. Cache Creek drains a highly erodible landscape with numerous sources of mercury (Hg) leading to elevated Hg loading to downstream habitats. To enhance Hg retention within the basin, the United States Geological Survey studied the use of the coagulants ChitoVan (organic/shell amino-based), Ferralyte (ferric-sulfate), and Ultrion, (polyaluminum-chloride) in CCSB. The present study used lab-scale soil-water incubations to assess concerns about the coagulant-treated wetland soils releasing absorbed substances and/or enhancing MeHg production after rewetting with and without the addition of organic matter (OM). Under rewetted conditions without OM added, MeHg levels remained low in water (0.12±0.06 ng/L) and soil (1.2±0.04 µg/kg dw) despite coagulant treatment. The incubations reached oxidation-reduction potential levels associated with nitrate and manganese reduction, conditions not typically associated with Hg methylation. OM addition resulted in depressed oxidation reduction potential and a short-lived burst of MeHg production peaking at day 4 (32.79±0.05 ng/L in water, and 7.31±0.4 µg/kg dw in soil) in coagulant-treated and control soils, followed by a rapid decrease in water and soil MeHg after day 4, which occurred before sulfate disappeared on day 8. The increase in MeHg was likely due to enhanced microbial activity and increased inorganic mercury bioavailability associated with the addition of the OM, whereas the decrease was likely due to demethylation being favored under more reducing conditions. Sulfide buildup and high molecular weight dissolved OM may have also suppressed Hg methylation by decreasing inorganic Hg bioavailability. Patterns of inorganic Hg concentration in water mirrored those of MeHg, with peak concentrations of 77.5±0.12 ng/L during day 2. Results indicate that rewetted coagulant-treated soils are not a source of MeHg, unless under elevated OM loading. OM addition appeared to stimulate microbial activity and generate an ephemeral window of MeHg production. Thus, managing OM loading could potentially limit net MeHg production and bioaccumulation in wetland settings like CCSB.

2.2 Introduction

Mercury (Hg) is a significant threat to both terrestrial and aquatic ecosystems. Key anthropogenic Hg sources include abandoned Hg, gold and silver mines, fossil fuels combustion, Hg recycling facilities, and chemical production facilities for bleach, plastics, chlor-alkali processes, electronics, and lighting

(Eckley et al., 2020). Once Hg is released, it can be transported through the atmosphere and deposited on the land and water either as Hg gas or inorganic Hg (IHg) forms (Driscoll et al., 2013). Anthropogenic emissions exceed natural emission by sevenfold, significantly impacting Hg deposition (Sonke et al., 2023). In wetlands, lakes, and reservoirs, the conversion of IHg to methylmercury (MeHg) by microorganisms is the primary process of concern (Hsu-Kim et al., 2013; Ullrich et al., 2001). Because MeHg is a neurotoxin that bioaccumulates and biomagnifies in aquatic food webs, it poses a health risk to wildlife and humans. Accordingly, over 80% of marine and freshwater fish sampled by the Global Fish and Community Mercury Monitoring Project contained elevated Hg concentrations based on the U.S. Environmental Protection Agency (USEPA) reference dose (Evers et al., 2013). In California, half of rivers and lakes are placed under fish consumption advisories (SWRCB, 2017a). Thus, there is a global need to control MeHg generation and accumulation in the aquatic ecosystems (Eckley et al., 2020)

The production and accumulation of MeHg depends on several site-specific and interrelated environmental conditions. Two important factors are the activity of microbes capable of IHg methylation and the bioavailability of IHg in the environment (Peterson et al., 2023; Poulin et al., 2023; Ullrich et al., 2001). Most commonly, sulfate-reducing bacteria (SRB) (Campeau and Bartha, 1985; Gilmour et al., 1992) and iron-reducing bacteria (FeRB) are associated with MeHg production (Fleming et al., 2006; Kerin et al., 2006). However, in freshwater ecosystems methylating archaea and microbes across the full environmental oxidation-reduction (redox) potential spectrum have been identified with hgcAB genes capable of methylating Hg (Regnell and Watras, 2019; Sonke et al., 2023). The bioavailability of IHg depends on its association with chemical ligands and its partitioning between dissolved and solid phases. MeHg production has been associated with dissolved IHg sulfide (HgS) species with neutral charge, nanoparticles HgS species, and IHg complexes with thiols (Benoit et al., 2001; Graham et al., 2012; Schaefer et al., 2011; Tian et al., 2021; Zhou et al., 2017). However, the bioavailability of the Hg-complexes to microbes may differ among microbial consortia (Sonke et al., 2023).

Furthermore, the bioavailability of IHg and the activity of Hg-methylating microbes are affected by redox potential, pH, concentrations of sulfate, sulfide, iron, and chloride, and the quality and quantity of dissolved organic matter (DOM) (Bigham et al., 2016; Frohne et al., 2012). For instance, in the oxic/anoxic boundary layer and in anoxic waters with circumneutral pH, obligate anaerobe microbes can take up bioavailable IHg and produce MeHg (Frohne et al., 2012; Ullrich et al., 2001). Likewise, high DOM content can be associated with high methylation rates by stimulating microbial activity via labile organic carbon as an electron donor for metabolism (Mazrui et al., 2016; Schuster et al., 2008). DOM can also facilitate or inhibit bacterial uptake for Hg methylation by the formation of Hg-DOM complexes. For example, IHg bound to low molecular weight thiol-groups of the DOM are commonly associated with MeHg production, while high

molecular weight DOM binding with IHg may inhibit Hg methylation (Miller, 2006; Ravichandran, 2004). This highlights the crucial role of Hg-DOM complexation for Hg transformation and transportation (Wang et al., 2022). Consequently, the adsorption of Hg-DOM complexes, including binding to soils and sediments through coagulation and flocculation, ion exchange, and adsorption, is expected to be the principal mechanism for Hg removal and MeHg production control in high DOM ecosystems (Babel et al., 2003; Henneberry et al., 2011).

The net balance between Hg methylation and MeHg demethylation ultimately determines the concentration of MeHg in the environment (Helmrich et al., 2022). Soil and sediments of wetlands, lakes, and reservoirs, in addition to being suitable for Hg methylation, also serve as hotspots for MeHg demethylation (Oremland et al., 1995; Pak and Bartha, 1998). There are two biotic demethylation pathways: 1) reductive demethylation by aerobic microorganisms with the mer gene system, which may be used to detoxify their environment, and 2) oxidative demethylation, an anaerobic co-metabolic process in which SRB and methanogens oxidize MeHg to form IHg and carbon dioxide and/or methane (Barkay and Gu, 2022; Du et al., 2019; Marvin-DiPasquale et al., 2000). Demethylation may also occur abiotically in surface waters via photochemical degradation, for which terminal products are still not clear (Du et al., 2019; Klapstein and O'Driscoll, 2018).

In this context, our study focuses on the Cache Creek Settling Basin (CCSB), a wetland like environment in California, USA, used to capture and retain sediment in Cache Creek before it discharges into the Yolo Bypass. Cache Creek drains an area of naturally elevated Hg soils and wastes from historic mining operations. The trapping of the sediment also serves to capture this particulate Hg, leading to the CCSB being named in two total maximum daily load (TMDL) regulations (Cache Creek, Delta MeHg) to limit Hg transport and its impact on the biologically sensitive downstream Sacramento-San Joaquin Delta (California Water Boards, 2022). To enhance Hg capture and retention in CCSB, the U.S. Geological Survey (USGS), in cooperation with USEPA, assessed the use of different coagulants (ChitoVan, an organic/shell amino-based coagulant; Ferralyte, a ferric-sulfate-based coagulant; and Ultrion, a polyaluminum chloride-based coagulant) at the bench and field scale. Coagulation with metal-based salts, through the association with oxyhydroxides-DOM and flocculation, increases particle size, resulting in higher settling velocities and better retention of suspended material and associated metals (Henneberry et al., 2011; Stumpner et al., 2015). Several studies have identified coagulation as a potential management practice to improve Hg retention in contaminated wetlands (Henneberry et al., 2016; Henneberry et al., 2012; Bachand et al., 2019; Diaz Arriaga et al., 2023; Lv et al., 2012; Mangold et al., 2014; Weerasooriya et al., 2006). However, Stumpner et al. (2015) detected that a portion of the floc can solubilize upon rewetting, resulting in MeHg liberation if soil is subjected to dry/wet cycles. Hence, there is

some concern about the potential for coagulant-treated wetland soils to liberate absorbed substances and increase net Hg-methylation after rewetting in CCSB.

Our study evaluated the potential for the three coagulant-treated soils, sourced from the USGS field experiment, to liberate or produce MeHg under rewetted and deoxygenated conditions in comparison to untreated control soil. We conducted 16-day laboratory incubations and monitored THg in water, and MeHg in water and soil. Additionally, we examined other aqueous compounds including manganese, iron, aluminum, sulfate, dissolved organic carbon (DOC), ammonia, and phosphate to identify additional environmental concerns and provide insights into the underlying Hg-methylation processes. A secondary aim of our study was to evaluate the potential of coagulant-treated soils to release MeHg under typical Hg-methylating conditions. We performed an additional "stress test" incubation in which algal-derived OM (spirulina powder) was added at the beginning of the incubation. We hypothesized that ChitoVan- and Ultrion-treated soils would retain Hg better under standard rewetting conditions compared to the control soil, because of their perceived lack of sensitivity to reducing conditions based on their respective chemical compositions. Conversely, we anticipated that upon rewetting Ferralyte-treated soil would release more Hg, DOM, and sulfate, to the solution phase with the potential to enhance subsequent MeHg production. This information is important in confirming that coagulation is an environmentally sound management practice to enhance Hg capture in managed aquatic ecosystems like CCSB.

2.3 Methods

2.3.1 Site Description and Sample Collection

CCSB, located in the Sacramento Valley, was designed to trap sediment from the Cache Creek watershed (Fig. 2-1). While the CCSB is effective at trapping particulate Hg, it is a net MeHg source to the Delta (Wood et al., 2010). Samples for this study were collected from mesocosms receiving four treatments (3 different coagulants and one control) located in three replicate groups (A, B, C) (Fig. 2-2). The coagulants included ChitoVan^{TM} (Dungeness Environmental, Everett, WA, USA), Ferralyte®8131 (NALCO, Naperville, IL, USA), and Ultrion^{TM} 8186 (NALCO, Naperville, Ill.). One mesocosm (A3-ChitoVan) was lost over the course of the field experiment during storm flows. An additional sample for ChitoVan was collected from group B to balance the statistical design of the incubation data analysis. Soil samples were collected during 2018 and stored refrigerated in sealed plastic bags. The bags were subsampled in 2020 and transported to UC Merced (UCM) under refrigerated and dark conditions. Water for the incubations was collected from Cache Creek at the Rumsey gaging station (USGS site 11451800) in May-June of 2021.

2.3.2 Soil Characterization

The soils were homogenized in the UCM lab and passe through a size 10 sieve. Then, we collected two subsamples of 50 g of soil in falcon tubes for soil characterization. One subsample was shipped to the USGS laboratories to analyze for tin-reducible reactive Hg (R-Hg), as well as a limited number of THg and MeHg analyses for inter-laboratory quality control comparison. The other subsample was analyzed at UCM using standard methods for water content, percentage lost on ignition (LOI), total Hg (THg), MeHg, R-Hg with thiol extraction method, and total iron, aluminum, and manganese. See supplemental material (Table S1) for details of analytical methods.

2.3.3 Incubation Experiments

The laboratory incubations were divided into two experiments, rewetting under nitrogen gas atmosphere conditions, or “standard test”, and rewetting under nitrogen gas atmosphere conditions with OM addition (spirulina powder), which we called the “stress test.” Food-grade Spirulina was purchased from Micro Ingredients brand (Montclair, CA, USA). Spirulina powder was the chosen type of OM after testing soil-water systems response to acetate-pyruvate and acetate-pyruvate-sulfate addition in select soils. Results from these pre-incubations showed no MeHg accumulation in water or soil after 10 days, suggesting the system might need a more natural and complex source of bioavailable carbon.

The standard test had three incubation sets (groups A, B, C) that included the three treated soils and the control soil at six points in time: 0, 1, 2, 4, 8, and 16 days, with a total of 87 bottles, including 12 randomly selected replicates, and one bottle blank (water with no sediment). The stress test had a total of 28 bottles: 24 bottles (four treatments at six time points) from group C, three random replicates, and one bottle blank. The incubation replicates were individual bottles developed to assess replicability of experimental incubations. The incubation replicates and original incubations typically had a relative percent difference of less than 10% for the range of parameters assessed (see Table S2). We also prepared a soil-free control incubation (designated W+SP) that included 0.5 g of spirulina powder in 200 mL of Cache Creek water. Note, spirulina powder was assessed for THg and amounted to less than 0.15 ng of Hg being added to the incubation bottle.

The incubation preparation for both sets of experiments (standard and stress test) included 50 g of each treated soil and the control in individual 250 ml Teflon bottles. We placed the bottles inside a nitrogen gas atmosphere glove box for two days to promote initial deoxygenated conditions. For the stress test experiments, 0.5 g of spirulina powder was added to the bottles with soil before placing them inside the glove box. The spirulina addition was equivalent to approximately twice the total OM concentration measured in the soil based on LOI measurements (Table 2-1). Cache Creek water was also deoxygenated by bubbling with the

nitrogen gas atmosphere of the glove box. After deoxygenation, 200 g of water was added to the bottles with soil inside the glove box. The bottles were closed and vigorously shaken forming a slurry before taking them outside the glove box. The incubation bottles were placed on their side on a shaker table at 150 RPM at room temperature (~20 ^{o}C) and covered with aluminum foil to mimic dark conditions until the sampling day.

On each sampling day, select bottles were placed in the centrifuge at 12,000 RPM and 22°C for 40 minutes to separate water from solids. The water and soil of each bottle incubation were then destructively sampled. Clean, calibrated probes (HACH HQ40d multi meter, HACH MTC10101 ORP probe, Loveland, CO) were used to measure pH and redox potential in the supernatant water inside the glove box. Redox potential values were converted to the standard hydrogen electrode (Eh) following the Nernst equation temperature correction (Nordstrom and Wilde, 2005). The supernatant water was filtered with pre-combusted 0.3 µm glass-fiber filters. For THg and MeHg analysis, 80 ml of water were directly filtered into a trace-metals clean fluorinated polyethylene bottle (Nalgene) and preserved with trace-metal-free grade hydrochloric acid (0.4% v/v). For DOC characteristics assessment, 30 ml of water were filtered directly into 50 ml falcon tubes, refrigerated, and shipped on ice within 2-3 days of sampling to the USGS for analysis. For the other analytes, 10 ml of filtered water was poured into 15 ml falcon tubes. One falcon tube was for iron, aluminum, and manganese, which was preserved with 1% v/v of nitric acid, and a second tube was for nutrients and anions (no acid addition), which was frozen. Soil samples were frozen and then freeze dried for later analysis.

2.3.4 Water and Sediment Analyses

While briefly described here, see Table S1 and Table S2 in Appendix for details of analytical methods, including detection limits and quality control metrics. Water samples from both experiments were analyzed for filtered THg and MeHg, total metals (iron, aluminum, and manganese), nutrients (ammonia, nitrate plus nitrite, and phosphate), anions (sulfate and chloride), and DOC characteristics (DOC, $SUVA_{254}$). THg analysis was performed on a MERX-T (Brooks Rand Instruments, Seattle, WA, USA) using cold vapor atomic fluorescence spectroscopy (CVAFS) based on the method 1631 (USEPA, 1994). Samples for MeHg analysis were distilled (2 h at 125°C with nitrogen gas flow of less than 50 ml/min) before being measured on a MERX-M (Brooks Rand Instruments, Seattle, WA, USA) using ethylation, gas chromatography and CVAFS based on the method 1630 (USEPA, 1998). Hg analyses followed strict quality control standards including method blanks, matrix spikes (MS/MSD), analytical duplicates, and ongoing procedure recovery (OPR). Average MS/MSD and OPR samples were inside 75-125% range, and the method blanks were <0.1 ng/L. Batches that did not meet these criteria were rerun and/or flagged. We analyzed

metals using inductively coupled plasma optical emission spectrometry (ICP-OES) on an Optima 5300 DV (USEPA,1994). Nutrients were analyzed on a LACHAT QuikChem 8500 autoanalyzer using standard colorimetric methods by air-segmented continuous-flow absorption spectrophotometry (Antweiler et al., 1996). Phosphate was measured as soluble reactive phosphorus via reagent addition to filtered water samples. Anions were measured at the USGS Microbial Biogeochemistry Laboratory (Earth System Processes Division, Menlo Park, CA) via ion chromatography (USEPA, 1993). DOC and optical properties analyses were analyzed at the USGS Organic Matter Research Laboratory (Sacramento, CA). Total DOC concentration was measured using high-temperature combustion total organic carbon analyzer (Model TOC-VCHS; Shimadzu Scientific Instruments, Columbia, Maryland) according to USEPA method 415.3 (Potter and Wimsatt, 2009). Optical properties characterization was performed on an Aqualog® Spectrofluorometer (Horiba Scientific, Edison, New Jersey) using methods outlined in Hansen et al. (2016).

For soils, THg before incubation experiments was analyzed on a Milestone Direct Mercury Autoanalyzer (DMA 80) via thermal decomposition, amalgamation, and atomic absorption spectrometry, based on method 7473 on dry weight basis (USEPA 2007). MeHg analysis of soil was performed before incubation experiments, and in standard and stress tests. MeHg was extracted from ~0.2 g of homogenized, freeze-dried soil followed by digestion with 2.5 ml of 25% KOH in methanol (USEPA, 1996). Micro-aliquots of digestant were then analyzed for MeHg in water as detailed above, excluding the distillation step. THg and MeHg soil analyses also followed strict quality control standards including method blanks, MS/MSD, analytical duplicates, certified reference material checks, and OPRs. Inter-laboratory comparisons of soil characterization between UCM and the USGS Microbial Biogeochemistry Laboratory (Earth System Processes Division, Menlo Park, CA) yielded a relative percent difference of 14.8% (n = 4) for soil THg, and 1.4% (n = 4) for soil MeHg. “Reactive” Hg (R-Hg) in soil before incubation experiments was measured at the USGS Microbial Biogeochemistry Laboratory (Earth System Processes Division, Menlo Park, CA) following the USGS tin reduction of Hg(II) method (Marvin-DiPasquale and Flanders, 2007). We also analyzed R-Hg at UCM following the thiol extraction method by the addition of 1 mM of glutathione in 1 g of soil and 10 ml of Cache Creek water during 30 min (Ticknor et al., 2015). Total acid extractable iron (Fe_{TAE}), manganese (Mn_{TAE}) and aluminum (Al_{TAE}) were measured in 0.25 g of freeze-dried soil using microwave digestion (Method 3052) in acid (concentrated HNO_3 and HCl) followed by filtration and ICP-OES analysis as noted above (USEPA, 1996). Measurement of soil-extractable iron was measured in a two-step sequential extraction based on the USGS method (Marvin-DiPasquale, 2020). The acid extractable iron (Fe_{AE}) fraction (0.5 M HCl) targeted dissolved and surface-bound Fe(II) and Fe(III), and amorphous Fe(III) hydroxides. The citrate/dithionite-extractable iron (Fe_{DE}) fraction targeted major iron-oxide minerals and amorphous iron-silicates, but not crystalline silicate minerals. From the same extraction fluids

measured for total Fe, we measured aluminum (Al_{AE}) and manganese (Mn_{AE}) in the acid extractable and dithionite-extractable (Al_{DE}, Mn_{DE}) fractions by ICP-OES. Results are presented in dry weight basis as the least square mean ± standard error of the three mesocosms and treatments, including the control (mean, n = 11) in Table 2-1.

2.3.5 Statistical Analysis

Statistical analyses were developed in RStudio (version 4.3.3). When necessary to meet the assumptions of normality, concentrations/masses were log-transformed before applying the models. For statistical analysis purposes, ChitoVan data included two incubations groups labeled as B, since A samples were not available. Soil characterization statistical analyses used the statistical packages for Linear Mixed Effects (LME) model (nlme, lme4 and lmerTest) with the method of restricted maximum likelihood (REML). For the model, we designated Treatments (control, ChitoVan, Ferralyte, Ultrion) and mesocosms Groups (A, B, C) as fixed effects. Mesocosm Groups were also considered as random effects to account for variability in the soil. Significant differences were compared using one-way analysis of variance type II (ANOVA) with a significance level set at $p < 0.05$. Additional Tukey honestly significant difference pairwise post-hoc test (Tukey HSD) results were determined using package emmeans for Treatments, Groups, and Treatments x Groups as correlated factors with a $p < 0.05$. The initial conditions statistical comparison between standard and stress test during day 0 and soil or Cache Creek water from characterization analysis used the Welch two sample t-test comparing the means with n=4.

Data from the standard test, in which treatments were run in triplicate, were analyzed using LME model with the method of REML. In this analysis, Treatments and Days were fixed effects and were also treated as correlated fixed factors (Treatments x Days). In addition, to account for variability, mesocosm Groups were designated as random effects. To determine significant differences among the multiple compounds analyzed, results were compared using one-way analysis of variance type III (ANOVA) with a significance level set at $p < 0.001$. Least square means were estimated using lsm() function with a confidence interval of 95% and degrees of freedom estimated with method Satterthwaite.

For the stress test comparison (one incubation set prepared with mesocosm group C) against standard test group C, we used the LME model with the method of REML. The model included Test (standard and stress), Treatments, Days of incubation, and Test x Day as fixed factors. As Treatment in the standard incubation demonstrated minor differences, we included this variable also as the random effect. Least square means were estimated using lsm() function with a confidence interval of 95% and degrees of freedom estimated with method

Satterthwaite. To compare the significant difference, we used one-way analysis of variance type III (ANOVA) with a significance level set at $p < 0.001$. Additional Tukey HSD results were determined for Test x Day, as correlated factors, with a $p < 0.05$. The interaction term helped evaluate any significant interaction between day and stress test incubation not always seen in the standard test.

2.4 Results

2.4.1 Soil Characterization

During the soil characterization, soils showed no statistical difference among mesocosm groups or treatments (Table 2-1). Soils had a mean water content of 15.9 ± 3.3% (mean plus/minus standard error, n = 11) and a LOI of 0.52% ± 0.06. THg concentration was 299 ± 23.7 µg/kg and MeHg was 2.19 ± 0.26 µg/kg, with MeHg representing on average 0.72% of THg. Tin extractable "reactive" Hg averaged 10.3 ± 1.0 µg/kg, while glutathione extractable "reactive" Hg averaged 14.5 ± 3.1 µg/kg. This suggests that 3-7% of THg in the soil is potentially bioavailable, but the high variability in the glutathione extractable "reactive" Hg complicates the interpretation of the metric. Total iron (Fe_{TAE}) in microwaved, acid-digested samples averaged 39.5 ± 5.7 g/kg. Acid-extractable Fe (Fe_{AE}) averaged 4.5 ± 0.2 g/kg and citrate-dithionite-extractable Fe (Fe_{DE}) averaged 11.8 ± 0.4 g/kg. The average value for Al_{TAE} was 30.8 ± 0.9 g/kg soil, Al_{AE} was 1.9 ± 0.09 g/kg, and Al_{DE} was 1.6 ± 0.1 g. Finally, total manganese (Mn_{TAE}) showed average values of 0.95 ± 0.06 g/kg, with 0.43 ± 0.03 g/kg for Mn_{AE} and 0.48 ± 0.04 g/kg for Mn_{DE}. Ultrion-treated soils and Ferralyte-treated soils did not show an enrichment in any of the aluminum fractions or iron fractions, respectively, compared to control soils. This was to be expected as the dosing rates for the coagulants were a fraction of background levels measured in soils.

2.4.2 Incubation Experiments

2.4.2.1 Inorganic Mercury and Methylmercury

For the standard incubation, Hg in solution (Fig. 2-3) and Hg in the solid phase (Fig. 2-4), generally did not show any dramatic changes during the standard incubation (Table 2-3 and S3). During day 0, water MeHg concentration was higher (0.16 ± 0.04 ng/L, n = 4) compared to levels measured in filtered Cache Creek water used for the incubations (0.06 ± 0.02 ng/L, n = 3), though the differences were not significant ($t_{(4)}$= -2.08, p=0.11) (Table 2-2). MeHg concentration in solution (Fig. 2-3A) decreased during the 16 days ($F_{5,46}$ =7.03, $p < 0.001$, Table 2-3), especially from day 0 to 4 (from 0.12 ± 0.04 ng/L to 0.041 ± 0.04) (Table S3). For IHg in the solution phase, during day 0, concentrations were statistically significantly higher (13.2 ± 0.03, n = 4) than filtered Cache Creek water (average of 4.95±1.4 ng/L, n = 4) used to make the slurries ($t_{(6)}$= -4.63,

p=0.01, n = 4) (Table 2-2). Over the course of the standard incubation, IHg in the water (Fig. 2-3B) decreased with incubation time ($F_{5,46}$ =10.12, $p < 0.001$, Table 2-3) and the changes in concentration were significant in day 1, and 4 to 16, decreasing from 12.38 ± 0.71 on day 0 to 6.41 ± 0.71 on day 16 (Table S3). IHg concentration in water was also significantly different among treatments ($F_{5,46}$ = 3.05, $p < 0.04$, Table 2-3), with the control being higher (10.06 ± 0.59 ng/L) than the coagulant treatments (Table S3). In addition, group C ($F_{2,46}$ = 14.11, $p < 0.001$, Table 2-3) resulted in lower IHg in water concentration with 6.31 ± 0.71 ng/L compared to the other two groups, A and B (Table S3).

Also in the standard test, MeHg:THg ratio (Fig. 2-3C) showed significant differences among treatments, groups, and days (Table 2-3). MeHg:THg ratio values increased after day 4 ($F_{5,46}$ = 5.26, $p < 0.001$, Table 2-3), and the differences in MeHg:THg ratio were statistically significantly higher in group C and in the control soil (0.01 ± 0.01) (Table S3). Finally, % MeHg mass in solution of the total MeHg mass (soil plus water) (Fig. 2-3D) in the incubations typically accounted for only 0.02±0.005% (Fig. 3-3D). The % mass of MeHg solution decreased with incubation time ($F_{5,46}$ = 4.43, $p < 0.01$, Table 2-3) with 0.072 ± 0.03% on day 0 to 0.031 ± 0.03% on day 16 (Table S3). For the soil phase, MeHg concentration in treatments and the control at day 0 (1.10 ± 0.03 µg/kg dw, n = 4) was lower than values measured during the soil characterization (2.32 ± 0.03 µg/kg dw, n = 3) prior to the experiment ($t_{(5)}$= 8.9, p=0.0003) (Table 2-2). MeHg mass in soil (Fig. 3-4A) did not show a statistically significant difference among treatments, group, days, nor interaction during the 16-day incubation (Table 2-3, Table S3). However, the Log k_d value (L/kg) (Fig. 2-4B) increased with incubation time ($F_{5,46}$ = 5.00, $p < 0.001$, Table 3-3) with higher values during day 4 and 16 (4.22 ± 0.02) (Table S3).

Compared to the standard test, Hg cycling showed significant differences in the stress test, with the addition of OM to the soils and water with incubation time (Fig. 2-3E-H, Table 2-4). IHg and MeHg in water through incubation days were three orders of magnitude greater than those observed in the rewetting incubation (F_{33} = 13.58, $p < 0.001$; F_{33} = 95.36, $p < 0.001$; respectively, Table 2-4, S6). Additionally, MeHg (0.26± 0.13) and IHg (17.99±0.05) concentrations in water during day 0 were significantly higher compared to Cache Creek water characterization ($t_{(4)}$= -4.02, p=0.01, and $t_{(6)}$= -4.39, p=0.008, respectively) (Table 2-2). In general, MeHg and IHg concentrations in solution increased rapidly in the first two to four days of incubation (Table S7), peaking at around 33.8±0.13 ng/L for MeHg at day 4 and 77.5±0.12 ng/L for IHg (107.5±0.13 ng/L for THg) at day 2 (Fig. 2-3E-F, Table S6, S7). The increase was short-lived as MeHg and IHg concentrations started to decrease after day 2 to 4, approaching the initial concentrations by day 8 (Fig. 2-3E-F; Table S6, S7). Following day 8, MeHg and IHg concentrations decreased more slowly, although changes in concentration between day 8 and 16 were not significant (Table S7). The treated soils seem to show higher concentrations of IHg in water compared to the control, particularly

for the Ferralyte treatment, during day 1 to 2 of the incubation. However, as the incubations did not have a replication set, the statistical analysis was not possible. MeHg:THg ratio in water increased after day 1 to 0.36±0.03 by day 4, coincidental with the accumulation of relatively high concentrations of MeHg in water, then decreased to 0.28±0.03 on day 8, and remained quasi-steady for the remainder of the incubation (Fig. 2-3G, Table S6, S7). Lastly, %MeHg in water of total MeHg mass in incubation showed a significant temporal pattern peaking at 2.04±0.02% on day 2, decreasing by day 16 to 0.88±0.02% (Fig. 2-3H, Table S6, S7).

In the soil of the stress test, MeHg mass (Fig. 2-4C) followed a similar pattern as in the water with significant differences with incubation time compared to the standard test ($F_{33} = 3.89$, $p < 0.001$, Table S6, S7). Initial (day 0) MeHg concentration in soil (3.45±0.04 µg/kg dw) was higher ($t_{(4)} = -4.51$, $p=0.01$) than values measured during the soil characterization (2.31±0.02 µg/kg dw), as well as those observed in the soil in the initial standard test incubations (1.10±0.01 µg/kg dw) on day 0 ($t_{(4)} = -8.86$, $p=0.0006$) (Table 2-2). MeHg in the soil had a significant increase by day 4 to a concentration of 7.31±0.4 µg/kg (Table S6). Then, the concentration significantly decreased to 3.12±0.4 µg/kg through day 16, returning to near initial conditions (Table S6, S7). The log MeHg k_d value (L/kg) significantly dropped from 4.12±0.08 to 2.47±0.08 on the first two days when MeHg concentration in water significantly increased (Fig. 2-4D, Table S6, S7). Values then leveled off at 3.01±0.08 after day 8 as water MeHg decreased relative to soil MeHg (Table S6, S7).

2.4.2.2 Aqueous Parameters: Redox Potential, pH, Manganese, and Sulfate

Redox potential, pH, manganese, and sulfate were monitored as primary indicators of microbial activity in the incubations (Fig. 2-5). In the standard incubation, the decrease in redox potential (Eh) (Fig. 2-5A) was significant ($F_{5,46} = 4.76$, $p < 0.01$, Table 2-5), over the 16-day period, especially for day 4, decreasing from 330 ± 0.49 mV at day 0 to 51.4 ± 0.5 mV at day 4 (Table S4). On the contrary, changes in pH were not significant (Table 2-5), decreasing from 8.24 ± 0.004 on day 0 to 7.84 ± 0.01 on day 16 (Table S4). Manganese (Fig. 2-3C) increased steadily over time ($F_{5,46} = 21.27$, $p< 0.0001$, Table 2-5), changing from 0.14 ± 0.05 mg/L on day 4 to 1.26 ± 1.46 mg/L on day 16 (Table S4). Manganese concentration in ChitoVan^{TM} treatment was lower (1.14 ± 0.47) compared to the other treatments ($F_{3,72} = 30.17$, $p < 0.0001$) (Table 2-5, S4). Sulfate (Fig. 3D) concentration changes were not significant throughout the experiment (Table 2-5) with concentrations in the range of 81 ± 0.2 mg/L to 206 ± 0.2 mg/L (Table S4).

For the stress test incubation, OM addition led to the same general patterns for Eh ($F_{33} = 90.97$, $p < 0.001$), pH ($F_{33} = 28.53$, $p < 0.001$), and manganese ($F_{33} = 43.62$, $p < 0.001$), but a greater magnitude than the standard incubation without OM addition (Fig. 2-5E-H; Table 2-6). Eh decreased from 247±8.92 mV at day 0

to –75.3±8.92 mV by day 8 when it leveled out (no statistical differences) (Fig 2-3E; Table 2-6, S8, S9). pH decreased from 8.06 ± 0.03 on day 0 to 6.9 ± 0.03 by day 4 when it leveled out for the remainder of the incubation (Fig. 2-3F, Table S8, S9). In contrast to the incubation without OM added, Mn concentrations in the stress test significantly increased from day 2 (Table S8) and reached 4.74±0.19 mg/L by day 4 before leveling out for the remainder of the incubation (Fig. 2-3G, Table S8, S9). Sulfate concentration, contrary to the standard test ($F_{33} = 272.6$, $p < 0.001$, Table 2-6), significantly decreased from 170.7±1.04 at day 2 to 109.9±1.04 mg/L by day 4 reaching levels below detection on day 8 (Fig. 32-H; Table S8, S9).

2.4.2.3 Aqueous Parameters: Metals, Nutrients, and Dissolved Organic Carbon

Supporting aqueous parameters were also assessed including iron, aluminum, ammonia, nitrate, and phosphate (Fig. 2-6), and DOC and SUVA (Fig. 2-7). In the standard incubation, the concentration of iron in the solution phase (Fig. 2-6A) remained relatively consistent but differences by treatments were statistically significant ($F_{3,72} = 3.44$, $p < 0.05$, Table 2-5). Iron concentration in Ferralyte treatment was higher (0.15 ± 0.03 mg/L) compared to the other coagulant-treated soils and the control (Table S5). Aluminum concentration (Fig. 2-6B) also remained low through the experiment, but differences in treatments ($F_{3,72} = 16.12$, $p < 0.00001$) and days ($F_{5,72} = 19.27$, $p < 0.00001$) were significant (Table 2-5). In the soil with ChitoVan, aluminum concentration was higher (0.11 ± 0.06 mg/L) during day 4 compared to the other treatments (Table S5). Ammonia concentrations (Fig. 2-6C) increased through incubation time for all treatments ($F_{5,46} = 19.27$, $p < 0.00001$, Table 2-5), particularly during the initial eight days of the incubation ($F_{5,46} = 16.12$, $p < 0.00001$, Table 2-5) from 0.18 ± 0.10 mg-N/L to 2.63 ± 0.10 mg-N/L (Table S5). But the shell-based ChitoVan-treated soil displayed the most elevated ammonia concentration 2.71 ± 0.09 mg-N/L (Table S5). Nitrate (Fig. 2-6D) decreased throughout incubation time ($F_{5,46} = 9.44$, $p < 0.00001$, Table 2-5), particularly significant by day 8 (2.86 ± 0.24 mg-N/L on day 0 to 2.51 ± 0.24 mg-N/L on day 8) (Table S5). Finally, phosphate concentration (Fig 2-6E) was relatively stable throughout the incubation; however, phosphate concentration differed among treatments ($F_{3,72} = 15.52$, $p < 0.00001$, Table 2-5) with ChitoVan (1.01 ± 0.08 mg-P/L) and Ultrion (0.9 ± 0.08 mg-P/L) treatments significantly higher (Table S5).

When OM was added to the incubations, iron concentrations increased compared to the standard incubation ($F_{33} = 3.75$, $p < 0.05$, Table 2-6). (Fig. 2-4F). Iron increased from 0.10±0.29 mg/L on day 1 to 2.05±0.29 mg/L on day 4 (Table 2-6, S10, S11). Then, iron concentrations decreased to 1.59±0.29 mg/L on day 8 and had no significant changes by the end of the incubation (Table S10, S11). Among treatments, Ferralyte and Ultrion iron concentrations seemed to be higher than ChitoVan and the control, however, due to the small sample size we could not determine statistical significance or a significant drop from day 8 to 16 (Table 2-

6). For total aluminum (F_{33} =14.84, $p < 0.001$, Table 2-6, S10, S11), the treated soils and the control showed a significant increase in concentration, from 0.02±0.02 mg/L on day 4 to 0.13±0.02 mg/L on day 8 compared to the standard test (Fig. 2-4G, Table S10 and S11). For ammonia, compared to the standard test, the concentration increased steadily from day 0 to 16 (F_{33} =6.03, $p < 0.001$, Table 2-6, S11). Ammonia concentration increased from 0.9±0.02 mg-N/L on day 0 to 73.7 ±0.02 mg-N/L on day 16 (Fig 2-4H, Table S10, S11). Nitrate disappeared after day one in all the treatments, similar to the standard incubation (Fig. 2-4I, Table 2-6). Phosphate concentrations increased steadily starting day 1 through day 8, compared to the standard test (F_{33} =7.81, $p < 0.001$, Table 2-6, S10). Concentrations at day 1 were 1.77±0.9 mg-P/L and increased to 8.73±0.9 mg-P/L by day 16 (Fig. 2-4J, Table S10, and S11). ChitoVan-treated soil seemed to have a higher increase throughout the incubation.

Results for DOC (Fig. 2-5A) in the standard incubation showed concentrations at around 9.56 mg/L to 18.81 mg/L during day 0 (Table S5) with significant differences among treatments ($F_{3,72}$ = 16.72, $p < 0.001$) and group ($F_{2,72}$ = 2.21, $p < 0.001$) (Table 2-5). The control treatment showed higher values (15.64 ± 2.1 mg/L) compared to the coagulant-treated soils, as well as in group B and C (Table S5). DOC concentration also appeared to differ among days, but these results were not statistically significant ($F_{3,72}$ = 2.21, p= 0.06, Table 2-5). For $SUVA_{254}$ (Fig. 2-5B), values increased from 0.31 ± 0.03 on day 0 to 0.35 ± 0.03 on day 16 suggesting a pattern, but differences were not significant (Table 2-5 and Table S5). In the stress test incubation, DOC concentrations at day 0 were double (48.07±13.6 mg/L) compared to the standard test at day 0 (11.15±13.6 mg/L) (F_{33} = 19.35, p= 0.001, Table 2-6, S10, S11). DOC increased from day 0 to 8, peaking at 266.63±13.6 mg/L, then decreased after day 8 to around 84.84±13.6 mg/L for all treatments (Fig. 5C, Table S10, S11). The $SUVA_{254}$ values were similar (1.45±0.04 L/mg-C·m) at day 0 for the stress test and standard test incubations, the differences were significant after day 2 (F_{33} = 19.97, p= <0.001) (Fig. 2-5D; Table 2-6, S10, S11). $SUVA_{254}$ values dropped on day 2 (0.91±0.04 L/mg-C·m), increased on day 4 (1.16±0.04 L/mg-C·m), and dropped again on day 8 (0.86±0.04 L/mg-C·m) (Table S10 and S11).

2.5 Discussion

2.5.1 Rewetting Effect

Contrary to previous studies that show reflooded conditions in soils enhanced MeHg production (Stumpner et al., 2015; Ullrich et al., 2001), the standard incubation showed no net MeHg accumulation after rewetting in any of the treated soils (ChitoVan, Ferralyte, and Ultrion) or the control after 16 days (Table 2-3). However, we saw ammonia accumulation in water throughout the incubation, likely due to OM degradation, while nitrate concentration decreased, suggesting microbial denitrification (Table 2-5, S5; Fig.2-6 C-D). In addition,

water accumulated manganese starting in day 2, likely driven by microbially-mediated reductive dissolution of manganese oxides (Davison, 1993) (Table 2-5, S4; Fig. 2-5C). These results indicate that conditions were not sufficiently reduced to favor iron or sulfate reduction, suspected by the lack of iron accumulation and sulfate consumption (Table 2-5, S4, S5; Fig. 2-5D and 2-6A), which are typically associated with high methylation rates. Instead, the system was slightly lowered from its initial redox state and maintained conditions typically associated with nitrate and manganese reduction (Fig. 2-5A, Table S4):

Reduction of NO_3^- (denitrification)

$$4NO_3^- + 16H^+ + 2CH_2O \leftrightarrow 2N_2 + 10H_2O + 2CO_2$$

Reduction of Mn^{4+} to Mn^{2+}

$$4MnO_2 + 8H^+ + 2CH_2O \leftrightarrow 4Mn^{2+} + 2CO_2 + 6H_2O$$

The fact that soils were in an initially aerated, with elevated levels of oxidized redox-sensitive manganese and iron (Fe_{DE} ~30% and Mn_{DE} ~52%, Table 2-1), likely combined with low levels of labile OM, a key driver of IHg methylation (Beulig et al., 2018; Eckley et al., 2021; Ravichandran, 2004), suppressed the activity of SRB, which have long been considered as the main Hg-methylator organisms (Compeau and Bartha, 1985).

There has been a growing interest in the apparent synergy between nitrate and manganese reduction and MeHg accumulation in aquatic systems, and the possibility that nitrate and manganese-reducing organisms may methylate IHg (Alpers et al., 2014; Balogh et al., 2004; Beutel et al., 2020; Sonke et al., 2023). Despite the identification of nitrate reducers with the *hgc*$_A$+ genes in multiple studies, direct implications in MeHg production have not been established in freshwater environments (Bridou et al., 2018; Peterson et al., 2023; Sonke et al., 2023). However, a possible overlapping of anaerobic microbial processes, such manganese reduction with sulfate reduction, was also acknowledged as potentially responsible for these correlations. In this incubation study, the accumulation of manganese, presumably the result of microbial manganese oxide reduction, and the loss of nitrate, as the result of denitrification, did not correspond with MeHg accumulation, suggesting in CCSB the linkage is not causal (Fig. S1). Other studies have shown the importance of FeRB as main contributors of IHg methylation during mildly redox conditions (Fleming et al., 2006). FeRB mediated rates for Hg methylation appear to be higher in iron-rich systems with labile carbon, low sulfate concentration, and under nonacidic pH (Warner et al., 2003). In our standard incubations FeRB appear to be inactive (Fig. 2-6A, Table S5), even with the high Fe concentration in the soil, since redox potential (205±1.58 mV) was above levels that facilitate high rates of iron reduction (and possible Hg

methylation) (Table S4, Fig. 2-5A) (Tuner and Patrick, 1968; Madigan and Martinko, 2006).

While there was not a substantial increase in MeHg concentration in the standard test experiment, MeHg and IHg in water showed a pattern of initial accumulation followed by loss. The patterns were consistent for the control and the coagulant-treated soils (Fig. 2-3A-B, Table 2-3, S3). This observation was also seen in the increase in MeHg:THg ratio and in the downward trend in the %MeHg in the water (as percentage of total mass of MeHg in soil and water in experimental bottle) (Fig 2-3C-D, Table 2-3, S3). During the initial Hg release to water, IHg concentration in the water is lower in the soils treated with the coagulants compared to the control, suggesting enhanced Hg sorption capacity to the soils treated with coagulates (Table 2-3 and S3). Additionally, ChitoVan-treated soil showed statistically significant higher levels of ammonia in water throughout the incubation in comparison to the control soil and the other treatments (Table 2-5, Fig. 2-6B). Higher ammonia concentration (3.64±0.16 mg/L) after day 8 of the incubation for ChitoVan-treated soil is likely due to ChitoVan's amine-rich composition which includes partial deacetylation of chitin from shells of shrimp and other crustaceans (Table S5). Interestingly, soils treated with aluminum-based Ultrion and iron-based Ferralyte did not show an obvious pattern of aluminum or iron release, not even an initial flush to water, compared to the other treated-soils and the control, likely due to the low solubility of aluminum hydroxides and Fe(III) at circumneutral pH. Still, Ferralyte differences among treatments were significant (Table 2-5 and Table S5).

2.5.2 Key Drivers of Mercury Cycling

Organic matter quantity and quality (composition) are key controllers of Hg cycling in aquatic ecosystems (Frohne et al., 2012). Several studies report a positive correlation between high MeHg concentrations and methylation rates with high OM concentration in aquatic systems (Bigham et al., 2017; Cossa et al., 2014; Gagnon et al., 1997; Ullrich et al., 2001). In addition, studies have shown that soils enriched with algal organic carbon, besides increasing methylation rates, can affect IHg speciation via the release of aromatic, low molecular weight thiols and forming bioavailable Hg-thiol complexes (Peterson et al., 2023; Wang et al., 2023). In our stress test experiment, the addition of OM appeared to stimulate microbial growth, leading to alterations in environmental conditions that promoted MeHg production. Over the course of the first 8 days of incubation, DOC accumulated, and $SUVA_{254}$ values decreased (Fig. 2-7 C-D, Table 2-5), suggesting OM degradation from particulate to dissolved form with preferential loss of the oxidized, aromatic groups possibly fueling microbial activity (Kellerman et al., 2015; Weishaar et al., 2003). Simultaneously, redox potential had rapid and prominent drop indicative of the microbial activity (Fig. 2-5A, Table 2-5, S8). Moreover, the incubations exhibited the accumulation of other compounds associated with anaerobic microbial processes including ammonia, manganese,

phosphate, iron, and the depletion of nitrate (Fig. 2-5G and Fig. 2-6F-J, Table 2-5, S9, S11). Of note is the apparent phosphate release from ChitoVan by the end of the incubation (Fig. 2-4J). A recent review reported high phosphate adsorption capacity for chitosan-based adsorbents/coagulants, but the study noted that desorption patterns are not well characterized (Wujcicki and Kluzczka, 2023). Our results suggest that ChitoVan may release phosphate to surrounding water under highly reduced conditions. Further, MeHg in water and soil had an immediate increase, peaking in concentration during days 2 to 4 as seen with the increase in MeHg:THg ratio (Fig. 2-6G, Table 2-4, S6, S7). Interestingly, during peak production, redox conditions measured in the incubation water were moderately reduced (97±8.92 to 1.34±8.92 mV), higher than values typically associated with activity of SRB (Jones and Ingle, 2005) (Table S8).

High concentrations of MeHg observed with OM stimulation in the stress test incubations could be attributed to the heterogeneity of redox conditions and/or the activity of multiple Hg-methylating microbes. Redox potential could have been lower inside aggregates facilitating SRB activity. Studies in wetland soils report redox processes occurring spatially at the microscale and mesoscale, even when the macroscale redox potential indicates a tendency away from such processes (Alewell et al., 2006; Lacroix et al., 2023). In the stress test incubation, the relatively lower, but significant (Table S9), sulfate concentration during day 2 and 4 suggests some SRB activity despite the redox potential indicating conditions favorable for nitrate and manganese reduction (Fig. 2-3H, Table S8, S9). An increase in labile OM may have also enhanced multiple biogeochemistry cycles, in turn stimulating multiple Hg-methylating bacteria such as FeRB (Ebinghaus et al., 1994; Fleming et al., 2006). This idea is supported by the fact that iron concentration in water, an indicator of FeRB activity (Davidson, 1993), had a significant increase from day 1 to 4 (Fig. 2-6F, Table S11), coincidentally with the rapid rise in water and soil MeHg (Fig. 2-3E and 2-4C, Table 2-5, S7). In addition, studies have shown that iron reducers capable of reducing manganese are also Hg-methylators (Bravo et al., 2018; Peterson et al., 2023). Finally, FeRB and SRB could also contribute to MeHg production via direct interspecies electron transfer between these microorganisms in anaerobic environments. This could suggest that in CCSB soils, SRB may rely on FeRB to degrade more complex organic substrates to more biodegradable fractions, thereby enhancing SRB activity and the production of MeHg (Shi et al., 2016; Yu et al., 2018). Additionally, interactions of SRB with methanogens, as redox potential dropped, could have also contributed to the rise in MeHg. Laboratory research has demonstrated that the interaction of these two organisms increases potential Hg-methylation rates by a factor of 2 to 9 compared to monocultures under low sulfate concentrations (Yu et al., 2018).

Another factor that could contribute to the increase in MeHg concentration under mildly reducing conditions, at least for the water phase, is the reductive dissolution of manganese and iron oxides releasing associated MeHg-DOM (Cossa et al., 2014; Cossa and Gobeil, 2000). Manganese accumulation was significant

started between days 1 to 2, while iron significant accumulation started between days 1 to 4, both concurrent with MeHg buildup in water, day 0 to 4 (Fig. 4G, 3F, and 4C, Table 7, S8, and S10). This process could also account for some of the increase in water IHg concentration during the first two days of incubation (Fig. 3F, Table 6). Although most of the Hg is associated to the soil OM, some Hg-DOM complexes could also be bound with iron- and manganese-hydroxides and clays. Iron and manganese oxides have large surface areas and high capacity to absorb and co-precipitate with Hg-DOM, and to release them during their redox sensitive dissolution (Ullrich, 2001). Clays may also play a role as they have high specific surface area, great adsorption properties for Hg-DOM, and a large potential for ion exchange (Gorski et al., 2013). The release of Hg-DOM complexes from oxyhydroxides and clays may have also favored the increase in IHg bioavailability and promoted MeHg production in the incubations.

2.5.2 Ephemeral Methylation Window

MeHg production in the stress test incubation was short-lived, highlighting the ephemeral nature of MeHg in aquatic sediments (Fig. 2-3E, 2-4C) (Hintelmann et al., 2000). After day 4, MeHg concentration in water and soil decreased (Table 2-4, S6, S7) while still having favorable conditions for MeHg production, including reduced conditions, neutral pH, and ample sulfate (sulfate was not depleted until day 8) (Table S8, S9). From day 8 to 16, changes in MeHg concentration and mass were not significant (Table 2-4, S7). This can be interpreted as the system approaching a quasi-steady state, as seen in other water and sediment incubations (Compeau and Bartha, 1985; Ullrich et al., 2001).

The fact that MeHg decreased in both water and soil, as well as the increase in the log k_d value, indicate that there was a true loss mechanism, as opposed to sorption/desorption processes exchanging MeHg between water and soil phases (Fig. 2-6E-G, Table 2-4, S7). When redox conditions in soil-water systems are reduced to potentials favorable for MeHg demethylation, microbial demethylation can overtake methylation resulting in a negative net MeHg production (Marvin-DiPasquale et al., 2000; Ullrich et al., 2001). In the stress test incubations, when conditions were more oxidized, IHg could be bioavailable, but Hg-methylators like FeRB and SRB had low activity. As redox potential dropped in the presence of ubiquitous iron oxides in soils and moderate sulfate concentrations in water, FeRB and SRB became active. This resulted in a “methylation window” for net MeHg production under mildly reduced conditions in the early days of the stress test incubation. Then, as redox potential continued to decrease, the buildup in sulfide concentration, from high SRB activity, and possibly high molecular-weight DOM could induce low IHg bioavailability via the formation of less bioavailable charged Hg-S complexes and Hg-polysulfide complexes (Poulin et al., 2017; Ullrich et al., 2001; Zhang et al., 2012). Subsequently, the oxidative pattern for MeHg

demethylation could have been favored by certain SRB, FeRB and some methanogens as conditions in the incubation continued to shift towards highly reduced, closing the methylation window (Barkay and Gu, 2022; Fuhrman et al., 2021; Ullrich et al., 2001).

Sulfur species are deeply correlated to SRB activity and IHg bioavailability, thereby limiting or enhancing MeHg production (Ullrich et al., 2001). In the stress test incubation, from day 0 to 8, sulfate was available to stimulate SRB activity, which likely produced MeHg (Figs. 2-3E, 2-4C, and 2-5H, Table 2-4 and 2-6). However, as MeHg accumulation started to decrease in water and soil after day 4, and sulfate concentrations remained relatively high (109.95±1.04 mg/L at day 4) (Table 2-4, 2-6, S7, and S9). It appears that sulfate limitation was not the main mechanism driving the observed decrease in MeHg concentration. Sulfate concentrations of less than around 0.1 mM (~10 mg/L) are generally required to limit SRB activity (Ingvorsen et al., 1981; Ullrich et al., 2001), and such limiting concentrations were not observed in water until around day 8 (Fig. 2-3H, Table 2-6). Nevertheless, the presence of sulfide, a byproduct of SRB activity, may have had an important effect on Hg methylation by inhibiting IHg bioavailability. This could explain the decrease in MeHg after day 4 in water and soil (Fig. 2-3E and 2-4C, Table 2-6 and S9). The decrease in IHg bioavailability could be the result of IHg forming negatively charged disulfide complexes unable to cross bacteria cell membranes (Hsu-Kim et al., 2013; Liem-Nguyen et al., 2017; Regnell and Watras, 2019; Slowey and Brown, 2007). IHg can also precipitate with sulfide producing metacinnabar (β-$HgS_{(s)}$) resulting in a sink for IHg (Poulin et al., 2017):

$$Hg^{2+} + HS^{-} \leftrightarrow HgS_{(s)} \qquad \text{Log k: -38.6}$$

This β-$HgS_{(s)}$ sink could explain the decrease of IHg in water in the stress test incubation after day 4 (Fig. 2-3F; Table 2-4, S6, and S7). Results from PhreeqC 3.6.2 calculations (LLNL database) suggest a very low sulfide concentration (6.1×10^{-6} mg/L) needed for β-$HgS_{(s)}$ precipitation, considering the redox conditions and the concentrations of iron, sulfate, chloride, ammonia, manganese, and IHg in incubation experiments and general water chemistry (calcium, and bicarbonate concentrations) of Cache Creek watershed (Rytuba et al., 2015, USGS Rumsey station). Thus, β-$HgS_{(s)}$ precipitation could be a factor that decreased IHg bioavailability and suppressed MeHg production.

The decrease in iron accumulation in water for Ferralyte-and-Ultrion-treated soils (Fig. 2-6F), starting after around day 6 (Table 2-6, S11), could be also attributed to the presence of sulfide, as iron can be lost from water via precipitation with sulfide as mackinawite (FeS_m):

$$Fe^{2+} + HS^{-} \leftrightarrow H^{+} + FeS(s)$$

Reported solubility products for FeS_m show a pK_{sp} of 2.6-3.8, indicating a high affinity between iron and sulfide (Beutel et al., 2020; Cook, 1984; Murray, 1995; Slowey and Brown, 2007). PhreeqC 3.6.2 calculation (LLNL database) indicates that a low sulfide concentration (0.069 mg/L) was needed for FeS_m precipitation in the incubations (Cache Creek alkalinity data from USGS Rumsey Station). Indeed, an observed lack of obvious sulfide smell (intense putrid odor may have masked sulfide odor) in the incubations suggests that, even with sulfate depletion, sulfide levels remained low. Hence, the decrease in iron concentration in the incubations could also be attributed to other processes, such as Fe(II) sorbing back to the soil oxides and clays possibly associated with DOM (Catruillet et al., 2016; Gu et al., 2019; Zhu et al., 2018). DOC concentrations exhibited a similar decline to iron after day 8, suggesting some sorption into the soil (Fig. 2-7C, Table 2-6, S11). Additionally, another plausible explanation could be the precipitation of iron and phosphate as vivianite (Heiberg et al., 2012; Rothe et al., 2016). Phosphate concentrations (5-15 mg/L) towards the end of the incubation support the possibility of vivianite precipitation with relatively high iron concentrations (1 mg/L) (Fig. 2-6F and 2-6J). Calculations with PhreeqC 3.6.2 yield a vivianite saturation index (SI) of 1.2 (Cache Creek alkalinity data from USGS Rumsey Station). SI (log activity/equilibrium constant) values higher than 0 indicate a thermodynamic tendency for precipitation.

$$2HPO_4^{2-} + 3Fe^{2+} + 8H_2O \leftrightarrow Fe_3(PO_4)_2(H_2O)_8 + 2H^+ \qquad \text{Log k: -4.7}$$

Another possible mechanism for the decrease in MeHg concentration under sulfidic conditions is a proposed demethylation pathway via the abiotic formation of volatile dimethylmercury (DMeHg) (Barkay and Gu, 2022). Marine systems with high MeHg to sulfide ratio can favor the formation of DMeHg (Jonsson et al., 2016; Kanzler et al., 2018; Ullrich et al., 2001). Some experimental data indicates that this reaction may also occur in freshwater systems under high MeHg concentrations, promoting the loss of MeHg from this system (Kanzler et al., 2018). MeHg can apparently react with sulfide to form bis(methylmercuric) sulfide (DMeHg-S). This compound can then degrade into HgS and DMeHg, which is lost from the aqueous phase via volatilization. The stress test incubation appeared to follow the criteria for potential abiotic demethylation, including high MeHg to sulfide ratio and anoxic conditions. Despite the need for further research on freshwater ecosystems, Kanzler et al. (2018) argue that the loss of MeHg from aquatic systems, often attributed to microbial process, may be primarily abiotic in nature.

2.5.3 Initial Changes in Soil Methylmercury

While not a focus of this study, there appeared to be short-term changes in soil MeHg concentration at the very start of our experimental incubations (Table 2-2). In the standard test incubation, MeHg in soil at day 0 was lower compared to initial soil characterization, 1.10± 0.03 µg/kg dw versus 2.32± 0.03 µg/kg dw ($t_{(5)}$=

8.9, p=0.0003,). On the contrary, during the stress test incubation, MeHg in soil was higher, 3.45±0.04 µg/kg dw compared to the standard test, 2.32±0.03 µg/kg dw ($t_{(4)}$= -4.51, p=0.01). Note that "day 0" incubations were not technically sampled until around 2 hours after the initial mixing of soil and water, and in the case of the stress test also the addition of spirulina OM. Mass balance considerations indicate that these changes in soil concentration were not related to gain or loss from the water phase, or through the addition of OM with low THg concentration (~0.3 µg/kg dw). In addition, incubations were managed under low light conditions precluding photo-related reactions. These rapid changes suggest a rapid abiotic process. In the standard incubation, a possible loss mechanism for MeHg in the soil was the solubilization of colloids with high affinity for Hg, including MeHg, which were inadvertently captured on filters during sample filtration. Studies show that colloids play an important role in regulating freshwater partitioning of both IHg and MeHg, especially in Eh ranges from 0-300 mV (Babiarz et al., 2001; Gfeller et al., 2021; Z. Wang et al., 2021). The apparent production of MeHg in the stress test incubations may be related to OM addition and solubilization. Humic compounds in DOM can promote abiotic formation of MeHg from IHg (Celo et al., 2005; Weber, 1993), particularly the hydrophobic basic component in fresh algal-derived DOM (Liang et al., 2024). This suggests a causal link between OM addition and MeHg production upon rewetting in the stress test incubation. Initial rewetted conditions in the stress test with bioavailable DOM and IHg may have also stimulated activity of aerobic/facultative bacteria capable of aerobic methylation as a hypothesized IHg detoxification process (Cao et al., 2021; Xiang et al., 2020).

2.6. Conclusions

Soil-Water laboratory incubations in this study aimed to assess whether coagulant-treated soils produced or released MeHg under rewetted, deoxygenated conditions. This was a concern because coagulant-treated soils could release previously sorbed Hg-DOM complexes after being rewetted. In addition, Ferralyte-treated soil containing sulfate and iron could potentially stimulate Hg methylation. However, the incubations showed little net MeHg release or production with redox potential indicative of mildly reduced conditions (nitrate and manganese reduction) over 16 days. Upon rewetting, the coagulant-treated soils showed better sorption capacity than the control soil, with lower concentrations of IHg in the water phase. However, ChitoVan-treated soil released higher levels of ammonia and phosphate, which could have implications for algae production and water quality.

The stress test incubations showed that the addition of OM at a concentration of around twice that of native soils appeared to stimulate anaerobic bacterial activity, including FeRB and SRB, producing MeHg up to day 4. The pattern was consistent in both coagulant-treated and control soils, suggesting there is not a clear enactment of the coagulant treatments on MeHg production. Initial IHg bioavailability was not the main issue determining MeHg production as it

seems that up to 7% (~21 µg/kg) of the THg in the soil was potentially bioavailable and reactive (based on RHg measurements, Table 2-1), which would have been equivalent to 5.2 µg/L of THg in the water phase (considering 200 ml of water and 50 g of soil). This suggests that the supply and catabolism of labile carbon was a key limiting factor for microbial Hg-methylation activity, as suspected in other studies (Beuling et al., 2018; Peterson et al., 2023).

After day 4, the methylation window closed demonstrating that MeHg production in closed aquatic sediments loaded with OM is short-lived. Low redox conditions and sulfide accumulation likely decreased Hg methylation and possibly enhanced MeHg demethylation, as seen with MeHg concentration decreasing from the water and soil phase. Moreover, low bioavailability of IHg, possibly caused by β-$HgS_{(s)}$ precipitation and/or formation of high molecular weight Hg-DOM complexes under sulfidic conditions, could have also suppressed the production of MeHg. In addition, a possible abiotic demethylation pattern could have also contributed to the decrease in MeHg via the formation of HgS and volatile DMeHg. Hence, it seems that under OM loading, CCSB soils could generate a potential concern for MeHg release, whether or not they are treated with the three coagulants. In the end, results suggest that managing OM loading to CCSB could limit net MeHg production and bioaccumulation.

2.7. References

Ackerman, J. T., Kraus, T. E. C., Fleck, J. A., Krabbenhoft, D. P., Horwath, W. R., Bachand, S. M., Herzog, M. P., Hartman, C. A., and Bachand, P. A. M. (2015). Experimental Dosing of Wetlands with Coagulants Removes Mercury from Surface Water and Decreases Mercury Bioaccumulation in Fish. Environmental Science and Technology, 49(10), 6304–6311. https://doi.org/10.1021/acs.est.5b00655

Alewell, C., Paul, S., Lischeid, G., Küsel, K., and Gehre, M. (2006). Characterizing the Redox Status in Three Different Forested Wetlands with Geochemical Data. Environmental Science and Technology, 40(24), 7609–7615. https://doi.org/10.1021/es061018y

Alpers, C. N., Fleck, J. A., Marvin-DiPasquale, M., Stricker, C. A., Stephenson, M., and Taylor, H. E. (2014). Mercury cycling in agricultural and managed wetlands, Yolo Bypass, California: Spatial and seasonal variations in water quality. Science of The Total Environment, 484, 276–287. https://doi.org/10.1016/j.scitotenv.2013.10.096

Barkay, T., and Gu, B. (2022). Demethylation─The Other Side of the Mercury Methylation Coin: A Critical Review. ACS Environmental Au, 2(2), 77–97. https://doi.org/10.1021/acsenvironau.1c00022

Antweiler, R. C., Patton, C. J., and Taylor, H. E. (1996). Automated, Colorimetric methods for determination of nitrate plus nitrite, nitrite, ammonium, and

orthophosphate ions in natural water samples. U.S.G.S. Report, Report 93, 1–28.

Babel, S., & Kurniawan, T. A. (2005). Various treatment technologies to remove arsenic and mercury from contaminated groundwater: an overview. Proceedings of the Southeast Asian Water Environment, 1.

Babiarz, C. L., Hurley, J. P., Hoffmann, S. R., Andren, A. W., Shafer, M. M., and Armstrong, D. E. (2001). Partitioning of Total Mercury and Methylmercury to the Colloidal Phase in Freshwaters. Environmental Science and Technology 35 (24), 4773-4782. https://doi.org/10.1021/es010895v

Bachand, S.M., Oyewo, O.A., Maity, A. (2019). Aliminium-and iron-based coagulation for in-situ removal of dissolved organic carbon, disinfection byproducts, mercury and other constituents from agricultural drain water. Ecol. Eng. 156

Balogh, S. J., Nollet, Y. H., and. Swain, E. B. (2004). Redox chemistry in Minnesota streams during episodes of increased methylmercury discharge. Environmental Science and Technology 38, 4921–4927

Benoit, J. M., Mason, R. P., Gilmour, C. C., & Aiken, G. R. (2001). Constants for mercury binding by dissolved organic matter isolates from the Florida Everglades. Geochimica et Cosmochimica Acta, 65(24), 4445-4451.

Beulig, F., Røy, H., Glombitza, C., Jørgensen, B.B. (2018). Control on rate and pathway of anaerobic organic carbon degradation in the seabed. Proc Natl Acad Sci USA. 115:367–72.

Beutel, M., Fuhrmann, B., Herbon, G., Chow, A., Brower, S., and Pasek, J. (2020). Cycling of methylmercury and other redox-sensitive compounds in the profundal zone of a hypereutrophic water supply reservoir. Hydrobiologia, 847(21), 4425–4446. https://doi.org/10.1007/s10750-020-04192-3

Bigham, G. N., Murray, K. J., Masue-Slowey, Y., and Henry, E. A. (2017). Biogeochemical controls on methylmercury in soils and sediments: Implications for site management: Geochemical Controls on Mercury Methylation. Integrated Environmental Assessment and Management, 13(2), 249–263. https://doi.org/10.1002/ieam.1822

Bravo, A. G., Zopfi, J., Buck, M., Xu, J., Bertilsson, S., Schaefer, J. K., Poté, J., and Cosio, C. (2018). Geobacteraceae are important members of mercury-methylating microbial communities of sediments impacted by wastewater releases. The ISME Journal, 12(3), 802–812. https://doi.org/10.1038/s41396-017-0007-7

Bridou, R., Rodriguez-Gonzalez, P., Stoichev, T., Amouroux, D., Monperrus, M., Navarro, P., Tessier, E., and Guyoneaud, R. (2018). Methylation and dealkykation of tin compounds by sulfate- and nitrate-reducing bacteria. Chemosphere, 208, 871–879. https://doi.org/10.1016/j.chemosphere.2018.06.030

Burns, D. A., Aiken, G. R., Bradley, P. M., Journey, C. A., and Schelker, J. (2013). Specific ultra-violet absorbance as an indicator of mercury sources in an Adirondack River basin. Biogeochemistry, 113(1–3), 451–466. https://doi.org/10.1007/s10533-012-9773-5

California Water Board, Central Valley R5. (2023). Total Mercury Daily Loads, accessed 22 June 2024, https://www.waterboards.ca.gov/centralvalley/water_issues/tmdl

Cao, D., Chen, W., Xiang, Y., Mi, Q., Liu, H., Feng, P., Shen, H., Zhang, C., Wang, Y., and Wang, D. (2021). The efficiencies of inorganic mercury bio-methylation by aerobic bacteria under different oxygen concentrations. Ecotoxicology and Environmental Safety, 207, 111538. https://doi.org/10.1016/j.ecoenv.2020.111538

Catrouillet, C., Davranche, M., Dia, A., Bouhnik-Le Coz, M., Demangeat, D., Gruau, G. (2016). Does As(III) interact with Fe(II), Fe(III) and organic matter through ternary complexes? Journal of Colloid and Interface Science, 470, 153-161. https://doi.org/10.1016/j.jcis.2016.02.047.

Celo, V., Lean, D.R.S., Scott, S.L. (2006). Abiotic methylation of mercury in the aquatic environment. Science of the Total Environment 368, 126–137 https://doi.org/10.1016/j.scitotenv.2005.09.043

Chiasson-Gould, S. A., Blais, J. M., and Poulain, A. J. (2014). Dissolved Organic Matter Kinetically Controls Mercury Bioavailability to Bacteria. Environmental Science and Technology, 48(6), 3153–3161. https://doi.org/10.1021/es4038484

Compeau, G. C., and Bartha, R. (1985). Sulfate-Reducing Bacteria: Principal Methylators of Mercury in Anoxic Estuarine Sediment. Appl. Environ. Microbiol., 50(2), 498–502.

Cook, R. B. (1984). Distributions of Ferrous Iron and Sulfide in an Anoxic Hypolimnion. Canadian Journal of Fisheries and Aquatic Sciences, 41(2), 286–293. https://doi.org/10.1139/f84-033

Cossa, D., Garnier, C., Buscail, R., Elbaz-Poulichet, F., Mikac, N., Patel-Sorrentino, N., Tessier, E., Rigaud, S., Lenoble, V., and Gobeil, C. (2014). A Michaelis–Menten type equation for describing methylmercury dependence on inorganic mercury in aquatic sediments. Biogeochemistry, 119(1–3), 35–43. https://doi.org/10.1007/s10533-013-9924-3

Cossa, D., and Gobeil, C. (2000). Mercury speciation in the Lower St. Lawrence Estuary. 57.

Davison, W. (1993). Iron and manganese in lakes. Earth-Science Reviews, 34(2), 119–163. https://doi.org/10.1016/0012-8252(93)90029-7

De Parsia, E.R., Fleck, J.A., Krabbenhoft, D.P., Hoang, K., Roth, D., and Randall, P. (2019). Coagulant and sorbent efficacy in removing mercury from surface waters in the Cache Creek watershed, California: U.S. Geological Survey Open-File Report 2019–1001, 46p., https://doi.org/10.3133/ofr20191001

Diaz Arriaga, F.A., Katz, L.E. and Lawler, D.F. (2023).Mercury–dissolved organic matter interactions: insights on the removal of both pollutants in conventional drinking water treatment. Aquat Sci 85, 64. https://doi.org/10.1007/s00027-023-00950-2

Domagalski, J. L., Slotton, D. G., Alpers, C. N., Suchanek, T. H., Churchill, R., Bloom, N., Ayers, S. M., and Clinkenbeard, J. (2004). Summary and

Synthesis of Mercury Studies in the Cache Creek Watershed , California , 2000-2001. Mercury, 36.

Driscoll, C. T., Mason, R. P., Chan, H. M., Jacob, D. J., & Pirrone, N. (2013). Mercury as a global pollutant: sources, pathways, and effects. Environmental Science & Technology, 47(10), 4967-4983.

Du, H., Ma, M., Igarashi, Y., and Wang, D. (2019). Biotic and Abiotic Degradation of Methylmercury in Aquatic Ecosystems: A Review. Bulletin of Environmental Contamination and Toxicology, 102(5), 605–611. https://doi.org/10.1007/s00128-018-2530-2

Ebinghaus, R., Hintelmann, H., and Wilken, R. D. (1994). Mercury-cycling in surface waters and in the atmosphere Species analysis for the investigation of transformation and transport properties of mercury. Fresenius' Journal of Analytical Chemistry, 350(1–2), 21–29. https://doi.org/10.1007/BF00326247

Eckley, C. S., Gilmour, C. C., Janssen, S., Luxton, T. P., Randall, P. M., Whalin, L., and Austin, C. (2020). The assessment and remediation of mercury contaminated sites: A review of current approaches. Science of the Total Environment, 707, 136031. https://doi.org/10.1016/j.scitotenv.2019.136031

Eckley, C. S., Luxton, T. P., Stanfield, B., Baldwin, A., Holloway, J., McKernan, J., and Johnson, M. G. (2021). Effect of organic matter concentration and characteristics on mercury mobilization and methylmercury production at an abandoned mine site. Environmental Pollution, 271, 116369. https://doi.org/10.1016/j.envpol.2020.116369

Evers, D., Digangi, J., Petrlik, J., Buck, D., Šamánek, J., Beeler, B., Turnquist, M., Hatch, S., and Regan, Kevin. (2013). Global mercury hotspots: New evidence reveals mercury contamination regularly exceeds health advisory levels in humans and fish worldwide. Technical Report https://doi.org/10.13140/RG.2.2.23895.24481.

Fleck, J., Marvin-DiPasquale, M., Alpers, C.N. (2018). Cache Creek Settling Basin Mesocosms Study. [Power Point Slides]

Fleming, E. J., Mack, E. E., Green, P. G., and Nelson, D. C. (2006). Mercury Methylation from Unexpected Sources: Molybdate-Inhibited Freshwater Sediments and an Iron-Reducing Bacterium. Applied and Environmental Microbiology, 72(1), 457–464. https://doi.org/10.1128/AEM.72.1.457-464.2006

Frohne, T., Rinklebe, J., Langer, U., du Laing, G., Mothes, S., and Wennrich, R. (2012). Biogeochemical factors affecting mercury methylation rate in two contaminated floodplain soils. Biogeosciences, 9(1), 493–507. https://doi.org/10.5194/bg-9-493-2012

Fuhrmann, B. C., Beutel, M. W., O'Day, P. A., Tran, C., Funk, A., Brower, S., Pasek, J., and Seelos, M. (2021). Effects of mercury, organic carbon, and microbial inhibition on methylmercury cycling at the profundal sediment-water interface of a sulfate-rich hypereutrophic reservoir. Environmental Pollution, 268, 115853. https://doi.org/10.1016/j.envpol.2020.115853

Gagnon, C., Pelletier, É., and Mucci, A. (1997). Behaviour of anthropogenic mercury in coastal marine sediments. Marine Chemistry, 59(1–2), 159–176. https://doi.org/10.1016/S0304-4203(97)00071-6

Gfeller, L., Weber, A., Worms, I., Slaveykova, V. I., and Mestrot, A. (2021).Mercury mobility, colloid formation and methylation in a polluted Fluvisol as affected by manure application and flooding–draining cycle, Biogeosciences, 18, 3445–3465. https://doi.org/10.5194/bg-18-3445-2021

Gilmour, C. C., Henry, E. A., & Mitchell, R. (1992). Sulfate stimulation of mercury methylation in freshwater sediments. Environmental Science & Technology, 26(11), 2281-2287.

Gilmour, C. C., Podar, M., Bullock, A. L., Graham, A. M., Brown, S. D., Somenahally, A. C., Johs, A., Hurt, R. A., Bailey, K. L., and Elias, D. A. (2013). Mercury Methylation by Novel Microorganisms from New Environments. Environmental Science and Technology, 47(20), 11810–11820. https://doi.org/10.1021/es403075t

Gorski, C. A., Klüpfel, L. E., Voegelin, A., Sander, M., and Hofstetter, T. B. (2013). Redox Properties of Structural Fe in Clay Minerals: 3. Relationships between Smectite Redox and Structural Properties. Environmental Science and Technology, 47(23), 13477–13485. https://doi.org/10.1021/es403824x

Graham, A. M., Aiken, G. R., & Gilmour, C. C. (2012). Dissolved organic matter enhances microbial mercury methylation under sulfidic conditions. Environmental Science & Technology, 46(5), 2715-2723.

Gu, S., Gruau, G., Dupas, R., Petitjean, P., Li, O., Pinay, G. (2019). Respective roles of Fe-oxyhydroxide dissolution, pH changes and sediment inputs in dissolved phosphorus release from wetland soils under anoxic conditions. Geoderma, 338, 365-374. https://doi.org/10.1016/j.geoderma.2018.12.034.

Hansen, A.M., Kraus, T.E.C., Pellerin, B.A., Fleck, J.A., Downing, B.D., Bergamaschi, B.A. (2016). Optical properties of dissolved organic matter (DOM): Effects of biological and photolytic degradation. Limnology and Oceanography, 61 1015-1032.

Heiberg, L., Koch, C.B., Kjaergaard, C., Jensen, H.S. and Hansen, H.C.B. (2012), Vivianite Precipitation and Phosphate Sorption following Iron Reduction in Anoxic Soils. J. Environ. Qual., 41: 938-949. https://doi.org/10.2134/jeq2011.0067

Helmrich, S., Vlassopoulos, D., Alpers, C. N., and O'Day, P. A. (2022). Critical review of mercury methylation and methylmercury demethylation rate constants in aquatic sediments for biogeochemical modeling. Critical Reviews in Environmental Science and Technology, 52(24), 4353–4378. https://doi.org/10.1080/10643389.2021.2013073

Henneberry, Y. K., Kraus, T. E., Fleck, J. A., Krabbenhoft, D. P., Bachand, P. M., & Horwath, W. R. (2011). Removal of inorganic mercury and methylmercury from surface waters following coagulation of dissolved organic matter with metal-based salts. Science of the Total Environment, 409(3), 631-637

Henneberry, Y. K., Kraus, T. E. C., Nico, P. S., and Horwath, W. R. (2012). Structural stability of coprecipitated natural organic matter and ferric iron under reducing conditions. Organic Geochemistry, 48, 81–89. https://doi.org/10.1016/j.orggeochem.2012.04.005

Henneberry, Y., Kraus, T. E. C., Krabbenhoft, D. P., and Horwath, W. R. (2016). Investigating the Temporal Effects of Metal-Based Coagulants to Remove Mercury from Solution in the Presence of Dissolved Organic Matter. Environmental Management, 57(1), 220–228. https://doi.org/10.1007/s00267-015-0601-2

Hintelmann, H., and Harris, R. (2004). Application of multiple stable mercury isotopes to determine the adsorption and desorption dynamics of Hg (II) and MeHg to sediments. Marine Chemistry, 90(1-4), 165-173. https://doi.org/10.1016/j.marchem.2004.03.015

Hintelmann, H., Keppel-Jones, K. and Evans, R.D. (2000), Constants of mercury methylation and demethylation rates in sediments and comparison of tracer and ambient mercury availability. Environmental Toxicology and Chemistry, 19, 2204-2211.https://doi.org/10.1002/etc.5620190909

Hsu-Kim, H., Kucharzyk, K. H., Zhang, T., and Deshusses, M. A. (2013). Mechanisms Regulating Mercury Bioavailability for Methylating Microorganisms in the Aquatic Environment: A Critical Review. Environmental Science and Technology, 47(6), 2441–2456. https://doi.org/10.1021/es304370g

Ingvorsen, K., Zeikus, J. G., and Brock, T. D. (1981). Dynamics of Bacterial Sulfate Reduction in a Eutrophic Lake. Applied and Environmental Microbiology, 42(6), 1029–1036. https://doi.org/10.1128/aem.42.6.1029-1036.1981

Jones, B. D., and Ingle, J. D. (2005). Evaluation of redox indicators for determining sulfate-reducing and dechlorinating conditions. Water Research, 39(18), 4343–4354. https://doi.org/10.1016/j.watres.2005.09.006

Jones, D. S., Johnson, N. W., Mitchell, C. P. J., Walker, G. M., Bailey, J. v., Pastor, J., and Swain, E. B. (2020). Diverse Communities of hgcAB+Microorganisms Methylate Mercury in Freshwater Sediments Subjected to Experimental Sulfate Loading. Environmental Science and Technology, 54(22), 14265–14274. https://doi.org/10.1021/acs.est.0c02513

Jonsson, S., Mazrui, N. M., and Mason, R. P. (2016). Dimethylmercury Formation Mediated by Inorganic and Organic Reduced Sulfur Surfaces. Scientific Reports, 6(1), 27958. https://doi.org/10.1038/srep27958

Kanzler, C. R., Lian, P., Trainer, E. L., Yang, X., Govind, N., Parks, J. M., and Graham, A. M. (2018). Emerging investigator series: Methylmercury speciation and dimethylmercury production in sulfidic solutions. Environmental Science: Processes and Impacts, 20(4), 584–594. https://doi.org/10.1039/C7EM00533D

Kellerman, A., Kothawala, D., Dittmar, T. et al. Persistence of dissolved organic matter in lakes related to its molecular characteristics. (2015). Nature Geosci 8, 454–457, https://doi.org/10.1038/ngeo2440

Kerin, E. J., Gilmour, C. C., Roden, E., Suzuki, M. T., Coates, J. D., & Mason, R. (2006). Mercury methylation by dissimilatory iron-reducing bacteria. Applied and Environmental Microbiology, 72(12), 7919-7921.

Kim, E.-H., Mason, R. P., Porter, E. T., and Soulen, H. L. (2006). The impact of resuspension on sediment mercury dynamics, and methylmercury production and fate: A mesocosm study. Marine Chemistry, 102(3–4), 300–315. https://doi.org/10.1016/j.marchem.2006.05.006

Klapstein, S. J., and O'Driscoll, N. J. (2018). Methylmercury Biogeochemistry in Freshwater Ecosystems: A Review Focusing on DOM and Photodemethylation. Bulletin of Environmental Contamination and Toxicology, 100(1), 14–25. https://doi.org/10.1007/s00128-017-2236-x

Kraus, T. E. C., Bergamaschi, B. A., Hernes, P. J., Doctor, D., Kendall, C., Downing, B. D., and Losee, R. F. (2011). How reservoirs alter drinking water quality: Organic matter sources, sinks, and transformations. Lake and Reservoir Management, 27(3), 205–219. https://doi.org/10.1080/07438141.2011.597283

Lacroix, E.M., Aeppli, M., Boye, K., Brodie, E., Fendorf, S., Keiluweit, M., Naughton, H.R., Noël, V., and Sihi, D. (2023). Consider the Anoxic Microsite: Acknowledging and Appreciating Spatiotemporal Redox Heterogeneity in Soils and Sediments. ACS Earth and Space Chemistry, 7 (9), 1592-1609. https://doi.org/10.1021/acsearthspacechem.3c00032

Liang, H., Pei, F., Ge. J., Xu, P., Wang, M., Liang, P., Zhang, J., Wu, S., and Wong, M.H. (2024). Algae decomposition released dissolved organic matter subfractions on dark abiotic mercury methylation. Ecotoxicology and Environmental Safety. 270, 115914. https://doi.org/10.1016/j.ecoenv.2023.115914

Liem-Nguyen, V., Skyllberg, U., and Björn, E. (2017). Thermodynamic Modeling of the Solubility and Chemical Speciation of Mercury and Methylmercury Driven by Organic Thiols and Micromolar Sulfide Concentrations in Boreal Wetland Soils. Environmental Science and Technology, 51(7), 3678–3686. https://doi.org/10.1021/acs.est.6b04622

Luo, H., Cheng, Q., He, D., Sun, J., Li, J., and Pan, X. (2023). Recent advances in microbial mercury methylation: A review on methylation habitat, methylator, mechanism, and influencing factor. Process Safety and Environmental Protection, 170, 286–296. https://doi.org/10.1016/j.psep.2022.12.007

Lv, J., Luo, L., Zhang, J., Christie, P., and Zhang, S. (2012). Adsorption of mercury on lignin: Combined surface complexation modeling and X-ray absorption spectroscopy studies. Environmental Pollution, 162, 255–261. https://doi.org/10.1016/j.envpol.2011.11.012

Madigan, M.T., and Martinko, J.M. (2006). Brok Biology of Microorganisms. 11th Edition. Pearson Prentice Hall, (p. 114).

Mangold, J. E., Park, C. M., Liljestrand, H. M., and Katz, L. E. (2014). Surface complexation modeling of Hg(II) adsorption at the goethite/water interface using the Charge Distribution Multi-Site Complexation (CD-MUSIC)

model. Journal of Colloid and Interface Science, 418, 147–161. https://doi.org/10.1016/j.jcis.2013.10.066

Marvin-DiPasquale, M. (2020). USGS Iron Speciation in Sediment (p. 8).

Marvin-DiPasquale, M. C., Alpers, C. N., and Fleck, J. A. (2009). Mercury, Methylmercury, and Other Constituents in Sediment and Water from Seasonal and Permanent Wetlands in the Cache Creek Settling Basin and Yolo Bypass, Yolo County, California, 2005−06. Open File Report 2009-1182, 69.

Marvin-DiPasquale, M., Agee, J., McGowan, C., Oremland, R. S., Thomas, M., Krabbenhoft, D., and Gilmour, C. C. (2000). Methyl-Mercury Degradation Pathways: A Comparison among Three Mercury-Impacted Ecosystems. Environmental Science and Technology, 34(23), 4908–4916. https://doi.org/10.1021/es0013125

Marvin-DiPasquale, M. and Flanders, J.R. USGS. (2007). Determination of Reactive Mercury in Sediments by Direct Tin-Reduction of Inorganic Hg(II), Purge and Trap, and Cold Vapor Atomic Fluorescence Spectrometry (p. 22).

Mazrui, N. M., Jonsson, S., Thota, S., Zhao, J., and Mason, R. P. (2016). Enhanced availability of mercury bound to dissolved organic matter for methylation in marine sediments. Geochimica et Cosmochimica Acta, 194, 153–162. https://doi.org/10.1016/j.gca.2016.08.019

Miller, C. L. (2006). The Role of Organic Matter in the Dissolved Phase Speciation and Solid Phase Partitioning of Mercury. Thesis Dissertation, University of Maryland, College Park, 173.

Murray, T. E. (1995). The correlation between iron sulfide precipitation and hypolimnetic phosphorus accumulation during one summer in a softwater lake. Canadian Journal of Fisheries and Aquatic Sciences, 52(6), 1190–1194. https://doi.org/10.1139/f95-115

Nordstrom, D. K., & Wilde, F. D. (2005). Reduction-6.5 oxidation potential (electrode method). US Geological Survey TWRI Book, 9.

Oremland, R. S., Miller, L. G., Dowdle, P., Connell, T., & Barkay, T. A. M. A. R. (1995). Methylmercury oxidative degradation potentials in contaminated and pristine sediments of the Carson River, Nevada. Applied and Environmental Microbiology, 61(7), 2745-2753.

Pak, K. R., & Bartha, R. (1998). Mercury methylation and demethylation in anoxic lake sediments and by strictly anaerobic bacteria. Applied and Environmental Microbiology, 64(3), 1013-1017.

Peterson, B. D., Poulin, B. A., Krabbenhoft, D. P., Tate, M. T., Baldwin, A. K., Naymik, J., Gastelecutto, N., and McMahon, K. D. (2023). Metabolically diverse microorganisms mediate methylmercury formation under nitrate-reducing conditions in a dynamic hydroelectric reservoir. The ISME Journal, 17(10), 1705–1718. https://doi.org/10.1038/s41396-023-01482-1

Potter, B. B. and J. Wimsatt. Method 415.3, Rev. 1.2: Determination of Total Organic Carbon and Specific UV Absorbance at 254 nm in Source Water

and Drinking Water. U.S. Environmental Protection Agency, Washington, DC, 2009.

Poulin, B. A., Gerbig, C. A., Kim, C. S., Stegemeier, J. P., Ryan, J. N., and Aiken, G. R. (2017). Effects of Sulfide Concentration and Dissolved Organic Matter Characteristics on the Structure of Nanocolloidal Metacinnabar. Environmental Science and Technology, 51(22), 13133–13142. https://doi.org/10.1021/acs.est.7b02687

Poulin, B. A., Tate, M. T., Ogorek, J., Breitmeyer, S. E., Baldwin, A. K., Yoder, A. M., Harris, R., Naymik, J., Gastelecutto, N., Hoovestol, C., Larsen, C., Myers, R., Aiken, G. R., Krabbenhoft, D. P. (2023). Biogeochemical and hydrologic synergy control mercury fate in an arid land river-reservoir system. Environ. Sci.: Processes Impacts. 25, 912– 928, DOI: 10.1039/D3EM00032J

Ravichandran, M. (2004). Interactions between mercury and dissolved organic matter—a review. Chemosphere, 55(3), 319–331. https://doi.org/10.1016/j.chemosphere.2003.11.011

Regnell, O., and Watras, C. J. (2019). Microbial Mercury Methylation in Aquatic Environments: A Critical Review of Published Field and Laboratory Studies. Environmental Science and Technology, 53(1), 4–19. https://doi.org/10.1021/acs.est.8b02709

Rothe, M., Kleeber, A., Hupfer, M. (2016). The occurrence, identification and environmental relevance of vivianite in waterlogged soils and aquatic sediments. Earth-Science Reviews, 158, 51-64. https://doi.org/10.1016/j.earscirev.2016.04.008

Rytuba, J.J., Hothem, R.L., Brussee, B.E., Goldstein, D.N., and May, J.T., 2015, Environmental assessment of water, sediment, and biota collected from the Bear Creek watershed, Colusa County, California: U.S. Geological Survey Open-File Report 2013–1070, 83 p., http://dx.doi.org/10.3133/ofr20131070.

Sanei, H., and Goodarzi, F. (2006). Relationship between organic matter and mercury in recent lake sediment: The physical–geochemical aspects. Applied Geochemistry, 21(11), 1900–1912. https://doi.org/10.1016/j.apgeochem.2006.08.015

Schaefer, J. K., Letowski, J., and Barkay, T. (2002). Mer -Mediated Resistance and Volatilization of Hg(II) Under Anaerobic Conditions. Geomicrobiology Journal, 19(1), 87–102. https://doi.org/10.1080/014904502317246192

Schaefer, A. M., Stavros, H. C. W., Bossart, G. D., Fair, P. A., Goldstein, J. D., & Reif, J. S. (2011). Associations between mercury and hepatic, renal, endocrine, and hematological parameters in Atlantic bottlenose dolphins (Tursiops truncatus) along the eastern coast of Florida and South Carolina. Archives of Environmental Contamination and Toxicology, 61, 688-695.

Schuster, P.F., Shanley, J.B., Marvin-DiPasquale, M. et al. (2008). Mercury and Organic Carbon Dynamics During Runoff Episodes from a Northeastern

USA Watershed. Water Air Soil Pollut 187, 89–108. https://doi.org/10.1007/s11270-007-9500-3

Shi, L., Dong, H., Reguera, G. et al. (2016). Extracellular electron transfer mechanisms between microorganisms and minerals. Nat Rev Microbiol 14, 651–662 https://doi.org/10.1038/nrmicro.2016.93

Slowey, A. J., and Brown, G. E. (2007). Transformations of mercury, iron, and sulfur during the reductive dissolution of iron oxyhydroxide by sulfide. Geochimica et Cosmochimica Acta, 71(4), 877–894. https://doi.org/10.1016/j.gca.2006.11.011

Sonke, J. E., Angot, H., Zhang, Y., Poulain, A., Björn, E., and Schartup, A. (2023). Global change effects on biogeochemical mercury cycling. Ambio, 52(5), 853–876. https://doi.org/10.1007/s13280-023-01855-y

State Water Resources Control Board. (2017a). State Water Resources Control Board 2014 and 2016 California Integrated Report Clean Water Act Sections 303(d) and 305(b). Staff Report. October 3

Stumpner, E. B., Kraus, T. E. C., Fleck, J. A., Hansen, A. M., Bachand, S. M., Horwath, W. R., DeWild, J. F., Krabbenhoft, D. P., and Bachand, P. A. M. (2015). Mercury, monomethyl mercury, and dissolved organic carbon concentrations in surface water entering and exiting constructed wetlands treated with metal-based coagulants, Twitchell Island, California. Data Series, 36. http://pubs.er.usgs.gov/publication/ds950

Tian, L., Guan, W., Ji, Y., He, X., Chen, W., Alvarez, P. J., & Zhang, T. (2021). Microbial methylation potential of mercury sulfide particles dictated by surface structure. Nature Geoscience, 14(6), 409-416.

Turner, F.T., and Patrick, W.H. (1968). Chemical Changes in Waterlogged Soils as a Result of Oxygen Depletion. Transactions of the 9th International Congress of Soil Science, 4, 53-65

Ullrich, S. M., Tanton, T. W., and Abdrashitova, S. A. (2001). Mercury in the Aquatic Environment: A Review of Factors Affecting Methylation. Critical Reviews in Environmental Science and Technology, 31(3), 241–293. https://doi.org/10.1080/20016491089226

USEPA. (1993). Method 300.0, Revision 2.1: Determination of Inorganic Anions by Ion Chromatography.

USEPA. (1994). "Method 200.7: Determination of Metals and Trace Elements in Water and Wastes by Inductively Coupled Plasma-Atomic Emission Spectrometry," Revision 4.4. Cincinnati, OH

USEPA. (1994). Determination of Mercury in Water by Cold Vapor Atomic Absorption Spectrometry Method 245.1. Environmental Monitoring Systems Laboratory Office of Research and Development, 1–18.

USEPA. (1996). Method 3052. Microwave Assisted Acid Digestion of Silic (Vol. 66, Issue December, pp. 37–39).

USEPA. (1998). Method 1630 Methyl Mercury in Water by Distillation, Aqueous Ethylation, Purge and Trap, and Cold Vapor Atomic Fluorescence Spectrometry Engineering and Analysis Division (4303). Science And Technology, 4303.

USEPA. (2007). Mercury total (organic and 7439-97-6 inorganic). Methods, February.1–17. https://www.epa.gov/sites/production/files/2015-07/documents/epa-7473.pdf

Wang, T., Zhao, D., Liu, J., Zhang, T., Wang, X., Liu, T., Wang, S., Liu, G., Liu, B., and Liu, Y. (2023). Effects of abiotic mineral transformation of FeS on the dynamic immobilization of Cr(VI) in oxic aquatic environments. Science of the Total Environment, 894, 164991. https://doi.org/10.1016/j.scitotenv.2023.164991

Wang, Y., Liu, J., Liem-Nguyen, V., Tian, S., Zhang, S., Wang, D., and Jiang, T. (2022). Binding strength of mercury (II) to different dissolved organic matter: The roles of DOM properties and sources. Science of the Total Environment, 807, 150979. https://doi.org/10.1016/j.scitotenv.2021.150979

Wang, Z., Akbar, S., Sun, Y., Gu, L., Zhang, L., Lyu, K., Huang, Y., and Yang, Z. (2021). Cyanobacterial dominance and succession: Factors, mechanisms, predictions, and managements. Journal of Environmental Management, 297, 113281. https://doi.org/10.1016/j.jenvman.2021.113281

Warner, K. A., Roden, E. E., and Bonzongo, J. C. (2003). Microbial mercury transformation in anoxic freshwater sediments under iron-reducing and other electron-accepting conditions. Environ. Sci. Technol. 37, 2159–2165

Weber, J. H. (1993). Review of possible paths for abiotic methylation of mercury(II) in the aquatic environment. Chemosphere, 26(11), 2063–2077. https://doi.org/10.1016/0045-6535(93)90032-Z

Weerasooriya, R., Seneviratne, W., Kathriarachchi, H. A., and Tobschall, H. J. (2006). Thermodynamic assessment of Hg(II)-gibbsite interactions. Journal of Colloid and Interface Science, 301(2), 452–460. https://doi.org/10.1016/j.jcis.2006.05.054

Weishaar, J.L., Aiken, G.R., Bergamaschi, B.A., Fram, M.S., Fuji, R., Mopper, K. (2003). Evaluation of specific ultraviolet absorbance as an indicator of the chemical composition and reactivity of dissolved organic carbon. Environ Sci Technol;37:4702–8. https://doi.org/10.1021/es030360x

Wujcicki, Ł.; Kluczka, J. (2023). Recovery of Phosphate(V) Ions from Water and Wastewater Using Chitosan-Based Sorbents Modified— A Literature Review. Int. J. Mol. Sci. 24, 12060. https://doi.org/ 10.3390/ijms241512060

Xiang, Y., Wang, Y., Shen, H., and Wang, D. (2020). The draft genome sequence of Pseudomonas putida strain TGRB4, an aerobic bacterium capable of producing methylmercury. Current Microbiology, 77(4), 522-527. https://doi.org/10.1007/s00284-019-01670-3

Yu, R.-Q., Reinfelder, J. R., Hines, M. E., and Barkay, T. (2018). Syntrophic pathways for microbial mercury methylation. The ISME Journal, 12(7), 1826–1835. https://doi.org/10.1038/s41396-018-0106-0

Zhang, T., Kim, B., Levard, C., Reinsch, B.C., Lowry, G.V., Deshusses, M.A. et al. (2012) Methylation of mercury by bacteria exposed to dissolved, nanoparticulate, and microparticulate mercuric sulfides. Environmental

Science and Technology, 46(13), 6950–6958. https://doi.org/10.1021/es203181m

Zhu, S., Chen, B., He, M., Huang, T., & Hu, B. (2017). Speciation of mercury in water and fish samples by HPLC-ICP-MS after magnetic solid phase extraction. Talanta, 171, 213-219.

Zhu, Y., Liu, J., Goswami, O. et al. (2018). Effects of humic substances on Fe(II) sorption onto aluminum oxide and clay. Geochem Trans 19, 3. https://doi.org/10.1186/s12932-018-0048-5

Table 2-1. Cache Creek Settling Basin Soil Characterization

	Control	Chitovan	Ferralyte	Ultrion	Tukey HSD
Water Content (%)	17.2±2.25	14.8±2.25	14.5±2.25	17.1±2.25	*ns*
Wet:Dry ratio (g wet/g dry)	1.2±0.06	1.2±0.06	1.2±0.06	1.3±0.06	*ns*
LOI %	0.5±0.06	0.6±0.06	0.5±0.06	0.5±0.06	*ns*
MeHg (µg/kg)	2.32±0.14	2.23±0.14	2.02±0.14	2.22±0.14	*ns*
THg (µg/kg)	286±9.89	298±9.89	311±9.89	299±9.89	*ns*
Thiol-RHg (µg/kg)	28±2.67	24±2.67	25±2.67	28±2.67	*ns*
RHg (µg/kg)	10±1.06	9±1.06	11±1.06	11±1.06	*ns*
Fe_{TAE} (g-Fe/kg)	38±1.12	41±1.12	38±1.12	41±1.12	*ns*
Fe_{AE} (g-Fe/kg)	4±0.12	5±0.12	4±0.12	5±0.12	*ns*
Fe_{DE} (g-Fe/kg)	12±1.09	12±1.09	11±1.09	12±1.09	*ns*
Al_{TAE} (g-Al/kg)	33±1.07	30±1.07	30±1.07	30±1.07	*ns*
Al_{AE} (g-Al/kg)	2.0±1.09	1.7±1.09	1.8±1.09	2.0±1.09	*ns*
Al_{DE} (g-Al/kg)	1.6±0.12	1.6±0.12	1.4±0.12	1.6±0.12	*ns*
Mn_{TAE} (g-Mn/kg)	0.9±0.06	1.0±0.06	0.9±0.06	1.0±0.06	*ns*
Mn_{TAE} (g-Mn/kg)	0.4±0.16	0.4±0.16	0.4±0.16	0.5±0.16	*ns*
Mn_{DE} (g-Mn/kg)	0.4±0.07	0.5±0.07	0.5±0.07	0.5±0.08	*ns*

Notes: Values are least square means ± standard error of study sites A, B, and C. Results are presented in dry weight basis. "Reactive" Hg (R-Hg) in soil following the USGS tin reduction of Hg(II) method. Thiol-RHg was measured following the thiol (glutathione) extraction method. Iron (Fe), manganese (Mn), and aluminum (Al) fractions were analyzed after microwave digestion with ICP-OES. (Fe, Al, Mn)TAE: Total metal in concentrated acid (HNO_3 + HCl); (Fe, Al, Mn)AE: Acid-extractable metal (0.5 M HCl); and (Fe, Al, Mn)DE: Citrate/dithionite-extractable metal. Tukey's honestly significant difference (Tukey HSD) pairwise post hoc test results are included. *ns* indicates the treatments (control, ChitoVan, Ferralyte, Ultrion) and groups (A, B, C) do not differ among them.

Table 2-2. Comparison of mercury parameters during initial conditions

	Standard Test	Stress Test	Cache Creek Soil	Cache Creek water
MeHg water, ng/L	0.16 ± 0.04	0.26±0.13		0.06 ±0.02
Inorganic mercury water, ng/L	9.21±0.05	17.99±0.05		4.95±1.4
MeHg soil, µg/kg dw	1.10±0.01	3.45±0.04	2.31±0.02	

Note: Values are standard means ± standard error of study sites, for the standard test, and treatments, for the stress test.

Table 2-3. Standard test incubation significant determinants for mercury parameters estimated using ANOVA.

Parameter	N	Variable	dF	F-statistic	P-value
MeHg water	3	Treatment	46	1.67	0.19
	5	**Day**	**46**	**7.03**	**<0.001**
	2	Group	46	0.22	0.81
	15	Treatment x Day	46	1.15	0.34
IHg water	**3**	**Treatment**	**46**	**3.05**	**0.04**
	5	**Day**	**46**	**10.12**	**<0.001**
	2	**Group**	**46**	**14.11**	**<0.001**
	15	Treatment x Day	46	0.19	0.99
MeHg: THg water	**3**	**Treatment**	**72**	**2.07**	**0.02**
	5	**Day**	**72**	**2.39**	**0.05**
	2	**Group**	**72**	**5.26**	**0.01**
	15	Treatment x Day	72	2.26	0.08
% MeHg solution of total MeHg mass in incubation	3	Treatment	72	0.97	0.41
	5	**Day**	**72**	**4.43**	**0.002**
	2	Group	72	1.52	1.00
	15	Treatment x Day	72	1.27	0.65
MeHg soil	3	Treatment	46	1.82	0.16
	5	Day	46	1.09	0.37
	2	Group	46	1.31	0.28
	15	Treatment x Day	46	0.93	0.54
Log Kd (soil/water)	3	Treatment	46	0.58	0.63
	5	**Day**	**46**	**5.00**	**<0.001**
	2	Group	46	0.29	0.75
	18	Treatment x Day	46	1.26	0.26

Notes: Statistical results to compare the different mercury water/soil parameters measured between the coagulant-treated soils (ChitoVan, Ferralyte, Ultrion) and the control soil, and among groups (A, B, C) and days of incubation (0, 1, 2, 4, 8, 16). Table shows the individual linear mixed effect model fit by REML where Treatment, Group, and Treatment x Day were fixed variables, and the Group was also the random effect. ANOVA was estimated with Satterhwaite's method with $p < 0.05$ using RStudio. Values in bold are statistically significant.

Table 2-4. Stress Test compared to Standard Test significant determinants for mercury parameters estimated using ANOVA.

Parameter	Type	N	Df	F	Prob>F
MeHg water	Test	1	33	2959.01	<0.001
	Day	5	33	83.59	<0.001
	Treatment	3	0	0.7	1
	Test:Day	5	33	95.36	<0.001
IHg water	Test	1	33	514.65	<0.001
	Day	5	33	48.47	<0.001
	Treatment	3	0	0.618	1
	Test:Day	5	33	13.58	<0.001
MeHg:THg	Test	1	33	1.76	<0.001
	Day	5	33	14.07	<0.001
	Treatment	3	33	0.93	0.43
	Test:Day	5	33	6.88	<0.001
%MeHg-solution	Test	1	33	567.14	<0.001
	Day	5	33	67.11	<0.001
	Treatment	3	33	1.88	0.15
	Test:Day	5	33	68.73	<0.001
Soil MeHg	Test	1	33	266.56	<0.001
	Day	5	33	8.27	<0.001
	Treatment	3	0	0.19	1
	Test:Day	5	33	3.89	<0.001
Log Kd	Test	1	33	851.78	<0.001
	Day	5	33	28.75	<0.001
	Treatment	3	0	1.4	0.99
	Test:Day	5	33	42.94	<0.001

Notes: Statistical results to compare the different mercury water/soil parameters measured between the tests (stress test and standard test) among treatments (control, ChitoVan, Ferralyte, Ultrion) and days of incubation (0, 1, 2, 4, 8, 16). Stress test included mesocosm group C with spirulina organic matter addition. The standard test included the results only from mesocosm group C. Table shows the individual linear mixed effect model fit by REML per parameter where Treatment, Test, Day and Test x Day were fixed variables. Treatment was also the random effect due to the low variability response during the previous standard test statistical analysis. ANOVA was estimated with Satterhwaite's method with $p < 0.001$ using RStudio. Interpretation of the Test x Day term indicates that there was a significant interaction between day and stress test incubation not always seen in the standard test, thus each test had a different "day" effect.

Table 2-5. Standard test incubation significant determinants for aqueous parameters estimated using ANOVA.

Parameter	N	Variable	dF	F-statistic	P-value
Redox potential	3	Treatment	46	0.0005	0.99
	5	**Day**	**46**	**4.76**	**<0.001**
	2	Group	46	0.42	0.657
	15	Treatment x Day	46	0.002	1.00
pH	3	Treatment	46	0.44	0.72
	5	Day	46	6.58	0.06
	2	Group	46	0.56	0.57
	15	Treatment x Day	46	0.39	0.97
Manganese	**3**	**Treatment**	**72**	**30.1761**	**<0.001**
	5	**Day**	**72**	**21.72**	**<0.001**
	2	Group	72	4.45	0.06
	15	Treatment x Day	72	1.53	0.11
Sulfate	3	Treatment	72	1.08	0.36
	5	Day	72	1.41	0.23
	2	Group	72	0.70	0.49
	15	Treatment x Day	72	1.27	0.24
Iron	**3**	**Treatment**	**72**	**3.44**	**0.04**
	5	Day	72	0.91	0.48
	2	Group	72	0.27	0.84
	15	Treatment x Day	72	1.34	0.20
Aluminum	**3**	**Treatment**	**46**	**16.12**	**<0.001**
	5	**Day**	**46**	**19.27**	**<0.001**
	2	Group	0	0.09	1.00
	15	Treatment x Day	46	0.43	0.96
Ammonia	**3**	**Treatment**	**46**	**19.27**	**<0.001**
	5	**Day**	**46**	**16.12**	**<0.001**
	2	Group	46	3.43	0.04
	15	Treatment x Day	46	1.44	0.16
Nitrate	3	Treatment	46	1.69	0.18
	5	**Day**	**46**	**9.44**	**<0.001**
	2	Group	46	1.46	0.24
	15	Treatment x Day	46	0.42	0.96
Phosphate	**3**	**Treatment**	**72**	**15.51**	**<0.001**
	5	Day	72	1.21	0.32
	2	Group	72	3.19	0.05
	15	Treatment x Day	72	0.49	0.93

DOC	**3**	**Treatment**	**72**	**16.72**	**<0.001**
	5	**Day**	**72**	**2.21**	**0.06**
	2	**Group**	**72**	**32.45**	**<0.001**
	15	Treatment x Day	72	0.61	0.85

Notes: Statistical results to compare the different aqueous parameters measured between the coagulant-treated soils (ChitoVan, Ferralyte, Ultrion) and the control soil, and among groups (A, B, C) and days of incubation (0, 1, 2, 4, 8, 16). Table shows the individual linear mixed effect model fit by REML where Treatment, Group, and Treatment x Day were fixed variables, and the Group was also the random effect. For $SUVA_{254}$ values, the model was inconclusive. ANOVA was estimated with Satterhwaite's method with $p < 0.05$ using RStudio. Values in bold are statistically significant.

Table 2-6. Stress Test compared to Standard Test significant determinants for aqueous parameters estimated using ANOVA.

Parameter	Type	N	Df	F	Prob> F	Parameter	Type	N	Df	F	Prob> F
Redox Potential	Test	1	33	186.6	<0.001	**Ammonia**	Test	1	33	459.7	<0.001
	Day	5	33	61.1	<0.001		Day	5	33	3.9	<0.001
	Treatment	3	0	0.4	0.7531		Treatment	3	33	23.2	0.01
	Test:Day	5	33	90.9	<0.001		Test:Day	5	33	6.0	<0.001
pH	Test	1	33	786.8	<0.001	**Nitrate**	Test	1	33	3.3	0.076
	Day	5	33	195.0	<0.001		Day	5	33	4.6	0.0027
	Treatment	3	0	5.28	1		Treatment	3	0	1.3	0.289
	Test:Day	5	33	28.5	<0.001		Test:Day	5	33	0.9	0.4939
Manganese	Test	1	33	531.1	<0.001	**Phosphate**	Test	1	33	364.3	<0.001
	Day	5	33	68.5	<0.001		Day	5	33	8.7	<0.001
	Treatment	3	33	1.1	0.37		Treatment	3	33	4.2	0.01
	Test:Day	5	33	43.6	<0.001		Test:Day	5	33	7.8	<0.001
Sulfate	Test	1	33	879.6	<0.001	**DOC**	Test	1	33	228.4	<0.001
	Day	5	33	296.2	<0.001		Day	5	33	19.33	<0.001
	Treatment	3	0	26.9	1		Treatment	3	33	2.2	0.09
	Test:Day	5	33	272.6	<0.001		Test:Day	5	33	19.3	<0.001
Iron	Test	1	33	24.9	<0.001	**SUVA**	Test	1	33	215.3	<0.001
	Day	5	33	3.92	0.006		Day	5	33	13.2	<0.001
	Treatment	3	33	0.83	0.49		Treatment	3	0	1.9	1
	Test:Day	5	33	3.7	0.0085		Test:Day	5	33	16.9	<0.001
Aluminum	Test	1	33	4.8	<0.001						
	Day	5	33	2.8	<0.001						
	Treatment	3	0	0.7	1						
	Test:Day	5	33	14.84	<0.001						

Notes: Statistical results to compare the different aqueous parameters measured between the tests (stress test and standard test) among treatments (control, ChitoVan, Ferralyte, Ultrion) and days of incubation (0, 1, 2, 4, 8, 16). Stress test included mesocosm group C with spirulina organic matter addition. The standard test included the results only from

mesocosm group C. Table shows the individual linear mixed effect model fit by REML per parameter where Treatment, Test, Day and Test x Day were fixed variables. Treatment was also the random effect due to the low variability response during the previous standard test statistical analysis. ANOVA was estimated with Satterhwaite's method with $p < 0.01$ using RStudio. Interpretation of the interaction term indicates that there was a significant interaction between day and stress test incubation not always seen in the standard incubation. Interpretation of the interaction term indicates that there was a significant interaction between day and stress test incubation not always seen in the standard test, thus each test had a different "day" effect.

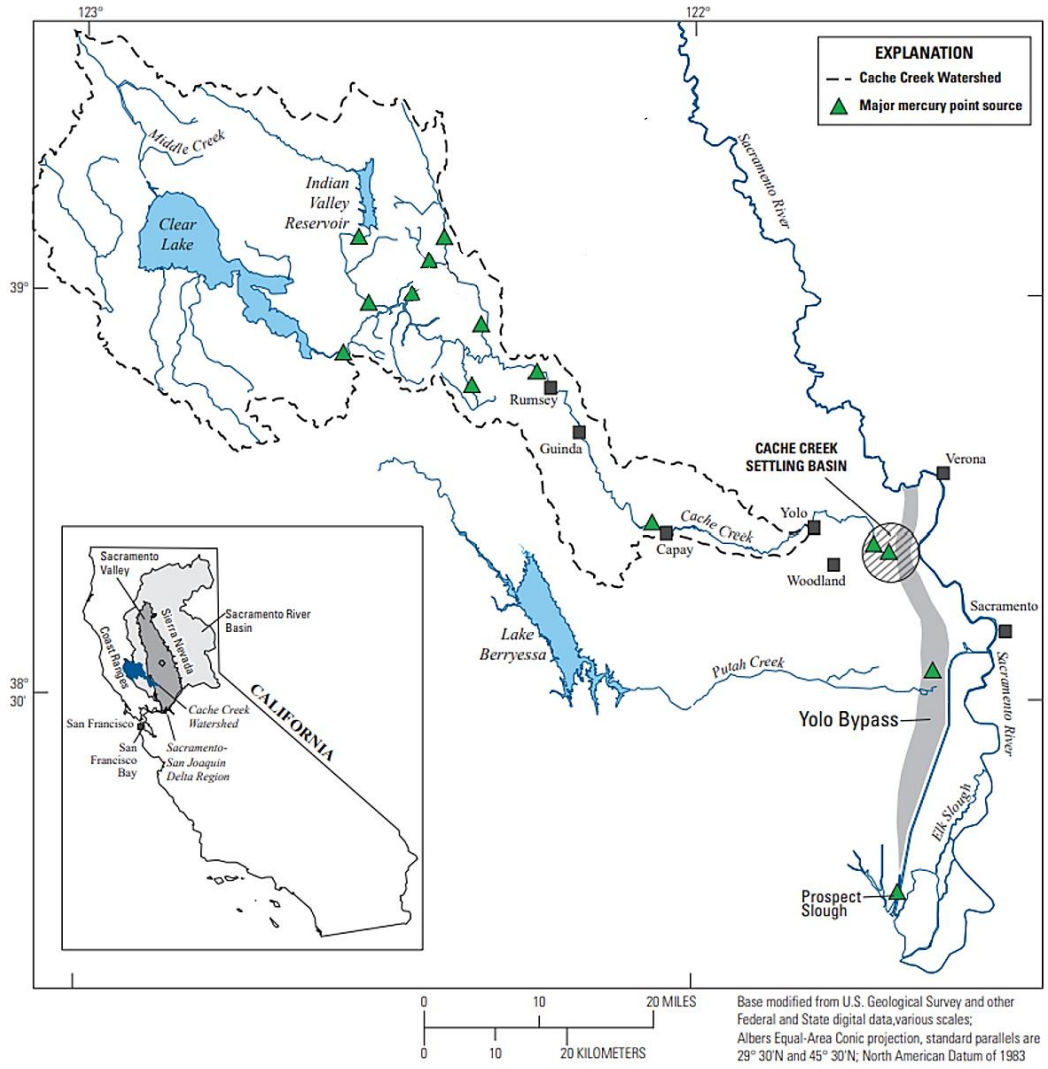

Figure 2-1 Map of the location of Cache Creek Settling Basin showing Cache Creek watershed, the major mercury points sources, and the connection of the Yolo Bypass with the Sacramento-San Joaquin Delta. Modified from De Parsia and others (2019).

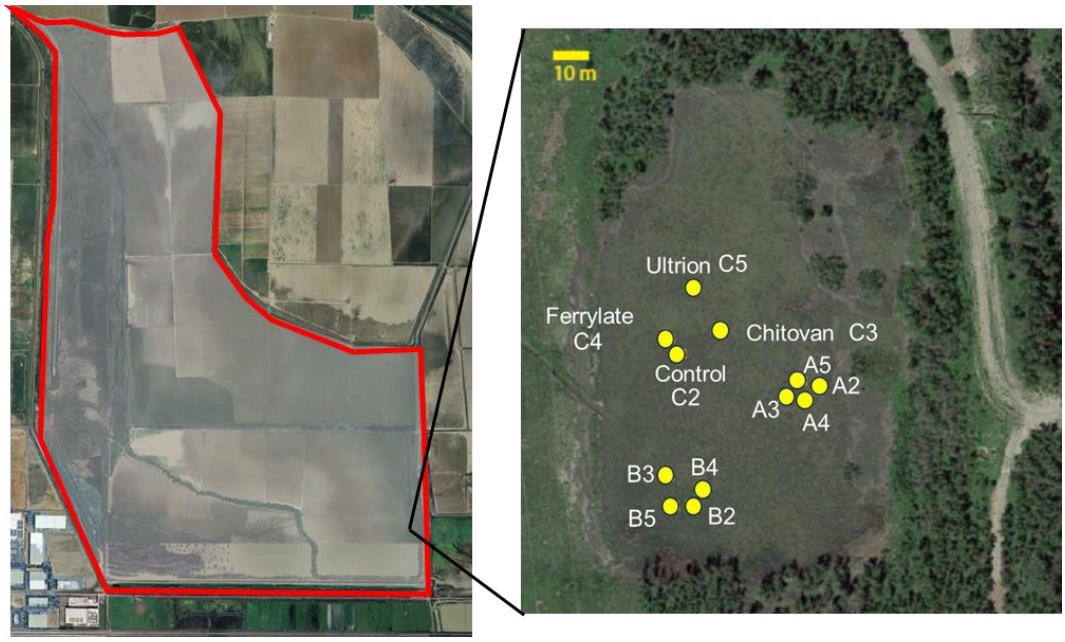

Figure 2-2 Map showing Cache Creek Settling Basing study site and mesocosm locations A, B and C. Numbers represent the different coagulants with 2: the control, 3: Chitovan coagulant, 4: Ferralyte, and 5: Ultrion (compliments of J. Fleck, USGS).

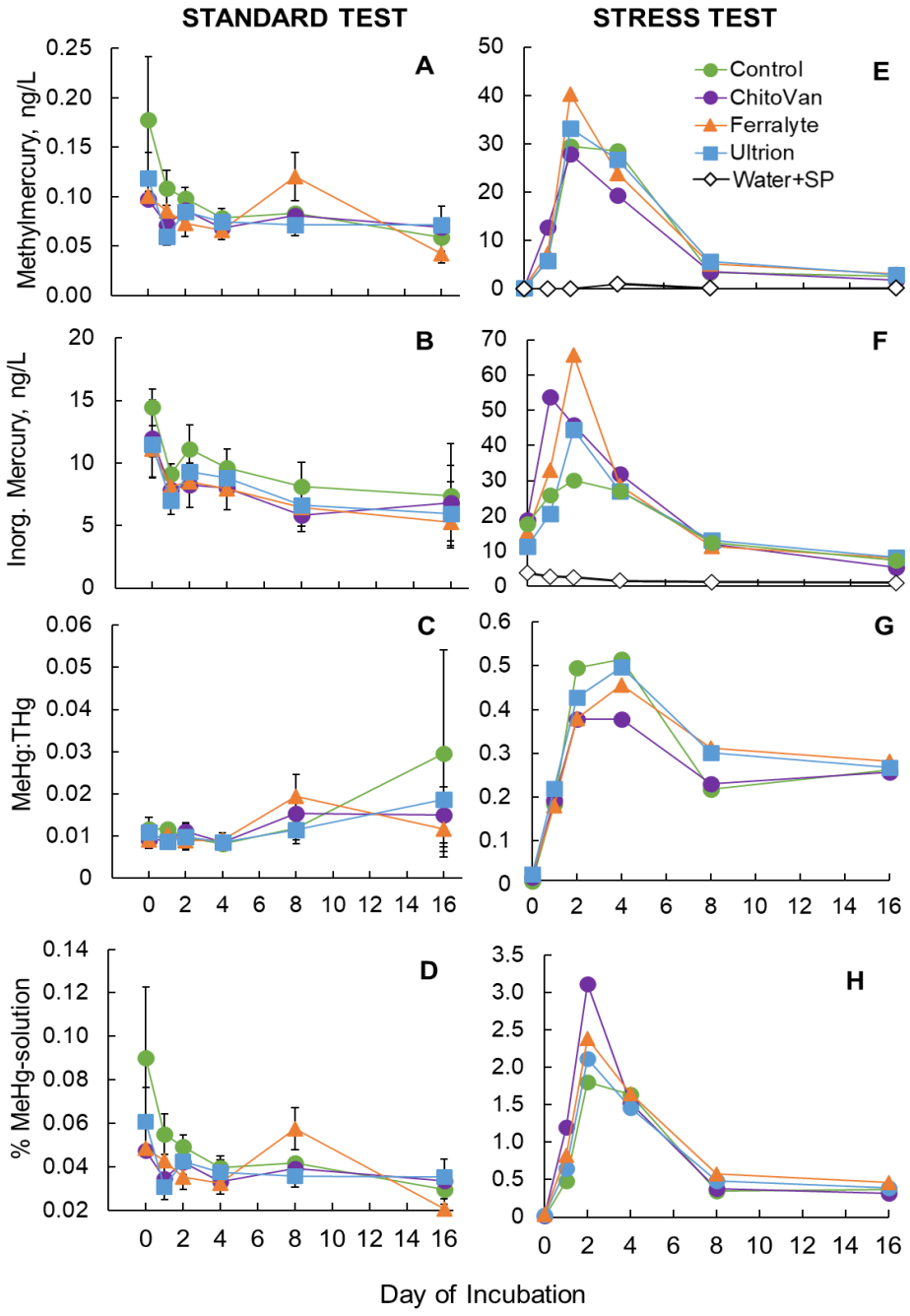

Figure 2-3 Mercury and methylmercury in water. Left side, standard test with control and three coagulant treatments (ChitoVan, Ferralyte and Ultrion) replicated at three stations (A, B and C). Error bars are plus/minus one standard error of triplicate incubations. Right side, stress test with spirulina organic matter (SP) addition in control soil for station C and a water+SP control. From top to bottom: methylmercury concentration, inorganic mercury concentration, ratio of methylmercury to total mercury, and percentage of methylmercury in water relative to methylmercury in water plus sediment. Note difference in vertical scale for all figures.

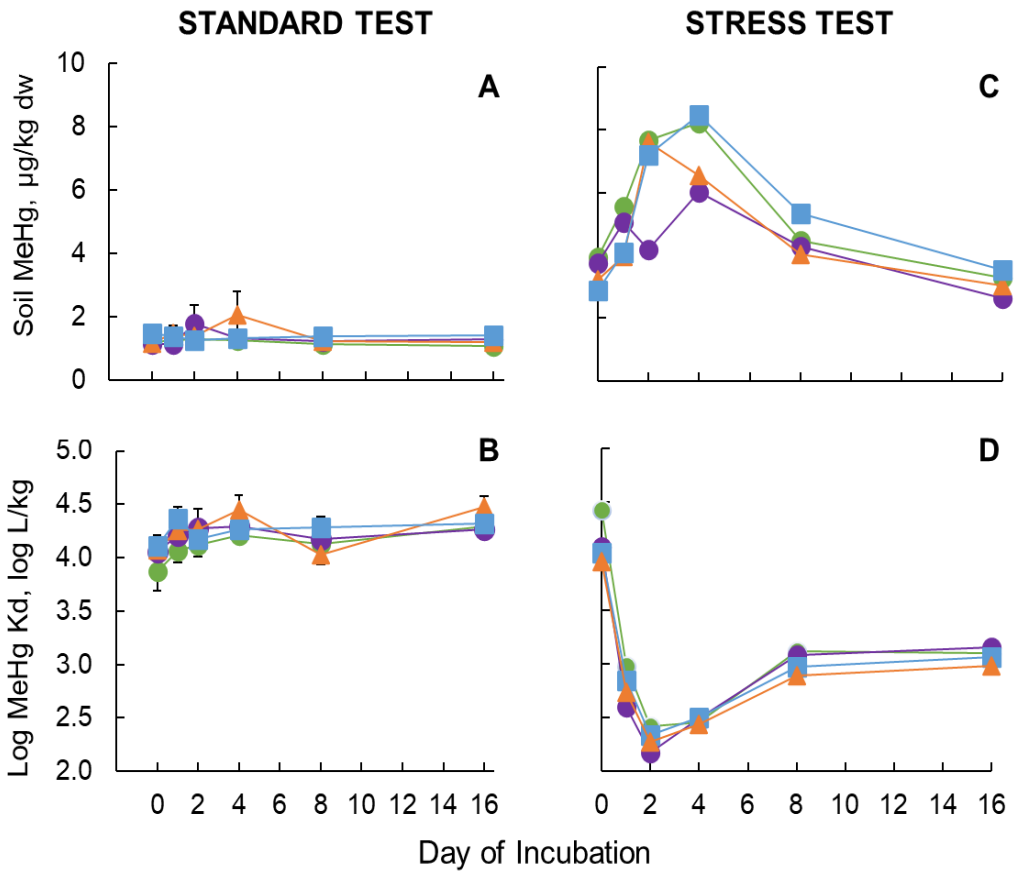

Figure 2-4 Methylmercury (MeHg) in soil. Left side, standard test with mean values from control and three coagulant treatments (ChitoVan, Ferralyte and Ultrion) replicated at three stations (A, B and C). Error bars are plus/minus one standard error of triplicate incubations. Right side, stress test with spirulina organic matter addition in control soil for station C. From top to bottom: methylmercury mass in soil (dw: dry weight) and log methylmercury Kd value (log of methylmercury soil concentration divided by water concentration).

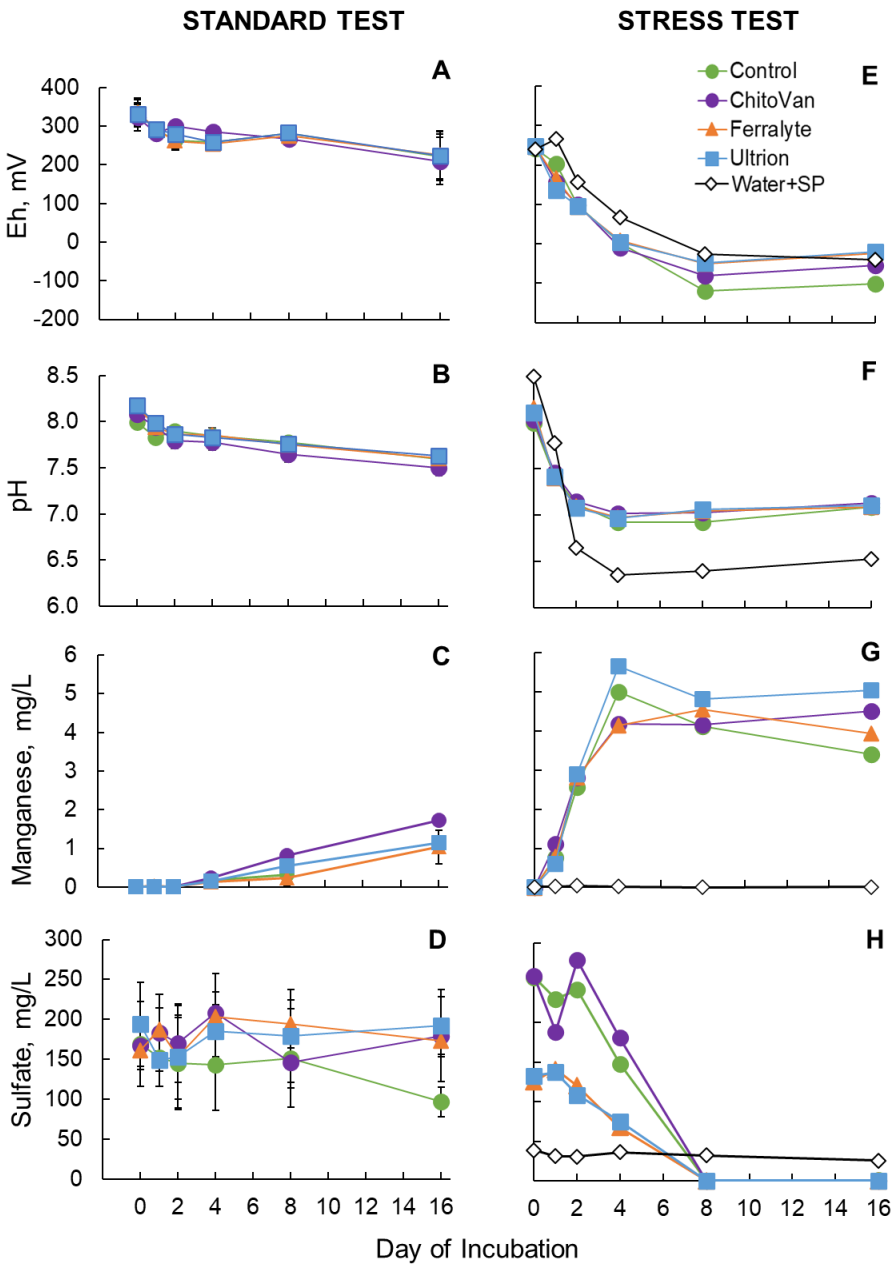

Figure 2-5 Primary aqueous parameters. Left side, standard test with mean values from control and three coagulant treatments (ChitoVan, Ferralyte and Ultrion) replicated at three stations (A, B and C). Error bars are plus/minus one standard error of triplicate incubations. Right side, stress test with spirulina organic matter (SP) addition in control soil for station C and a water+SP control. From top to bottom: redox potential (Eh), pH, manganese, and sulfate.

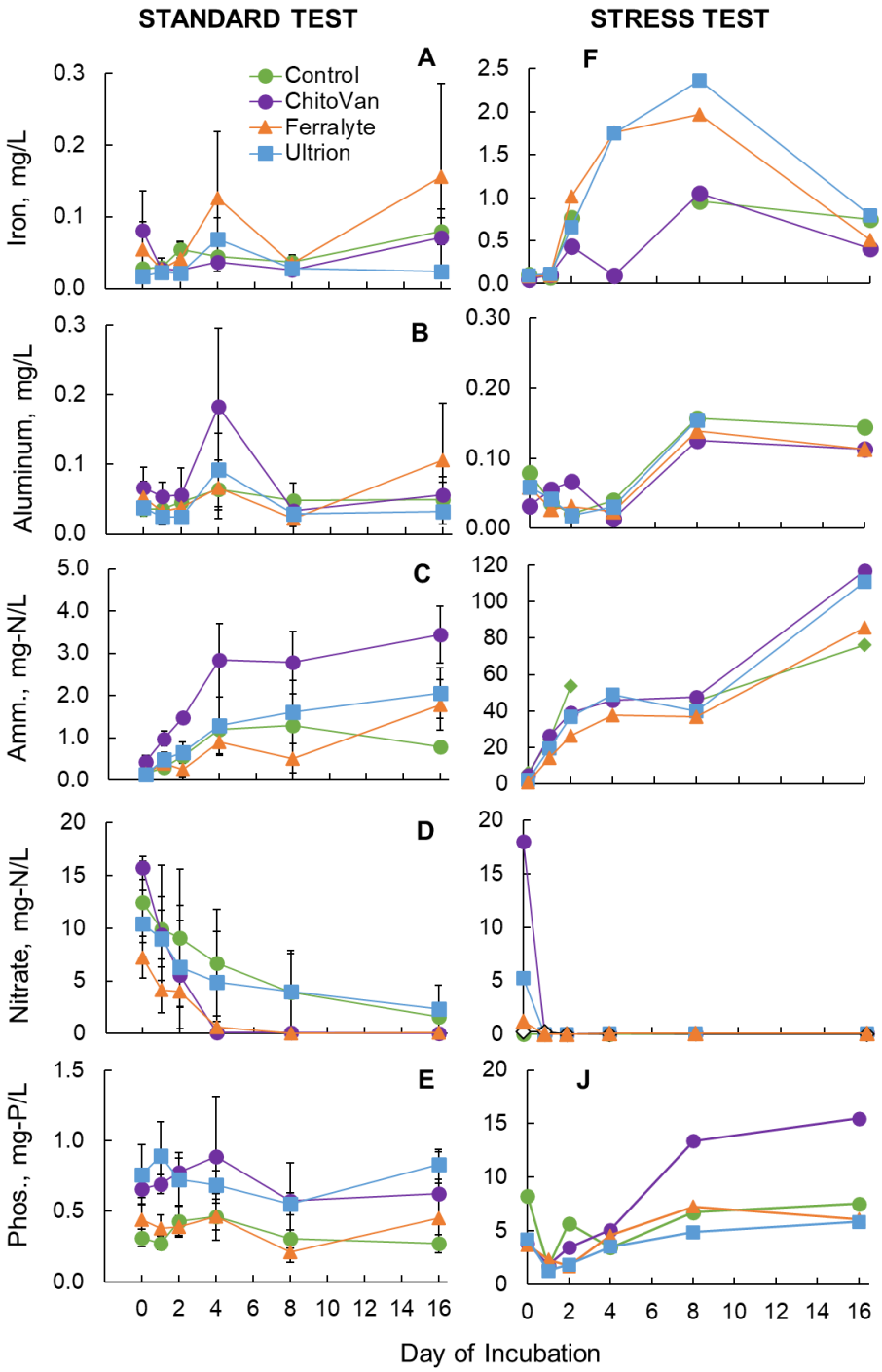

Figure 2-6 Supporting aqueous parameters. Left side, standard test with mean values from control and three coagulant treatments (ChitoVan, Ferralyte and Ultrion) replicated at three stations (A, B and C). Error bars are plus/minus one standard error of triplicate incubations. Right side, stress test with spirulina organic matter addition in control soil for station C. From top to bottom: iron (total), aluminum (total), ammonia (as N), nitrate (as N), and phosphate (as P). Note difference in vertical scale for iron, ammonia, and phosphate.

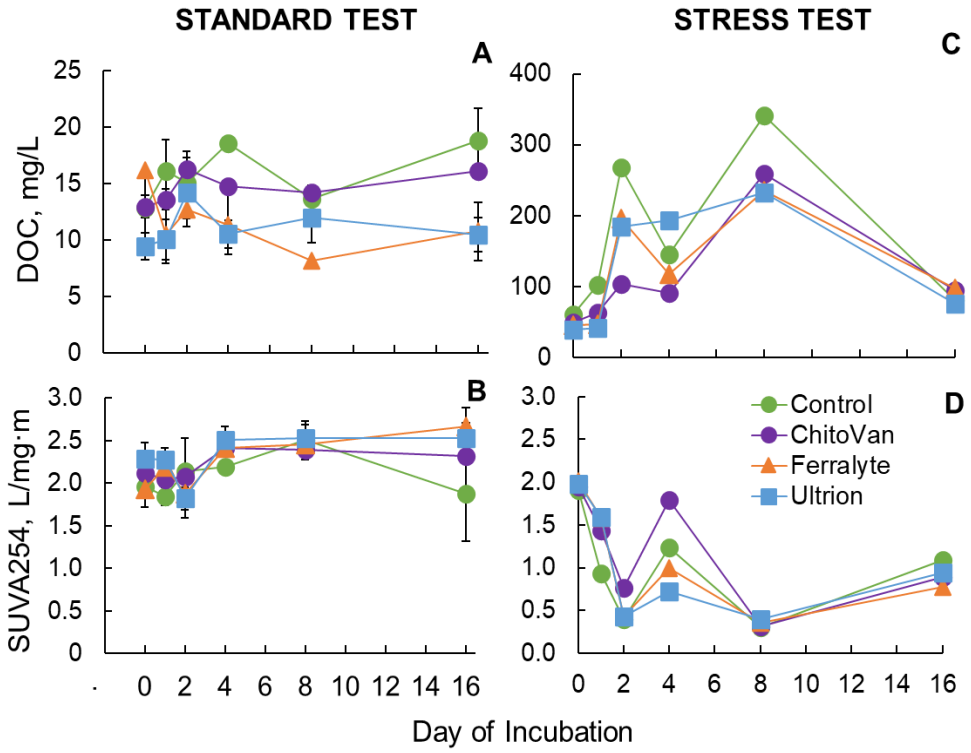

Figure 2-7 Dissolved organic carbon (DOC) concentration (top) and $SUVA_{254}$ (bottom). Left side, standard test with control and three coagulant treatments (ChitoVan, Ferralyte and Ultrion) replicated at three stations (A, B and C) mean values. Error bars are plus/minus one standard error of triplicate incubations. To facilitate statistical analysis, ChitoVan data includes two B incubations since A samples were not available. Right side, stress test with spirulina organic matter addition in control soil for station C. Note difference in vertical scale for DOC.

3. ALGAL ORGANIC MATTER ADDITION OPENS EPHEMERAL MERCURY METHYLATION WINDOW IN MILDLY MERCURY-CONTAMINATED SOILS

3.1 Abstract

Dissolved organic matter (DOM) plays a significant role in the mercury (Hg) cycle by mediating biogeochemical processes within aquatic ecosystems. However, the specific effects of DOM composition on Hg methylation are not entirely understood. As anthropogenic pollution and climate change exacerbate water quality degradation, DOM loading in the form of algae growth in surface waters is increasing, which could potentially promote methylmercury (MeHg) production and its bioaccumulation in biota. To study the effects of algal organic matter loading on the Hg cycle in mildly contaminated wetland soils (total Hg ~0.3 mg/kg dry weight), we added spirulina powder over a concentration range (0.025 g, 0.05 g, 0.1 g, 0.2 g, and 0.4 g) to 250 ml lab-scale soil-water incubations. We analyzed total Hg and MeHg in water and soil and characterized DOM in water using adsorption and fluorescence spectroscopy. The addition of a gradient in spirulina organic matter (SpOM) stimulated a gradient in microbial activity. At high SpOM addition (> 0.1 g), microbial activity increased substantially and generated specific DOM optical signatures. The Hg "methylation window" appeared to open due to an increase in quinoid-like moieties and microbial-sourced DOM, which likely provided labile carbon for microbial activity and growth. This microbial growth may have favored synergistic activity of iron- and sulfate-reducing bacteria and other non-Hg-methylating microbes. In addition, the enrichment of low-molecular-weight DOM appears to have promoted IHg bioavailability. Peak MeHg accumulation in soil (~5 µg/kg) and water (~30 ng/L) was observed at days 2 and 4. However, the methylation window was short-lived, with MeHg levels decreasing in water and soil after day 4, indicating the dominance of MeHg demethylation over Hg methylation. Changes in DOM optical properties and increasingly reduced conditions are possible indicators of this shift in the microbial community. Additionally, a decrease in Hg methylation rates could be associated with lower IHg bioavailability by the formation of larger HgS-DOM complexes. Results suggest that there is a threshold in algal DOM loading at which an ephemeral Hg methylation window may open at the sediment-water interface of aquatic ecosystems. Findings suggest that the optical properties of DOM could be useful indicators of MeHg production in aquatic ecosystems, providing valuable insights into Hg cycling.

3.2 Introduction

The transformation of inorganic mercury (IHg) to methylmercury (MeHg) in aquatic environments is a major concern worldwide (Driscoll et al., 2013; Hsu-Kim et al., 2013). MeHg binds to proteins bioaccumulating into upper trophic levels where it possess a significant health threat for wildlife and humans that

consume contaminated prey (Chetelat et al., 2020). IHg transformations and MeHg bioaccumulation in inland waters are associated with wetlands, rivers, reservoirs, and lakes, where consumption of Hg-contaminated fish is the major MeHg exposure route (Bravo et al., 2018). Most of the IHg input into these ecosystems originates from over 500 years of anthropogenic emissions (Amos et al., 2013; Sonke et al., 2023). Despite global efforts to decrease mercury (Hg) emissions (i.e., the Minamata Convention), MeHg bioaccumulation in fish is still a problem. The main reason is that MeHg concentration does not directly correlate to the amount of IHg in the ecosystem; low levels of environmental Hg pollution can still result in elevated Hg levels in biota (Ullrich et al., 2001). In fact, the net MeHg concentration in the environment is the result of the balance between two processes, Hg methylation and MeHg demethylation (Helmrich et al., 2022). Hg methylation, produced mainly by anaerobic bacteria, depends on multiple biogeochemical conditions, including oxidation-reduction (redox) potential, pH, sulfate concentration, organic matter, microbial activity, and IHg bioavailability, many of which are undergoing alterations due to climate change (Bigham et al., 2016; Peterson et al., 2023; Sonke et al., 2023; Ullrich et al., 2001; Poulin et al., 2023). Biotic MeHg demethylation is performed by aerobic microorganisms with the *mer* gene system, possibly to detoxify their environment, and by anaerobic microbes such as SRB and methanogens as a result of co-metabolic processes (Barkay and Gu, 2022; Lu et al., 2017; Marvin-DiPasquale and Oremland, 1998).

Among the biogeochemical conditions influencing MeHg production, methylation rates are largely dependent on the activity of Hg-methylating bacteria and IHg bioavailability for methylation (Ullrich et al., 2001; Poulin et al., 2023). Both are strongly related to the size and chemical speciation of dissolved and particulate organic matter (DOM, POM) (He et al., 2019; Liem-Nguyen et al. 2016). In a recent study using different types of sediments, the < 0.5 µm size fraction of glutathione-Hg and of two-coordinated-thiol-Hg contributed the most leachable and potentially bioavailable pool of Hg (Xu et al., 2021). Hg uptake (passive permeation, active transport pathways or carbon metabolism) and methylation rates appeared to vary with different microbial strains (Tang et al., 2020). MeHg is produced by archaea and bacteria across the redox spectra with the *hgcAB* genes (Parks et al., 2013; Regnell and Watras, 2019; Sonke et al., 2023). Particularly, MeHg has been associated with sulfate-reducing bacteria (SRB) and iron-reducing bacteria (FeRB) (Campeau and Bartha, 1985; Gilmour et al., 1992; Fleming et al., 2006). In mildly anoxic and sulfidic soils and porewaters, there is a positive correlation between DOM content and SRB activity, as DOM contributes to microbial growth and activity of heterotrophic methylating microorganisms (Graham et al., 2012; Li et al., 2019). Specifically, low-molecular-weight (LMW) DOM composed of proteins, sugars, and starches tends to be especially bioavailable for microbial metabolism, thereby accelerating Hg methylation rates, compared to larger DOM molecules (Bravo et al., 2018; Eckley et al., 2021).

Additionally, autochthonous DOM (e.g., algal biomass) is more bioavailable as an electron donor for Hg methylators compared to allochthonous DOM (e.g., terrestrial stems and leaves) (Liem-Nguyen et al. 2016).

IHg bioavailability, DOM has a dual role as it influences IHg speciation and IHg desorption-dissolution kinetics (Jonsson et al., 2016; Liem-Nguyen et al. 2016). From the IHg pool, the known bioavailable aqueous species for Hg-methylating microbes are the neutral and amorphous Hg-sulfide (HgS) complexes. These include HgS-DOM polynuclear clusters (0.5− 2μm), nanoparticulate (<0.5 μm) HgS (HgS_{NP}), nanoparticulate metacinnabar (β-HgS(s)), and LMW Hg-thiol complexes (Benoit et al., 2001; Graham et al., 2012; Schaefer et al., 2011; Tian et al., 2021; Zhou et al., 2017). Likewise, recently formed Hg-DOM complexes may be more bioavailable for microbes than aged Hg-DOM complexes that tend to be more stable or crystalline (Miller, 2006). In addition, the stimulatory effects of DOM on MeHg production are also attributed to the dissolution of HgS minerals, resulting in the formation of bioavailable nanoscale β-HgS(s) (Graham et al., 2013; Waples et al., 2005). Once MeHg is formed, DOM can facilitate its transport and solubility through complexation, enhancing MeHg bioaccumulation by moving MeHg-DOM complexes to biologically-active surface waters (Marvin-DiPasquale et al., 2009; Ravichandran, 2004). DOM can also decrease IHg bioavailability by inhibiting the aggregation of bioavailable β-HgS(s) (Gerbig et al., 2011; Graham et al., 2013). Moreover, the association of IHg with high-molecular-weight DOM can impede microbial methylation, as the complexes are too large to cross the bacterial cell membranes (Miller, 2006; Ravichandran, 2004). Humic and fulvic acid fractions of DOM can also decrease IHg bioavailability by photochemically reducing IHg to volatile elemental Hg(0) in the presence of reactive oxygen species generated by solar radiation (Driscoll et al., 2013). In addition, optical signatures indicative of DOM type show that specific DOM composition can affect MeHg photodegradation (Fleck et al., 2014).

Nutrient loading and warmer temperatures, associated with increased human activities and climate change, have resulted in widespread eutrophication and elevated DOM loading of aquatic ecosystems (Lambert et al., 2022). Seasonal anoxia, harmful algae blooms, and fresh organic matter decomposition appear to have enhanced MeHg production and subsequent bioaccumulation in some freshwater aquatic ecosystems (Noh et al., 2018). As a consequence in recent years, the impact of algal-derived organic matter (AOM) on Hg cycling in aquatic ecosystems has received greater attention (Catalán et al., 2021; Lei et al., 2019; Y. Wang et al., 2022; Wu et al., 2022). In a comparative experiment between organic matter types, AOM enhanced methylation rates by 1 to 2 orders of magnitude compared to terrestrial organic matter (Wu et al., 2022). Other authors suggest that AOM may enhance or decrease IHg bioavailability by influencing the dissolution and aggregation processes, structural order, and surface properties of HgS_{NP} (Wang et al., 2022). In addition, proteins and aminoacids (such as tyrosine, tryptophan) in AOM have been associated with promoting in situ Hg methylation

(Zhao et al., 2017) and higher Hg methylation rates (Lescord et al., 2018; Wu et al., 2024). With the complex nature of Hg cycling and DOM, information regarding the implications of DOM characteristics and composition on MeHg production in aquatic ecosystems merits further research (Fleck et al., 2014; Wu et al., 2024).

To study the effects of AOM on the Hg cycle, we applied a range of spirulina organic matter loading (0.025 g, 0.05 g, 0.1 g, 0.2 g and 0.4 g to 250 ml bottles) to 16-day laboratory incubations. The microcosm included water from Cache Creek and soil from Cache Creek Settling Basin (CCSB), Sacramento, California, USA. The experiment builds upon previous efforts by the United States Geological Survey (USGS) in CCSB to enhance Hg capture and retention through the application of coagulants (De Parsia et al., 2019; Rodal-Morales, in preparation). Previous results highlighted the importance of DOM in enhancing Hg methylation in CCSB soils (Rodal-Morales et al., in preparation). During this incubation experiment, we analyzed total Hg (THg) and other parameters in water, MeHg in soil and water, and characterized the quality of DOM using adsorption spectra and fluorescence spectroscopy. These techniques have proven to be effective in assessing DOM characteristics in various aquatic environments (Carstea et al., 2020; Downing et al., 2009; Hansen, 2019) and could provide insight into the relationship between DOM composition, microbial activity, and IHg bioavailability (Cui et al., 2022; Fleck et al., 2014). For this study, our two aims were: 1) to evaluate if there is a threshold at which AOM loading stimulates MeHg production, and 2) to measure optical characteristics of incubation water to qualitatively assess microbial AOM degradation and its relationship with the MeHg cycle.

3.3 Methods

3.3.1 Study Site

CCSB, located in the Sacramento Valley, California, USA was designed to control sediment deposition from the Cache Creek watershed before being transported to the Yolo Bypass and the ecologically sensitive Sacramento-San Joaquin Delta. The Cache Creek watershed drains an area of naturally elevated Hg soils, including hydrothermal activity and active mineral springs and deposits, and wastes derived from historical Hg and gold mines (Higgins and Kamman, 2010). While trapping significant amounts of particulate Hg, the CCSB is a source of MeHg production, releasing an estimated 160 g of MeHg annually to the Yolo Bypass (Marvin-DiPasquale et al., 2009). Thus, this wetland-like environment is appropriate for the study of environmental factors that influence IHg methylation. For this laboratory study, we used soil samples from the southeast region in CCSB previously collected by the USGS in 2018 (De Parsia et al., 2019; Rodal-Morales, in preparation) and water samples collected by the USGS from Cache Creek at Rumsey USGS index station during May of 2022. At UC Merced, we homogenized the soil samples with a size 10 sieve and filtered the water using

GF/F filters. Collected soils were in an oxidized state with elevated levels of redox-sensitive manganese (~52%) and iron (~30%). Water content of soil was around 16% and loss on ignition around 0.6%. THg concentrations in CCSB soil and Cache Creek water were 299 µg/kg and 1.1 ng/L, respectively. Initial MeHg concentrations in CCSB soil and Cache Creek water were 2.14 µg/kg and 0.06 ng/L, respectively (Table 3-1). See Rodal-Morales et al. (in preparation) for more details on the study site and soil characterization.

3.3.2 Spirulina Powder

Spirulina powder from Micro Ingredients brand (Montclair, California, USA) was the form of AOM used for the incubations. Spirulina is a photosynthetic bacterium, from the group *Cyanobacteria Prochlorales*, also known as green blue algae. Chemical analysis notes that spirulina is made up of 60 to 70% proteins, 13% carbohydrates, and 4 to 7% lipids (Ali and Saleh, 2012). Spirulina typically contains around 1% calcium, phosphorus, potassium, and sodium, as well as trace amounts of naturally sulfur compounds, especially sulfate (Ali and Saleh, 2012; Ashworth, 2024).

3.3.3 Incubation Design and Sampling

The microcosm experiment was designed to measure MeHg concentrations in water and soil under five different AOM loadings over a 16-day anaerobic laboratory incubation. Spirulina organic matter (SpOM) was added at 0.025 g, 0.05 g, 0.1 g, 0.2 g, and 0.4 g to 250 ml Teflon bottles mixed with 50 g of CCSB soil and 200 g of Cache Creek filtered water. The upper limit loading was informed based on the “Stress-test” (0.5 g f SpOM) from previous incubation experiments in collaboration with the USGS which showed MeHg production (Rodal-Morales, in preparation). The addition of 0.5 g f SpOM was equivalent to approximately twice the total OM concentration measured in the soil based on LOI measurements (Table 3-1). The preparation included a deoxygenation step where the bottles (with the soil and spirulina) were placed inside a glove box flushed with nitrogen gas for two days. We also bubbled Cache Creek water with the nitrogen atmosphere of the glove box during the same time. After two days inside the glove box, we added the water to the bottles with soil and SpOM and heavily shook them. Then, the slurry incubation bottles were placed on their side on a shaker table at 150 RPM at room temperature (~21°C) and covered with aluminum foil until sampling. The bottles were destructively sampled for water THg, water and soil MeHg, and other water quality parameters (iron, aluminum, manganese, ammonia, nitrate, phosphate, sulfate, chloride), and dissolved organic carbon (DOC) characteristics at six time points (0, 1, 2, 4, 8, and 16 days). The incubations included a control, CCSB soil with no SpOM, six randomly selected replicates, and two Cache Creek water blanks. This set up resulted in a total of 46 bottles. The incubation replicates, developed to assess the replicability of the experimental mesocosms, typically had a relative percent difference of around 14% for the range of parameters assessed.

When sampling, we placed the selected bottles in the centrifuge at 12,000 RPM and 22°C for 40 minutes to separate water from soil. Then, we measured pH and redox potential using clean and calibrated probes (HACH HQ40d multi meter, HACH MTC10101 ORP probe, Loveland, CO) inside the glove box. Redox potential values were converted to the hydrogen electrode (Eh) following the Nernst equation temperature correction (Nordstrom and Wilde, 2005). Finally, we filtered the supernatant water through pre-combusted 0.3 µm glass-fiber filters and preserved it for later analysis. The preservation included acid addition and fridge storage, including 0.4% by volume trace-metals grade hydrochloric acid for THg and MeHg and 1% by volume trace-metals grade nitric acid for iron, aluminum, and manganese. For ammonia, nitrate, phosphate, sulfate, and chloride, samples were frozen. DOC samples for optical measurements were refrigerated and shipped on ice within 2-3 days of sampling to the USGS for analysis. Soil samples were frozen and later freeze-dried for further analyses.

3.3.4 Analyses

The water analyses included THg and MeHg, total metals (iron and manganese), nutrients (ammonia, nitrate plus nitrite, and phosphate), anions (sulfate and chloride), and DOC characteristics (DOC concentration and optical properties). We analyzed THg analyzed using cold vapor atomic fluorescence spectroscopy (CVAFS) based on the method USEPA 1631 on a MERX-T (Brooks Rand Labs, Seattle, WA, USA) (USEPA, 1994). MeHg water samples were distilled (2 h at 125°C with nitrogen gas flow < 50 ml/min) before being measured on a MERX-M (Brooks Rand Labs, Seattle, WA, USA) using ethylation, gas chromatography, and CVAFS according to the method USEPA 1630 (USEPA, 1998). In all incubations, IHg concentration in water was estimated as THg concentration minus MeHg concentration. For soil, MeHg was extracted from ~0.2 g of homogenized, freeze-dried soil followed by digestion with 2.5 ml of 25% KOH in methanol (USEPA, 1996). Digestant was then analyzed for MeHg in water as detailed above. Two soil samples were sent for inter-lab MeHg analysis comparison to Brooks Brand Laboratory (Seattle, Washington, USA). The relative percent difference for the UC Merced and Brooks Rand Laboratory MeHg soil analyses was 16.7% (n = 2). Hg analyses followed strict quality control standards including method blanks (<0.1 ng/L), matrix spikes (75-125% range), analytical duplicates, and ongoing procedure recovery (75-125% range). Reporting limits were 0.2 ng/L for THg and 0.02 ng/L for MeHg. Batches that did not meet quality control criteria were rerun or flagged (See Appendix). We analyzed metals using inductively coupled plasma optical emission spectrometry (ICP-OES) on an Optima 5300 DV with a reporting limit of 0.01 mg/L (USEPA,1994). Nutrients were analyzed on a LACHAT QuikChem 8500 autoanalyzer using standard colorimetric methods by air-segmented continuous-flow absorption

spectrophotometry (Antweiler et al., 1996). Reporting limits were 0.02 mg-N/L for ammonia and nitrate and 0.02 mg-P/L for phosphate (analyzed as soluble reactive phosphate). Anions were measured using ion chromatography on a Dionex ICS-2000 following the method USEPA 300.1 with a reporting limit of 0.4 mg/L (USEPA, 1997).

DOM composition was evaluated using derivations of absorbance and fluorescence properties analyzed at the USGS Organic Matter Research Laboratory (Sacramento, California, USA). DOM optical properties are related to the light sensitive (chromophoric) portions of the DOM pool that absorb or fluoresce in the ultraviolet and visible spectra. Spectral absorbance (A) was measured at 1 nm increments between 200 and 750 nm in a 0.01 m quartz cuvette using a CARY-300 spectrophotometer (Agilent Technologies, Santa Clara, CA, USA). Independent spectral slopes were calculated for multiple wavelength ranges using a non-linear least-squares curve fitting technique for each spectral range (Boss and Zaneveld, 2003; Del Vecchio and Blough, 2002) using MatLab R2008a (MathWorks, Natick, Massachusetts, USA). Fluorescence was measured using a SPEX Fluoromax-4 spectrofluorometer equipped with a 150 W Xenon lamp (Horiba Jobin Yvon, NJ, USA) at excitation wavelengths (ex) of 200 nm to 440 nm at 10 nm increments and emission wavelengths (em) of 300 nm to 600 nm at 5 nm increments on room temperature (25°C) in a 1 cm quartz cell. Results are reported in Raman-normalized fluorescent units (RU) (Gu and Kenny, 2009). Individual diagnostics regions such as F and B, and other DOM compositional indicators like the fluorescence index (FI) and humic index (HI), were identified according to previous efforts (Table S6). DOC concentration was measured using high-temperature combustion total organic carbon analyzer (Model TOC-VCHS; Shimadzu Scientific Instruments, Columbia, Maryland) according to USEPA Method 415.3 (Potter and Wimsatt, 2005). There appeared to be DOC contamination in some samples, making DOC concentration results somewhat uncertain. However, an assessment of DOC concentration versus absorbance showed that the contamination appeared to be a simple organic solvent (e.g., methanol) which did not have a significant absorbance or fluorescence signature. Thus, we concluded that the DOC optical characteristics of the collected dataset were valid. In addition, as we were mostly interested in the quality and optical characteristics of the DOM, the lack of complete DOC concentration dataset did not undermine the overall experiment.

3.4 Results

3.4.1 Aqueous Parameters: redox potential, pH, manganese, and sulfate

In general, there was a negative gradient in redox potential, indicative of more reduced conditions, as the amount of spirulina addition increased in the incubations (Fig. 3-1A). At the beginning of the experiment, the incubations with 0.025 g, 0.05 and 0.1 g SpOM, as well as the control, started at a higher redox

potential (400 mV). In contrast, the incubations with 0.2 and 0.4 g SpOM at day 0 (~2 hours after soil flooding) started with a lower redox potential (250 mV). Looking at the redox potential temporal patterns, the control showed minimal variations after day 4, stabilizing at 300 mV. For the incubations with 0.025 and 0.05 g SpOM, the redox potential dropped to 150 mV by day 16. For the incubation with 0.1 g SpOM, redox potential decreased to -200 mV in 8 days. The redox potential for the incubations with 0.2 and 0.4 g SpOM dropped from 250 mV to -250 mV during the first 4 days. Interestingly, for the 0.2 and 0.1 g SpOM treatments, there was an increase in redox potential from day 8 to 16, reaching -100 mV. On the contrary, the incubation with 0.4 g SpOM showed a continuous value of -200 mV by the end of the experiment. For pH (Fig. 3-1B), values showed a more prominent drop with higher SpOM addition. pH levels started at 7.5 to 8 and dropped to more circumneutral conditions (7 to 6.8) in all samples. The incubations with 0.1 and 0.2 g SpOM showed higher pH values (~7.9) at day 0 compared to the rest of the treatments. The control had a continued drop in pH after day 4 while the incubations with SpOM addition showed the main drop in pH during the first 2 days.

Manganese concentration increased progressively with the addition of SpOM (Fig. 3-1C). In the control, the continuous accumulation started on day 4 reaching a concentration of 1.4 mg/L by day 16. Incubations with 0.025 and 0.5 g SpOM showed manganese accumulation after day 2, with peak concentrations of 2 to 3 mg/L at day 16. For the incubations with 0.1 and 0.2 g SpOM, manganese accumulation started on day 1 and reached peak concentrations of around 3.5 mg/L on day 8. Manganese concentrations remained relatively steady for the rest of the incubation period. Lastly, for the incubation with 0.4 g SpOM, manganese accumulation started on day 1 and peaked at 5.2 mg/L on day 4, then dropped to 4.7 mg/L by day 16. For iron (Fig. 3-1D), accumulation started on day 2 only for the incubations with 0.1, 0.2, and 0.4 g of SpOM, which coincided with lower redox conditions. In the incubation with 0.1 g SpOM, iron was continuously released after day 4, with a final concentration of 1.7 mg/L at day 16. The incubations with 0.2 g and 0.4 g of SpOM addition showed similar behavior, a progressive release of iron starting at day 2, followed by a decrease in concentration after day 8 to around 1.4 mg/L by the end of the incubation.

Results for sulfate (Fig. 3-1E) showed minimal changes in concentration for the control, 0.025, 0.05, and 0.1 g SpOM addition with values ranging from 60 to 140 mg/L. However, for the 0.2 and 0.4 g SpOM incubations, there was a continuous decrease in concentration after day 4, with sulfate being depleted by day 16. Finally, phosphate (Fig. 3-1F) showed a quasi-steady concentration for the control and a gradient in accumulation at day 4 for the different SpOM treatments. Phosphate concentration showed a dramatic increment for 0.1 and 0.2 g SpOM addition. On the contrary, for the 0.4 g SpOM addition, phosphate concentration decreased back to initial conditions. While some DOC concentration data appeared compromised, data from this study and a related study (Rodal-Morales, in

preparation) indicate that DOC in water was 10-20 mg/L in control incubations and 200-300 mg/L in incubations with 0.4 g SpOM addition. Intermediate SpOM additions likely had concentrations between these extremes. DOC concentration showed a general trend of increasing from days 0 to 8 and then decreasing from days 8 to 16 (Fig. S6).

3.4.2 Mercury and Methylmercury in water and soil

Overall, there was no Hg accumulation in the water and soil phase for the control, 0.025 and 0.05 g SpOM incubations (Fig. 3-2). Patterns of Hg accumulation for the 0.2 and 0.4 g of SpOM incubations were similar but differed in magnitude and accumulation day. Both treatments showed a short-lived Hg accumulation which returned to initial conditions by day 16. Starting with MeHg in water (Fig. 3-2A), for the 0.2 g SpOM incubation MeHg peaked on day 4 at 14 ng/L then decreased to initial conditions by day 16. For the 0.4 g SpOM addition, MeHg concentration had a rapid increase, peaking at 27 ng/L on day 4, then steadily decreasing to 2.7 ng/L by day 16. For water IHg (Fig. 3-2B), the 0.1 g SpOM addition appeared to be slightly enriched to around 24 ng/L after day 8. For the 0.2 g SpOM addition, IHg peaked on day 1 at 47 ng/L then steadily decreased to background levels. The 0.4 g SpOM addition peaked at 90 ng/L on day 2, sharply decreased to 27 ng/L by day 8, and slowly declined to 15 ng/L by day 16. The %MeHg in water (Fig. 3-2C) ranged from 0.05 to 2.3% during MeHg accumulation in early days of the 0.2 and 0.4 g SpOM addition. The MeHg to IHg ratio followed the same pattern as MeHg in water showing values of around 0.1 to 0.5 for the incubations with more SpOM addition (0.2 g and 0.4 g) (Fig. 3-2D).

In soil, MeHg mass mostly followed the same behavior as MeHg concentration in water (Fig. 3-2E). There was no variation in MeHg mass for the control and the incubations with 0.025 and 0.05 g SpOM addition. The 0.1 g SpOM incubation showed a minimal increase in soil MeHg mass to 1.6 ug/kg, returning to initial conditions by day 8. For the 0.2 g of SpOM incubation, there was a continuous increase in soil MeHg after day 1, peaking at 3 ug/kg during day 4, then steadily decreasing to around 1 ug/kg by day 16. For the 0.4 g SpOM incubation, MeHg in the soil had a continuous increase during the first four days to 5.4 µg/kg, then a steady decline to initial conditions by day 16. Finally, MeHg log K_d (soil/water) (Fig. 3-2F) was steady at around 4 for the control, 0.025, and 0.05 g SpOM incubations. The 0.1 g SpOM incubation demonstrated a small change in log K_d from 4 to 3.3 by day 4, then returned to initial conditions by day 8. For 0.2 and 0.4 g SpOM incubations, log K_d dropped from 4 to around 2.5 during the first day, for both incubations, as MeHg concentration in water increased. Log K_d steadily increased to around 3.5 in the 0.2 g SpOM addition and 2.9 in the 0.4 g SpOM addition by day 16.

3.4.3 Optical Characterization of Dissolved Organic Matter

Patterns of DOM optical properties also showed a gradient in measurements related to the gradient in SpOM addition (Fig. 3-3 and 3-4). Fluorescence intensity measurements in region F (Flr_F), previously referred as FDOM (Fig. 3-3A), is reportedly related to quinoid-like DOM, which are functional active groups in humic substances normally not associated with labile carbon (Downing et al., 2009). Region F fluorescence intensity was higher at day 0 in microcosms with higher SpOM addition. For example, the day 0 value was 2.5 RU for the control addition and 30 RU for the 0.2- 0.4 g SpOM addition (Fig. 3-3A and 3-4). All treatments showed a general pattern of decreasing in fluorescence region F as a function of incubation time, returning close to background conditions (~2 RU) by day 8 (Fig. 3-3A). The fluorescence in B region (Flr_B) is related to amino acids-, protein-, and phenols-like DOM (Coble, 1996, 1990; Stedmon et al., 2003), normally associated with tyrosine, a highly bioavailable fraction of DOM (Weishaar et al., 2003). Region B fluorescence intensity interestingly showed an increase from day 0 to 4 only for the incubations with 0.2 (61 RFU) and 0.4 g (150 RFU) SpOM addition (Fig. 3-3B and 3-4). Most of the increase in fluorescence for these high SpOM treatments happened during day 1 to 2. The fluorescence index (FI) (Fig. 3-3C) allows to identify the source or type of the DOM pool. Values higher than 1.8 are normally related to bacterially derived DOM, while values lower than 1.4 are associated to terrestrial derived DOM (Cory et al., 2010). FI at day 0 increased with increasing SpOM addition, from 1.7 in the control to 3 in the 0.4 g SpOM treatments (Fig. 3-3C and 3-4). FI followed a similar decrement pattern to the fluorescence region F, returning to background (control) conditions by day 8. Finally, the spectral slope ($Sag_{275\text{-}295}$) is reportedly an indicator of DOM with high molecular weight (< 0.01) or LMW (> 0.02) (Blough and Del Vecchio, 2002; Helms et al., 2008). LMW DOC is of especial interests because it tends to be more labile for microbes and can enhance IHg bioavailability. The most obvious patterns were seen for the 0.1, 0.2, and 0.4 g SpOM additions, with an initial increase between days 1 to 2, followed by a decrease to a steady value around day 8 (Fig. 3-3D). For these three treatments, both the peak and the final steady state value of $Sag_{275\text{-}295}$ was higher with higher SpOM addition. The most dramatic pattern was for the 0.4 g SOM addition, which peaked at 0.035 on day 1, then steadily dropped to 0.026 by day 8. For the description of the other fluorescence parameters analyzed see Appendix section (Table S7, Fig.S2).

3.5 Discussion

3.5.1 Algal Organic Matter Stimulates Microbial Activity

The addition of SpOM appears to have notably increased the presence of quinoid- and protein-like moieties, which likely had the potential to be metabolized by heterotrophs. Within the initial 2 h following the mixing of water, soil, and AOM (day 0), there was evidence of SpOM solubilization, indicated by relative differences in optical properties in incubation water with higher SpOM

addition. The incubations were gradually enriched in regions indicative of microbial/algal DOM sources (FI index and region N) and in protein-like components of DOM (regions B and T), recognized as bioavailable substrates for microbial growth (Cammack et al., 2004; Fleck et al., 2014). Interestingly, there was also a gradual enrichment in humic- and fulvic-like DOM compounds (fluorescence regions A, C, M, and D), especially in the quinoid-like DOM moiety (region F), with high SpOM addition (Fig 3-3, 3-4, S2, Table S2). Humic-like substances (CH aromatics and OH polysaccharides) were also identified in an AOM characterization study with the common cyanobacteria *Microcystis* and red tide dinoflgellate *Alexandrium tamarense* (Villacorte et al., 2015). Considering the aliphatic and reduced nature of AOM (Villacorte et al., 2015; Wu et al., 2024), another possible explanation for the humic-like DOM enrichment after SpOM addition in our incubations could be the presence of fully reduced quinones-like moieties, detectable as aromatic carbon, thus having a humic-like DOM response (Cory and Mcknight, 2005).

The observed changes in optical properties as the incubation progressed suggest a stimulation of microbial activity. Labile organic matter plays a crucial role in the biogeochemical cycles as electron donor for microbial reactions (Bravo et al., 2017; Lei et al., 2019). As SpOM dissolved, the release of small carbon compounds (LMW DOM), as suggested by $Sag_{275\text{-}295}$ enrichment (Fig. 3-3D), likely fueled the growth and activity of multiple types of microbes, possibly including syntrophs and heterotrophs (Eckley et al., 2021; Peterson et al., 2023; Zhu et al., 2024). Interestingly, these bacteria appeared to consume the quinoid-like DOM (fluorescence region F) and the microbial-source DOM (FI index) over the course of incubation (Fig. 3-3A), despite these indicators not being traditionally associated with the most bioavailable forms of carbon as the protein-like DOM (fluorescence region B and T). However, quinones could enhance electron transfer within the lipid bilayer of bacteria cell membranes (Rich and Marecha; 2012), potentially facilitating microbial reactions, such as denitrification (Aranda-Tamaura et al., 2007). In addition, Lescord et al. (2018) showed that biotic MeHg production was related to the amount of microbial-based OM (FI index), as seen in our incubations. On the other hand, the unexpected enrichment in tyrosine-like DOM (region B) with incubation time may result from active heterotrophs releasing extracellular byproducts during their biosynthesis and growth (Fig. 3-3B) (Cammack et al., 2004, Zhu et al., 2024). Hernes et al. (2009) showed this region could represent more than tyrosine-like DOM component and could be an indicator of an OM degradation byproduct. Moreover, the decrease in fluorescence values in the humic-like regions through time could be attributed to microbial activity breaking the SpOM components into simpler molecules (Tranvik, 1988), as suggested by the decrease in the HIX index (Fig. 3-4 and S2, Table S7).

Other signals of microbial activity in the incubations (Fig. 3-1) included the drop in pH and redox potential (from oxidized to reduced conditions),

accumulation (manganese, iron) or loss (nitrate, sulfate) of aqueous parameters indicative of microbial reduction, and indicators of organic matter mineralization including accumulation of ammonia and phosphate (Davidson, 1993; Henze et al., 1995; Reineke, 2001; Rysgaard et al., 1994). For example, the control showed minimal changes by the end of the incubation, with redox conditions reaching levels associated with manganese and nitrate reduction. This was accompanied with modest ammonia (~1 mg/L) and manganese (~1 mg/L) accumulation, and nitrate depletion likely driven by denitrification processes (Fig. 3-1). But at SpOM addition of 0.1 g and above, the incubations had drastic redox potential decreases and the changes in aqueous parameters were more evident. We saw iron accumulation (>1 mg/L), likely due to microbial reduction of iron oxides, and the probable co-release of sorbed phosphate, reaching concentrations of 3.9 mg-P/L (Davidson, 1993). Additionally, a decrease in fulvic-like DOM coincided with the release of iron into the water (Fig. S2). Studies shown that fulvic acids could enhance the microbial reductive dissolution of iron oxides by FeRB, accelerating reduced iron release, as seen after day 2 in our incubations (Song et al., 2023). The highest addition of SpOM (0.2 and 0.4 g) showed a burst of microbial activity and reached highly reduced conditions likely associated with SRB activity, as indicated by the decrease in sulfate concentration (Fig. 3-1).

It was in these two high AOM treatments where MeHg was also observed (Fig. 3-2). High amounts of SpOM appeared to stimulate the activity of Hg-methylating microbes. Several studies have reported a positive correlation between high MeHg concentrations and methylation rates with high OM concentration (Bigham et al., 2017; Cossa & Gobeil, 2000; Gagnon et al., 1997; Ullrich et al., 2001). Particularly, AOM has been identified as a significant electron donor for microbial metabolisms, enhancing Hg methylation (Herrero Ortega et al., 2018; Wang et al., 2023; Zhao et al., 2021). In the 0.2 and 0.4 g treatments, MeHg started accumulating on day 1, when the system was associated to mildly reduced conditions (100 mV). But peak MeHg accumulation in soil and water occurred during day 2 and 4, with depressed redox potential (-200 mV) associated with FeRB and SRB activity (Fig. 3-1A) (Marvin-DiPasquale et al., 2014; Reineke, 2001).

3.5.2 Ephemeral Methylation Window

In natural environments, the net production of MeHg is the result of both Hg methylation and MeHg demethylation processes, leading in many cases to a short-lived net MeHg accumulation (Hintelmann et al., 2000), or as we called it, the methylation window (Fig. 3-2, 3-5). It seems that in our experimental incubations with elevated SpOM addition, we had an ephemeral methylation window from days 0 to 4, which was followed by a decline in both soil and water from day 4 to 8. MeHg production was mostly associated with the soil phase (Fig. 3-2F). For instance, during peak MeHg production only 2% of the MeHg was observed in water (Fig. 2C), demonstrating MeHg's high affinity to the soil phase (Hintelmann et al., 2004). Additionally, Hg and DOM optical properties patterns

suggest that the system was reaching to a new quasi-steady condition under the anoxic conditions by the end of the incubation.

Below we discuss a conceptual model of these observed dynamics (Fig. 3-5) within a framework of three stages of MeHg production including. Stage I: Opening the methylation window; Stage II: Closing the methylation window; and Stage III: Anoxic quasi-steady conditions.

3.5.2.1 Stage I: Opening the Methylation Window

In the incubations with elevated SpOM loading (>0.1 g), MeHg accumulated in both soil and water, suggesting the methylation window opened from day 1 to 4. Multiple factors could contribute to its opening, including SpOM dissolution, desorption processes, and microbial activity (Fig. 3-5). Withing the first 24 h, it is possible that solid-phase Hg (MeHg and IHg) from CCSB soil (POM) was liberated to the aqueous phase by binding to dissolved organic ligands following the dissolution of SpOM.

$$Hg^{2+} - POM \rightarrow Hg^{2+} + -DOM$$
$$MeHg - POM \rightarrow MeHg + -DOM$$

Dissolved organic ligands originated from soil organic carbon are recognized for acting like carriers, facilitating the mobilization of heavy metals, including Hg, in sediment-water systems (Zeng et al., 2024). Dissolution of the SpOM appeared to enrich the aqueous phase with LMW DOM, suggested by the increase in $Sag_{275\text{-}295}$ values early in the incubation (Fig. 3-3D). In conjunction, desorption processes associated to the reductive dissolution of manganese oxides, iron oxides, and clays might have also released Hg-DOM complexes to the aqueous phase (Gagnon et al., 1997; Cossa & Gobeil, 2000). Manganese started accumulating during day 0-1 and iron started accumulating around day 2, both coinciding with MeHg and IHg buildup (Fig. 1C-D, 2). The release of IHg-DOM by these processes, possibly associated to LMW thiols (R-SH^-), like cysteine (R-SH_{cys}), and even humic acids (La) into the water phase may have also increased IHg bioavailability and helped opening the methylation window early in the incubations. Some examples of the possible reactions occurring during the first two hours in the incubations are:

$$R - SH^- + Hg^{2+} \rightarrow Hg - R - SH^+$$
Log k 25.8-32.2 (Haitzer et al., 2002)

$$R - SH_{cys} + Hg^{2+} \rightarrow Hg - R - SH_{cys}{}^+$$
Log k 14.4 (Ravichandran 2004)

$$La + Hg^{2+} \rightarrow Hg - La^{2+}$$
Log k 3.6 (Tipping, 2007)

Another factor contributing to the opening of the methylation window was the increased activity of multiple microbial communities due to the rise in labile carbon resulting from the dissolution of SpOM. (Fig. 3-5). The enrichment in fluorescence region F (quinoid-like DOM) and FI index (showing microbial source DOM), followed by their decline, coincided with the changes in water parameters and MeHg buildup during the incubation, suggesting microbes used this type of DOM as substrate (Fig. 3-1, 3-2 and 3-3A and 3-3C). $Sag_{275\text{-}295}$ values also decreasing after day 1 could indicate microbial activity consuming labile carbon (LMW DOM) (Fig. 3-3D). Hg-thiol complexes could be rapidly utilized by SRB, likely increasing the Hg methylation rates (Regnell and Watras, 2019).

$$SO_4^{2-} + Hg - R - SH^+ \xrightarrow{SRB} HS^{2-} + H_2O + HCO_3^- + MeHg$$

Additionally, the progressive increase in fluorescence region B, as region F and FI index were decreasing, could be interpreted as microbes releasing a byproduct component during their biosynthesis and growth (Laspidou and Rittmann, 2002; Zhu et al., 2024) (Fig. 3-3B).

The enrichment in microbial communities likely increased Hg methylators, such as FeRB and SRB, which contributed to the opening of the methylation window. Previous studies have observed that AOM stimulates the growth and abundance of Hg-methylating microbes (Lei et al., 2019; Mazrui et al., 2016; Zhu et al., 2024). In the high SpOM incubations, iron concentration increased and sulfate concentration decreased during MeHg production suggesting the activity of FeRB and SRB, two main Hg-methylating microbes (Compeau & Bartha, 1984; Fleming et al., 2006; Marvin-DiPasquale et al., 2014). A simultaneous activity of FeRB and SRB early in the incubations, when the bulk redox conditions were favorable for nitrate and manganese reduction, could be explained firstly, by heterogeneity of redox conditions inside micro aggregates (Alewell et al., 2006; Lacroix et al., 2023). Secondly, studies have shown that syntropy between microbial species is important for Hg methylation, including typical non-methylators with Hg methylators (Bae et al., 2014; Xu et al., 2019; Yu et al., 2018; Zhou et al., 2022). For example, FeRB and SRB through direct exchange of electrons could contribute to MeHg production (Shi et al., 2016). This suggests that in CCSB, SRB may depend on various organisms, including FeRB, to break down complex organic substrates to more biodegradable fractions, leading to the production of MeHg (Shi et al., 2016; Yu et al., 2018; Zhou et al., 2022).

3.5.2.2 Stage II: Closing the Methylation Window

Following day 4, despite favorable methylation conditions (elevated sulfate and DOC, and circumneutral pH), the methylation window closed as the rate of MeHg demethylation increased over the rate of Hg methylation. MeHg levels in both soil and water, and the MeHg:THg ratio decreased indicating a true loss mechanism in our soil-water system (Fig. 3-2). Two factors might have contributed

to its closing, MeHg demethylation by microbes and a decrease in IHg bioavailability (Fig. 3-5). MeHg demethylation can overtake Hg methylation when redox potential is reduced to conditions favorable for microbial demethylation, in the absence of photolytic demethylation (Marvin-DiPasquale et al., 2000; Ullrich et al., 2001). As redox potential continued to drop in the incubations (-250 mV on day 4), the oxidative pattern for MeHg demethylation could have been favored by certain types of fermentative microbes, in addition to SRB and FeRB (Bridou et al., 2010). DOM optical properties also suggest a shift in microbial activity after day 4 as the change in fluorescence flattened out in region F and ceased increasing in region B (Zhu et al., 2024). Then, a presumed buildup in sulfide concentration, from high SRB activity, could have led to low IHg bioavailability via the formation of less bioavailable charged Hg-S complexes and Hg-polysulfide complexes with DOM (Hsu-Kim et al., 2013; Poulin et al., 2017; Ullrich et al., 2001; Jay et al., 2000):

$$Hg^{2+} + HS^{-} \rightarrow HgSH^{+} \qquad \text{Log k } 22.3$$

$$Hg^{2+} + 2HS^{-} \rightarrow Hg(SH)_2 \qquad \text{Log k } 40.37$$

These complexes cannot permeate bacteria cell membranes (Liem-Nguyen et al., 2017; Regnell and Watras, 2019), leading to a decrease in IHg bioavailability, and consequently a decline in Hg methylation rates in the incubations. Moreover, IHg can precipitate with sulfide producing metacinnabar (β-HgS(s)) resulting in a sink for bioavailable IHg (Poulin et al., 2017). PhreeqC 3.6.2 calculations (LLML database) using data from day 4 suggest a sulfide concentration of 1.64×10^{-5} mg/L would result in HgS precipitation (Cache Creek alkalinity data from USGS Rumsey Station). This β-HgS(s) sink could explain the dramatic decrease in water IHg after day 2 (Fig. 3-2B).

3.5.2.3 Stage III: Anoxic quasi-steady state

During the last 8 days of the incubation, optical and Hg-related parameters approached a quasi-steady state returning to values close to the control incubation by day 18 (Fig. 3-5). Similar results of incubations reaching a quasi-steady state were seen in other studies of Hg cycling in aquatic sediment (Compeau and Bartha, 1985; Ullrich et al., 2001). DOM optical properties, during this anoxic, low-redox-potential period, suggest a transition to low microbial activity as the primary organic substrates were being depleted. This apparent substrate depletion could be indicated by relatively steady fluorescent signal in regions F, FI and B after day 8. For the Hg cycle, it is likely that low MeHg demethylation processes, carried by SRB and possibly methanogens, were still occurring (Barkay et al., 2003; Fuhrmann et al., 2021). This is indicated by the ongoing decrease of MeHg in water and soil phase, as well as stable redox potential values (-300 mV) associated with methanogenesis production (Reineke, 2001). The depletion of sulfate in the highest SpOM loaded incubations also suggests suppressed SRB activity sometime between day 8 to 16.

In addition, IHg bioavailability likely remained low due to SRB activity producing sulfide, which as noted above, can bind with IHg (Poulin et al., 2017; Regnell and Watras, 2019). During this stage, we saw indirect evidence for sulfide production. For example, in the 0.2 and 0.4 g SpOM incubations, Fe concentration in water dropped after day 8 (Fig. 3-4D). A potential sink for Fe is precipitation with sulfide as mackinawite (FeS_m), a common process in lakes with anoxic bottom waters (Davison, 1993). Reported solubility products for FeS_m show a pKsp of 2.6-3.8, indicating a high affinity between iron and sulfide (Beutel et al., 2020; Cook, 1984; Murray, 1995; Slowey and Brown, 2007). PhreeqC 3.6.2 calculations (LLML database) suggest that FeS_m precipitation could occur with a sulfide concentration of 0.07 mg/L in the presence of around 2.5 mg/L of iron observed during day 8 of incubation (Cache Creek alkalinity data from USGS Rumsey Station).

3.6 Environmental Considerations

In CCSB soils, the addition of AOM at elevated loading was a key stimulator of MeHg production. Initial SpOM degradation likely increased labile carbon, as indicated by initially elevated fluorescence in region F (quinoid like-DOM), FI index (microbial source DOM), and $Sag_{275\text{-}295}$ (an indicator of LMW DOM). This bioavailable carbon appears to have enhanced both microbial activities, including Hg methylators, and potentially IHg bioavailability as well. The stimulated microbial activity possibly facilitated syntrophic interactions between non-Hg-methylating and Hg-methylating microbes. These interactions appeared to be especially important between FeRB and SRB, which could have prompted substantial MeHg production early in the incubations. After day 4, the incubations transitioned to more reduced conditions, resulting in MeHg demethylation overpowering Hg methylation. This was evidenced by the decline in soil and water MeHg and in the shift in DOM optical properties, including slower drops in region F fluorescence and FI index and ceased accumulation in region B fluorescence between day 4 and 8. After day 8, most of the DOM optical properties and the Hg cycle were transitioning to an anoxic quasi-steady state due to an apparent decrease in microbial activity attributed to the depletion of the main substrate regions (FI index and F). Hence, optical properties of DOM appear to correspond to the opening and closing of the methylation window, which are driven by contrasting patterns of microbial activity and IHg bioavailability. Interest in developing real-time in situ monitoring of DOM optical properties via fluorescence spectroscopy is growing (Jaffé et al., 2008; Lescord et al., 2018, Fleck et al., 2014). Our work suggests that these efforts could provide valuable supporting data to better understand the Hg cycling in aquatic ecosystems.

With human activities and climate change modifying hydrologic conditions, promoting nutrient enrichment, and increasing water temperature, the occurrence of algal blooms in lakes, rivers, and wetlands are becoming more frequent (Cheng et al., 2019; Dodd and Smith, 2016; Refsnider et al., 2021).

Our study suggests that excessive external loading of AOM, and/or nutrients that stimulate algal growth, to wetlands with mild Hg contamination could enhance MeHg production. While scaling our experiment to an actual wetland sediment-water environment is challenging, we attempt to do so here to better understand what levels of AOM may support MeHg production in wetland systems. Our experiments showed that the addition of >0.1 g SpOM (~0.05 g-C) crossed a threshold for Hg methylation, with MeHg production increasing substantially with increasing AOM addition. Considering the areal scale of the microcosm (~10 cm^2), this is roughly equivalent to an AOM areal carbon loading of 50 g-C/m^2. Carbon fixation rates by phytoplankton in shallow eutrophic lakes can reach 0.5-1 g-C/m^3·h (Horne and Goldman, 1994). Assuming a carbon fixation rate of 0.5 g-C/m^3·h, a 1-m-deep water column, and a 12-hour period of photosynthesis, yields an areal carbon fixation rate of 6 g-C/m^2. This indicates our estimated loading of 50 g-C/m^2 is the carbon-equivalent of an intense algae "bloom" spanning around 12 days. Thus, our >0.1 g SpOM loading rates appear high in magnitude compared to what might be expected in a wetland setting. However, wetlands are complex systems that include multiple sources of organic matter loading including external loading, planktonic algae growth, periphyton growth, litter from growing macrophytes, bottom detritus and surficial sediments (Kadlec and Wallace, 2008). A typical standing stock of carbon in a densely vegetated eutrophic wetland is on the order of 300 g-C/m^2. In this context, the SpOM loading rate of 50 g-C/m^2 is not so extreme, though the difference in carbon quality available to support microbial processes (e.g., low quality macrophyte litter versus high quality AOM) needs to be acknowledged.

Finally, a unique characteristic of our study was that the incubations were a closed system. These systems under one-time OM loading showed a short-lived methylation window followed by a transition to an anoxic quasi-steady state with regards to Hg-related water and sediment quality parameters. However, this might not be a realistic model of natural wetlands, which can have sediment-water interface conditions that oscillate between aerobic and anaerobic conditions depending on patterns of hydrology, nutrient loading and autochthonous and allochthonous productivity. These environmental variations might open the methylation window on multiple occasions, favoring recurrent pulses of MeHg uptake in biota. For example, studies adjacent to the CCSB in the Yolo Bypass showed that seasonal wetlands and permanently flooded wetlands have different MeHg cycling behaviors driven by hydrological dynamics (Windham-Myers et al., 2018). Seasonally flooded wetlands produce high MeHg during and after the growing season regulated by the availability of labile carbon that controls microbial Hg methylation, apparently demonstrating a pulsed pattern of Hg uptake into biota. Conversely, permanently flooded wetlands exhibited less annual MeHg production, which was attributed to higher MeHg degradation rates and limited IHg bioavailability. This is an analog to our closed system incubations, which after an initial burst of MeHg production exhibited an extended anoxic period with a closed methylation window. Furthermore, studies by Tanner et al. (2018)

suggested that enhancing aerobic conditions in wetlands could restrict the activity of Hg-methylating microbes, maintaining a closed methylation window. The status of dissolved oxygen and redox conditions in aquatic ecosystem are well-recognized factors affecting many aspects of water quality. As detailed in our study, oxidized versus reduced conditions were driving indicators for the methylation window, where mildly reduced conditions seemed to open the methylation window allowing the activity of multiple methylating microbes. In contrast, highly reduced conditions appeared to close it by favoring MeHg-demethylating microbes.

3.7 References

Alewell, C., Paul, S., Lischeid, G., Küsel, K., and Gehre, M. (2006). Characterizing the Redox Status in Three Different Forested Wetlands with Geochemical Data. Environmental Science and Technology, 40(24), 7609–7615. https://doi.org/10.1021/es061018y

Ali, S. K., and Saleh, A. M. (2012). Spirulina-an overview. International journal of Pharmacy and Pharmaceutical sciences, 4(3), 9-15.

Amos, Helen, J., Daniel, J. ,. Streets David G, and Sunderland Elsie M. (2013). Legacy impacts of all-time anthropogenic emissions on the global mercury cycle.

Antweiler, R. C., Patton, C. J., and Taylor, H. E. (1996). Automated, Colorimetric methods for determination of nitrate plus nitrite, nitrite, ammonium, and orthophosphate ions in natural water samples. U.S.G.S. Report, Report 93, 1–28

Barkay, T., and Gu, B. (2022). Demethylation─The Other Side of the Mercury Methylation Coin: A Critical Review. ACS Environmental Au, 2(2), 77–97. https://doi.org/10.1021/acsenvironau.1c00022

Aranda-Tamaura, C., Estrada-Alvarado, M. I., Texier, A.-C., Cuervo, F., Gómez, J., and Cervantes, F. J. (2007). Effects of different quinoid redox mediators on the removal of sulphide and nitrate via denitrification. Chemosphere, 69(11), 1722–1727. https://doi.org/10.1016/j.chemosphere.2007.06.004

Ashworth, G. (2024). Sulphur dioxide in commercially produced microalgae. Food Science and Technology. https://doi.org/10.1002/fsat.3510_2.x

Bae, H.-S., Dierberg, F.E., Ogram, A. (2014). Syntrophs dominate sequences associated with the mercury methylation-related gene hgcA in the water conservation areas of the Florida Everglades. Appl. Environ. Microbiol. 80, 6517–6526. https://doi.org/ 10.1128/AEM.01666-14.

Barkay, T., and Gu, B. (2022). Demethylation─The Other Side of the Mercury Methylation Coin: A Critical Review. ACS Environmental Au, 2(2), 77–97. https://doi.org/10.1021/acsenvironau.1c00022

Beutel, M., Fuhrmann, B., Herbon, G., Chow, A., Brower, S., and Pasek, J. (2020). Cycling of methylmercury and other redox-sensitive compounds in the profundal zone of a hypereutrophic water supply reservoir. Hydrobiologia, 847(21), 4425–4446. https://doi.org/10.1007/s10750-020-04192-3

Bigham, G. N., Murray, K. J., Masue-Slowey, Y., and Henry, E. A. (2017). Biogeochemical controls on methylmercury in soils and sediments: Implications for site management: Geochemical Controls on Mercury Methylation. Integrated Environmental Assessment and Management, 13(2), 249–263. https://doi.org/10.1002/ieam.1822

Blough NV, and DelVecchio R. (2002). Chromophoric DOM in the coastal environment. In: Hansel DA, Carlson CA, editors. Biogeochemistry of marine dissolved organic matter. San Diego: Academic Press; 509–46.

Bravo, A. G., Zopfi, J., Buck, M., Xu, J., Bertilsson, S., Schaefer, J. K., Poté, J., and Cosio, C. (2018). Geobacteraceae are important members of mercury-methylating microbial communities of sediments impacted by wastewater releases. The ISME Journal, 12(3), 802–812. https://doi.org/10.1038/s41396-017-0007-7

Bridou R, Monperrus M, Gonzalez PR, Guyoneaud R, Amouroux D. (2011). Simultaneous determination of mercury methylation and demethylation capacities of various sulfate-reducing bacteria using species-specific isotopic tracers. Environ Toxicol Chem. 30(2):337-44. https://doi.org/10.1002/etc.395.

Cammack, W. K. L., Kalff, J., Prairie, Y. T., and Smith, E. M. (2004). Fluorescent dissolved organic matter in lakes: Relationships with heterotrophicmetabolism. Limnology and Oceanography, 49(6), 2034–2045. https://doi.org/10.4319/lo.2004.49.6.2034

Carstea, E. M., Popa, C. L., Baker, A., and Bridgeman, J. (2020). In situ fluorescence measurements of dissolved organic matter: A review. Science of the Total Environment, 699, 134361. https://doi.org/10.1016/j.scitotenv.2019.134361

Catalán, N., Pastor, A., Borrego, C. M., Casas-Ruiz, J. P., Hawkes, J. A., Gutiérrez, C., Von Schiller, D., and Marcé, R. (2021). The relevance of environment vs. Composition on dissolved organic matter degradation in freshwaters. Limnology and Oceanography, 66(2), 306–320. https://doi.org/10.1002/lno.11606

Cheng, B., Xia, R., Zhang, Y., Yang, Z., Hu, S., Guo, F., & Ma, S. (2019). Characterization and causes analysis for algae blooms in large river system. Sustainable Cities and Society, 51, 101707.

Chételat, J., Ackerman, J. T., Eagles-Smith, C. A., & Hebert, C. E. (2020). Methylmercury exposure in wildlife: a review of the ecological and physiological processes affecting contaminant concentrations and their interpretation. Science of the Total Environment, 711, 135117.

Coble PG. (1996). Characterization of marine and terrestrial DOM in seawater using excitation emission matrix spectroscopy. Mar Chem, 52:325–36.

Coble PC, Green S, Blough NV, Gagosian RB. (1990). Characterization of dissolved organic mat ter in the Black Sea by fluorescence spectroscopy. Nature, 348:432–5.

Compeau, G. C., & Bartha, R. (1985). Sulfate-Reducing Bacteria: Principal Methylators of Mercury in Anoxic Estuarine Sedimentt. Appl. Environ. Microbiol., 50(2), 498–502.

Cook, R. B. (1984). Distributions of Ferrous Iron and Sulfide in an Anoxic Hypolimnion. Canadian Journal of Fisheries and Aquatic Sciences, 41(2), 286–293. https://doi.org/10.1139/f84-033

Cory R, Miller MP, McKnight DM, Guerard JJ, Miller PL. (2010). Effect of instrument-specific re sponse on the analysis of fulvic acid fluorescence spectra. Limnol Oceanogr Methods, 8, 67–78.

Cory RM, McKnight DM. (2005). Fluorescence spectroscopy reveals ubiquitous presence of ox idized and reduced quinones in dissolved organic matter. Environ Sci Technol, 39, 8142–9.

Cossa, D., and Gobeil, C. (2000). Mercury speciation in the Lower St. Lawrence Estuary. 57.

Cui, H., Zhao, Y., Zhao, L., and Wei, Z. (2022). Characterization of mercury binding to different molecular weight fractions of dissolved organic matter. Journal of Hazardous Materials, 431, 128593. https://doi.org/10.1016/j.jhazmat.2022.128593

Davison, W. (1993). Iron and manganese in lakes. Earth-Science Reviews, 34(2), 119–163. https://doi.org/10.1016/0012-8252(93)90029-7

De Parsia, E.R., Fleck, J.A., Krabbenhoft, D.P., Hoang, K., Roth, D., and Randall, P. (2019). Coagulant and sorbent efficacy in removing mercury from surface waters in the Cache Creek watershed, California: U.S. Geological Survey Open-File Report 2019–1001, 46 p., https://doi.org/10.3133/ofr20191001.

Dodds, W. K., & Smith, V. H. (2016). Nitrogen, phosphorus, and eutrophication in streams. Inland Waters, 6(2), 155-164. https://doi.org/10.5268/IW-6.2.909).

Downing, B. D., Boss, E., Bergamaschi, B. A., Fleck, J. A., Lionberger, M. A., Ganju, N. K., Schoellhamer, D. H., and Fujii, R. (2009). Quantifying fluxes and characterizing compositional changes of dissolved organic matter in aquatic systems in situ using combined acoustic and optical measurements. Limnology and Oceanography: Methods, 7(1), 119–131. https://doi.org/10.4319/lom.2009.7.119

Driscoll, C. T., Mason, R. P., Chan, H. M., Jacob, D. J., and Pirrone, N. (2013). Mercury as a Global Pollutant: Sources, Pathways, and Effects. Environmental Science & Technology, 47(10), 4967–4983. https://doi.org/10.1021/es305071v

Du, H., Ma, M., Igarashi, Y., and Wang, D. (2019). Biotic and Abiotic Degradation of Methylmercury in Aquatic Ecosystems: A Review. Bulletin of Environmental Contamination and Toxicology, 102(5), 605–611. https://doi.org/10.1007/s00128-018-2530-2

Eckley, C. S., Luxton, T. P., Stanfield, B., Baldwin, A., Holloway, J., McKernan, J., and Johnson, M. G. (2021). Effect of organic matter concentration and characteristics on mercury mobilization and methylmercury production at

an abandoned mine site. Environmental Pollution, 271, 116369. https://doi.org/10.1016/j.envpol.2020.116369

Fleck, J. A., Gill, G., Bergamaschi, B. A., Kraus, T. E. C., Downing, B. D., and Alpers, C. N. (2014). Concurrent photolytic degradation of aqueous methylmercury and dissolved organic matter. Science of the Total Environment, 484, 263–275. https://doi.org/10.1016/j.scitotenv.2013.03.107

Fuhrmann, B. C., Beutel, M. W., O'Day, P. A., Tran, C., Funk, A., Brower, S., Pasek, J., and Seelos, M. (2021). Effects of mercury, organic carbon, and microbial inhibition on methylmercury cycling at the profundal sediment-water interface of a sulfate-rich hypereutrophic reservoir. Environmental Pollution, 268, 115853. https://doi.org/10.1016/j.envpol.2020.115853

Fleming, E. J., Mack, E. E., Green, P. G., and Nelson, D. C. (2006). Mercury Methylation from Unexpected Sources: Molybdate-Inhibited Freshwater Sediments and an Iron-Reducing Bacterium. Applied and Environmental Microbiology, 72(1), 457–464. https://doi.org/10.1128/AEM.72.1.457-464.2006

Gagnon, C., Pelletier, É., and Mucci, A. (1997). Behaviour of anthropogenic mercury in coastal marine sediments. Marine Chemistry, 59(1–2), 159–176. https://doi.org/10.1016/S0304-4203(97)00071-6

Gerbig, C. A., Kim, C. S., Stegemeier, J. P., Ryan, J. N., and Aiken, G. R. (2011). Formation of Nanocolloidal Metacinnabar in Mercury-DOM-Sulfide Systems. Environmental Science & Technology, 45(21), 9180–9187. https://doi.org/10.1021/es201837h

Gilmour, C. C., Podar, M., Bullock, A. L., Graham, A. M., Brown, S. D., Somenahally, A. C., Johs, A., Hurt, R. A., Bailey, K. L., and Elias, D. A. (2013). Mercury Methylation by Novel Microorganisms from New Environments. Environmental Science & Technology, 47(20), 11810–11820. https://doi.org/10.1021/es403075t

Gorski, C. A., Klüpfel, L. E., Voegelin, A., Sander, M., and Hofstetter, T. B. (2013). Redox Properties of Structural Fe in Clay Minerals: 3. Relationships between Smectite Redox and Structural Properties. Environmental Science & Technology, 47(23), 13477–13485. https://doi.org/10.1021/es403824x

Graham, A. M., Aiken, G. R., and Gilmour, C. C. (2012). Dissolved Organic Matter Enhances Microbial Mercury Methylation Under Sulfidic Conditions. Environmental Science & Technology, 46(5), 2715–2723. https://doi.org/10.1021/es203658f

Graham, A. M., Aiken, G. R., and Gilmour, C. C. (2013). Effect of Dissolved Organic Matter Source and Character on Microbial Hg Methylation in Hg–S–DOM Solutions. Environmental Science & Technology, 47(11), 5746–5754. https://doi.org/10.1021/es400414a

Gu, S., Gruau, G., Dupas, R., Petitjean, P., Li, O., Pinay, G. (2019). Respective roles of Fe-oxyhydroxide dissolution, pH changes and sediment inputs in

dissolved phosphorus release from wetland soils under anoxic conditions. Geoderma, 338, 365-374. https://doi.org/10.1016/j.geoderma.2018.12.034.

Gu Q, Kenny JE. (2009). Improvement of inner filter effect correction based on determination of effective geometric parameters using a conventional fluorimeter. Anal Chem, 81, 420–6.

Haitzer, M., Aiken, G. R., & Ryan, J. N. (2002). Binding of mercury(II) to dissolved organic matter: The role of the mercury-to-DOM concentration ratio. *Environmental Science and Technology*, *36*(16), 3564–3570. https://doi.org/10.1021/es025699i

Hansen, A. M. (2019). Strategies to suppress internal loads of metals in sediments. E3S Web of Conferences, 98, 09009. https://doi.org/10.1051/e3sconf/20199809009

He, M., Tian, L., Braaten, H. F. V., Wu, Q., Luo, J., Cai, L.-M., Meng, J.-H., and Lin, Y. (2019). Mercury–Organic Matter Interactions in Soils and Sediments: Angel or Devil? Bulletin of Environmental Contamination and Toxicology, 102(5), 621–627. https://doi.org/10.1007/s00128-018-2523-1

Helms JR, Stubbins A, Ritchie JD, Minor EC, Kieber DJ, Mopper K. (2008). Absorption spectral slopes and slope ratios as indicators of molecular weight, source, and photobleaching of chromophoric dissolved organic matter. Limnol Oceanogr, 53, 955–69.

Henneberry, Y. K., Kraus, T. E. C., Nico, P. S., and Horwath, W. R. (2012). Structural stability of coprecipitated natural organic matter and ferric iron under reducing conditions. Organic Geochemistry, 48, 81–89. https://doi.org/10.1016/j.orggeochem.2012.04.005

Henze, M., Gujer, W., Mino, T., Matsuo, T., Wentzel, M. C., and Marais, G. V. R. (1995). Wastewater and biomass characterization for the activated sludge model no. 2: biological phosphorus removal. Water Science and Technology, 31(2), 13-23.

Hernes, P. J., Bergamaschi, B. A., Eckard, R. S., and Spencer, R. G. (2009). Fluorescence-based proxies for lignin in freshwater dissolved organic matter. Journal of Geophysical Research: Biogeosciences, 114(G4).

Herrero Ortega, S., Catalán, N., Björn, E., Gröntoft, H., Hilmarsson, T. G., Bertilsson, S., Wu, P., Bishop, K., Levanoni, O., and Bravo, A. G. (2018). High methylmercury formation in ponds fueled by fresh humic and algal derived organic matter. Limnology and Oceanography, 63(S1). https://doi.org/10.1002/lno.10722

Higgins, S. A., and Kamman, G. R. (2010). Watershed-based assessment of hydrologic and geomorphic conditions in cache creek through capay valley. Kamman Hydrology & Engineering, Inc., San Rafael, CA, 107.

Hintelmann, H., and Harris, R. (2004). Application of multiple stable mercury isotopes to determine the adsorption and desorption dynamics of Hg (II) and MeHg to sediments. Marine Chemistry, 90(1-4), 165-173. https://doi.org/10.1016/j.marchem.2004.03.015

Hintelmann, H., Keppel-Jones, K. and Evans, R.D. (2000), Constants of mercury methylation and demethylation rates in sediments and comparison of tracer

and ambient mercury availability. Environmental Toxicology and Chemistry, 19, 2204-2211. https://doi.org/10.1002/etc.5620190909

Horne, A.J. and Goldman, C.R. (1994). Limnology. Second edition. McGraw-Hill, 576 pp

Hsu-Kim, H., Kucharzyk, K. H., Zhang, T., and Deshusses, M. A. (2013). Mechanisms Regulating Mercury Bioavailability for Methylating Microorganisms in the Aquatic Environment: A Critical Review. Environmental Science & Technology, 47(6), 2441–2456. https://doi.org/10.1021/es304370g

Jaffé, R., McKnight, D., Maie, N., Cory, R., McDowell, W. H., & Campbell, J. L. (2008). Spatial and temporal variations in DOM composition in ecosystems: The importance of long-term monitoring of optical properties. Journal of Geophysical Research: Biogeosciences, 113(G4).

Jay, J. A., Morel, F. M., & Hemond, H. F. (2000). Mercury speciation in the presence of polysulfides. *Environmental Science & Technology*, *34*(11), 2196-2200.

Jones, D. S., Johnson, N. W., Mitchell, C. P. J., Walker, G. M., Bailey, J. v., Pastor, J., and Swain, E. B. (2020). Diverse Communities of hgcAB+Microorganisms Methylate Mercury in Freshwater Sediments Subjected to Experimental Sulfate Loading. Environmental Science and Technology, 54(22), 14265–14274. https://doi.org/10.1021/acs.est.0c02513

Jonsson, S., Mazrui, N. M., and Mason, R. P. (2016). Dimethylmercury Formation Mediated by Inorganic and Organic Reduced Sulfur Surfaces. Scientific Reports, 6(1), 27958. https://doi.org/10.1038/srep27958

Kadlec, R.H. and Wallace, S., 2008. Treatment Wetlands, 2nd Edition. CRC press.

Klapstein, S. J., and O'Driscoll, N. J. (2018). Methylmercury Biogeochemistry in Freshwater Ecosystems: A Review Focusing on DOM and Photodemethylation. Bulletin of Environmental Contamination and Toxicology, 100(1), 14–25. https://doi.org/10.1007/s00128-017-2236-x

Lacroix, E. M., Aeppli, M., Boye, K., Brodie, E., Fendorf, S., Keiluweit, M., Naughton, H. R., Noël, V., and Sihi, D. (2023). Consider the Anoxic Microsite: Acknowledging and Appreciating Spatiotemporal Redox Heterogeneity in Soils and Sediments. ACS Earth and Space Chemistry, 7(9), 1592–1609. https://doi.org/10.1021/acsearthspacechem.3c00032

Lambert, T., Perolo, P., Escoffier, N., and Perga, M.-E. (2022). Enhanced bioavailability of dissolved organic matter (DOM) in human-disturbed streams in Alpine fluvial networks. Biogeosciences, 19(1), 187–200. https://doi.org/10.5194/bg-19-187-2022

Laspidou, C. S., & Rittmann, B. E. (2002). A unified theory for extracellular polymeric substances, soluble microbial products, and active and inert biomass. *Water research*, *36*(11), 2711-2720.

Lei, P., Nunes, L. M., Liu, Y.-R., Zhong, H., and Pan, K. (2019). Mechanisms of algal biomass input enhanced microbial Hg methylation in lake sediments. Environment International, 126, 279–288. https://doi.org/10.1016/j.envint.2019.02.043

Lescord, G. L., Emilson, E. J. S., Johnston, T. A., Branfireun, B. A., and Gunn, J. M. (2018). Optical Properties of Dissolved Organic Matter and Their Relation to Mercury Concentrations in Water and Biota Across a Remote Freshwater Drainage Basin. Environmental Science & Technology, 52(6), 3344–3353. https://doi.org/10.1021/acs.est.7b05348

Li, M., Drosos, M., Hu, H., He, X., Wang, G., Zhang, H., Hu, Z., and Xi, B. (2019). Organic amendments affect dissolved organic matter composition and mercury dissolution in pore waters of mercury-polluted paddy soil. Chemosphere, 232, 356–365. https://doi.org/10.1016/j.chemosphere.2019.05.234

Liem-Nguyen, V., Skyllberg, U., and Björn, E. (2017). Thermodynamic Modeling of the Solubility and Chemical Speciation of Mercury and Methylmercury Driven by Organic Thiols and Micromolar Sulfide Concentrations in Boreal Wetland Soils. Environmental Science and Technology, 51(7), 3678–3686. https://doi.org/10.1021/acs.est.6b04622

Marvin-DiPasquale, M., Agee, J., McGowan, C., Oremland, R. S., Thomas, M., Krabbenhoft, D., and Gilmour, C. C. (2000). Methyl-Mercury Degradation Pathways: A Comparison among Three Mercury-Impacted Ecosystems. Environmental Science & Technology, 34(23), 4908–4916. https://doi.org/10.1021/es0013125

Marvin-DiPasquale, M. C., Alpers, C. N., and Fleck, J. A. (2009). Mercury, Methylmercury, and Other Constituents in Sediment and Water from Seasonal and Permanent Wetlands in the Cache Creek Settling Basin and Yolo Bypass, Yolo County, California, 2005−06. Open File Report 2009-1182, 69.

Marvin-DiPasquale, M., Windham-Myers, L., Agee, J. L., Kakouros, E., Kieu, L. H., Fleck, J. A., Alpers, C. N., and Stricker, C. A. (2014). Methylmercury production in sediment from agricultural and non-agricultural wetlands in the Yolo Bypass, California, USA. Science of the Total Environment, 484, 288–299. https://doi.org/10.1016/j.scitotenv.2013.09.098

Mazrui, N. M., Jonsson, S., Thota, S., Zhao, J., and Mason, R. P. (2016). Enhanced availability of mercury bound to dissolved organic matter for methylation in marine sediments. Geochimica et Cosmochimica Acta, 194, 153–162. https://doi.org/10.1016/j.gca.2016.08.019

Mergler, D., Anderson, H.A., Hing Man Chan, L., Mahaffey, K.R., Murray, M., Sakamoto, M., and Stern, A.H. (2007). Methylmercury Exposure and Health Effects in Humans: A Worldwide Concern. AMBIO: A Journal of the Human Environment 36(1), 3-11. https://doi.org/10.1579/0044-7447(2007)36[3:MEAHEI]2.0.CO;2

Murray, T. E. (1995). The correlation between iron sulfide precipitation and hypolimnetic phosphorus accumulation during one summer in a softwater lake. Canadian Journal of Fisheries and Aquatic Sciences, 52(6), 1190–1194. https://doi.org/10.1139/f95-115

Noh, S., Kim, J., Hur, J., Hong, Y., and Han, S. (2018). Potential contributions of dissolved organic matter to monomethylmercury distributions in temperate

reservoirs as revealed by fluorescence spectroscopy. Environmental Science and Pollution Research, 25(7), 6474–6486. https://doi.org/10.1007/s11356-017-0913-2

Peterson, B. D., Poulin, B. A., Krabbenhoft, D. P., Tate, M. T., Baldwin, A. K., Naymik, J., Gastelecutto, N., and McMahon, K. D. (2023). Metabolically diverse microorganisms mediate methylmercury formation under nitrate-reducing conditions in a dynamic hydroelectric reservoir. The ISME Journal, 17(10), 1705–1718. https://doi.org/10.1038/s41396-023-01482-1

Potter, B. B., and Wimsatt, J. C. (2005). Method 415.3. Measurement of total organic carbon, dissolved organic carbon and specific UV absorbance at 254 nm in source water and drinking water. US Environmental protection agency, Washington, DC.

Poulin, B. A., Tate, M. T., Ogorek, J., Breitmeyer, S. E., Baldwin, A. K., Yoder, A. M., Harris, R., Naymik, J., Gastelecutto, N., Hoovestol, C., Larsen, C., Myers, R., Aiken, G. R., Krabbenhoft, D. P. (2023). Biogeochemical and hydrologic synergy control mercury fate in an arid land river-reservoir system. Environ. Sci.: Processes Impacts. 25, 912– 928, DOI: 10.1039/D3EM00032J

Ravichandran, M. (2004). Interactions between mercury and dissolved organic matter—a review. Chemosphere, 55(3), 319–331. https://doi.org/10.1016/j.chemosphere.2003.11.011

Regnell, O., and Watras, Carl. J. (2019). Microbial Mercury Methylation in Aquatic Environments: A Critical Review of Published Field and Laboratory Studies. Environmental Science & Technology, 53(1), 4–19. https://doi.org/10.1021/acs.est.8b02709

Refsnider, J. M., Garcia, J. A., Holliker, B., Hulbert, A. C., Nunez, A., & Streby, H. M. (2021). Effects of harmful algal blooms on stress levels and immune functioning in wetland-associated songbirds and reptiles. Science of the Total Environment, 788, 147790.

Reineke, W. (2001). Aerobic and Anaerobic Biodegradation Potentials of Microorganisms. In B. Beek (Ed.), Biodegradation and Persistance (Vol. 2K, pp. 1–161). Springer-Verlag. https://doi.org/10.1007/10508767_1

Rich, P.R., Maréchal, A. (2012). Electron transfer chains: structures, mechanisms and energy coupling. S.J. Ferguson (Ed.), Comprehensive Biophysics, Comprehensive Biophysics, vol. 8, Elsevier Academic Press Inc, San Diego. 72-93

Rysgaard, S., Risgaard-Petersen, N., Niels Peter, S., Kim, J., & Lars Peter, N. (1994). Oxygen regulation of nitrification and denitrification in sediments. Limnology and Oceanography, 39(7), 1643-1652.

Shi, L., Dong, H., Reguera, G. et al. (2016). Extracellular electron transfer mechanisms between microorganisms and minerals. Nat Rev Microbiol 14, 651–662 https://doi.org/10.1038/nrmicro.2016.93

Song, C., Sun, S., Wang, J., Gao, Y., Yu, G., Li, Y., Liu, Z., Zhang, W., and Zhou, L. (2023). Applying fulvic acid for sediment metals remediation:

Mechanism, factors, and prospect. Frontiers in Microbiology, 13, 1084097. https://doi.org/10.3389/fmicb.2022.1084097

Sonke, J. E., Angot, H., Zhang, Y., Poulain, A., Björn, E., and Schartup, A. (2023). Global change effects on biogeochemical mercury cycling. Ambio, 52(5), 853–876. https://doi.org/10.1007/s13280-023-01855-y

Stedmon CA, Markager S, Bro R. (2003). Tracing dissolved organic matter in aquatic environ ments using a new approach to fluorescence spectroscopy. Mar Chem, 82, 239–54.

Tipping, E. (2007). Modelling the interactions of Hg (II) and methylmercury with humic substances using WHAM/Model VI. *Applied geochemistry*, *22*(8), 1624-1635.

Tranvik, L. J. (1988). Availability of dissolved organic carbon for planktonic bacteria in oligotrophic lakes of differing humic content. Microbial Ecology, 16(3), 311–322. https://doi.org/10.1007/BF02011702

Ullrich, S. M., Tanton, T. W., and Abdrashitova, S. A. (2001). Mercury in the Aquatic Environment: A Review of Factors Affecting Methylation. Critical Reviews in Environmental Science and Technology, 31(3), 241–293. https://doi.org/10.1080/20016491089226

USEPA. (1993). Method 300.1 Determination of Inorganic Anions in Drinking Water by Ion Chromatography. Revision 1.0.

USEPA. (1994). Method 200.7: Determination of Metals and Trace Elements in Water and Wastes by Inductively Coupled Plasma-Atomic Emission Spectrometry, Revision 4.4. Cincinnati, OH

USEPA. (1994). Determination of Mercury in Water by Cold Vapor Atomic Absorption Spectrometry Method 245.1. Environmental Monitoring Systems Laboratory Office of Research and Development, 1–18.

USEPA. (1996). Method 3052. Microwave Assisted Acid Digestion of Silic (Vol. 66, Issue December, pp. 37–39).

USEPA. (1996). Method 3052. Microwave Assisted Acid Digestion of Silic (Vol. 66, Issue December, pp. 37–39).

USEPA. 1997. “Method 300.1: Determination of Inorganic Anions in Drinking Water by Ion Chromatography,” Revision 1.0. Cincinnati, OH

USEPA. (1998). Method 1630 Methyl Mercury in Water by Distillation, Aqueous Ethylation, Purge and Trap, and Cold Vapor Atomic Fluorescence Spectrometry Engineering and Analysis Division (4303). Science And Technology, 4303.

USEPA. (2007). Mercury total (organic and 7439-97-6 inorganic). Methods, February.1–17. https://www.epa.gov/sites/production/files/2015-07/documents/epa-7473.pdf

Villacorte, L. O., Ekowati, Y., Neu, T. R., Kleijn, J. M., Winters, H., Amy, G., Schippers, J. C., and Kennedy, M. D. (2015). Characterisation of algal organic matter produced by bloom-forming marine and freshwater algae. Water Research, 73, 216–230. https://doi.org/10.1016/j.watres.2015.01.028

Wang, T., Zhao, D., Liu, J., Zhang, T., Wang, X., Liu, T., Wang, S., Liu, G., Liu, B., and Liu, Y. (2023). Effects of abiotic mineral transformation of FeS on

the dynamic immobilization of Cr(VI) in oxic aquatic environments. Science of the Total Environment, 894, 164991. https://doi.org/10.1016/j.scitotenv.2023.164991

Wang, Y., Liu, J., Liem-Nguyen, V., Tian, S., Zhang, S., Wang, D., and Jiang, T. (2022). Binding strength of mercury (II) to different dissolved organic matter: The roles of DOM properties and sources. Science of the Total Environment, 807, 150979. https://doi.org/10.1016/j.scitotenv.2021.150979

Waples, J. S., Nagy, K. L., Aiken, G. R., and Ryan, J. N. (2005). Dissolution of cinnabar (HgS) in the presence of natural organic matter. Geochimica et Cosmochimica Acta, 69(6), 1575–1588. https://doi.org/10.1016/j.gca.2004.09.029\

Weishaar JL, Aiken GR, Bergamaschi BA, Fram MS, Fuji R, Mopper K. (2003). Evaluation of spe cific ultraviolet absorbance as an indicator of the chemical composition and reac tivity of dissolved organic carbon. Environ Sci Technol, 37, 4702–8.

Windham-Myers, L., Marvin-DiPasquale, M., Stricker, C. A., Agee, J. L., Kieu, L. H., & Kakouros, E. (2014). Mercury cycling in agricultural and managed wetlands of California, USA: experimental evidence of vegetation-driven changes in sediment biogeochemistry and methylmercury production. Science of the Total Environment, 484, 300-307.

Wu, Z., Li, Z., Shao, B., Chen, J., Cui, X., Cui, X., Liu, X., Zhao, Y. X., Pu, Q., Liu, J., He, W., Liu, Y., Liu, Y., Wang, X., Meng, B., and Tong, Y. (2024). Differential response of Hg-methylating and MeHg-demethylating microbiomes to dissolved organic matter components in eutrophic lake water. Journal of Hazardous Materials, 465, 133298. https://doi.org/10.1016/j.jhazmat.2023.133298

Wu, Z., Li, Z., Shao, B., Zhang, Y., He, W., Lu, Y., Gusvitskii, K., Zhao, Y., Liu, Y., Wang, X., and Tong, Y. (2022). Impact of dissolved organic matter and environmental factors on methylmercury concentrations across aquatic ecosystems inferred from a global dataset. Chemosphere, 294, 133713. https://doi.org/10.1016/j.chemosphere.2022.133713

Xu, J., Buck, M., Ekl¨ of, K., Ahmed, O.O., Schaefer, J.K., Bishop, K., Skyllberg, U., Bj¨orn, E., Bertilsson, S., Bravo, A.G.(2019). Mercury methylating microbial communities of boreal forest soils. Sci. Rep.. 9, 1–13. https://doi.org/10.1038/ s41598-018-37383-z.

Yu, R.-Q., Reinfelder, J. R., Hines, M. E., and Barkay, T. (2018). Syntrophic pathways for microbial mercury methylation. The ISME Journal, 12(7), 1826–1835. https://doi.org/10.1038/s41396-018-0106-0

Zeng, K., Huang, X., Guo, J., Dai, C., He, C., Chen, H., and Xin, G. (2024). Microbial-driven mechanisms for the effects of heavy metals on soil organic carbon storage: A global analysis. Environment International, 184, 108467. https://doi.org/10.1016/j.envint.2024.108467

Zhao, L., Chen, H., Lu, X., Lin, H., Christensen, G. A., Pierce, E. M., and Gu, B. (2017). Contrasting Effects of Dissolved Organic Matter on Mercury Methylation by Geobacter sulfurreducens PCA and Desulfovibrio

desulfuricans ND132. Environmental Science & Technology, 51(18), 10468–10475. https://doi.org/10.1021/acs.est.7b02518

Zhao, Q., Wang, J., OuYang, S., Chen, L., Liu, M., Li, Y., and Jiang, F. (2021). The exacerbation of mercury methylation by Geobacter sulfurreducens PCA in a freshwater algae-bacteria symbiotic system throughout the lifetime of algae. Journal of Hazardous Materials, 415, 125691. https://doi.org/10.1016/j.jhazmat.2021.125691

Zhao, X., Zhang, T., Chen, X., Guo, M., Meng, X., Wang, X., & Bai, S. (2023). Exploring the resilience of constructed wetlands to harmful algal blooms disturbances: A study on microbial response mechanisms. Bioresource Technology, 383, 129251.

Zhou, X. Q., Qu, X. M., Yang, Z., Zhao, J., Hao, Y. Y., Feng, J., ... and Liu, Y. R. (2022). Increased water inputs fuel microbial mercury methylation in upland soils. Journal of Hazardous Materials, 439, 129578.

Zhu, Y., Liu, J., Goswami, O. et al. (2018). Effects of humic substances on Fe(II) sorption onto aluminum oxide and clay. Geochem Trans 19, 3. https://doi.org/10.1186/s12932-018-0048-5

Zhu, Q. Z., Yin, X., Taubner, H., Wendt, J., Friedrich, M. W., Elvert, M., ... & Middelburg, J. J. (2024). Secondary production and priming reshape the organic matter composition in marine sediments. Science Advances, 10(20), eadm8096.

Table 3-1. Cache Creek Settling Basin Soil Characteristics in a dry weight basis

Water content %	15.9 ± 3.3
LOI %	0.55 ± 0.6
Total Mercury, ug/kg	299 ± 23.7
Methyl Mercury, ug/kg	2.14 ± 0.26
Reactive Mercury, ug/kg	10.3 ± 1
Total Iron units, g-Fe/kg	40 ± 5.7
Total Manganese units, g-Mn/kg	0.94 ± 0.6
Total Aluminum units, g-Al/kg	30.6 ± 0.9

Values are mean and standard deviation (n=11) of soil samples across the study site.

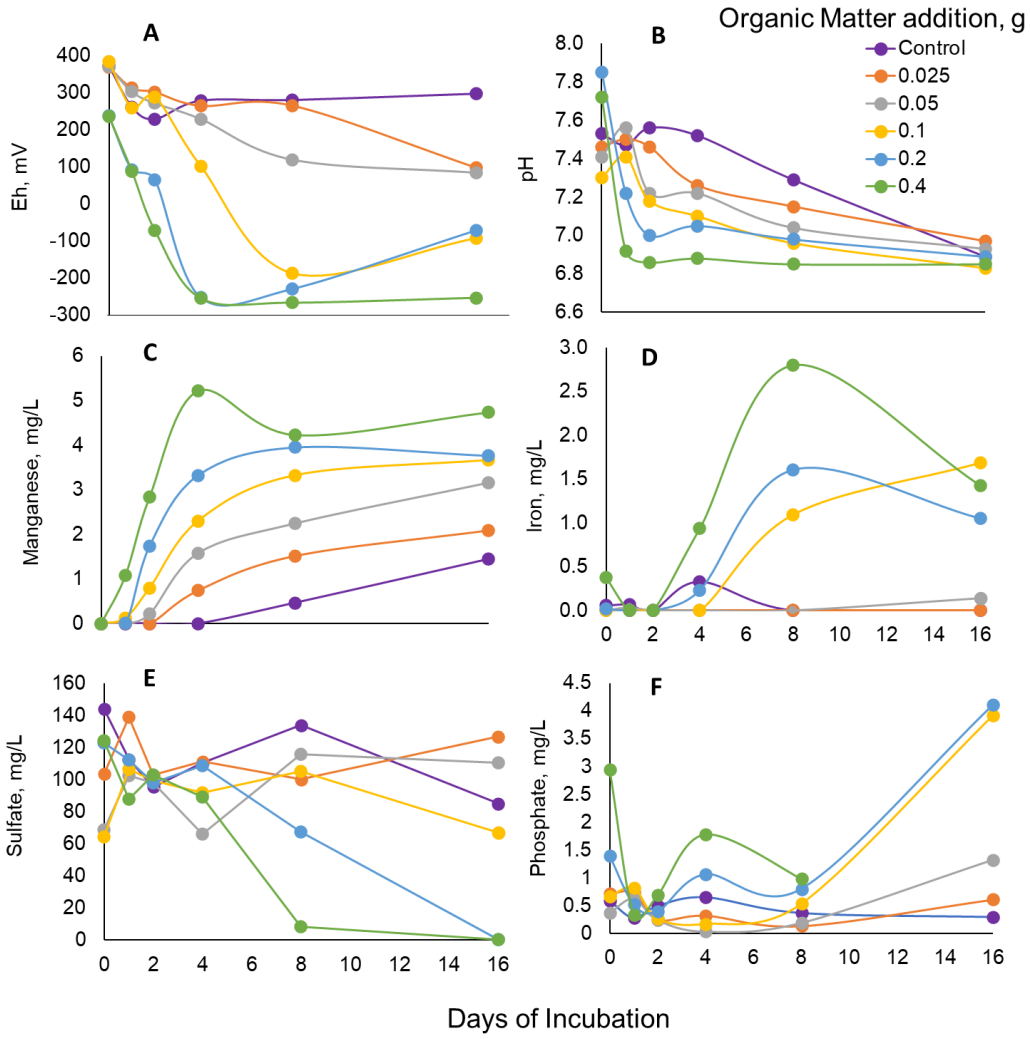

Figure 3-1 Variation in Eh, pH, and aqueous concentrations with incubation time and gradient in spirulina organic matter additions (0.025 g, 0.05 g, 0.1 g, 0.2 g, 0.4 g, and control). A) oxidation-reduction potential (Eh), B) pH, C) manganese, D) iron, E) sulfate, and F) phosphate concentrations in water.

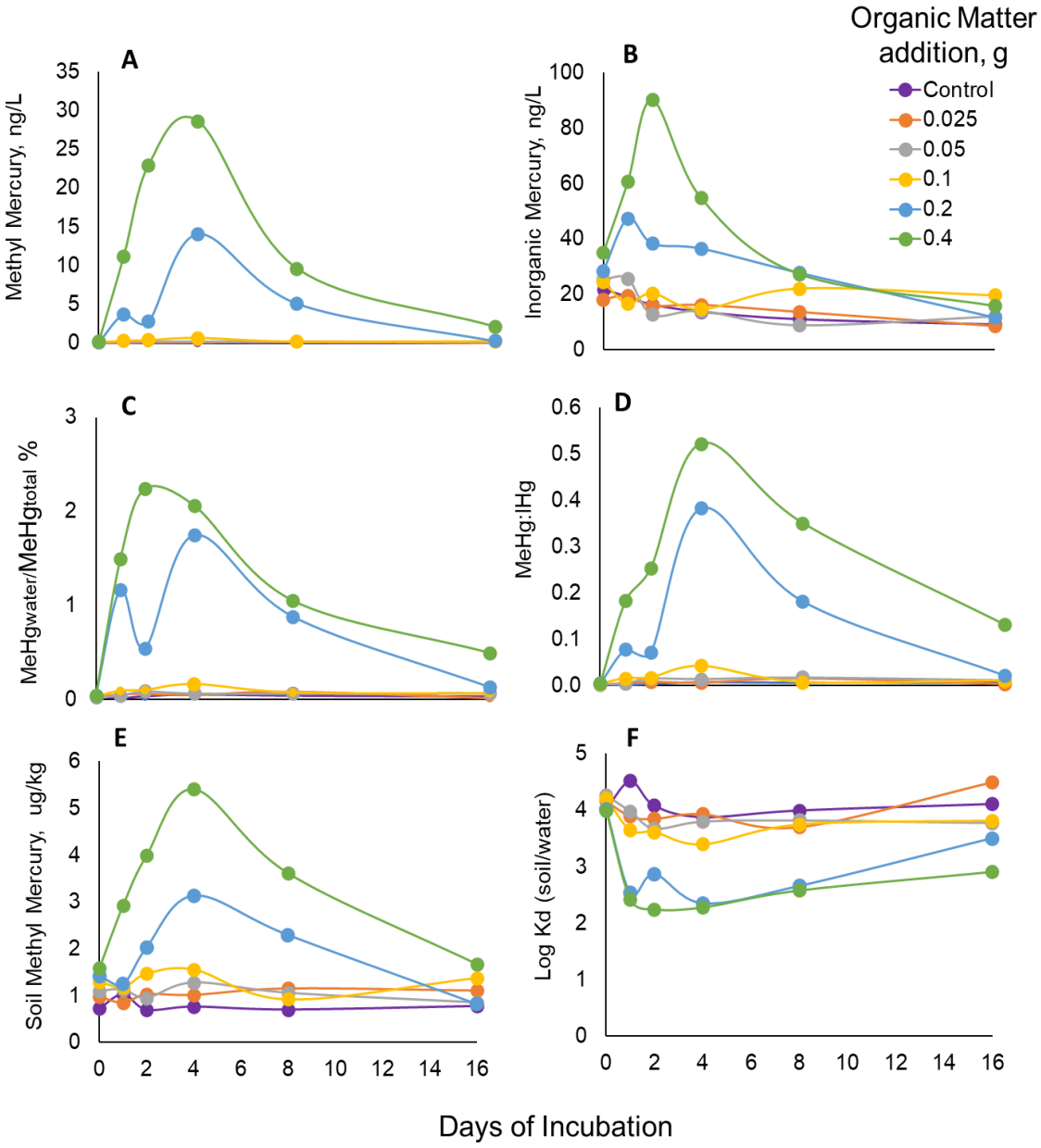

Figure 3-2 Mercury and methylmercury in water and soil with incubation time with the gradient in spirulina organic matter additions, 0.025 g, 0.05 g, 0.1 g, 0.2 g, 0.4 g, and the control. A) Methylmercury (MeHg) in water, B) Inorganic mercury, IHg (total Hg minus MeHg) in water, C) %MeHg in water (MeHg in water divided by MeHg water plus MeHg soil), D) MeHg:IHg ratio in water, E) Soil MeHg, and F) Partitioning coefficient, Log Kd, for MeHg in soil relative to water with Kd units of L/Kg.

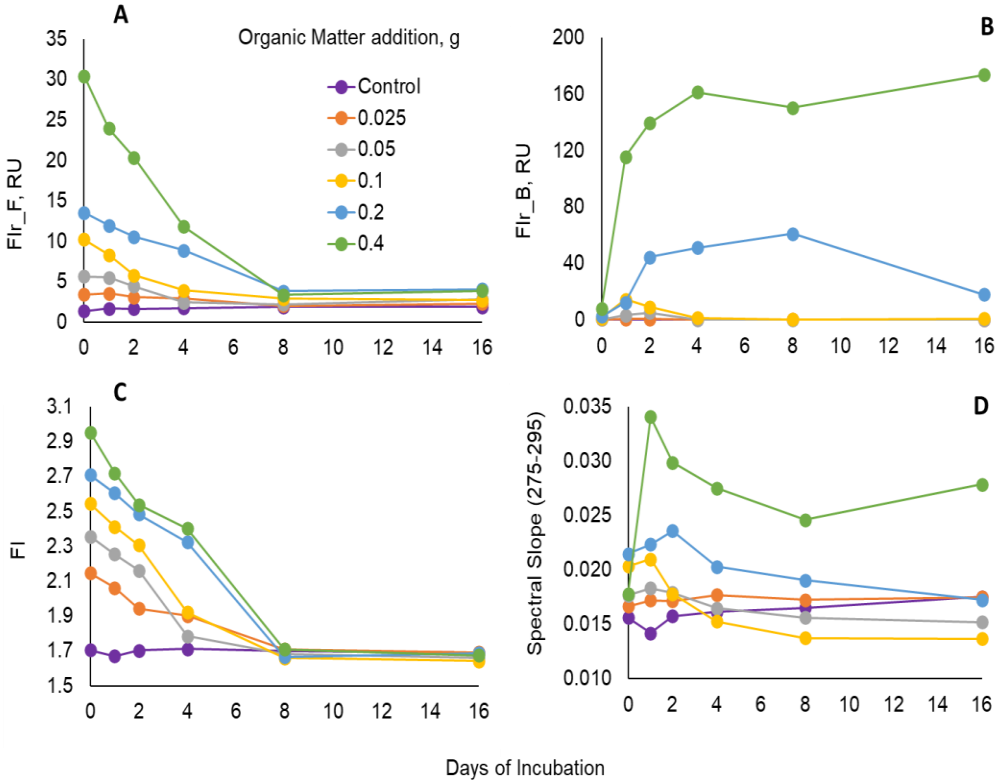

Figure 3-3 Dissolved organic matter (DOM) optical properties with incubation time and gradient in spirulina organic matter additions (0.025 g, 0.05 g, 0.1 g, 0.2 g, and 0.4 g, and control). A) Fluorescence in region F (Flr_F, RU), quinoid-like DOM, B) Fluorescence in region B (Flr_B, RU), a byproduct of microbial activity, C) Fluorescence Index (FI), indicative of microbial DOM source (>1.8), and D) $SS_{(275\text{-}295)}$, indicative of low molecular weight DOM (>0.02).

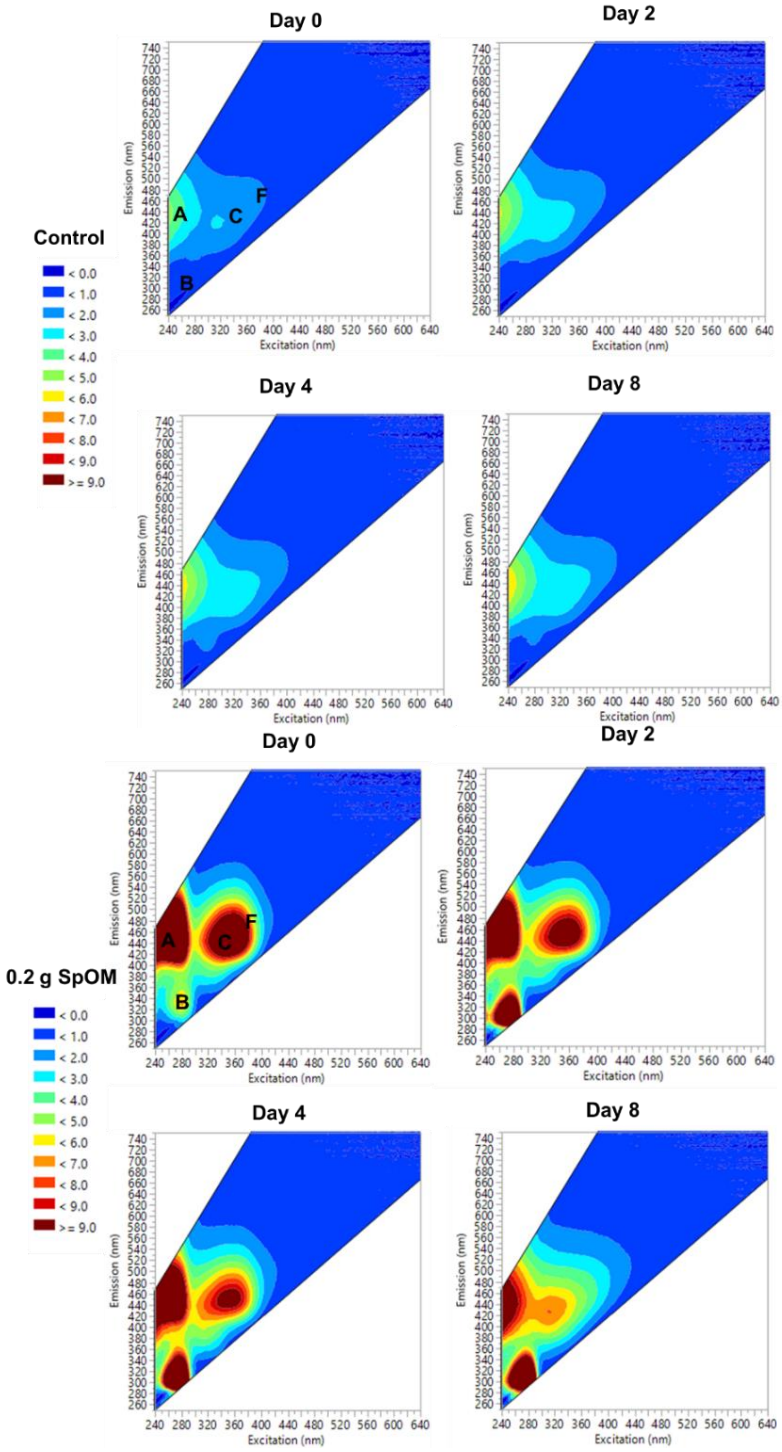

Figure 3-4 Changes in the excitation-emission matrix (EEM) fluorescence intensity spectra at day 0, 2, 4, and 8 for the control incubation (top) and the 0.2 g of spirulina organic matter addition (bottom). Colors blue to red indicate lower to higher fluorescence intensities. Select named regions and areas used for calculating indicators are labeled in figures on the left. See Table S1 for description and Table S2 for interpretations of named regions.

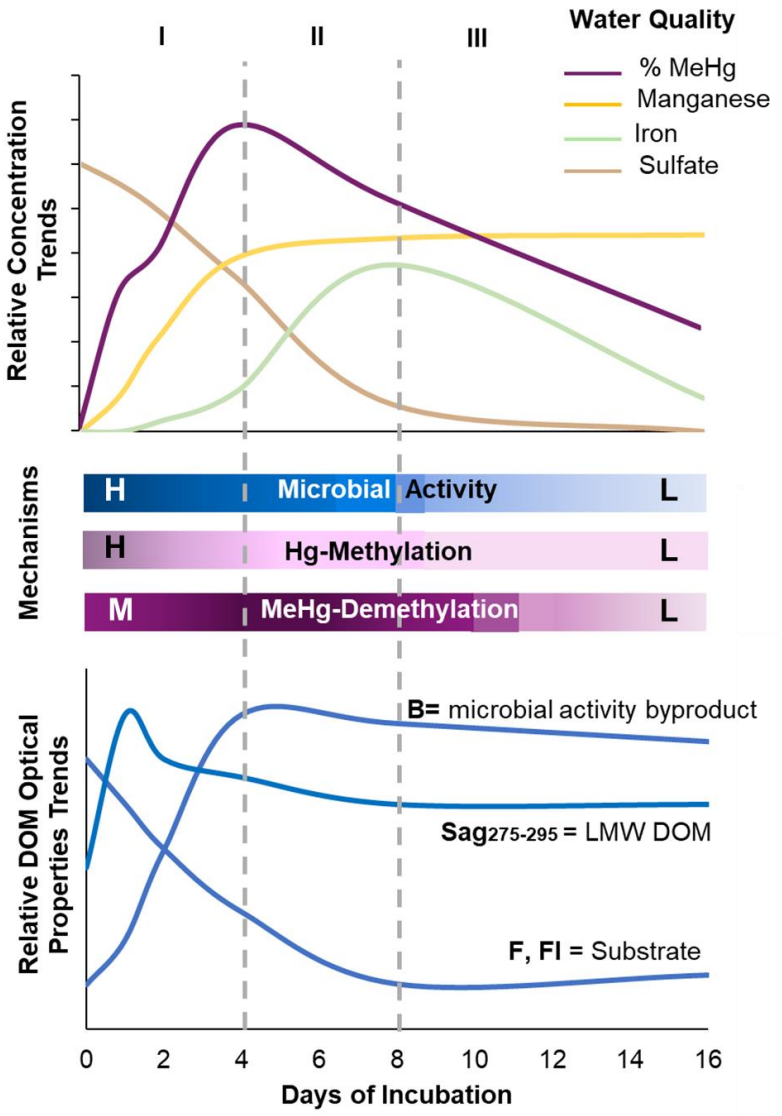
I
II
III
Water Quality
% MeHg
Manganese
Iron
Sulfate
Relative Concentration Trends
Mechanisms
H
Microbial Activity
L
H
Hg-Methylation
L
M
MeHg-Demethylation
L
Relative DOM Optical Properties Trends
B= microbial activity byproduct
Sag275-295 = LMW DOM
F, FI = Substrate
0
2
4
6
8
10
12
14
16
Days of Incubation

Figure 3-5 Conceptual model for the production on methyl mercury (MeHg) with the addition of spirulina organic matter with key aspects studied including water quality, dissolved organic matter (DOM) optical properties, and the mechanisms behind the mercury cycle. Top figure presents relative water concentration trends: % MeHg of the total mercury in soil-water system as an indicator of net MeHg production; and manganese, iron, and sulfate as indicators of oxidation-reduction potential status. Bottom figure represents select DOM optical properties including region B as an indicator of a microbial activity byproduct; fluorescence index (FI) and fluorescence region F as indicators of labile carbon (substrate) type, microbial source DOM and quinoid-like DOM, respectively; and $Sag_{275\text{-}295}$ as an indicator of LMW DOM. The intensity of key mechanisms is shown in the middle and includes microbial activity in blue, and Hg methylation in pink, and MeHg demethylation in purple. H: high, M: medium, L: low.

Stage I (day 0 to 4): Opening the Methylation Window. SpOM addition leads to high microbial activity with drop in F and FI and increase in B and increases inorganic mercury bioavailability of Hg-LMW DOM with a spike in $Sag_{275\text{-}295}$, opening the methylation window. Main substrate for microbial activity appeared to be quinoid-like DOM and microbial source DOM, region F and FI, respectively. Multiple microbial communities and syntropy interactions were enhanced, including multiple Hg-methylating organisms including iron-reducing (increase in iron) and sulfate-reducing (drop in sulfate) bacteria.

Stage II (day 4 to 8): Closing the Methylation Window. Transition to high MeHg demethylation rates with a decrease in net MeHg production. This is caused by reduced conditions favoring the activity of MeHg-demethylating microbes (high). Changes in the DOM properties might suggest the shift in microbial communities with a steeper slope in the substrate F and FI regions and ceased accumulation in fluorescence region B. IHg bioavailability is possibly affected by sulfide build up and DOM, forming Hg-S and Hg-DOM complexes decreasing Hg methylators activity.

Stage III (day 8 to 16): Anoxic quasi-steady state. This period represents high MeHg demethylation rates at the beginning and the transition of the incubations system to a new quasi-steady state where the microbial activity is limited due to a depletion of substrate and sulfate. Iron and mercury are probably complexing/precipitating with sulfide and DOM and returning to the soil phase.

APPENDIX

Table S1a. Cache Creek Settling Basin quality assurance and quality control data from the multiple analyzes developed for the standard and stress text incubation in chapter 2

Analyte	Matrix	MDL	MDL (final units)	RL	RL (final units)	DUP RD (%)	DUP N	DUP USGS-UCM RD (%)	DUP USGS-UCM N	OPR Mean Recovery(%)	OPR N	MS Mean Recovery (%)	MS N
THg	Soil charact	1.0	µg/kg dry wt.	2.0	µg/kg dry wt.	7	12	7	4	93	2	-	-
MeHg	Soil charact	0.1	µg/kg dry wt.	0.2	µg/kg dry wt.	23	4	4	4	99	2	75	2
Thiol-RHg	Soil charact	-	µg/kg dry wt.	0.5	µg/kg dry wt.	13	22	-	-	99	18	-	-
Water Content (%)	Soil charact	-	% wet wt.	1	% wet wt.	14	16	-	-	-	-	-	-
LOI %	Soil charact	-	% dry wt.	0.9	% dry wt.	-	-	-	-	-	-	-	-
Fe TAE_ICP-OES	Soil charact	-	mg/kg wet wt.	4	mg/kg wet wt.	16	2	-	-	-	-	-	-
Al TAE_ICP-OES	Soil charact	-	mg/kg wet wt.	4	mg/kg wet wt.	15	2	-	-	-	-	-	-
Mn TAE_ICP-OES	Soil charact	-	mg/kg wet wt.	4	mg/kg wet wt.	7	2	-	-	-	-	-	-
THg	water	0.02	ng/L	0.2	ng/L	19	15	-	-	90	24	-	-
MeHg	water	0.015	ng/L	0.03	ng/L	11	33	-	-	91	46	94	44

NO3-NO2	water	-	mg-N/L	0.025	mg-N/L	-	-	-	-	102	9	-	-
NH4_Low	water	-	mg-N/L	0.025	mg-N/L	26	5	-	-	108	5	-	-
PO4_Low	water	-	mg-P/L	0.025	mg-P/L	38	6	-	-	100	6	-	-
NH4_High	water	-	mg-N/L	0.25	mg-N/L	16	1	-	-	80	3	-	-
PO4_High	water	-	mg-P/L	0.1	mg-P/L	31	1	-	-	102	3	-	-
Fe	water	-	ug/L	10	ug/L	10	5	-	-	-	-	-	-
Mn	water	-	ug/L	10	ug/L	30	5	-	-	-	-	-	-
Al	water	-	ug/L	10	ug/L	19	5	-	-	-	-	-	-
Cl	water	0.2	mg/L	0.5	mg/L	7	19	-	-	-	-	100	7
SO4	water	0.2	mg/L	0.5	mg/L	5	16.0	-	-	-	-	102	7
THg	soil	1.0	µg/kg dry wt.	2.0	µg/kg dry wt.	10	13	-	-	-	-	-	-
MeHg	soil	0.10	µg/kg dry wt.	0.2	µg/kg dry wt.	10	8	-	-	96	21	110	32
Spirulina	powder	1.0	µg/kg dry wt.	2.0	µg/kg dry wt.	5	3	-	-	-	-	-	-

Table S1b. Cache Creek Settling Basin quality assurance and quality control data from the multiple analyzes developed for the standard and stress text incubation in chapter 2

Analyte	Check Standard Recovery (%)	Check Standard N	STD	STD N	CRM Name	CRM Type	CRM Lot Number	CRM Certified Value	CRM Certified Units	CRM Mean Recovery (%)	CRM N	Blanks Mean	Blanks N	Method Blank Mean	Method Blank N
THg	-	-	-	-	TORT-2	Lobster hepatopancreas	na	270± 0.06	µg/kg	93	2	0.42	2	0.18	2
MeHg	-	-	-	-	SQC 1238-50G	Soil	LRAB 9919	14.8± 0.5	µg/kg	119	2	-	-	0.065	2
Thiol RHg	-	-	-	-	-	-		-	-	-	-	-	-	0.081	10
Water Content (%)	-	-	-	-	-	-		-	-	-	-	-	-	-	-
LOI %	-	-	-	-	-	-		-		-	-	-	-	-	-
Fe TAE_ICP-OES	97	2	1.63	14	-	-		-	-	-	-	4.4	2	-	-
Al TAE_ICP-OES	102	4	1.83	14	-	-		-	-	-	-	3.1	3	-	-
Mn TAE_ICP-OES	94	2	1.59	14	-	-		-	-	-	-	0.38	1	-	-
THg	-	-	-	-	-	-		-	-	-	-	0.28	4.0	0.17	20.0

MeHg	-	-	-	-	-	-		-	-	-	-	0.08	4	0.005	10
NO3 -NO2	-	-	-	-	-	-		-	-	-	-	-	-	-	-
NH4_Low	-	-	-	-	-	-		-	-	-	-	-	-	-	-
PO4_Low	-	-	-	-	-	-		-	-	-	-	-	-	-	-
NH4_High	-	-	-	-	-	-		-	-	-	-	-	-	-	-
PO4_High	-	-	-	-	-	-		-	-	-	-	-	-	-	-
Fe	99	5	2.73	113	-	-		-	-	-	-	9.77	7	-	-
Mn	102	5	3.82	113	-	-		-	-	-	-	6.84	5	-	-
Al	101	5	14.58	105	-	-		-	-	-	-	8.50	7	-	-
Cl	-	-	-	-	-	-		-	-	-	-	21.3	4	0.05	5
SO4	-	-	-	-	-	-		-	-	-	-	0.2	4	0	5
THg	-	-	-	-	TORT-2	Lobster hepatopancreas	na	270± 0.06	µg/kg	90	13	0.70	5	0.08	8
MeHg	-	-	-	-	SQC 1238-50G	Sediment	LRAB 9919	14.8± 0.5	µg/kg	101	14	-	-	0.29	6
Spirulina	-	-	-	-	1573a	Tomato leaves	na	0.034	mg/kg	85	4	0.77	2	0.17	2

Table S2a. Cache Creek Settling Basin standard incubation presenting replication, blanks and Cache Creek water at Rumsey station data for quality and variability control in chapter 2

Location	Treatment	Code	Incubation Sample Day	Sample Date (m/dd/yyyy)	Sample ID	Replicate	pH	Eh (mV)	MeHg (ng/L)	THg (ng/L)	NO3-NO2 (mg-N/L)	NH4 (mg-N/L)	PO4 (mg-P/L)	Fe (µg/L)	Mn (µg/L)	Al (µg/L)
CCSB	Ultrion	A5	1	5/11/2021	A5-1	NO	7.72	288.3	0.076	7.19	15.70	0.25	0.95	19.13	-1.61	11.50
CCSB	Ultrion	A5	1	5/12/2021	A5-1 REP	YES	7.82	280.9	0.072	7.52	16.80	0.26	0.73	26.84	-1.33	22.47
CCSB	Control	A2	2	5/12/2021	A2-2	NO	7.95	183.3	0.116	12.7	5.53	0.19	0.55	43.54	-1.47	40.70
CCSB	Control	A2	2	5/12/2021	A2-2 REP	YES	8.07	184.1	0.083	10.80	7.35	0.23	0.49	20.66	-1.55	28.59
CCSB	Ferralyte	A4	16	5/26/2021	A4-16	NO	7.73	277.6	0.042	3.8	0.08	0.66	0.21	415.10	197.90	269.9
CCSB	Ferralyte	A4	16	5/26/2021	A4-16 REP	YES	7.87	244.3	0.055	3.52	0.07	0.50	0.24	36.49	2.53	49.43
CCSB	ChitoVan	B3	0	5/17/2021	B3-0	NO	8.15	259.1	0.097	9.26	16.20	0.16	0.57	191.50	1.69	124.0
CCSB	ChitoVan	B3	0	5/17/2021	B3-0 REP	YES	8.07	272.5	0.107	11.1	14.30	0.08	0.37	60.8	-1.378	38.77
CCSB	Ultrion	B5	8	5/25/2021	B5-8	NO	7.59	258.4	0.093	8.13	0.07	1.28	0.54	18.87	743.10	16.51
CCSB	Ultrion	B5	8	5/25/2021	B5-8 REP	YES	7.66	256.1	0.082	7.16	0.07	1.11	0.70	23.22	647.6	24.19

CCSB	Ultrion	C5	0	6/7/2021	C5-0	NO	8.21	273.6	0.084	5.78	5.25	0.32	0.34	16.01	-1.27	59.14
CCSB	Ultrion	C5	0	6/7/2021	C5-0 REP	YES	8.21	273.6	0.080	5.85	5.75	0.38	0.39	19.74	-1.797	50.67
CCSB	ChitoVan	C3	1	6/8/2021	C3-1	NO	8.15	242.7	0.069	6.65	13.90	1.28	0.80	11.68	-0.56	76.46
CCSB	ChitoVan	C3	1	6/8/2021	C3-1 REP	YES	8.12	247.2	0.029	6.49	13.00	1.40	0.87	13.68	0.947	31.06
CCSB	Ferralyte	C4	2	6/9/2021	C4-2	NO	7.80	245.0	0.099	7.6	6.76	0.01	0.48	19.63	-2.13	26.30
CCSB	Ferralyte	C4	2	6/9/2021	C4-2 REP	YES	7.82	253.0	0.097	7.29	0.06	0.85	0.43	39.44	394.3	155.2
CCSB	Control	C2	4	6/11/2021	C2-4	NO	7.74	234.8	0.070	7.54	0.07	2.84	0.76	35.35	361.20	142.7
CCSB	Control	C2	4	6/11/2021	C2-4 REP	YES	7.54	233.3	0.095	7.03	0.07	2.36	0.71	NA	NA	NA
CCSB	ChitoVan+Spirulina	C3-sp	1	6/15/2021	C3-sp-1	NO	7.45	125.5	12.8	66.6	0.11	26.20	1.81	106.10	1118	55.83
CCSB	ChitoVan+Spirulina	C3-sp	1	6/15/2021	C3-sp-1-REP	YES	7.19	83.5	22.0	60.3	0.04	36.10	4.23	267.70	1699	20.60
CCSB	Ferralyte+Spirulina	C4-sp	2	6/16/2021	C4-sp-2	NO	7.09	63.0	40.3	99.1	0.06	26.55	1.72	1012	2800	30.77
CCSB	Ferralyte+Spirulina	C4-sp	2	6/16/2021	C4-sp-2-REP	YES	7.07	64.5	32.6	101	0.07	33.50	2.91	985.1	2854	21.42
CCSB	Ultrion+Spirulina	C5-sp	4	6/18/2021	C5-sp-4	NO	6.96	-26.7	26.8	53.8	0.07	49.00	3.54	1750	5644	31.27
CCSB	Ultrion+Spirulina	C5-sp	4	6/18/2021	C5-sp-4-REP	YES	6.94	8.6	27.9	58.1	0.06	42.80	3.52	3518	4971	38.51
CCSB	Blank	Blank_A	16	5/26/2021	Blank_A	NO	NA	NA	0.214	0.259	0.08	0.00	0.01	233	137	15.46

CCSB	Blank	Blank_B1	8	6/22/2021	Blank_B1	NO	8.64	325.6	0.060	0.186	NA	0.13	0.19	30.73	8.30	114.8
CCSB	Blank	Blank_B2	17	6/23/2021	Blank_B2	NO	NA	NA	0.046	0.377	0.08	0.09	0.08	2.75	-0.50	18.77
CCSB	Blank	Blank_C	15	6/29/2021	Blank_C	NO	NA	NA	0.00	0.316	0.07	0.00	0.00	9.10	-1.65	15.13
CCSB	Cache Creek at Rumsey	CCRW_1	1	5/11/2021	Rumsey_1	NO	NA	NA	0.068	8.81	NA	NA	NA	NA	NA	NA
CCSB	Cache Creek at Rumsey	CCRW_2	8	5/25/2021	Rumsey_2	NO	NA	NA	0.059	1.05	NA	NA	NA	NA	NA	NA
CCSB	Cache Creek at Rumsey	CCRW_3	17	6/23/2021	Rumsey_3	NO	NA	NA	0.021	1.2	NA	NA	NA	NA	NA	NA
CCSB	Cache Creek at Rumsey	CCRW_4	8	6/15/2021	Rumsey_4	NO	NA	NA	0.081	1.14	NA	NA	NA	NA	NA	NA

Table S2b. Cache Creek Settling Basin standard incubation presenting replication, blanks and Cache Creek water at Rumsey station data for quality and variability control in chapter 2

Location	Treatment	Code	Incubation Sample Day	Sample Date (mm/dd/yyyy)	Sample ID	Replicate	DOC (mg/L)	SUVA 254 (L/mg-m)	SO4 (mg/L)	SO4 (mM)	Cl (mg/L)	Cl (mM)	Soil MeHg (µg/kg) dry wt.	Soil THg (µg/kg) dry wt.
CCSB	Ultrion	A5	1	5/11/2021	A5-1	NO	6.8	2.36	154	1.61	359	10.11	1.28	297
CCSB	Ultrion	A5	1	5/12/2021	A5-1 REP	YES	7.9	2.55	193	2.01	220	6.20	1.26	290
CCSB	Control	A2	2	5/12/2021	A2-2	NO	10.8	2.00	113	1.18	162	4.58	1.06	308
CCSB	Control	A2	2	5/12/2021	A2-2 REP	YES	9.8	2.04	78	0.81	94	2.64	1.10	326
CCSB	Ferralyte	A4	16	5/26/2021	A4-16	NO	5.6	3.12	161	1.68	165	4.65	1.08	321
CCSB	Ferralyte	A4	16	5/26/2021	A4-16 REP	YES	4.4	2.58	145	1.51	127	3.58	1.22	289
CCSB	ChitoVan	B3	0	5/17/2021	B3-0	NO	11.6	2.13	163	1.70	142	4.02	1.35	312
CCSB	ChitoVan	B3	0	5/17/2021	B3-0 REP	YES	11.7	2.14	112	1.16	104	2.92	1.15	314
CCSB	Ultrion	B5	8	5/25/2021	B5-8	NO	16.2	2.47	284	2.96	146	4.12	1.18	320
CCSB	Ultrion	B5	8	5/25/2021	B5-8 REP	YES	15.7	2.50	274	2.85	168	4.73	1.20	319
CCSB	Ultrion	C5	0	6/7/2021	C5-0	NO	9.1	1.91	100	1.04	140	3.96	1.40	300

CCSB	Ultrion	C5	0	6/7/2021	C5-0 REP	YES	9.2	1.91	125	1.30	157	4.42	1.37	304
CCSB	ChitoVan	C3	1	6/8/2021	C3-1	NO	15.0	1.99	277	2.89	165	4.65	1.10	314
CCSB	ChitoVan	C3	1	6/8/2021	C3-1 REP	YES	16.8	1.92	257	2.67	165	4.66	1.80	312
CCSB	Ferralyte	C4	2	6/9/2021	C4-2	NO	14.9	1.90	151	1.58	168	4.73	1.86	310
CCSB	Ferralyte	C4	2	6/9/2021	C4-2 REP	YES	14.9	2.17	153	1.59	142	4.02	1.20	314
CCSB	Control	C2	4	6/11/2021	C2-4	NO	13.8	2.37	258	2.68	156	4.40	1.23	287
CCSB	Control	C2	4	6/11/2021	C2-4 REP	YES	16.8	2.43	244	2.54	162	4.57	1.26	292
CCSB	ChitoVan+Spirulina	C3-sp	1	6/15/2021	C3-sp-1	NO	62.3	1.43	188	1.96	175	4.93	5.04	289
CCSB	ChitoVan+Spirulina	C3-sp	1	6/15/2021	C3-sp-1-REP	YES	129.4	0.78	211	2.20	155	4.36	5.71	310
CCSB	Ferralyte+Spiruli na	C4-sp	2	6/16/2021	C4-sp-2	NO	196.1	0.43	120	1.25	155	4.36	7.59	290
CCSB	Ferralyte+Spiruli na	C4-sp	2	6/16/2021	C4-sp-2-REP	YES	177.8	0.52	115	1.19	152	4.28	7.91	316
CCSB	Ultrion+Spirulina	C5-sp	4	6/18/2021	C5-sp-4	NO	193.8	0.73	75	0.78	153	4.33	9.15	335
CCSB	Ultrion+Spirulina	C5-sp	4	6/18/2021	C5-sp-4-REP	YES	242.0	0.59	70	0.72	135	3.81	11.86	381
CCSB	Blank	Blank_A	16	5/26/2021	Blank_A	NO	2.2	0.007	0.32	0.003	95	2.19	-	-
CCSB	Blank	Blank_B1	8	6/22/2021	Blank_B1	NO	0.7	0.002	0.08	0.001	0.57	0.016	-	-
CCSB	Blank	Blank_B2	17	6/23/2021	Blank_B2	NO	0.6	0.001	0.09	0.001	0.67	0.019	-	-

CCSB	Blank	Blank_C	15	6/29/2021	Blank_C	NO	0.5	0.002	0.26	0.003	0.20	0.006	-	-
CCSB	Cache Creek at Rumsey	CCRW_1	1	5/11/2021	Rumsey_1	NO	NA	NA	NA	-	NA	-	-	-
CCSB	Cache Creek at Rumsey	CCRW_2	8	5/25/2021	Rumsey_2	NO	NA	NA	NA	-	NA	-	-	-
CCSB	Cache Creek at Rumsey	CCRW_3	17	6/23/2021	Rumsey_3	NO	NA	NA	NA	-	NA	-	-	-
CCSB	Cache Creek at Rumsey	CCRW_4	8	6/15/2021	Rumsey_4	NO	NA	NA	NA	-	NA	-	-	-

Table S3. Standard Test mercury parameters from LME model. Results include least square mean (LSM) and standard error (SE) with its correspondence p value

LME MODEL	MeHg water			IHg water			MeHg:THg water			%MeHg mass water			MeHg soil			Log Kd (soil/water)		
Parameter	**LSM**	**SE**	**p**	**LSM**	**SE**	**p**	**LSM**	**SE**	**p**	**LSM**	**SE**	**p**	**LSM**	**SE**	**p**	**LSM**	**SE**	**p**
Control	0.13	0.06	2.20E-16	10.06	0.59	2.02E-21	0.01	0.01	1	0.03	0.002	1	0.08	0.04	0.04	0.06	0.02	1.65E-57
ChitoVan	0.12	0.03	2.20E-16	8.20	0.59	5.57E-18	0.01	0.01	1	0.02	0.002	1	0.10	0.04	0.01	0.06	0.02	1.24E-57
Ferralyte	0.12	0.03	2.20E-16	7.98	0.59	1.47E-17	0.01	0.01	1	0.02	0.002	1	0.14	0.04	0.00	0.06	0.02	1.51E-57
Ultrion	0.12	0.03	2.20E-16	8.28	0.59	3.74E-18	0.01	0.01	1	0.02	0.002	1	0.14	0.04	0.00	0.06	0.02	1.42E-57
Day 0	0.12	0.08	2.20E-16	12.38	0.71	6.62E-22	0.01	0.01	1	0.02	0.003	1	0.09	0.04	0.03	0.09	0.02	1.53E-56
Day 1	0.08	0.04	2.20E-16	8.11	0.71	4.89E-15	0.01	0.01	1	0.02	0.003	1	0.12	0.04	0.01	0.06	0.02	6.79E-57
Day 2	0.08	0.04	2.20E-16	9.37	0.71	2.92E-17	0.01	0.01	1	0.02	0.003	1	0.14	0.04	0.00	0.05	0.02	7.28E-57
Day 4	0.07	0.04	2.20E-16	8.68	0.71	4.75E-16	0.01	0.01	1	0.02	0.003	1	0.16	0.04	0.00	0.05	0.02	4.97E-57
Day 8	0.08	0.04	2.20E-16	6.83	0.71	1.36E-12	0.01	0.01	1	0.02	0.003	1	0.09	0.04	0.03	0.03	0.02	8.38E-57
Day 16	0.06	0.04	2.20E-16	6.41	0.71	9.33E-12	0.02	0.01	1	0.02	0.003	1	0.09	0.04	0.03	0.04	0.02	4.60E-57
Site A	0.07	0.03	2.20E-16	9.12	0.61	2.96E-19	0.01	0.01	1	0.02	0.003	1	0.05	0.05	0.41	0.06	0.03	1.27E-47
Site B	0.07	0.03	2.20E-16	10.64	0.61	6.81E-22	0.01	0.01	1	0.02	0.003	1	0.12	0.05	0.04	0.06	0.03	6.79E-48

Site C	0.08	0.03	2.20E-16	6.13	0.61	3.55E-13	0.01	0.01	1	0.02	0.003	1	0.18	0.05	0.00	0.06	0.03	6.73E-48
Control: Day 0	0.06	0.08	1.80E-16	14.63	1.37	4.52E-14	0.01	0.03	1	0.02	0.005	1	0.08	0.06	0.22	0.08	0.02	1.40E-51
ChitoVan: Day 0	0.13	0.08	2.20E-16	12.06	1.37	1.88E-11	0.01	0.03	1	0.02	0.005	1	0.04	0.06	0.47	0.06	0.02	1.00E-51
Ferralyte: Day 0	0.14	0.08	2.20E-16	11.23	1.37	1.43E-10	0.01	0.03	1	0.02	0.005	1	0.07	0.06	0.23	0.06	0.02	5.05E-52
Ultrion: Day 0	0.05	0.08	6.86E-16	11.59	1.37	5.91E-11	0.01	0.03	1	0.02	0.005	1	0.18	0.06	0.01	0.06	0.02	6.67E-52
Control: Day 1	0.05	0.08	2.20E-16	9.22	1.37	2.24E-08	0.01	0.03	1	0.02	0.005	1	0.10	0.06	0.12	0.06	0.02	4.40E-52
ChitoVan: Day 1	0.12	0.08	2.20E-16	7.95	1.37	5.46E-07	0.01	0.03	1	0.02	0.005	1	0.06	0.06	0.32	0.06	0.02	3.99E-52
Ferralyte: Day 1	0.12	0.08	2.20E-16	8.24	1.37	2.67E-07	0.01	0.03	1	0.02	0.005	1	0.17	0.06	0.01	0.06	0.02	5.08E-52
Ultrion: Day 1	0.11	0.08	2.20E-16	7.05	1.37	5.21E-06	0.01	0.03	1	0.02	0.005	1	0.15	0.06	0.02	0.06	0.02	2.07E-52
Control: Day 2	0.13	0.08	2.20E-16	11.22	1.37	1.47E-10	0.01	0.03	1	0.02	0.005	1	0.11	0.06	0.09	0.06	0.02	5.79E-52
ChitoVan: Day 2	0.13	0.08	2.20E-16	8.31	1.37	2.20E-07	0.01	0.03	1	0.02	0.005	1	0.22	0.06	0.00	0.06	0.02	1.94E-52
Ferralyte: Day 2	0.12	0.08	2.20E-16	8.56	1.37	1.19E-07	0.01	0.03	1	0.02	0.005	1	0.12	0.06	0.06	0.06	0.02	4.07E-52
Ultrion: Day 2	0.13	0.08	2.20E-16	9.40	1.37	1.40E-08	0.01	0.03	1	0.02	0.005	1	0.11	0.06	0.09	0.06	0.02	5.34E-52
Control: Day 4	0.12	0.08	2.20E-16	9.68	1.37	6.95E-09	0.05	0.03	1	0.02	0.005	1	0.10	0.06	0.10	0.06	0.02	1.33E-52
ChitoVan: Day 4	0.11	0.08	2.20E-16	8.09	1.37	3.91E-07	0.01	0.03	1	0.02	0.005	1	0.12	0.06	0.06	0.06	0.02	3.34E-52
Ferralyte: Day 4	0.11	0.08	2.20E-16	8.02	1.37	4.62E-07	0.01	0.03	1	0.02	0.005	1	0.30	0.06	0.00	0.06	0.02	2.86E-52

Ultrion: Day 4	0.12	0.08	2.20E-16	8.92	1.37	4.79E-08	0.01	0.03	1	0.02	0.005	1	0.13	0.06	0.04	0.06	0.02	4.18E-52
Control: Day 8	0.12	0.08	2.20E-16	8.19	1.37	2.98E-07	0.01	0.03	1	0.02	0.005	1	0.05	0.06	0.39	0.06	0.02	6.36E-52
ChitoVan: Day 8	0.07	0.08	2.20E-16	5.89	1.37	8.60E-05	0.01	0.03	1	0.02	0.005	1	0.09	0.06	0.16	0.06	0.02	3.49E-52
Ferralyte: Day 8	0.07	0.08	2.20E-16	6.55	1.37	1.77E-05	0.01	0.03	1	0.02	0.005	1	0.09	0.06	0.13	0.08	0.02	4.83E-52
Ultrion: Day 8	0.08	0.08	2.20E-16	6.69	1.37	1.25E-05	0.01	0.03	1	0.02	0.005	1	0.14	0.06	0.03	0.06	0.02	3.97E-52
Control: Day 16	0.08	0.08	1.79E-20	7.43	1.37	2.01E-06	0.02	0.03	1	0.02	0.005	1	0.03	0.06	0.56	0.06	0.02	2.72E-52
ChitoVan: Day 16	0.08	0.08	2.30E-19	6.87	1.37	8.19E-06	0.02	0.03	1	0.02	0.005	1	0.10	0.06	0.11	0.06	0.02	1.63E-52
Ferralyte: Day 16	0.07	0.08	2.46E-22	5.30	1.37	3.33E-04	0.03	0.03	1	0.02	0.005	1	0.04	0.06	0.19	0.06	0.02	3.27E-52
Ultrion: Day 16	0.05	0.08	1.80E-19	6.04	1.37	5.99E-05	0.02	0.03	1	0.02	0.005	1	0.04	0.06	0.02	0.06	0.02	2.69E-52

Notes: Model estimated using R Studio using a Linear mixed model fit by REML. t-tests use Satterthwaite's method [lmerModLmerTest]. Least Squares means [ls_means] estimated with a 95% confidence level. Degrees of freedom estimated with method Satterthwaite.

Table S4. Standard Test aqueous parameters LME model. Results include least square mean (LSM) and standard error (SE) with its correspondence p value.

LME MODEL	Redox Potential			pH			Manganese ug/L			Sulfate mg/L		
Parameter	**LSM**	**SE**	**p**	**LSM**	**SE**	**p**	**LSM**	**SE**	**p**	**LSM**	**SE**	**p**
Control	206.10	1.58	2.61E-15	7.91	0.05	6.16E-128	0.55	0.47	1.16E-05	102.78	1.21	2.42E-36
ChitoVan	205.96	1.58	2.63E-15	7.91	0.05	6.87E-128	0.84	0.47	3.57E-10	167.22	1.21	3.70E-39
Ferralyte	204.78	1.58	2.72E-15	7.91	0.05	6.78E-128	0.47	0.47	2.56E-08	131.73	1.21	8.33E-38
Ultrion	207.62	1.58	2.49E-15	7.91	0.05	5.24E-128	0.31	0.47	4.76E-07	128.97	1.21	1.10E-37
Day 0	331.27	1.64	1.88E-15	8.23	0.06	7.66E-122	0.00	0.56	3.70E-02	165.69	1.26	1.86E-33
Day 1	293.84	1.64	3.87E-15	8.02	0.06	9.79E-122	0.00	0.56	3.91E-02	163.75	1.26	2.14E-33
Day 2	270.92	1.64	6.34E-15	7.86	0.06	1.20E-121	0.00	0.56	8.20E-03	135.71	1.26	2.22E-32
Day 4	51.45	1.64	3.16E-10	7.64	0.06	1.32E-121	0.14	0.56	6.91E-09	81.85	1.26	1.69E-29
Day 8	283.39	1.64	4.82E-15	7.61	0.06	1.78E-121	0.69	0.56	1.74E-10	152.74	1.26	5.06E-33
Day 16	199.40	1.64	4.21E-14	7.61	0.06	2.92E-121	1.25	0.56	4.68E-13	108.41	1.26	3.98E-31
Site A	298.11	1.99	1.17E-10	9.77	0.04	2.33E-132	0.54	0.52	5.18E-05	115.48	1.18	3.98E-41
Site B	125.17	1.99	8.68E-09	9.86	0.04	1.71E-132	0.88	0.52	1.56E-07	127.34	1.18	1.03E-41
Site C	234.66	1.99	3.79E-10	9.82	0.04	1.96E-132	0.65	0.52	2.12E-08	151.91	1.18	9.49E-43
Control: Day 0	334.14	2.10	5.50E-10	8.04	0.12	3.49E-100	0.01	1.05	7.09E-02	155.80	1.60	1.13E-16
ChitoVan: Day 0	327.63	2.10	6.02E-10	8.17	0.12	2.67E-100	0.00	1.05	4.24E-01	164.35	1.60	7.05E-17
Ferralyte: Day 0	332.96	2.10	5.59E-10	8.06	0.12	7.76E-100	0.00	1.05	2.24E-01	163.18	1.60	7.51E-17
Ultrion: Day 0	330.40	2.10	5.79E-10	8.33	0.12	1.96E-100	0.00	1.05	5.13E-01	180.35	1.60	3.10E-17
Control: Day 1	293.39	2.10	1.00E-09	9.82	0.12	6.02E-100	0.00	1.05	4.21E-01	146.99	1.60	1.90E-16
ChitoVan: Day 1	295.72	2.10	9.64E-10	7.92	0.12	4.14E-100	0.00	1.05	5.28E-01	173.98	1.60	4.26E-17
Ferralyte: Day 1	292.55	2.10	1.01E-09	7.92	0.12	4.16E-100	0.01	1.05	9.03E-02	185.98	1.60	2.37E-17
Ultrion: Day 1	293.70	2.10	9.95E-10	7.92	0.12	3.62E-100	0.00	1.05	1.95E-01	151.16	1.60	1.48E-16
Control: Day 2	262.76	2.10	1.66E-09	7.90	0.12	4.70E-100	0.01	1.05	9.24E-02	126.34	1.60	7.35E-16

ChitoVan: Day 2	279.73	2.10	1.25E-09	7.90	0.12	6.54E-100	0.01	1.05	6.35E-02	159.47	1.60	9.21E-17
Ferralyte: Day 2	261.31	2.10	1.70E-09	7.86	0.12	5.25E-100	0.00	1.05	3.81E-01	122.85	1.60	9.45E-16
Ultrion: Day 2	280.48	2.10	1.23E-09	7.86	0.12	5.26E-100	0.00	1.05	1.85E-01	137.04	1.60	3.55E-16
Control: Day 4	51.35	2.10	3.21E-06	7.86	0.12	5.48E-100	0.11	1.05	1.33E-02	126.16	1.60	7.44E-16
ChitoVan: Day 4	52.33	2.10	2.95E-06	7.86	0.12	6.93E-100	0.12	1.05	3.59E-05	206.91	1.60	9.30E-18
Ferralyte: Day 4	50.73	2.10	3.39E-06	7.83	0.12	5.43E-100	0.09	1.05	1.01E-04	42.24	1.60	1.59E-11
Ultrion: Day 4	51.40	2.10	3.20E-06	7.83	0.12	5.92E-100	0.12	1.05	8.26E-04	40.70	1.60	2.24E-11
Control: Day 8	282.62	2.10	1.19E-09	7.83	0.12	6.93E-100	0.21	1.05	2.51E-03	124.34	1.60	8.48E-16
ChitoVan: Day 8	289.89	2.10	1.06E-09	7.83	0.12	1.06E-99	0.76	1.05	9.76E-08	141.48	1.60	2.67E-16
Ferralyte: Day 8	277.70	2.10	1.29E-09	7.83	0.12	7.58E-100	0.32	1.05	8.18E-04	191.70	1.60	1.82E-17
Ultrion: Day 8	283.49	2.10	1.17E-09	7.83	0.12	7.42E-100	0.22	1.05	1.32E-04	161.41	1.60	8.28E-17
Control: Day 16	205.03	2.10	5.24E-09	7.74	0.12	1.27E-99	0.83	1.05	3.83E-03	25.97	1.60	1.35E-09
ChitoVan: Day 16	185.66	2.10	8.30E-09	7.74	0.12	1.74E-99	2.09	1.05	6.78E-09	163.81	1.60	7.26E-17
Ferralyte: Day 16	205.66	2.10	5.16E-09	7.74	0.12	1.21E-99	0.75	1.05	1.03E-07	173.08	1.60	4.46E-17
Ultrion: Day 16	201.93	2.10	5.62E-09	7.74	0.12	1.11E-99	0.73	1.05	2.87E-05	187.53	1.60	2.20E-17

Notes: Least squares mean had a confidence interval of 95% and degrees of freedom were estimated with method Satterthwaite in RStudio.

Table S5. Standard Test supportive aqueous parameters LME model. Results include least square mean (LSM) and standard error (SE) with its correspondence p value.

LME MODEL	Iron			Aluminum			Ammonia			Nitrate			Phosphate			DOC		
Parameter	**LSM**	**SE**	**p**	**LSM**	**SE**	**p**	**LSM**	**SE**	**p**	**LSM**	**SE**	**p**	**LSM**	**SE**	**p**	**LSM**	**SE**	**p**
Control	0.029	0.0004	2.29E-12	0.034	0.0003	1.000	1.523	0.085	1.09E-05	6.097	0.206	2.33E-11	1.388	0.077	9.40E-05	15.643	1.020	2.35E-63
ChitoVan	0.034	0.0004	5.57E-13	0.050	0.0003	1.000	2.708	0.085	2.26E-15	4.484	0.206	3.63E-09	1.010	0.077	5.64E-12	8.699	1.020	2.78E-63
Ferralyte	0.030	0.0004	1.75E-12	0.030	0.0003	1.000	1.538	0.085	7.45E-06	3.738	0.206	7.62E-08	1.477	0.077	6.48E-06	7.564	1.020	2.29E-59
Ultrion	0.027	0.0004	4.74E-12	0.031	0.0003	1.000	1.851	0.085	4.21E-09	5.534	0.206	1.12E-10	0.900	0.077	1.09E-12	7.629	1.020	1.28E-59
Day 0	0.024	0.0004	2.14E-10	0.034	0.0003	0.999	1.198	0.096	6.47E-02	12.425	0.238	6.67E-14	0.543	0.090	2.80E-07	7.802	1.024	4.04E-54
Day 1	0.025	0.0004	1.39E-10	0.033	0.0003	0.999	1.502	0.096	1.01E-04	8.064	0.238	2.29E-11	0.561	0.090	1.38E-07	7.968	1.024	1.02E-54
Day 2	0.032	0.0004	2.07E-11	0.034	0.0003	0.999	1.645	0.096	4.40E-06	5.533	0.238	4.90E-09	0.583	0.090	6.12E-08	9.164	1.024	8.17E-57
Day 4	0.040	0.0004	3.19E-12	0.056	0.0003	0.999	2.284	0.096	3.47E-11	3.371	0.238	6.27E-06	0.626	0.090	1.17E-08	11.405	1.024	3.23E-55
Day 8	0.025	0.0004	1.67E-10	0.027	0.0003	0.999	2.261	0.096	4.91E-11	2.862	0.238	6.10E-05	0.412	0.090	3.81E-05	11.941	1.024	7.64E-55
Day 16	0.038	0.0004	5.12E-12	0.034	0.0003	0.999	2.631	0.096	2.82E-13	2.514	0.238	3.43E-04	0.525	0.090	5.58E-07	12.439	1.024	5.74E-56
Site A	0.032	0.0005	1.70E-08	0.035	0.0002	1.000	1.530	0.115	6.08E-04	6.042	0.253	6.55E-09	0.508	0.086	3.90E-07	9.014	1.017	1.12E-62
Site B	0.039	0.0005	3.93E-09	0.038	0.0002	1.000	1.777	0.115	9.54E-06	5.590	0.253	1.89E-08	0.480	0.086	1.20E-06	10.670	1.017	8.13E-68

Site C	0.022	0.0005	2.30E-07	0.033	0.0002	1.000	2.334	0.115	2.85E-09	3.433	0.253	1.38E-05	0.636	0.086	2.24E-09	11.396	1.017	6.68E-67
Control: Day 0	0.029	0.0006	3.13E-06	0.038	0.0007	0.989	1.134	0.161	4.40E-01	13.266	0.429	2.64E-07	0.314	0.169	7.03E-02	8.023	1.049	1.05E-34
ChitoVan: Day 0	0.051	0.0006	1.47E-07	0.058	0.0007	0.989	1.412	0.161	3.81E-02	17.630	0.429	2.67E-08	0.657	0.169	3.30E-04	8.253	1.049	2.03E-35
Ferralyte: Day 0	0.013	0.0006	2.47E-04	0.016	0.0007	0.989	1.141	0.161	4.18E-01	8.776	0.429	7.11E-06	0.440	0.169	1.25E-02	7.818	1.049	4.85E-34
Ultrion: Day 0	0.018	0.0006	3.65E-05	0.035	0.0007	0.989	1.129	0.161	4.56E-01	11.613	0.429	7.70E-07	0.760	0.169	4.76E-05	7.159	1.049	1.09E-31
Control: Day 1	0.030	0.0006	2.75E-06	0.038	0.0007	0.989	1.288	0.161	1.24E-01	8.148	0.429	1.27E-05	0.274	0.169	1.12E-01	8.954	1.049	2.15E-37
ChitoVan: Day 1	0.023	0.0006	1.03E-05	0.044	0.0007	0.989	1.965	0.161	1.26E-04	10.921	0.429	1.26E-06	0.694	0.169	1.65E-04	8.430	1.049	6.09E-36
Ferralyte: Day 1	0.026	0.0006	6.05E-06	0.033	0.0007	0.989	1.362	0.161	6.16E-02	5.132	0.429	4.07E-04	0.380	0.169	2.95E-02	7.316	1.049	2.79E-32
Ultrion: Day 1	0.023	0.0006	1.01E-05	0.022	0.0007	0.989	1.477	0.161	1.97E-02	9.260	0.429	4.66E-06	0.896	0.169	3.27E-06	7.301	1.049	3.17E-32
Control: Day 2	0.054	0.0006	1.14E-07	0.047	0.0007	0.989	1.510	0.161	1.41E-02	7.179	0.429	3.37E-05	0.432	0.169	1.42E-02	8.691	1.049	1.10E-36
ChitoVan: Day 2	0.027	0.0006	4.55E-06	0.038	0.0007	0.989	2.463	0.161	1.20E-06	4.718	0.429	7.39E-04	0.779	0.169	3.32E-05	9.107	1.049	8.60E-38
Ferralyte: Day 2	0.033	0.0006	1.64E-06	0.032	0.0007	0.989	1.221	0.161	2.22E-01	5.607	0.429	2.15E-04	0.392	0.169	2.51E-02	8.138	1.049	4.58E-35
Ultrion: Day 2	0.021	0.0006	1.66E-05	0.022	0.0007	0.989	1.612	0.161	4.86E-03	4.935	0.429	5.39E-04	0.728	0.169	8.88E-05	8.519	1.049	3.35E-36
Control: Day 4	0.016	0.0006	7.06E-05	0.025	0.0007	0.989	1.922	0.161	1.95E-04	5.933	0.429	1.42E-04	0.461	0.169	9.07E-03	8.680	1.049	1.18E-36
ChitoVan: Day 4	0.035	0.0006	1.21E-06	0.108	0.0007	0.988	3.650	0.161	2.74E-10	2.089	0.429	9.26E-02	0.892	0.169	3.57E-06	8.753	1.049	7.42E-37
Ferralyte: Day 4	0.074	0.0006	2.01E-08	0.055	0.0007	0.989	1.841	0.161	4.47E-04	2.520	0.429	3.64E-02	0.463	0.169	8.86E-03	7.582	1.049	3.08E-33

Ultrion: Day 4	0.061	0.0006	5.98E-08	0.069	0.0007	0.988	2.105	0.161	3.18E-05	4.134	0.429	1.83E-03	0.687	0.169	1.90E-04	7.519	1.049	5.11E-33
Control: Day 8	0.036	0.0006	1.03E-06	0.039	0.0007	0.989	2.070	0.161	4.48E-05	4.026	0.429	2.18E-03	0.305	0.169	7.81E-02	8.440	1.049	5.69E-36
ChitoVan: Day 8	0.027	0.0006	5.15E-06	0.034	0.0007	0.989	3.644	0.161	2.83E-10	2.072	0.429	9.62E-02	0.575	0.169	1.41E-03	8.599	1.049	1.99E-36
Ferralyte: Day 8	0.014	0.0006	1.50E-04	0.013	0.0007	0.989	1.438	0.161	2.92E-02	2.06	0.42	9.75E-02	0.212	0.169	2.16E-01	19.512	1.049	9.25E-32
Ultrion: Day 8	0.029	0.0006	3.12E-06	0.030	0.0007	0.989	2.409	0.161	1.93E-06	3.893	[illegible]	2.73E-03	0.554	0.169	2.04E-03	7.880	1.049	3.02E-34
Control: Day 16	0.023	0.0006	1.10E-05	0.023	0.0007	0.989	1.422	0.161	3.42E-02	2.771	0.429	2.17E-02	0.182	0.169	2.87E-01	9.631	1.049	4.50E-39
ChitoVan: Day 16	0.053	0.0006	1.25E-07	0.043	0.0007	0.989	4.341	0.161	7.56E-12	2.066	0.429	9.76E-02	0.628	0.169	5.55E-04	9.085	1.049	9.81E-38
Ferralyte: Day 16	0.068	0.0006	3.09E-08	0.053	0.0007	0.989	2.631	0.161	2.97E-07	2.074	0.429	9.58E-02	0.454	0.169	1.01E-02	7.394	1.049	1.43E-32
Ultrion: Day 16	0.024	0.0006	8.82E-06	0.025	0.0007	0.989	2.949	0.161	2.57E-08	3.362	0.429	6.94E-03	0.834	0.169	1.13E-05	7.471	1.049	7.60E-33

Notes: Least squares mean had a confidence interval of 95% and degrees of freedom were estimated with method Satterthwaite in RStudio.

Table S6. Stress Test mercury parameters LME model. Results include least square mean (LSM) and standard error (SE) with its correspondence p value

	MeHg water			IHg water			MeHg:THg			%MeHgmass water / total MeHg mass			MeHg soil			Log Kg MeHg (water/soil)		
Parameter	**LSM**	**SE**	**Pr(>|t|)**	**LSM**	**SE**	**Pr(>|t|)**	**LSM**	**SE**	**Pr(>|t|)**	**LSM**	**SE**	**Pr(>|t|)**	**LSM**	**SE**	**Pr(>|t|)**	**LSM**	**SE**	**Pr(>|t|)**
Standard Test	0.08	0.05	<0.001	14.73	0.05	<0.001	0.01	0.03	<0.001	0.10	0.02	<0.011	1.53	0.16	1.000	4.26	0.31	<0.001
Stress Test	5.05	0.05	<0.001	17.99	0.05	0.004	0.32	0.03	<0.001	1.01	0.02	<0.012	4.96	0.16	0.001	2.96	0.31	0.833
Standard Test : Day 0	0.10	0.13	0.230	9.21	0.12	<0.001	0.01	0.03	<0.001	0.10	0.02	<0.013	1.27	0.40	0.001	4.09	0.08	<0.001
Stress Test : Day 0	0.26	0.13	<0.001	23.57	0.12	<0.001	0.01	0.03	<0.001	0.10	0.02	<0.014	3.45	0.40	0.001	4.12	0.08	<0.001
Standard Test : Day 1	0.06	0.13	0.230	6.36	0.12	1.000	0.01	0.03	<0.001	0.10	0.02	<0.015	1.33	0.40	0.160	4.37	0.08	0.936
Stress Test : Day 1	7.46	0.13	<0.001	38.86	0.12	<0.001	0.25	0.03	<0.001	1.02	0.02	<0.016	4.66	0.40	0.160	2.79	0.08	<0.001
Standard Test : Day 2	0.09	0.13	0.230	6.62	0.12	1.000	0.01	0.03	<0.001	0.09	0.02	<0.017	1.70	0.40	0.001	4.18	0.08	0.936
Stress Test : Day 2	29.96	0.13	<0.001	77.48	0.12	<0.001	0.32	0.03	<0.001	1.46	0.02	<0.018	6.66	0.40	0.001	2.30	0.08	<0.001
Standard Test : Day 4	0.08	0.13	0.230	5.10	0.12	1.000	0.01	0.03	<0.001	0.06	0.02	<0.019	1.89	0.40	0.003	4.35	0.08	0.936
Stress Test : Day 4	32.79	0.13	<0.001	52.98	0.12	<0.001	0.36	0.03	<0.001	2.04	0.02	<0.020	7.31	0.40	0.004	2.47	0.08	<0.001
Standard Test : Day 8	0.09	0.13	0.230	4.81	0.12	1.000	0.01	0.03	<0.001	0.04	0.02	<0.021	1.51	0.40	0.290	4.21	0.08	0.936
Stress Test : Day 8	4.35	0.13	<0.001	16.61	0.12	0.002	0.28	0.03	<0.001	0.59	0.02	<0.022	4.53	0.40	0.300	3.01	0.08	<0.001

Standard Test : Day 16	0.08	0.13	0.230	4.22	0.12	1.000	0.01	0.03	<0.001	0.04	0.02	<0.023	1.47	0.40	0.610	4.32	0.08	0.936
Stress Test : Day 16	2.61	0.13	<0.001	9.78	0.12	<0.001	0.23	0.03	<0.001	0.88	0.02	<0.024	3.12	0.40	0.520	3.07	0.08	<0.001
Treatment Control	0.13	0.07	0.110	11.82	0.07	<0.001	0.01	0.03	<0.001	0.84	0.01	<0.001	3.38	0.23	1.000	3.68	0.05	0.997
Treatment ChitoVan	0.12	0.07	0.110	12.06	0.07	0.863	0.01	0.03	<0.001	0.86	0.01	<0.002	2.98	0.23	1.000	3.59	0.05	0.997
Treatment Ferralyte	0.12	0.07	0.110	13.20	0.07	0.317	0.01	0.03	<0.001	0.86	0.01	<0.003	3.23	0.23	1.000	3.55	0.05	0.997
Treatment Ultrion	0.12	0.07	0.110	11.47	0.07	0.789	0.01	0.03	<0.001	0.84	0.01	<0.004	3.37	0.23	1.000	3.61	0.05	0.997
Day 0	0.16	0.09	<0.001	11.94	0.09	<0.001	0.01	0.03	<0.001	0.72	0.00	<0.005	2.36	0.28	0.910	4.11	0.04	0.980
Day 1	0.68	0.09	0.016	15.64	0.09	0.038	0.23	0.03	<0.001	0.85	0.00	<0.006	2.99	0.28	0.440	3.58	0.04	0.016
Day 2	1.72	0.09	0.719	22.65	0.09	0.073	0.32	0.03	<0.001	1.02	0.00	<0.007	4.10	0.28	0.290	3.24	0.04	0.420
Day 4	1.36	0.09	0.204	20.09	0.09	0.260	0.30	0.03	<0.001	0.96	0.00	<0.008	4.60	0.28	0.680	3.42	0.04	0.017
Day 8	0.63	0.09	0.620	8.33	0.09	<0.001	0.21	0.03	<0.001	0.80	0.00	<0.009	3.02	0.28	0.730	3.61	0.04	0.334
Day 16	0.06	0.09	0.199	4.48	0.09	<0.001	0.02	0.03	<0.001	0.79	0.00	<0.010	2.29	0.28	0.890	3.70	0.04	0.044

Notes: Least squares mean had a confidence interval of 95% and degrees of freedom were estimated with method Satterthwaite in RStudio.

Table S7. Stress Test mercury parameters from Tukey HSD analysis.

		Log MeHg Kd		MeHg water		%MeHg		MeHg/THg water		Soil MeHg		IHg water	
Parameter	**df**	**t.ratio**	**p.value**	**t.ratio**	**p.value**	**t.ratio**	**p.value**	**t.ratio**	**p.value**	**t.ratio**	**p.value**	**t.ratio**	**p.value**
C Day0 - sp Day0	33.00	-0.13	1.00E+00	-5.49	**2.38E-04**	2.06	6.54E-01	5.49	**2.40E-04**	-3.82	**2.35E-02**	-2.56	3.40E-01
C Day1 - sp Day1	33.00	15.03	**7.45E-14**	-25.84	**5.86E-14**	-15.74	**6.36E-14**	2.13	6.04E-01	-5.85	**8.59E-05**	-10.36	**4.21E-10**
C Day16 - sp Day16	33.00	11.49	**2.43E-11**	-18.99	**5.86E-14**	-12.13	**6.79E-12**	1.09	9.93E-01	-2.90	1.88E-01	-9.07	**1.09E-08**
C Day2 - sp Day2	33.00	17.30	**5.88E-14**	-31.49	**5.86E-14**	-19.06	**5.86E-14**	-2.80	2.26E-01	-8.68	**3.03E-08**	-13.69	**3.05E-13**
C Day4 - sp Day4	33.00	17.72	**5.87E-14**	-31.14	**5.86E-14**	-18.16	**5.87E-14**	-2.03	6.74E-01	-9.53	**3.30E-09**	-10.91	**1.12E-10**
C Day8 - sp Day8	33.00	10.76	**1.35E-10**	-20.87	**5.86E-14**	-11.48	**2.94E-11**	0.56	1.00E+00	-5.31	**4.01E-04**	-7.97	**2.06E-07**
sp Day0 - sp Day1	33.00	NA	NA	-23.65	**5.86E-14**	-14.63	**9.86E-14**	-2.24	5.37E-01	-2.13	6.06E-01	-7.09	**2.42E-06**
sp Day0 - sp Day16	33.00	NA	NA	-16.84	**5.93E-14**	-11.51	**2.70E-11**	-3.82	2.37E-02	0.58	1.00E+00	4.10	**1.16E-02**
sp Day0 - sp Day2	33.00	NA	NA	-35.21	**5.86E-14**	-19.92	**5.86E-14**	-7.17	**1.96E-06**	-5.64	**1.55E-04**	-14.12	**1.62E-13**
sp Day0 - sp Day4	33.00	NA	NA	-33.11	**5.86E-14**	-18.08	**5.87E-14**	-8.27	**9.13E-08**	-6.79	**5.72E-06**	-10.66	**2.00E-10**
sp Day0 - sp Day8	33.00	NA	NA	-20.06	**5.86E-14**	-12.17	**6.11E-12**	-3.23	9.42E-02	-1.90	7.52E-01	-0.43	1.00E+00
sp Day1 - sp Day16	33.00	-2.63	2.77E-01	5.64	**1.56E-04**	3.11	1.22E-01	-1.22	9.83E-01	2.71	2.66E-01	7.89	2.57E-07
sp Day1 - sp Day2	33.00	4.49	**3.43E-03**	-7.85	**2.90E-07**	-5.30	**4.16E-04**	-4.86	**1.45E-03**	-3.51	5.02E-02	-4.01	1.44E-02

sp Day1 - sp Day4	33.00	2.93	1.59E-01	-6.33	**2.13E-05**	-3.45	5.76E-02	-6.22	**2.95E-05**	-4.66	**2.52E-03**	-1.84	7.85E-01
sp Day1 - sp Day8	33.00	-2.07	6.11E-01	2.90	1.86E-01	2.45	4.01E-01	-1.22	9.84E-01	0.23	1.00E+00	4.84	1.50E-03
sp Day2 - sp Day16	33.00	-7.12	**1.93E-06**	13.50	**4.16E-13**	8.41	**6.31E-08**	3.69	3.26E-02	6.22	**2.93E-05**	11.79	**1.45E-11**
sp Day2 - sp Day4	33.00	-1.57	8.86E-01	1.52	9.24E-01	1.85	7.82E-01	-1.35	9.65E-01	-1.15	9.90E-01	2.16	5.90E-01
sp Day2 - sp Day8	33.00	-6.54	**1.01E-05**	10.75	**1.61E-10**	7.75	**3.83E-07**	3.65	3.59E-02	3.74	**2.86E-02**	8.76	**2.46E-08**
sp Day4 - sp Day16	33.00	-5.54	**1.79E-04**	11.98	**9.31E-12**	6.56	**1.09E-05**	5.00	**9.75E-04**	7.37	**1.11E-06**	9.64	**2.49E-09**
sp Day4 - sp Day8	33.00	-4.96	**9.22E-04**	9.25	**6.87E-09**	5.90	**7.25E-05**	4.99	**9.97E-04**	4.89	**1.32E-03**	6.62	**9.27E-06**
sp Day8 - sp Day16	33.00	-0.55	1.00E+00	2.74	2.50E-01	0.66	1.00E+00	0.01	1.00E+00	2.48	3.87E-01	3.04	1.41E-01

Notes: C represents standard test while sp represents stress test incubation. Significant differences are in bold with a $p<0.05$. The interaction term helped evaluate any significant interaction between day and stress test incubation not always seen in the standard test.

Table S8. Stress Test aqueous parameters LME model. Results include least square mean (LSM) and standard error (SE) with its correspondence p value

	Redox Potential			pH			Manganese mg/L			Sulfate mg/L		
Parameter	**LSM**	**SE**	**Pr(> l t l)**	**LSM**	**SE**	**Pr(> l t l)**	**LSM**	**SE**	**Pr(> l t l)**	**LSM**	**SE**	**Pr(> l t l)**
Standard Test	246.44	3.64	<0.001	7.82	0.014	<0.001	0.27	0.08	0.002	184.93	1.04	1
Stress Test	64.19	3.64	<0.001	7.27	0.014	0.023	2.83	0.08	<0.0001	38.09	1.04	0.89
Standard Test : Day 0	300.61	8.92	<0.001	8.18	0.034	0.6	0.01	0.08	0.95	179.47	1.04	0.49
Stress Test : Day 0	246.72	8.92	<0.001	8.06	0.034	<0.001	0.01	0.19	<0.0001	183.09	1.04	0.49
Standard Test : Day 1	268.63	8.92	1	8.17	0.034	0.6	0.02	0.19	0.95	190.57	1.04	0.49
Stress Test : Day 1	165.49	8.92	0.01	7.41	0.034	<0.001	0.82	0.19	<0.0001	170.72	1.04	0.45
Standard Test : Day 2	283.4	8.92	1	7.72	0.034	0.6	0.02	0.19	0.95	196.37	1.04	0.45
Stress Test : Day 2	97.24	8.92	<0.001	7.1	0.034	<0.001	2.76	0.19	<0.0001	192.48	1.04	0.003
Standard Test : Day 4	264.41	8.92	1	7.76	0.034	0.6	0.20	0.19	0.95	192.48	1.04	0.63
Stress Test : Day 4	1.34	8.92	<0.001	6.9	0.034	<0.001	4.74	0.19	<0.0001	109.95	1.04	<0.001
Standard Test : Day 8	261.41	8.92	1	7.62	0.034	0.6	0.44	0.19	0.95	148.41	1.04	<0.001
Stress Test : Day 8	-75.31	8.92	<0.001	7.01	0.034	<0.001	4.40	0.19	<0.0001	2.20	1.04	<0.001
Standard Test : Day 16	100.18	8.92	1	7.49	0.034	0.6	0.92	0.19	0.95	188.67	1.04	<0.001
Stress Test : Day 16	-50.36	8.92	<0.001	7.09	0.034	<0.001	4.22	0.19	<0.0001	2.36	1.04	<0.001
Treatment Control	152.35	5.16	0.928	7.48	0.021	<0.001	1.44	0.11	<0.0001	112.17	1.04	1
Treatment ChitoVan	153.02	5.16	0.406	7.54	0.021	0.045	1.56	0.11	<0.0001	108.85	1.04	0.82
Treatment Ferralyte	158.5	5.16	0.498	7.59	0.021	0.001	1.49	0.11	<0.0001	67.36	1.04	<0.001
Treatment Ultrion	157.37	5.16	0.487	7.57	0.021	0.003	1.71	0.11	<0.0001	60.28	1.04	<0.001
Day 0	273.66	6.31	<0.001	8.12	0.024	<0.001	0.01	0.14	0.61	181.27	1.04	<0.001
Day 1	217.06	6.31	0.017	7.79	0.024	0.877	0.42	0.14	0.98	181.27	1.04	0.65
Day 2	190.33	6.31	0.183	7.41	0.024	<0.001	1.39	0.14	0.987	184.93	1.04	0.532

Day 4	132.87	6.31	0.007	7.36	0.024	<0.001	2.47	0.14	0.487	145.47	1.04	0.612
Day 8	93.05	6.31	0.004	7.31	0.024	<0.001	2.42	0.14	0.123	18.17	1.04	0.368
Day 16	24.91	6.31	<0.001	7.29	0.024	<0.001	2.57	0.14	0.002	21.12	1.04	0.738

Notes: Least squares mean had a confidence interval of 95% and degrees of freedom were estimated with method Satterthwaite in RStudio.

Table S9. Stress Test aqueous parameters from Tukey HSD analysis.

		Eh		Mn		pH		SO4	
Parameter	**df**	**t.ratio**	**p.value**	**t.ratio**	**p.value**	**t.ratio**	**p.value**	**t.ratio**	**p.value**
C Day0 - sp Day0	33	4.270	**7.28E-03**	0.013	1.00E+00	2.638	3.00E-01	-0.089	1.00E+00
C Day1 - sp Day1	33	8.173	**1.20E-07**	-2.952	1.69E-01	15.498	**6.62E-14**	0.847	9.99E-01
C Day16 - sp Day16	33	11.929	**1.05E-11**	-12.133	**6.67E-12**	8.554	**4.29E-08**	33.707	**5.86E-14**
C Day2 - sp Day2	33	14.752	**9.05E-14**	-10.113	**7.67E-10**	13.380	**5.14E-13**	0.927	9.97E-01
C Day4 - sp Day4	33	20.846	**5.86E-14**	-16.691	**5.95E-14**	17.346	**5.88E-14**	4.300	**5.84E-03**
C Day8 - sp Day8	33	26.682	**5.86E-14**	-14.575	**1.02E-13**	13.233	**6.77E-13**	32.592	**5.86E-14**
sp Day0 - sp Day1	33	6.436	**1.57E-05**	-2.992	1.56E-01	14.446	**1.14E-13**	NA	NA
sp Day0 - sp Day16	33	23.541	**5.86E-14**	-15.495	**6.62E-14**	22.138	**5.86E-14**	NA	NA
sp Day0 - sp Day2	33	11.845	**1.27E-11**	-10.143	**7.13E-10**	21.965	**5.86E-14**	NA	NA
sp Day0 - sp Day4	33	19.444	**5.86E-14**	-17.408	**5.88E-14**	25.495	**5.86E-14**	NA	NA
sp Day0 - sp Day8	33	25.518	**5.86E-14**	-16.173	**6.13E-14**	24.141	**5.86E-14**	NA	NA
sp Day1 - sp Day16	33	17.104	**5.91E-14**	-12.503	**2.98E-12**	6.981	**3.31E-06**	32.970	**5.86E-14**
sp Day1 - sp Day2	33	5.408	**3.02E-04**	-7.151	**2.05E-06**	6.816	**5.30E-06**	-0.103	1.00E+00
sp Day1 - sp Day4	33	13.008	**1.05E-12**	-14.416	**1.17E-13**	9.969	**1.10E-09**	3.408	5.63E-02
sp Day1 - sp Day8	33	19.082	**5.86E-14**	-13.181	**7.47E-13**	8.967	**1.43E-08**	33.376	**5.86E-14**
sp Day2 - sp Day16	33	11.696	**1.78E-11**	-5.352	**3.55E-04**	0.168	1.00E+00	33.073	**5.86E-14**
sp Day2 - sp Day4	33	7.599	**5.82E-07**	-7.265	**1.48E-06**	3.169	1.08E-01	3.530	**4.21E-02**
sp Day2 - sp Day8	33	13.673	**3.12E-13**	-6.030	**5.05E-05**	2.152	5.92E-01	33.574	**5.86E-14**
sp Day4 - sp Day16	33	4.097	**1.15E-02**	1.913	7.44E-01	-3.006	1.52E-01	29.533	**5.86E-14**
sp Day4 - sp Day8	33	6.074	**4.45E-05**	1.235	9.82E-01	-1.026	9.96E-01	30.119	**5.86E-14**
sp Day8 - sp Day16	33	-1.977	7.04E-01	0.678	1.00E+00	-1.988	6.98E-01	-0.502	1.00E+00

Notes: C represents standard test while sp represents stress test incubation. Significant differences are in bold with a $p<0.05$. The interaction term helped evaluate any significant interaction between day and stress test incubation not always seen in the standard test.

Table S10. Stress Test supportive aqueous parameters LME model. Results include least square mean (LSM) and standard error (SE) with its correspondence p value

	Iron			Aluminum			Ammonia			Nitrate			Phosphate			DOC			SUVA		
Parameter	**LSM**	**SE**	**Pr(>|t|)**	**LSM**	**SE**	**Pr(>|t|)**	**LSM**	**SE**	**Pr(>|t|)**	**LSM**	**SE**	**Pr(>|t|)**	**LSM**	**SE**	**Pr(>|t|)**	**LSM**	**SE**	**Pr(>|t|)**	**LSM**	**SE**	**Pr(>|t|)**
Standard Test	0.03	0.13	0.86	0.04	0.02	1.00	1.53	0.02	<0.001	15.49	1.13	0.002	0.63	0.42	0.13	13.97	5.79	0.02	1.51	0.02	0.02
Stress Test	0.86	0.13	**<0.0001**	0.05	0.02	0.22	1.78	0.02	<0.001	7.92	1.13	0.002	5.16	0.42	<0.001	131.56	5.79	<0.001	1.11	0.02	0.58
Standard Test : Day 0	0.02	0.29	0.76	0.04	0.02	0.16	0.13	0.02	<0.001	16.95	1.99	0.000	0.49	0.90	0.50	11.15	13.59	<0.001	1.49	0.04	<0.001
Stress Test : Day 0	0.09	0.29	**3.13E-06**	0.05	0.02	0.15	0.90	0.02	<0.001	18.17	1.99	0.004	5.01	0.90	<0.001	48.07	13.59	<0.002	1.45	0.04	<0.002
Standard Test : Day 1	0.03	0.29	0.76	0.05	0.02	0.33	1.65	0.02	0.04	8.08	1.99	0.05	0.53	0.90	0.50	14.78	13.59	<0.003	1.45	0.04	0.24
Stress Test : Day 1	0.10	0.29	**<0.0001**	0.04	0.02	0.37	16.12	0.02	<0.001	1.05	1.99	0.97	1.77	0.90	<0.001	63.17	13.59	<0.004	1.25	0.04	0.11
Standard Test : Day 2	0.03	0.29	0.76	0.03	0.02	0.28	1.13	0.02	0.46	7.69	1.99	0.01	0.59	0.90	0.50	15.43	13.59	0.41	1.28	0.04	0.41
Stress Test : Day 2	0.72	0.29	**<0.0001**	0.03	0.02	**<0.001**	19.89	0.02	<0.001	0.37	1.99	0.97	3.17	0.90	<0.001	188.03	13.59	0.001	0.91	0.04	<0.001
Standard Test : Day 4	0.05	0.29	0.76	0.13	0.02	0.33	1.97	0.02	0.000	5.21	1.99	0.97	0.90	0.90	0.50	13.56	13.59	0.28	1.58	0.04	0.28
Stress Test : Day 4	2.05	0.29	**<0.0001**	0.03	0.02	**0.01**	37.71	0.02	<0.001	0.13	1.99	0.97	4.17	0.90	<0.001	136.60	13.59	<0.001	1.16	0.04	0.00
Standard Test : Day 8	0.02	0.29	0.76	0.02	0.02	0.21	2.46	0.02	0.02	4.66	1.99	0.98	0.58	0.90	0.50	12.72	13.59	0.26	1.62	0.04	0.26
Stress Test : Day 8	1.59	0.29	**<0.0001**	0.13	0.02	**0.01**	40.85	0.02	<0.001	0.06	1.99	0.98	8.07	0.90	<0.001	266.63	13.59	<0.001	0.86	0.04	<0.001

Standard Test : Day 16	0.02	0.29	0.76	0.01	0.02	0.35	3.16	0.02	0.00	3.32	1.99	0.97	0.70	0.90	0.50	16.17	13.59	0.24	1.43	0.04	0.24
Stress Test : Day 16	0.62	0.29	**<0.0001**	0.07	0.02	**0.02**	73.70	0.02	<0.001	0.04	1.99	0.97	8.73	0.90	<0.001	84.84	13.59	<0.001	1.07	0.04	0.001
Treatment Control	0.62	0.20	<0.0001	0.05	0.01	0.22	1.52	0.02	0.09	1.67	2.20	0.09	2.90	0.66	<0.001	91.75	8.59	<0.001	1.23	0.02	<0.001
Treatment ChitoVan	0.19	0.20	0.35	0.04	0.01	0.22	2.71	0.02	0.11	16.44	2.20	0.01	4.13	0.66	<0.001	62.09	8.59	<0.001	1.32	0.02	0.03
Treatment Ferralyte	0.46	0.20	0.02	0.04	0.01	0.17	1.54	0.02	0.08	2.80	2.20	0.86	2.44	0.66	<0.001	68.21	8.59	<0.001	1.30	0.02	0.09
Treatment Ultrion	0.50	0.20	0.17	0.04	0.01	0.44	1.85	0.02	0.81	2.94	2.20	0.41	2.04	0.66	<0.001	69.01	8.59	<0.001	1.27	0.02	0.26
Day 0	0.05	0.21	0.81	0.04	0.02	0.22	1.20	0.02	0.06	17.64	1.53	0.02	1.13	0.76	<0.001	29.61	9.70	0.01	1.34	0.03	<0.01
Day 1	0.07	0.21	0.76	0.04	0.02	0.28	1.50	0.02	0.000	12.68	1.53	0.14	1.15	0.76	0.09	38.97	9.70	0.01	1.34	0.03	0.46
Day 2	0.37	0.21	0.08	0.03	0.02	0.71	1.64	0.02	0.000	7.85	1.53	0.38	2.50	0.76	0.01	101.73	9.70	<0.001	1.14	0.03	0.37
Day 4	1.05	0.21	<0.0001	0.06	0.02	**<0.001**	2.28	0.02	<0.001	1.06	1.53	0.004	2.75	0.76	0.001	75.07	9.70	0.001	1.36	0.03	0.25
Day 8	0.81	0.21	<0.0001	0.06	0.02	0.22	2.26	0.02	<0.001	1.01	1.53	0.004	4.32	0.76	<0.001	139.67	9.70	0.001	1.19	0.03	0.12
Day 16	0.32	0.21	0.14	0.03	0.02	**0.01**	2.63	0.02	<0.001	1.01	1.53	0.004	4.73	0.76	<0.001	51.51	9.70	0.001	1.25	0.03	0.49

Table S11. Stress Test supportive aqueous parameters from Tukey HSD analysis.

		Aluminium		DOC		Fe		NH4		NO3		PO4		SUVA	
Parameter	**df**	**t.ratio**	**p.value**	**t.ratio**	**p.value**	**t.ratio**	**p.value**	**t.ratio**	**p.value**	**t.ratio**	**p.value**	**t.ratio**	**p.value**	**t.ratio**	**p.value**
C Day0 - sp Day0	33.00	-1.28	9.77E-01	-1.94	7.29E-01	-0.16	1.00E+00	-3.70	3.15E-02	0.71	1.00E+00	-3.61	3.93E-02	0.537	1.00E+00
C Day1 - sp Day1	33.00	0.83	9.99E-01	-2.54	3.52E-01	-0.18	1.00E+00	-11.80	**1.40E-11**	1.57	9.09E-01	-0.99	9.97E-01	2.891	1.89E-01
C Day16 - sp Day16	33.00	-4.84	1.53E-03	-3.71	3.10E-02	-1.48	9.35E-01	-17.83	**5.87E-14**	-0.01	1.00E+00	-6.43	**1.59E-05**	5.672	**1.39E-04**
C Day2 - sp Day2	33.00	0.13	1.00E+00	-9.06	**1.13E-08**	-1.70	8.56E-01	-14.90	**8.22E-14**	2.21	5.55E-01	-2.07	6.47E-01	8.471	**5.28E-08**
C Day4 - sp Day4	33.00	5.17	**5.90E-04**	-6.46	**1.48E-05**	-4.89	1.31E-03	-13.15	**8.01E-13**	0.00	1.00E+00	-2.61	3.14E-01	6.072	**4.41E-05**
C Day8 - sp Day8	33.00	-5.42	**2.90E-04**	-13.32	**5.69E-13**	-3.82	2.33E-02	-13.49	**4.25E-13**	0.00	1.00E+00	-5.99	**5.60E-05**	12.278	**4.78E-12**
sp Day0 - sp Day1	33.00	0.99	9.97E-01	-0.79	1.00E+00	-0.04	1.00E+00	-10.82	**1.38E-10**	2.38	4.44E-01	2.59	3.26E-01	6.152	**3.50E-05**
sp Day0 - sp Day16	33.00	-0.93	9.98E-01	-2.03	6.68E-01	-1.31	9.72E-01	-22.27	**5.86E-14**	2.38	4.46E-01	-2.99	1.56E-01	11.988	**9.05E-12**

sp Day0 - sp Day2	33.00	1.78	8.15E-01	-7.34	**1.18E-06**	-1.55	9.15E-01	-14.76	**9.02E-14**	2.39	4.42E-01	1.47	9.39E-01	20.708	**5.86E-14**
sp Day0 - sp Day4	33.00	2.20	5.58E-01	-4.65	2.61E-03	-4.81	**1.65E-03**	-16.00	**6.18E-14**	2.38	4.44E-01	0.67	1.00E+00	9.543	**3.17E-09**
sp Day0 - sp Day8	33.00	-2.91	1.85E-01	-11.47	**2.99E-11**	-3.67	**3.41E-02**	-16.14	**6.14E-14**	2.38	4.46E-01	-2.45	4.04E-01	26.782	**5.86E-14**
sp Day1 - sp Day16	33.00	-1.92	7.39E-01	-1.24	9.81E-01	-1.27	9.77E-01	-8.37	**7.12E-08**	0.00	1.00E+00	-5.58	**1.84E-04**	2.754	2.43E-01
sp Day1 - sp Day2	33.00	0.79	1.00E+00	-6.55	**1.12E-05**	-1.51	9.26E-01	-3.23	9.49E-02	0.00	1.00E+00	-1.12	9.91E-01	5.707	**1.26E-04**
sp Day1 - sp Day4	33.00	1.22	9.84E-01	-3.85	2.16E-02	-4.78	**1.82E-03**	-4.22	8.24E-03	0.00	1.00E+00	-1.92	7.39E-01	1.224	9.82E-01
sp Day1 - sp Day8	33.00	-3.90	**1.94E-02**	-10.68	**1.93E-10**	-3.64	**3.71E-02**	-3.83	2.28E-02	0.00	1.00E+00	-5.04	**8.69E-04**	7.024	**2.89E-06**
sp Day2 - sp Day16	33.00	-2.71	2.63E-01	5.31	**4.00E-04**	0.24	1.00E+00	-5.14	**6.58E-04**	-0.01	1.00E+00	-4.46	**4.35E-03**	-2.972	1.61E-01
sp Day2 - sp Day4	33.00	0.42	1.00E+00	2.70	2.70E-01	-3.26	8.84E-02	-0.99	9.97E-01	0.00	1.00E+00	-0.80	1.00E+00	-4.492	**3.94E-03**
sp Day2 - sp Day8	33.00	-4.69	**2.31E-03**	-4.12	1.07E-02	-2.12	6.12E-01	-0.60	1.00E+00	-0.01	1.00E+00	-3.92	1.84E-02	1.281	9.75E-01
sp Day4 - sp Day16	33.00	-3.14	1.16E-01	2.61	3.14E-01	3.50	5.08E-02	-4.14	1.02E-02	0.00	1.00E+00	-3.66	3.49E-02	1.532	9.19E-01
sp Day4 - sp Day8	33.00	-5.11	**7.07E-04**	-6.82	**5.18E-06**	1.14	9.90E-01	0.39	1.00E+00	0.00	1.00E+00	-3.12	1.21E-01	5.794	**9.82E-05**

sp Day8 - sp Day16	33.00	1.98	7.05E-01	9.43	**4.25E-09**	2.36	4.55E-01	-4.53	3.62E-03	0.00	1.00E+00	-0.54	1.00E+00	-4.270	7.19E-03

Notes: C represents standard test while sp represents stress test incubation. Significant differences are in bold with a $p<0.05$. The interaction term helped evaluate any significant interaction between day and stress test incubation not always seen in the standard test.

Table S12. Description of the fluorescence and adsorption properties used in Chapter 3. Modified from Fleck et al. (2014).

Parameter	Description	Property	Reference
$Sag_{275\text{-}295}$	Absorption spectral slope between 275 and 290 nm	Higher S values (>0.02) indicate low molecular weight material, decreasing aromaticity	Blough and Del Vecchio,2002; Helms et al., 2008
Flr A:C	Fluorescence intensity in region “A” relatively to region “C”	Indicator of biological or photochemical degradation of the humic fraction of DOM	Kothawala et al., 2012; Moran et al. 2000
Flr T:C	Fluorescence intensity in the "D" region relative to the "C" region	Higher T:C suggests more labile DOM relative to background humic-like DOM	Lochmuller and Saavedra, 1986; Stedmon et al., 2003
Flr D:C	Fluorescence intensity in the "D" region relative to the "C" region	Higher D:C suggests more terrestrial soil fulvic DOM relative to background humic DOM	Lochmuller and Saavedra, 1986; Stedmon et al., 2003
Flr F:C	Fluorescence intensity in the "F" region (FDOM) relative to the "C" region	Relatively more 'reduced' humic DOM structures than oxidized forms; more sensitive to photodegradation	Fleck et al., 2014
Flr M:C	Fluorescence intensity in the "M" region relative to the "C" region	Higher values suggest fresher DOM relative to background humic DOM; also, possible anthropogenic DOM (i.e., hydrocarbons)	Burdige et al., 2004; Coble, 1996; Helms et al., 2013; Para et al., 2010
Flr N:C	Fluorescence intensity in the "N" region relative to the "C" region	Higher values suggest more fresh/algal DOM relative to background humic DOM; possible anthropogenic DOM (i.e., hydrocarbons)	Coble, 1998
HIX	Humification Index The area under the 435-480 nm Em divided by the peak area	Indicator of source, diagenesis, and sorption capacity; higher values indicate an increasing degree of humification	Ohno, 2002

	300-345 nm plus 435-480 nm at Ex 254 nm.		
FI	Fluorescence Index Ratio of Em 470 nm and 520 nm at Ex 370 nm	Relative contribution of plant versus microbial source to the DOM pool	Cory et al. 2010
BIX	Biological Index Ratio of Em 380 nm and 430 nm at Ex 310 nm	Indicator of recent biological activity or recently produced DOM	Wilson and Xenopoulos, 2009
FLR_A	260 Ex – 450 Em	Relative amount of humic-like aromatic substances of terrestrial origin UV spectra	Coble, 1996; Stedmon et al., 2003
FLR_B	270 Ex – 305 Em	Relative amount of "protein-like" DOM	Coble, 1996; Stedmon et al., 2003
FLR_C	340 Ex – 440 Em	Relative amount of "humic-like" substances of terrestrial sources visible spectra	Coble, 1996; Stedmon et al., 2003
FLR_D	390 Ex – 510 Em	Relative amount of "fulvic-like" DOM	Coble, 1996; Stedmon et al., 2003
FLR_F	355 to 375 nm Ex – 440 to 500 nm Em	Relative amount of "quinoid-like" humic DOM	Dowing et al., 2009
FLR_M	300 Ex – 390 Em	Relative amount of humic (blue shifted) "marine-like" DOM	Coble, 1996; Stedmon et al., 2003
FLR_N	280 Ex – 370 Em	Relative amount of algal-derived DOM	Coble, 1996; Stedmon et al., 2003
FLR_T	275 Ex – 340 Em	Relative amount of "protein-like" DOM from microbial sources	Coble, 1996; Stedmon et al., 2003

Table S13. Results and Interpretations for the different fluorescence and adsorption properties analyzed in chapter 3.

Parameter	Control	0.4 g of OM addition	Possible Interpretation
Sag275-295	No dramatic changes in a range 0.015-0.017	Biggest increase at day 1 to 0.035. Decreased to 0.025 by day 8. Slightly increase by day 16 (0.027). Similar patterns for 0.1 g and 0.2 g of SP-OM addition. The other treatments did not show dramatic changes.	Increased in low molecular weight DOM compared to the control. 70% decreased from day 1 to 8.
Flr A:C	No dramatic changes at 1.7	Increased to 2.5 during the first 2 days. Decreased to control values by day 8. Quasi-steady state by day 16. Similar pattern in a gradient with OM addition for the other treatments.	Normally an indicator of humic DOM degradation. We saw an enrichment with spirulina addition (pigments signal or a humic released from spirulina) during day 0. Decreased with incubation time due to humic-type DOM degrading to simple molecules.
Flr T:C	No dramatic changes at 0.7	Progressive increase peaking at 6 by day 8. Quasi-steady state by day 16. Dramatic patterns are only seen for 0.2 g and 0.4 g of SpOM addition. Similar pattern for 0.2 g of SpOM addition. No dramatic changes for the other treatments.	Enrichment of microbially derived material until day 8 with the spirulina addition relative to humic-like DOM.
Flr D:C	No dramatic changes at 0.42	Started at lower ratio (0.2). Progressive increase until day 8 to 0.3. No dramatic changes after. Lower than control by the end of incubation.	Normally an indicator of terrestrial fulvic DOM enrichment. Lower with the treatments than the control as the spirulina is enriched with amino acids and protein-like DOM.
Flr F:C	No dramatic changes at 0.7	Progressive increase to 1.1 by day 2. Dramatic decrease by day 8 to lower values than the control (0.6). Similar pattern for the other treatments, showing higher values with higher OM addition.	Normally an indicator of more reduced humic DOM structures. Possibly showing that the reduced humic structures are being consumed by microbes.

Flr M:C	No dramatic changes at 0.9	Progressive increase to 1.1 by day 8, from lower values than the control (0.2). Quasi-steady state conditions in the remainder of incubation. Similar patterns for the other treatments showing a gradient but maintaining quasi steady state conditions lower than the control. Similar pattern for the other treatments, showing lower values with greater OM addition, ending at control values at day 16.	Higher proportion of freshly produced DOM in this case associated with microbial activity.
Flr N:C	No dramatic changes at 0.7	Increased progressive tendency by day 8 to 1.8. Quasi-steady state by day 16. The other SpOM addition treatments did not show dramatic changes.	Fresh algal DOM relative to background humic DOM and control.
HIX	No dramatic changes at 0.87	Decrease progressive pattern by day 8 to 0.3. Quasi-steady conditions after day 8. Similar pattern for 0.2 g of Sp-OM addition. The other treatments did not show dramatic changes.	Higher values tend to indicate humification. It seems that molecules kept breaking down until day 8. Less aromatic and higher C/N ratio.
FI	No dramatic changes at 1.7	Higher than control at day 0 (2.9). Progressive decrease to 1.7 by day 8. Quasi-steady until day 16 at control values. Similar pattern for the other treatments, showing higher values with OM addition.	Higher than 1.8 means contribution of microbial derived OM to the DOM pool.
BIX	No dramatic changes at 0.8	Started at lower values (0.43). Progressive increase until day 8 at 1.0. Quasi-steady for the remainder time. The other treatments showed no dramatic changes with lower values than the control with OM addition.	Normally values higher than 1 correspond to recently produced DOM. We only see that tendency with 0.4 g of SpOM treatment.
FLR_A	No dramatic changes at 1.5	Progressive decrease from 71.5 to 8.8 during the first 8 days. Quasi-steady for the remainder of incubation. In general, there is a positive gradient with OM addition during the initial conditions. Similar pattern for the other treatments.	Relative amount of humic-like, aromatic substances of terrestrial origin (Fellman et al., 2010). It seems that there is an increase in something with a similar response of humic-like DOM with SpOM addition.

FLR_B	No dramatic changes at 1	Progressive increase until day 4 at 160. Quasi-steady conditions by the end of the incubation ending at 173. Similar pattern for 0.2 g of SpOM addition with a progressive increase until day 8 at 61. No dramatic changes for the other treatments.	Relative protein-like DOM associated with "food." Other authors suggest it is a by-product of microbial activity. In this case, as it increased with what seems to be microbial activity, it may be associated with a by-product-type DOM.
FLR_C	No dramatic changes at 1.5	Day 0 started at 37. Progressive decrease by day 8 ending at 5.3. Quasi-steady by the end of the incubation, higher than the control. Positive gradient with OM addition, higher than the control. Treatments follow a similar pattern than the 0.4 g of SpOM addition.	Relative number of humic-like substances of terrestrial source (Stedmon and Markager 2005). It seems that there is an increase in something with a similar response of humic-like DOM with SpOM addition, possibly associated with the pigments or other components of the algae.
FLR_ D	No dramatic changes at 0.7	Initial conditions at 5 with no changes until day 2 showing a progressive decrease until day 8. Quasi-steady conditions after day 8. For the other treatments, there is a positive gradient with OM addition showing no dramatic changes with the development of the incubation.	Relative amount of fulvic-like DOM associated with microbes' substrate. We saw an enrichment but an apparent consumption after day 2 only with 0.4 g of SpOM addition.
FLR_F	No dramatic changes at 0.7	Higher than control at day 0 (30). Progressive decrease to 3.3 by day 8. Quasi steady until day 16 slightly higher than control values. Similar pattern for the other treatments, showing higher values with OM addition.	Relative amount of "quinoid-like" humic DOM. It seems that the spirulina addition enriched the DOM in a type of humic DOM similar to quinoid that acted as substrate (food) for microbes.
FLR_ M	No dramatic changes at 0.7	Initial conditions higher (9) than the control. Values decreased by day 1 and maintained quasi-steady for the remainder of incubation at 7. For the other treatments we saw a positive gradient with higher the OM addition	Relative amount of "marine-like" DOM. There was an enrichment with the SpOM addition by the end of the incubation.

		following a similar pattern than the 0.4 g of Sp-OM addition.	
FLR_ N	No dramatic changes at 0.7	Initial value higher than the control at 15, peaking at day 1 with 30. Decrease by day 2 to 10 and stayed in quasi steady conditions for the remainder of the incubation. Similar pattern for the other treatments, showing a gradient with Sp-OM addition. However, the highest the OM addition, the dramatic the peak.	Relative amount of algal derived DOM enriched with spirulina addition.
FLR_ T	No dramatic changes at 0.7	Similar pattern to region N. Initial value higher than the control at 20, peaking at day 1 with 55. Decrease by day 2 to 30 and stayed in quasi steady conditions for the remainder of the incubation. Similar pattern for the other treatments, showing a gradient with Sp-OM addition. However, the highest the OM addition, the dramatic the peak.	Relative amount of "protein-like" DOM from microbial sources (Moran et al., 2000) resembling amino acid tryptophan (Fellman et al., 2010).

Table S14a. Chapter 3 gradient in organic matter incubation experiment data set, including replication and blanks.

Location	OM Treatment	Sample Day	Date (dd/mm/yyyy)	Cache Creek Rumsey Water (g)	A2-C2 Mix Soil (g)	Spirulina (g)	pH	Redox (mV)	Eh mV	MeHg (ng/L)	THg (ng/L)	NO3-NO2 (mg-N/L)	NH4 (mg-N/L)	PO4 (ug-P/L)
CCSB	Control	0	19/09/2022	200.1	50.08	0	7.53	168.6	372.8	0.0699	21.9	33.0	0.00	587
CCSB	0.025	0	19/09/2022	200.06	50.09	0.02634	7.46	163.1	367.3	0.0679	18.2	19.0	0.18	713
CCSB	0.05	0	19/09/2022	200.07	50.2	0.05522	7.41	166.4	370.6	0.0603	25.4	8.4	0.35	371
CCSB	0.1	0	19/09/2022	200.08	50.1	0.101743	7.30	178.3	382.5	0.0819	24.4	6.6	0.45	661
CCSB	0.2	0	19/09/2022	200.08	50.3	0.20114	7.85	33.5	237.7	0.138	28.6	1.6	2.41	1390
CCSB	0.4	0	19/09/2022	200.06	50	0.40309	7.72	30.8	235.0	0.165	35.1	0.5	2.82	2950
CCSB	Control	1	20/09/2022	200.08	50.03	0	7.47	56.5	260.7	0.0314	19.1	27.6	0.05	280
CCSB	0.025	1	20/09/2022	200.05	50.12	0.02672	7.50	107.3	311.4	0.11	19.6	n.a.	0.43	739
CCSB	0.05	1	20/09/2022	200.06	50	0.05034	7.56	98.4	302.6	0.119	25.7	0.1	0.87	622
CCSB	0.1	1	20/09/2022	200.07	50.3	0.10204	7.41	53.7	257.9	0.27	15.9	0.1	1.82	817
CCSB	0.2	1	20/09/2022	200.12	50	0.20293	7.22	-112.4	91.8	3.69	50.9	0.3	2.75	518
CCSB	0.4	1	20/09/2022	200.02	50	0.40327	6.92	-116.9	87.3	11.1	71.7	0.4	4.55	331

CCSB	Control	2	21/09/2022	200.08	50.3	0	7.56	24.0	228.2	0.0586	16.4	0.1	0.19	494
CCSB	0.025	2	21/09/2022	200.13	50.01	0.02521	7.46	96.2	300.4	0.147	16	n.a.	0.78	252
CCSB	0.05	2	21/09/2022	200.05	50.1	0.05358	7.22	67.2	271.4	0.201	12.9	n.a.	1.17	241
CCSB	0.1	2	21/09/2022	200.09	50.3	0.10028	7.18	83.7	287.9	0.36	20.7	0.1	2.09	264
CCSB	0.2	2	21/09/2022	200.02	50.2	0.20248	7.00	-138.9	65.3	2.77	37	0.1	8.87	393
CCSB	0.4	2	21/09/2022	200.09	50.2	0.40116	6.86	-275.7	-71.5	22.9	113	0.3	7.68	688
CCSB	Control	4	23/09/2022	200.09	50.05	0	7.52	73.8	278.0	0.102	13.9	n.a.	0.28	649
CCSB	0.025	4	23/09/2022	200.13	50.18	0.02574	7.26	59.5	263.7	0.12	16.3	n.a.	1.12	323
CCSB	0.05	4	23/09/2022	200.06	50.01	0.05136	7.22	24.7	228.9	0.204	14.2	0.1	1.60	31.7
CCSB	0.1	4	23/09/2022	200.09	50.2	0.10069	7.10	-102.6	101.6	0.63	15.3	n.a.	2.81	167
CCSB	0.2	4	23/09/2022	200.06	50.2	0.20385	7.05	-456.5	-252.3	14	50.5	n.a.	4.35	1060
CCSB	0.4	4	23/09/2022	200.09	50.2	0.40118	6.88	-458.3	-254.1	28.6	83.3	n.a.	15.81	1780
CCSB	Control	8	27/09/2022	200.08	50.14	0	7.29	75.7	279.9	0.0713	11.2	n.a.	0.36	369
CCSB	0.025	8	27/09/2022	200.11	50.08	0.02604	7.15	59.8	264.0	0.229	13.9	n.a.	1.13	135
CCSB	0.05	8	27/09/2022	200.02	50.1	0.05067	7.04	-85.2	119.0	0.161	9.06	n.a.	2.27	191
CCSB	0.1	8	27/09/2022	200.06	50.3	0.10284	6.96	-391.1	-186.9	0.166	22.2	n.a.	3.01	531

CCSB	0.2	8	27/09/2022	200.09	50	0.20219	6.98	-433.2	-229.0	5.08	32.9	n.a.	4.45	798
CCSB	0.4	8	27/09/2022	200.08	50	0.40027	6.85	-470.1	-265.9	9.59	36.9	n.a.	16.57	979
CCSB	Control	16	05/10/2022	200.12	50.02	0	6.89	92.7	296.9	0.0603	9.27	n.a.	0.64	297
CCSB	0.025	16	05/10/2022	200.09	50.03	0.02591	6.97	-107.0	97.2	0.036	8.65	n.a.	1.06	610
CCSB	0.05	16	05/10/2022	200.08	50.1	0.05126	6.93	-120.3	83.9	0.143	12.2	n.a.	2.24	1320
CCSB	0.1	16	05/10/2022	200.11	50.3	0.10197	6.83	-296.4	-92.2	0.213	19.8	n.a.	2.98	3920
CCSB	0.2	16	05/10/2022	200.06	50.1	0.20331	6.89	-275.4	-71.2	0.258	12	n.a.	8.80	4110
CCSB	0.4	16	05/10/2022	200.1	50.1	0.40244	6.85	-457.1	-252.9	2.07	17.8	n.a.	9.06	218
CCSB	Control	16	19/09/2022	200.16	50.04	0	7.10	-161.9	42.3	0.101	8.3	n.a.	0.84	342
CCSB	0.025	2	20/09/2022	200.1	50.11	0.02507	7.44	98.4	302.6	0.119	19.8	n.a.	1.44	502
CCSB	0.05	1	21/09/2022	200.08	50.1	0.05286	7.52	90.8	295.0	0.138	23.4	n.a.	2.03	212
CCSB	0.1	4	23/09/2022	200.13	50.1	0.10265	7.16	-134.3	69.9	0.586	14.7	n.a.	5.48	858
CCSB	0.2	8	27/09/2022	200.13	50.2	0.20428	6.95	-476.4	-272.2	5.26	29.6	n.a.	8.14	2340
CCSB	0.4	0	05/10/2022	200.09	50.3	0.40372	7.84	27.0	231.2	0.173	27.1	0.8	3.64	-4.43
CCSB	Blank	--	27/09/2022	--	--	--	8.31	145.3	349.5	0.0261	0.446	n.a.	-0.03	-6.48
CCSB	Blank	--	05/10/2022	--	--	--	8.32	160.8	365.0	0.00241	0.5	0.1	-0.02	-22

CCSB	CC Water Rumsey	--	--	--	--	--	--	--	--	0.0123	1.49		-0.07	-23.2
CCSB	CC Water Rumsey	--	--	--	--	--	--	--	--	0.135	1.82		-0.07	-22.7
CCSB	Control	1	26/10/2022	200.46	50.1	0	6.72	150.8	355.0		17.1			
CCSB	0.1	16	26/10/2022	200.48	50.1	0.12492	6.83	-296.4	-92.2		19.8		3.49	

Table S14b.Chapter 3 gradient in organic matter incubation experiment data set, including replication and blanks.

Soil Sample Location	OM Treatment	Sample Day	Sample Date (dd/mm/yyyy)	Sample ID	Fe (mg/L)	Mn (mg/L)	Al (mg/L)	DOC (mg/L)	TN (mg/L)	SUVA254 (L/mg-m)	SO4 (mg/L)	Cl (mg/L)	Soil MeHg (pg/mg) dry wt.	Soil MeHg Flag
CCSB	Control	0	19/09/2022	A-0	0.057	-0.007	0.318	64	10.20	0.2452	144.093	121.3612	0.73	a
CCSB	0.025	0	19/09/2022	B-0	-0.035	-0.009	0.207	66	10.85	0.2955	103.4401	91.4867	0.98	a
CCSB	0.05	0	19/09/2022	C-0	-0.089	-0.009	0.085	70	11.13	0.3505	68.5202	53.4543	1.10	
CCSB	0.1	0	19/09/2022	D-0	-0.033	-0.008	0.144	72	11.66	0.4349	64.298	55.8706	1.30	
CCSB	0.2	0	19/09/2022	E-0	0.015	-0.007	0.196	67	14.36	0.5490	122.7105	109.8679	0.49	
CCSB	0.4	0	19/09/2022	F-0	0.379	0.002	0.488	100	24.67	1.2060	123.9823	107.8326	1.59	a
CCSB	Control	1	20/09/2022	A-1	0.067	-0.001	0.210	14	10.43	0.2982	112.4468	103.163	0.81	a
CCSB	0.025	1	20/09/2022	B-1	-0.119	0.023	0.052	134	5.00	0.3374	139.0246	143.0067	0.85	a

CCSB	0.05	1	20/09/2022	C-1	0.032	0.005	0.137	117	4.46	0.3686	102.3603	98.9411	1.13	
CCSB	0.1	1	20/09/2022	D-1	-0.009	0.121	0.114	57	4.23	0.4043	106.4038	140.5287	1.18	
CCSB	0.2	1	20/09/2022	E-1	-0.138	0.008	0.075	59	7.26	0.4446	112.2371	121.7087	1.25	
CCSB	0.4	1	20/09/2022	F-1	-0.038	1.076	0.051	208	22.87	0.6944	87.5777	108.8848	2.93	a
CCSB	Control	2	21/09/2022	A-2	-0.035	-0.215	0.079	67	4.35	0.3145	95.3701	90.6418	0.70	a
CCSB	0.025	2	21/09/2022	B-2	-0.074	-0.113	0.083	108	2.63	0.3438	102.7274	92.7871	1.30	a
CCSB	0.05	2	21/09/2022	C-2	-0.088	0.22	0.068	107	3.28	0.3793	97.9667	87.5074	0.95	
CCSB	0.1	2	21/09/2022	D-2	-0.076	0.795	0.068	49	5.04	0.4047	99.4423	133.0338	1.47	
CCSB	0.2	2	21/09/2022	E-2	-0.058	1.738	0.043	86	12.03	0.5379	97.9109	104.7148	2.03	
CCSB	0.4	2	21/09/2022	F-2	-0.055	2.835	0.059	236	29.53	0.8203	102.6466	123.7394	3.99	a
CCSB	Control	4	23/09/2022	A-4	0.33	-0.165	0.129	66	0.89	0.3310	110.3713	106.2442	0.77	a

CCSB	0.025	4	23/09/2022	B-4	-0.033	0.744	0.087	106	2.09	0.3810	111.1025	107.5233	1.02	a
CCSB	0.05	4	23/09/2022	C-4	-0.054	1.579	0.07	87	3.61	0.3898	66.0861	65.691	1.28	
CCSB	0.1	4	23/09/2022	D-4	-0.021	2.301	0.277	28	6.26	0.5231	91.7146	93.678	1.56	
CCSB	0.2	4	23/09/2022	E-4	0.231	3.324	0.052	66	10.35	0.7899	108.4623	108.2934	3.13	
CCSB	0.4	4	23/09/2022	F-4	0.934	5.21	0.053	157	24.89	1.1477	89.0037	107.2701	5.41	a
CCSB	Control	8	27/09/2022	A-8	1.287	0.462	0.061	64	0.88	0.3425	133.7007	121.1968	0.70	a
CCSB	0.025	8	27/09/2022	B-8	-0.086	1.518	0.095	98	2.48	0.3769	100.0312	91.1868	1.15	a
CCSB	0.05	8	27/09/2022	C-8	-0.016	2.244	0.061	51	4.46	0.4177	115.8125	124.3215	1.06	
CCSB	0.1	8	27/09/2022	D-8	1.095	3.325	0.041	28	6.99	0.6042	105.0905	103.2763	0.92	
CCSB	0.2	8	27/09/2022	E-8	1.078	3.95	0.042	80	15.55	0.8298	67.2995	116.8359	2.29	
CCSB	0.4	8	27/09/2022	F-8	2.8	4.228	0.068	172	26.95	1.0447	8.1863	108.4843	3.61	a
CCSB	Control	16	05/10/2022	A-16	-0.079	1.444	0.076	89	1.30	0.3576	84.8321	82.0923	1.01	a

CCSB	0.025	16	05/10/2022	B-16	-0.078	2.089	0.065	87	2.79	0.4134	126.7687	109.2773	1.11	
CCSB	0.05	16	05/10/2022	C-16	0.136	3.155	0.065	44	5.84	0.5351	110.3909	103.0924	0.85	
CCSB	0.1	16	05/10/2022	D-16				21	7.61	0.6002	66.934	90.7803	0.91	
CCSB	0.2	16	05/10/2022	E-16	1.048	3.763	0.336	64	18.03	0.7803	0.0929	138.6127	0.82	
CCSB	0.4	16	05/10/2022	F-16	1.427	4.733	0.053	132	38.47	0.9090	0.0919	134.4829	1.67	a
CCSB	Control	16	19/09/2022	A-16 rep	-0.085	1.583	0.096	76	1.18	0.3691	11.6005	11.8091	1.10	a
CCSB	0.025	2	20/09/2022	B-2 rep	-0.097	-0.163	0.077	104	2.18	0.3260	145.0081	131.8146	0.92	a
CCSB	0.05	1	21/09/2022	C-1 rep	-0.128	-0.199	0.047	119	4.56	0.3877	153.9286	148.8411	1.32	
CCSB	0.1	4	23/09/2022	D-4 rep	-0.005	2.279	0.056	27	5.77	0.5065	120.4878	106.291	1.34	
CCSB	0.2	8	27/09/2022	E-8 rep	2.128	3.393	0.058	51	9.01	0.8075	73.3974	123.3164	1.04	
CCSB	0.4	0	05/10/2022	F-0 rep	0.021	-0.229	0.146	89	19.35	1.0300	165.195	144.0313	1.11	a
CCSB	Blank	--	27/09/2022	Blank 1	-0.133	-0.232	0.042				0.1656	11.6989		

CCSB	Blank	--	05/10/2022	Blank 2	-0.119	-0.234	0.047				0.1667	20.351		
CCSB	CC Water Rumsey	--	--	CC-R-1	-0.125	-0.238	0.049	5	0.27	0.0059				
CCSB	CC Water Rumsey	--	--	CC-R-2	-0.137	-0.238	0.042	8	0.08	0.0124				
CCSB	Control	1	26/10/2022	A-1redo	-0.089	-0.232	0.102							
CCSB	0.1	16	26/10/2022	D-16redo	1.685	3.668	0.393							

Table S15. Chapter 3 mercury analyses quality assurance and control

QA/QC Parameters	THg	MeHg	MeHg
Matrix	water	water	soil
MDL	0.02	0.015	0.10
MDL_(final_units)	ng/L	ng/L	µg/kg dry wt.
RL	0.2	0.03	0.2
RL_(final_units)	ng/L	ng/L	µg/kg dry wt.
DUP_RD_(%)	2	12	11
DUP_N	2	3	4
REP_RD_(%)	7	8	19
REP_N	6	6	6
OPR_Mean_Recovery_(%)	94	93	94
OPR_N	9	11	15
MS_Mean_Recovery_(%)	-	85	80
MS_N	-	7	5
CRM_Name	-	-	SQC 1238-50G
CRM_Type	-	-	Soil
CRM_Lot_Number	-	-	LRAB9919
CRM_Certified_Value	-	-	14.8±0.5
CRM_Certified_Units	-	-	µg/kg
CRM_Mean_Recovery (%)	-	-	77
CRM_N	-	-	16
External_Lab_CRM	-	-	83
External_Lab_CRM_N	-	-	2
External_Lab_UCM_Dup_RD%	-	-	16
External_Lab_UCM_Dup_N	-	-	2

Blanks_Mean	0.55	0.01	-
Blanks_N	2.0	2	-
Method_Blank_Mean	0.07	0.008	0.04
Method_Blank_N	3.0	4	3
Source_xlsx	Study3_Table_Water_Soil_Data	Study3_Table_Water_Soil_Data	Soil_MeHg_Extraction
Soil MeHg "a" flag	CRM between 60-80%, Matrix spike between 75-125%		

Figure S1. Linear regressions for Standard Test and Stress Test for MeHg water with DOC, Sulfate, Iron and Manganese. Note: values are log transform

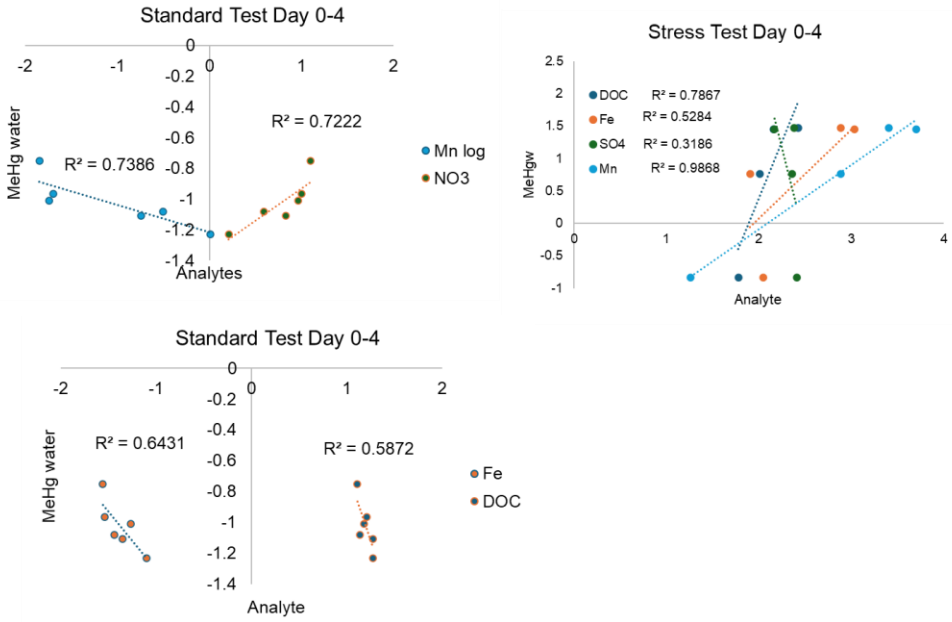

Figure S2. Fluorescence spectrometry figures from chapter 3